UNCLASSIFIED

REPORT DOCUMENTATION PAGE

AD-A204 995

DTIC ELECTE FEB 15 1989 S D

DTIC FILE COPY

(2)

1b. RESTRICTIVE MARKINGS	
2b. DECLASSIFICATION / DOWNGRADING SCHEDULE	3. DISTRIBUTION / AVAILABILITY OF REPORT: Approved for public release; distribution is unlimited.
4. PERFORMING ORGANIZATION REPORT NUMBER(S)	5. MONITORING ORGANIZATION REPORT NUMBER(S): AFOSR-TR- 89-0067
6a. NAME OF PERFORMING ORGANIZATION: Institute of Electrl & Electrnc	6b. OFFICE SYMBOL (If applicable): Eng Inc (IEEE)
6c. ADDRESS (City, State, and ZIP Code): 345 East 47th Street, New York, NY 10017	7a. NAME OF MONITORING ORGANIZATION: AFOSR/NP
	7b. ADDRESS (City, State, and ZIP Code): Building 410, Bolling AFB DC 20332-6448
8a. NAME OF FUNDING / SPONSORING ORGANIZATION: AFOSR	8b. OFFICE SYMBOL (If applicable): NP
	9. PROCUREMENT INSTRUMENT IDENTIFICATION NUMBER: AFOSR-88-0110
8c. ADDRESS (City, State, and ZIP Code): Building 410, Bolling AFB DC 20332-6448	10. SOURCE OF FUNDING NUMBERS

PROGRAM ELEMENT NO.	PROJECT NO.	TASK NO.	WORK UNIT ACCESSION NO.
61102F	2301	A1	

11. TITLE (Include Security Classification)

(U) ORGANIZATION OF THE 11TH IEEE SEMICONDUCTOR LASER CONFERENCE

12. PERSONAL AUTHOR(S)

Dr Wageman

13a. TYPE OF REPORT	13b. TIME COVERED	14. DATE OF REPORT (Year, Month, Day)	15. PAGE COUNT
Final	FROM 1 Mar 88 TO 30 Nov 88	Nov 1988	~~140~~ 221

16. SUPPLEMENTARY NOTATION

17. COSATI CODES			18. SUBJECT TERMS (Continue on reverse if necessary and identify by block number)
FIELD	GROUP	SUB-GROUP	
	20.06		

19. ABSTRACT (Continue on reverse if necessary and identify by block number)

The eleventh IEEE International Semiconductor Laser Conference was held, as scheduled, at the Westin Hotel in Boston MA from 29 Aug 88 - 1 Sep 88.

20. DISTRIBUTION / AVAILABILITY OF ABSTRACT: ☐ UNCLASSIFIED/UNLIMITED X ☐ SAME AS RPT. ☐ DTIC USERS	21. ABSTRACT SECURITY CLASSIFICATION: UNCLASSIFIED
22a. NAME OF RESPONSIBLE INDIVIDUAL: H R SCHLOSSBERG	22b. TELEPHONE (Include Area Code): (202) 767-4906 / 22c. OFFICE SYMBOL: AFOSR/NP

DD FORM 1473, 84 MAR — 83 APR edition may be used until exhausted. All other editions are obsolete.

SECURITY CLASSIFICATION OF THIS PAGE

UNCLASSIFIED

AUGUST 29 - SEPTEMBER 1, 1988

WESTIN HOTEL
Boston, Massachusetts

Sponsored by
THE IEEE
LASERS
AND
ELECTRO
OPTICS
SOCIETY

Support has been provided by the
Air Force Office of Scientific Research

CONFERENCE DIGEST

11th IEEE INTERNATIONAL SEMICONDUCTOR LASER CONFERENCE

AUGUST 29 - SEPTEMBER 1, 1988

WESTIN HOTEL
Boston, Massachusetts

Sponsored by
THE IEEE
LASERS
AND
ELECTRO
OPTICS
SOCIETY

Library of Congress Number 88-81947
IEEE Catalog Number 88CH-2609-6

Support has been provided by the
Air Force Office of Scientific Research

The papers in this book comprise the digest of the meeting mentioned on the cover and title page. They reflect the authors' opinions and are published as presented and without change, in the interests of timely dissemination. Their inclusion in this publication does not necessarily constitute endorsement by the editors, the Institute of Electrical and Electronic Engineers, Inc.

Library of Congress Number: 88-81947
IEEE Catalog Number 88CH-2609-6

Order from: IEEE Service Center
445 Hoes Lane
Piscataway, NJ 08855-1331

FOREWORD

Ivan Kaminow
Conference Chairman

Boston is one of my favorite cities. It is small and manageable yet varied and exciting. I spent four years here with my young family as a graduate student at Harvard and always enjoy a return visit. Much of its charm is afforded by the numerous college students ($1/4 \times 10^6$), ex-students and would-be-students. Many highly trained people, reluctant to leave the scene of their adolescence, can be found waiting on tables. The great universities (Harvard, MIT) and smaller ones (Brandeis, Tufts) have brought culture and high-tech industry (Polaroid, DEC, GTE) to the area.

Walks through the old neighborhoods (Newbury Street, North-End), university areas (Harvard Square) and the harbor (Faneuil Hall) are very pleasant and gastronomically rewarding. Excellent restaurants serving seafood, "natural-foods",, and European and Asian dishes are everywhere. A baseball game at nearby Fenway Park is a good excuse to have a few hot dogs and beers. The Gardner museum provides a delightful old-world setting for a special collection of old masters. Short drives to the North Shore or south to Cape Cod are very picturesque as are longer trips to the Berkshires in the west.

With these diversions, it may be difficult to focus on the business of the day—the 11th International Semiconductor Laser Conference. A glance at this Program will convince you that it is a worthy successor to the earlier meetings in Las Vegas (1967), Mexico City (1969), Boston (1972), Atlanta (1974), Nemunosato (1976), San Francisco (1978), Brighton (1980), Ottawa (1982), Rio de Janeiro (1984) and Kanazawa (1986). We seem to have settled into a two-year rhythm and may be seeing the emergence of a six-year continental modulation consisting of the sequence Asia (Australia), Americas, Europe (Africa).

Traditionally, the meeting has been small in scale to allow active discussion of all facets of current laser research. Thus, we don't have simultaneous sessions or invited talks. During the past 20 years, the depth of topics has grown from tentative claims that GaAs drives did in fact oscillate briefly under pulse excitation at 77K to documented performance characteristics of high-speed 1.5 μm DFB lasers. We owe a debt of gratitude to the International Technical Program Committee led by Bob Goodfellow for selecting papers from a very large group of excellent contributions.

I thank the Local Arrangements Committee under Jim Walpole for organizing the hotel facilities, banquet and spouses' program. In addition, I am grateful to Bob Wangemann and Wendy Rochelle of IEEE/LEOS, who managed the publications, registration and program selection. I also thank Russ Dupuis for looking after publicity and Howard Schlossberg for arranging a generous contribution from the Air Force Office of Scientific Research for conference organization. Many others who have given their time are listed elsewhere in this Program.

We all hope that you will learn interesting things and enjoy the Boston area.

FOREWORD

Bob Goodfellow
Program Chairman

I believe that the 11th IEEE International Semiconductor Laser Conference program promises to be one as exciting as ever, illustrating the diversity, maturity and advanced capabilities that semiconductor injection laser technology has attained. Reports of high power, narrow linewidth, stability, high frequency modulation, tunability and wavelength extensions are included in the program, along with others of yet more novel structures and new understanding. I therefore wish to thank all of the authors who submitted papers and to congratulate those whose papers were accepted. 170 papers were received and 90 were accepted for presentation by the program committee. This selection was a difficult task in view of the large number of excellent papers over a broad topic area, and in view of the short time allowed for the review procedure. I thank the program committee members and the sub-committee chairmen for this large effort and for their advise in compiling the program.

I am grateful to T. P. Lee and Gary Evans for the organisation of rump session discussions. Gary announced a competition to 'name the rump session' and gave example titles "101 ways to achieve a Swell Strehl", "101 (published) ways to not achieve a Swell Strehl" and "Coherent Arrays: On the edge or just scratching the surface?" which seemed to me to be of such excellence as to dissuade anyone else from entering the competition! Anyway I hope these rump sessions will be an opportunity for some controversy.

Another unpredictability at the moment is the post deadline session. This is often a very stimulating session at the Semiconductor Laser Conferences.

Could I remind you that John Bowers will guest edit a special issue of the IEEE Journal of Quantum Electronics. Following past conferences the special issues have proven to be valuable records of the laser advances of the period - I therefore recommend that the authors of all submissions consider pursuing publication by this route.

Finally I would like to thank Ivan Kaminow, the 1986 Conference Program Chairman, and the current Conference Chairman for all his help and advice. I hope all of those who attend enjoy and benefit from this meeting.

CONFERENCE COMMITTEE

Conference Chairman
Ivan P. Kaminow
AT&T Bell Laboratories
Crawford Hill Laboratory
Box 400 - Room HOH R-219
Holmdel, NJ 07733

Program Chairman
Bob Goodfellow
Optoelectronic Devices & Technology
Plessey Research Caswell Limited
Allen Clark Research Center
Caswell, Towcester, Northants
NN12 8EQ, England

Local Arrangements Chairman
James N. Walpole
M.I.T. Lincoln Laboratory
244 Wood Street, C-337
Lexington, MA 02173-0073

Treasurer
Donald R. Scifres
Spectra Diode Labs, Inc.
80 Rose Orchard Way
San Jose, CA 95134-1356

LEOS Technical Commitee Chairman
Larry Coldren
Dept. of Electrical Engineering
University of California, Room 4152
Santa Barbara, CA 93106

Secretary & Publicity Chairman
Russell D. Dupuis
AT&T Bell Laboratories
600 Mountain Avenue
Room MH 7C-327
Murray Hill, NJ 07974-2070

JQE Guest Editor
John E. Bowers
Dept. of Electrical Engineering
University of California
Room 3151
Santa Barbara, CA 93106

LOCAL ARRANGEMENTS COMMITTEE

James N. Walpole
Gary Evans
Donald M. Fye
Erich P. Ippen
R. Victor Jones
Robert Plastow
Dean Z. Tsang

ADVISORY GROUP

Zh. I. Alferov
Izuo Hayashi
Yasuo Nannichi
Jose E. Ripper
G.H.B. Thompson
Peter Eliseev
Hans Melchior
Tom L. Paoli
Yasuharu Suematsu
Amnon Yariv

LEOS EXECUTIVE OFFICE

LEOS Executive Officer
Robert T. Wangemann
Administrative Assistant
Kathleen Ruggeri
Conference Administrator
Wendy Rochelle

PROGRAM COMMITTEE

Bob Goodfellow, Chairman
Plessey Research Caswell Ltd.

Americas Subcommittee
T.P. Lee, Chairman
Bell Communications Research
Red Bank, NJ

Dan Botez
TRW Space & Technology
Redondo Beach, CA

P.D. Dapkus
University of Southern California
Los Angeles, CA

C.H. Henry
AT&T Bell Laboratories
Murray Hill, NJ

Z.L. Liau
M.I.T. Lincoln Laboratory
Lexington, MA

Robert Olshansky
GTE Laboratories, Inc.
Waltham, MA

Gary Evans
David Sarnoff Research Center
Princeton, NJ

M.A. Pollack
AT&T Bell Laboratories
Holmdel, NJ

Francisco Prince
Institute de Fisica, UNICAMP
Campinas, Brazil

Daniel Renner
Rockwell International Corp.
Dallas, TX

A.J. SpringThorpe
Bell Northern Research
Ottawa, Canada

William Streifer
Spectra Diode Laboratories
San Jose, CA

Kerry Vahala
California Institute of
Technology
Pasadena, CA

Asia & Australia Subcommittee
Michiharu Nakamura, Chairman
Hitachi, Ltd
Tokyo, Japan

Kenichi Iga
Tokyo Institute of Technology
Yokohama, Japan

Tetsuhiko Ikegami
NTT
Kanagawa, Japan

Takeshi Kamiya
Universitiy of Tokyo
Tokyo, Japan

Roy Lang
NEC Corporation
Kawasaki, Japan

Hirofumi Namizaki
Mitsubishi Electric Corporation
Hyogo, Japan

Yutaka Uematsu
Toshiba Corporation
Kawasaki, Japan

Qi Ming Wang
Academia Sinica
Beijing, China

Shigenobu Yamakoshi
Fujitsju Labs. Ltd.
Kanagawa, Japan

European Subcommittee
B. DeCremoux, Chairman
Thomsom-CSF/LSR
Orsay Cedex, France

G.A. Acket
Philips Research Labs
Eindhoven, Netherlands

M.-C. Amann
Siemens AG
Munich, F.R. Germany

J.-C. Bouley
CNET
Paris, France

J. Buus
Plessey Research Caswell Ltd.
Caswell, United Kingdom

S.A. Gurevich
USSR Academy of Sciences
Leningrad, USSR

P. Kirkby
Standard Telecommunications Laboratory
United Kingdom

Paul E. Lagasse
Universite of Ghent
Ghent, Belgium

Manfred H. Pilkuhn
Universität Stuttgart
Stuttgart, F.R. Germany

CONTENTS

MONDAY MORNING, AUGUST 29, 1988

Monday, August 29, 1988

MONDAY AFTERNOON, AUGUST 29, 1988

Session C: Quantum Wells I

Monday, August 29, 1988

Session D: High Speed Modulation

TUESDAY MORNING, AUGUST 30, 1988

Session E: Visible and Infrared

Tuesday, August 30, 1988

Session F: Quantum Wells II

Tuesday, August 30, 1988

Session G: Mode Locking and Fast Switching

TUESDAY AFTERNOON, AUGUST 30, 1988

Session H: Single Mode DFB & DBR Devices II

Tuesday, August 30, 1988

Session I: Grating Laser Dynamics & Stabilization

WEDNESDAY MORNING, AUGUST 31, 1988

Session J: Tunable Lasers

WEDNESDAY MORNING, AUGUST 31, 1988

Session K: Stabilization, Noise and Bistability

WEDNEDSAY AFTERNOON, AUGUST 31, 1988

Session L: High Power Fabry-Perot Lasers

THURSDAY MORNING, SEPTEMBER 1, 1988

Session N: Surface Emitters and Integration

Thursday, September 1, 1988

Session O: Four-Wave Mixing and Nonlinear Gain

Session P: Quantum Wells III

THURSDAY AFTERNOON, September 1, 1988

Session Q: Linewidth and Chirp Reduction

Thursday, September 1, 1988

Session R: Electrical Properties & Design

MONDAY, August 29, 1988

Session A: Single Mode DFB & DBR Devices I

A—1

Extremely Low Threshold InGaAsP/InP DFB PPIBH Laser Diode

Y.Ohkura,A.Takemoto,N.Yoshida,K.Isshiki,
S.Kakimoto,H.Namizaki,and W.Susaki
LSI R&D Laboratory, MITSUBISHI Electric Corporation
4-1 Mizuhara, Itami, Hyogo 664, Japan

We report on an extremely low threshold InGaAsP/InP DFB laser realized by an MOCVD/LPE hybrid process.

Very low threshold lasers play an important role in reduction of consumption of electricity and they can be modulated at high speed without bias currents[1]. However, satisfactorily low threshold InGaAsP/InP DFB lasers had not been realized, because most lasers have been fabricated by LPE which is difficult to control thickness of layers and can not preserve corrugation sufficiently. MOCVD is suited to overcome these problems. We have successfully fabricated extremely low threshold InGaAsP/InP DFB lasers with the PPIBH structure[2] by the MOCVD/LPE hybrid process.

To realize a very low threshold current and stable single longitudinal mode (SLM) laser, we make the cavity length (L) short and the coupling coefficient (κ) large, since the internal absorption loss is reduced with the cavity length, and the larger κ is necessary for shorter cavity length to achieve a stable SLM operation. Figure 1 shows a schematic drawing of the DFB-PPIBH laser fabricated by the MOCVD/LPE hybrid process. We use the MOCVD technique for the formation of double hetero-junction and the overgrowth on corrugation, because it has excellent abilities to control layer thickness and to preserve corrugation. We designed cavity length (L) and coupling coefficient (κ) as 150μm and 100cm^{-1}, respectively. Corrugation was formed of about 70nm height to have large coupling coefficient κ (100cm^{-1}).

Figure 2 shows the light-output/current characteristic of the device. A CW threshold current of 3.1mA and sidemode suppression ratio more than 35dB was achieved at R.T. This threshold value is the lowest so far as we know among InGaAsP/InP lasers including conventional Fabry-Perot type devices. These excellent properties are attributed to adequate device parameters ($L=150\mu m, \kappa L=1.5$) for both reduction of threshold current and stable SLM operation, and the high current confinement effect of PPIBH structure.

This extremely low threshold DFB laser has excellent modulation properties with no bias current. The responses and the lasing spectrum under 1 Gbit/sec RZ pseudo-randam modulation with zero bias condition are shown in Fig.3. The result suggests a potential of the high bit rate,long distance transmission without using bias current.

References 1. M.Nakamura et al.,Electron.Lett. 23, 1352 (1987)
2. A.Takemoto et al.,Electron.Lett. 23, 546 (1987)

88CH2609-8/88/0000/0002$1.00 1988IEEE

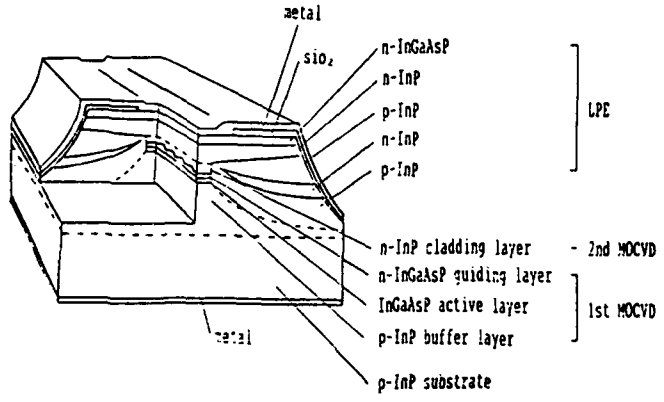

Fig.1 Schematic drawing of the DFB-PPIBH laser diode

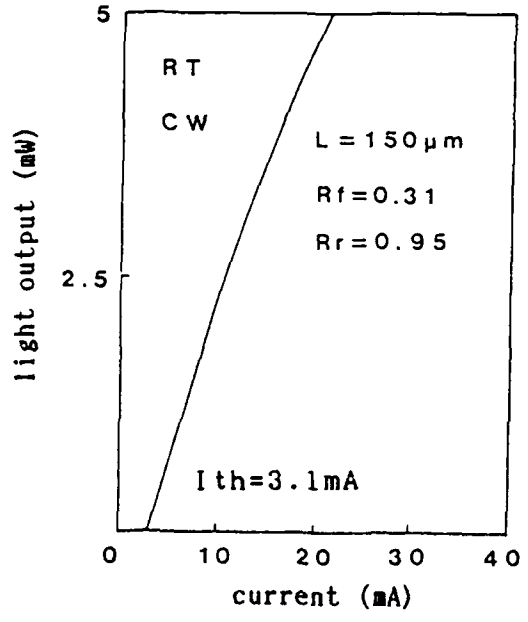

Fig.2 Light output versus current characteristic

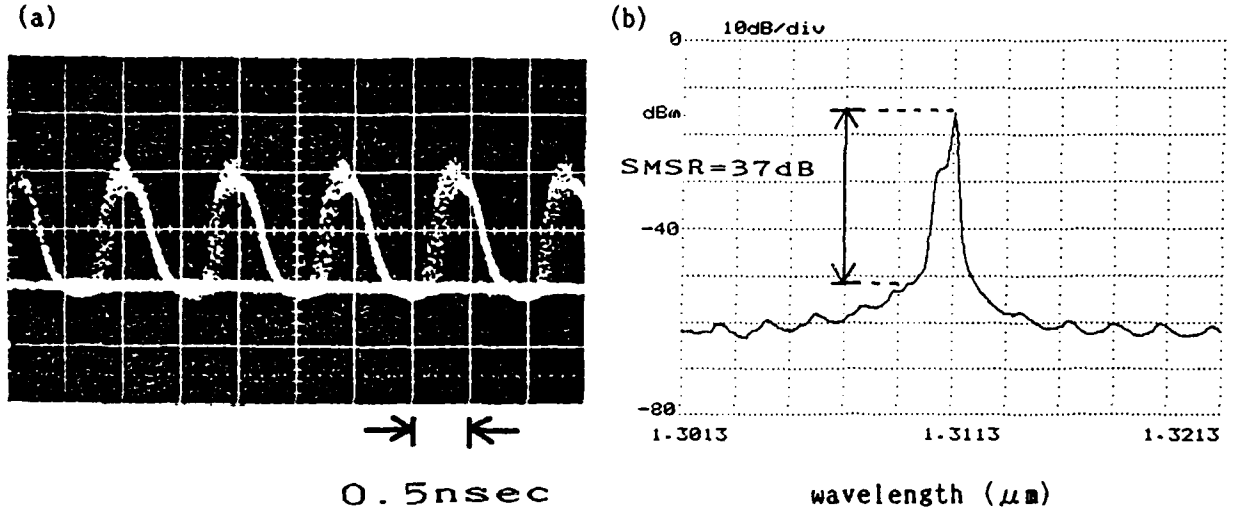

Fig.3 (a)responses and (b)lasing spectrum under 1 Gbit/sec RZ pseudo-random modulation with zero bias level

A—2

Ultra Low Threshold, High Bandwidth, Very Low Noise Operation of 1.52 μm GaInAsP/InP DFB - Buried Ridge Structure Laser Diodes Entirely Grown by MOCVD

M.KRAKOWSKI, D.RONDI, A.TALNEAU, Y.COMBEMALE, F.DEBORGIES, P.MAILLOT, P.RICHIN, R.BLONDEAU and B. de CREMOUX
Central Research Laboratory, THOMSON-CSF
Domaine de Corbeville, BP.10, 91401 ORSAY CEDEX, FRANCE

We have shown previously that low pressure metalorganic chemical vapor deposition (LP-MOCVD) is very promising for production of GaInAsP/InP distributed feedback (DFB) lasers with the ridge waveguide structure developed by Kaminow [1]. Few results have been reported on DFB lasers grown entirely by MOCVD, specially in the high frequency field.

Realization : Fig.1 shows the schematic diagram of DFB-BRS-LD. The first epitaxy consists of the growth of three layers on a Sn doped InP substrate : a 2 μm thick InP(N) confinement layer, a 0.2 μm thick undoped GaInAsP active layer (λ ~ 1.52 μm) and a 0.15 μm thick undoped GaInAsP guiding layer (λ ~ 1.3 μm). A second order grating with a period of 4670 Å and a depth of 750 Å is realized by holography on the guiding layer. The active strip, about 1.3 μm wide, is delineated by chemical etching. Next, a second epitaxy comprising a 1.5 μm thick InP(P) confinement layer and a 0.4 μm thick GaInAs(P^+) contact layer is realized. Then, ohmic contacts and deep proton implantation are achieved. 150 μm long lasers are mounted epi-side up on alumina.

Experimental results : Fig.2 shows a light-current characteristic of a DFB-BRS laser under CW operation. The best threshold current is 5 mA, which we suppose to be the lowest reported for DFB lasers, the average being 7 mA. The external differential quantum efficiency and series resistance are respectively 16 %/facet and 6 Ω. Side mode suppression ratio is 30 dB.

Fig.3 shows modulation characteristics of a DFB-BRS-LD (I_{th} = 7 mA) mounted in an optical module at 3 different polarization currents. Measurements were done with a 12 GHz bandwidth GaInAs PIN photodiode made in our laboratory. The modulation current is 4.5 mA peak to peak. At only 3 mA above threshold (modulation depth m of 75 %) the - 3 dB bandwidth B is 2.9 GHz. At 25 mA a little dip in the response due to parasitics of the package limits B at 6.4 GHz but a higher -3 dB point is obtained at 9.6 GHz which is supposed to be the real bandwidth of the laser. The evolution of bandwidth with the square root of emitted power from one facet is important : 9.6 GHz/$\sqrt{}$ mW between 10 mA and 25 mA. This is partly due to the detuning of the Bragg wavelength to the high energy side of the gain spectrum.

We calculated the relative intensity noise (RIN) of the DFB-BRS-LD from the measurements of the mean detector current and of the noise power by a spectrum analyser using amplifiers in the C band (4-8 GHz). Fig.4 shows the variation of the RIN with the pumping rate (I/I_{th}) at 4 GHz (low side of the resonance frequency) and 8 GHz (high side). At 4 GHz and 25 mA injection current we obtained a RIN of 4.2 10^{-16} s (- 154 dB/Hz). This figure is, to our knowledge, the lowest reported in this frequency range for a semiconductor laser and close to other best reported figures.

The DFB-BRS-LD fabricated by two steps MOCVD are usefull for R.F. optical systems.

Reference

[1] M.Razeghi, R.Blondeau, K.Kazmierski, M.Krakowski and B. de Cremoux "CW operation of 1.57 μm GaInAsP/InP distributed feedback lasers grown by low pressure metalorganic chemical vapor deposition" Appl. Phys. Lett., vol.45, n°7, Oct.1, 1984.

88CH2609-8/88/0000/0004$1.00 1988IEEE

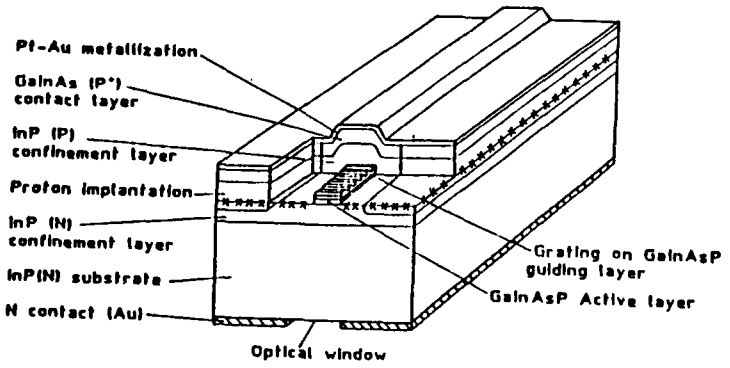

Fig.1 - Schematic diagram of DFB - buried ridge structure laser diode.

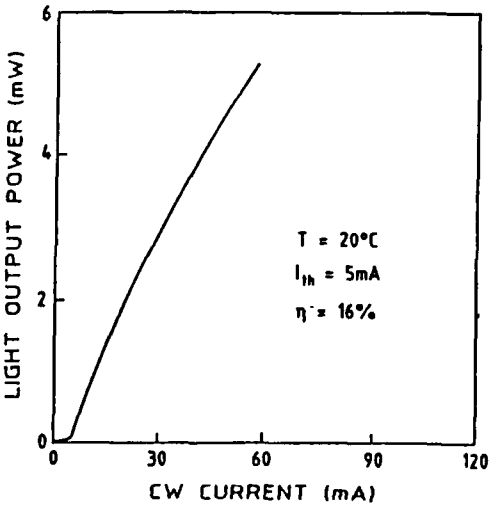

Fig.2 - CW light-current characteristic of DFB-BRS-LD at 20°C.

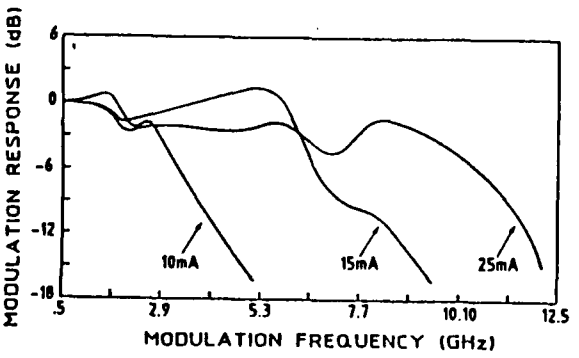

Fig.3 - Frequency responses of DFB-BRS-LD.

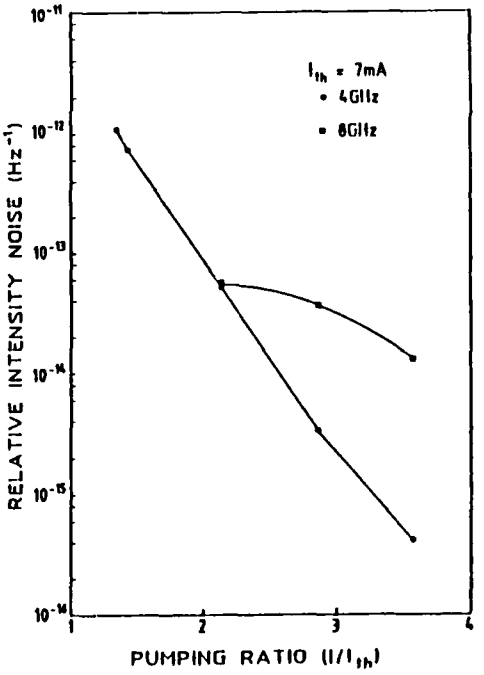

Fig.4 - RIN versus injection current of DFB-BRS-LD.

A—3

InGaAs/InGaAsP Multiple Quantum Well Distributed Feedback Lasers

U. Koren, B.I. Miller,T.L. Koch, K.-Y. Liou, G. Eisenstein , A. Shahar
AT&T Bell laboratories, Holmdel ,New Jersey, 07733

Multiple quantum well lasers have been reported extensively in the GaAs/GaAlAs material system. As optical fibers have a loss minimum at 1.55 micron wavelength, there is a strong motivation to develop quantum well devices in this wavelength range for the specific requirements of lightwave communication systems.

In the present paper we describe 1.5 micron wavelength InGaAs/InGaAsP quantum well (QW) distributed feedback (DFB) lasers grown entirely by atmospheric pressure metal organic vapor phase deposition (MOCVD) . Although QW - DFB lasers have been reported previously [1], the use of liquid phase epitaxy (LPE) limited the thicnesses and sharpness of the QW's. Here, the use of MOCVD permitted the growth of very narrow QW's with abrupt monoatomic interfaces [2].

InGaAs/InGaAsP Fabry-Perot seperate confinement heterostructure (SCH) QW lasers with cleaved mirrors have been shown to operate well [3] when the number of quantum wells was four or higher. In the present case, due to the large feedback provided by the DFB gratings, the number of quantum wells has been reduced to three. The longitudinal cross section of the device is shown in Fig. 1. The lateral structure was the semi-insulating blocked planar BH laser (SIPBH) configuration described previously [4]. The lasers have threshold currents of 20-30 ma with cavity length of 300-700 microns. Some devices operated in a single longitudinal mode at up to 10 mW CW output power. We have measured the linewidth of these devices using both Fabry-Perot and delayed self heterodyne techniques. Typical linewidth as a function of output power is shown in Fig. 2.

We have also fabricated a tunable phase shifted DFB laser by an addition of an intracavity passive QW phase modulator section as shown in Fig. 3. By adjusting the voltage on the phase modulator section every device could be operated with a single longitudinal mode and switching between single or double DFB mode operation was possible. Under single mode operation , small signal voltage modulation of the modulator section results in fast modulation of the effective refractive index due to the quantum confined electrooptic effect. The resulting FM modulation response of the laser diode as a function of frequency is shown in Fig 4.

REFERENCES

1. N.K. Dutta, S.G. Napholtz, A.B. Piccirilly, G. Przybylek. Appl.Phys. Lett. 48, 1419 (1986).

88CH2609-8/88/0000/0006$1.00 1988IEEE

2. B.I. Miller, E.F. Schubert, U. Koren, A. Ourmazd, A. Dayem, R.J. Capik. Appl. Phys.Lett. 49, 1384, (1986).
3. U. Koren, B.I. Miller, Y.K. Su, T.L. Koch, J.E. Bowers, Appl. Phys. Lett. 51, 1746, (1987).
4. U. Koren, B.I. Miller, G. Eisenstein R.S.Tucker, G. Raybon, R.J. Capik. Electron. Lett. 24, 138, (1988).

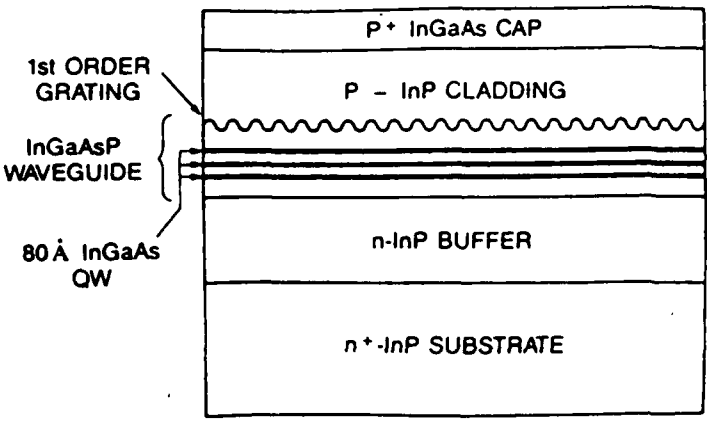

Fig.1. Schematic structure of the QW-DFB laser

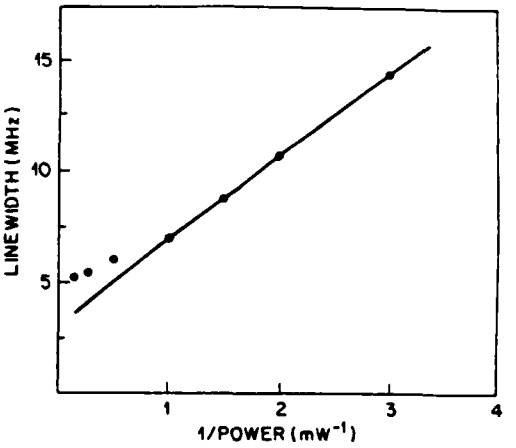

Fig. 2. Linewidth vs. output power

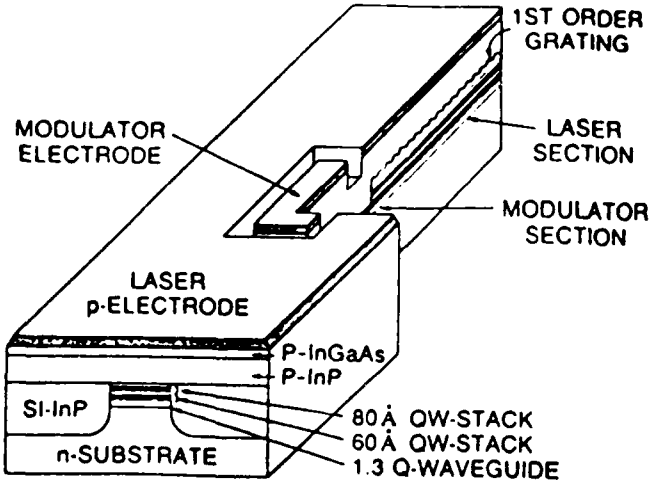

Fig.3. Schematic structure of a DFB laser with an integrated QW phase modulator

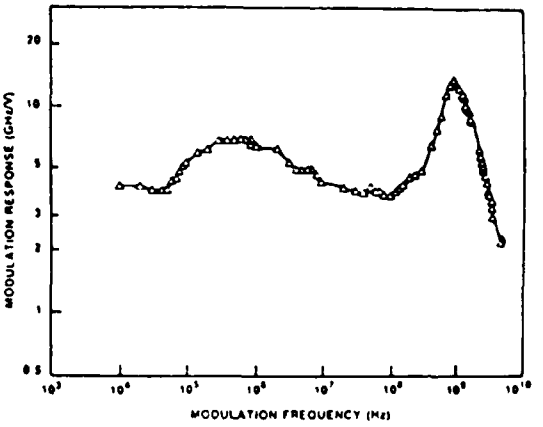

Fig. 4. FM modulation response.

A—4

DFB Lasers with a Crescent-Shaped Active Layer on a Corrugated p-type Substrate

Y. Ogawa, H. Horikawa, H. Wada, Y. Kawai, and M. Sakuta
Research Laboratory, OKI Electric Industry Co., Ltd.
550-5 Higashiasakawa, Hachioji, Tokyo 193

A high power DFB laser with a crescent-shaped active layer on a corrugated p-type substrate is reported: A maximum CW power of 70mW has been achieved and the sub-mode suppression ratio in single DFB mode operation ($<$ 10 mW) was 30 dB.

The basic structure, except for the corrugation, of the DFB laser is similar to a conventional Fabry-Perot VIPS-LD structure which takes advantage of a low leakage current to achieve high output power ($>$200mW) operation.[1] However, it has hardly been possible to introduce a corrugated structure into the VIPS-LD structure. We have, therefore, proposed a novel fabrication technique to overcome this difficulty and have confirmed that the laser operated under DFB mode.

Figure 1 shows a schematic diagram of the fabrication process. A first order grating was formed on a p-type InP substrate using conventional holographic lithography. A SiO_2 stripe film with a width of approximately 1.5 μm was then formed on the corrugated substrate to act as a mask for selective growth. Current blocking layers, an n-InP layer (0.5~1.0 μm thick) and a p-InP layer (1.0~1.5 μm thick), were then grown on the substrate outside of the SiO_2 mask by liquid phase epitaxy (LPE). Next, after removing the stripe mask with HF, a second stage of LPE was performed: a waveguide layer (λ_g=1.1 μm), a crescent-shaped active layer (λ_g=1.31 μm), an n-InP cladding layer and an n-GaInAsP contact layer were grown. After contact metallization, the wafer was cleaved into 300 μm-long cavity chips. The front facet was coated with an Al_2O_3 film with 5% reflectivity.

Figure 2 shows the L-I and dL/dI characteristics under CW operation at 20 ℃ for driving currents less than 60mA. A high slope efficiency of 0.36 W/A was obtained with a threshold current (I_{th}) of 27 mA. The lasing spectrum of the laser operating at 40mA (5mW output power) is shown in Fig. 3. These data show that this laser operated at 1.32 μm wavelength in a single DFB mode with a sub-mode suppression ratio of 30 dB.

Figure 4 shows the high output power operation characteristics with a maximum CW power as high as 70mW at a driving current of 400mA.
The driving current at which the output power saturated was higher than that of a conventional buried heterostructure(BH) DFB laser with the same chip size, slope efficiency, and I_{th}. This may be due to a lower leakage current in the new laser compared to that of the BH-DFB laser. Thus, the DFB lasers with a crescent-shaped active layer are thought to be preferable for high power use, although we have as yet only obtained the single DFB mode up to 10 mW. Above this output power level, the higher order DFB mode and/or TM mode began to oscillate. Single mode operation at higher power levels is expected by optimizing the parameters which control the mode: thicknesses of the waveguide and active layers, and the κL.

88CH2609-8/88/0000/0008$1.00 1988IEEE

1) S. Oshiba et al, J. Quantum Electronics, QE-23 (1987) 738

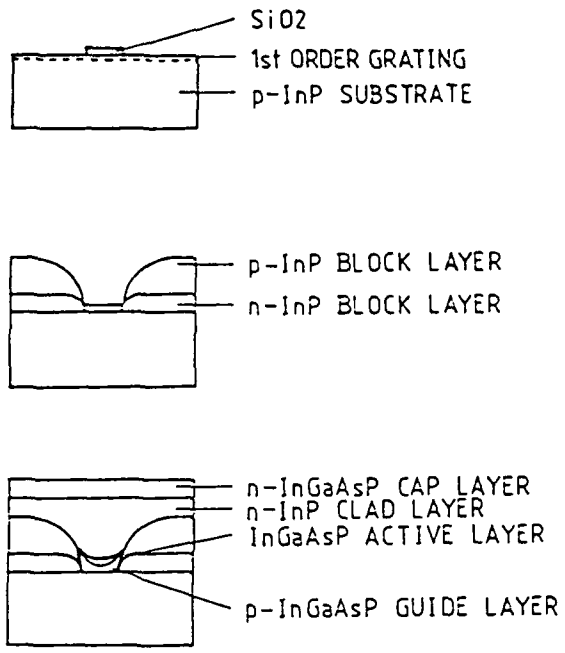

Fig. 1. schematic diagram of the fabrication process

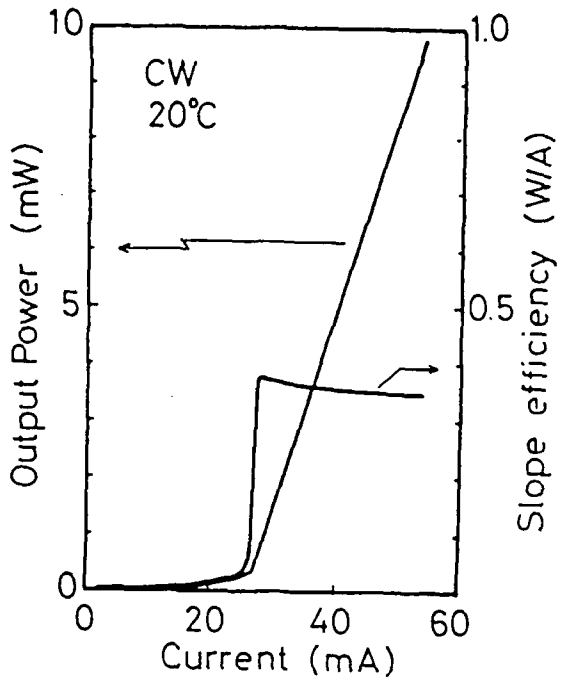

Fig. 2. L-I and dL/dI characteristics (CW, 20℃)

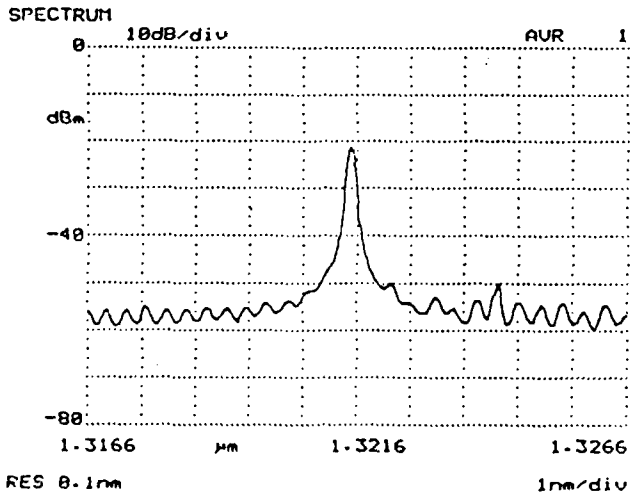

Fig. 3. spectrum of the laser operating at 40mA

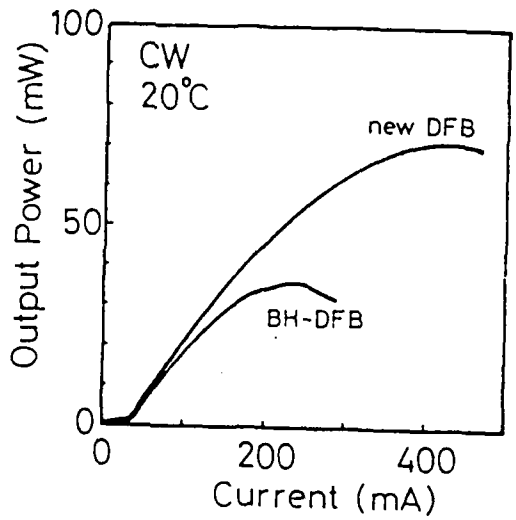

Fig. 4. high power operation characteristics (CW, 20℃)

A—5

1.5 μm GaInAsP/InP Distributed Reflector (DR) Dynamic Single-Mode (DSM) Lasers

K. Komori, S. Pellegrino, S. Arai, and Y. Suematsu

Department of Physical Electronics
Tokyo Institute of Technology
2-12-1 O-okayama, Meguro-ku, Tokyo 152, Japan

Dynamic Single mode (DSM) laser[1] with high efficiency and high power operation are very attractive light sources not only for long haul, high-bit rate optical communication systems but also for photonic integration. A phase-adjusted structure have been developed in DFB type lasers to realize superior properties of DSM operations and AR-HR coating[2] was adopted to improve the output efficiency of DSM operations, however it is unsuitable for monolithic integration or batch process for mass-production.

To solve these problems we propose a distributed reflector (DR) structure, in which the passive distributed reflector is used at one side of a active distributed reflector instead of the high reflection coating on the facet. We realized the DR laser by using the Bundle-Integraged-Guide (BIG) structure[3] for the first time, and obtained superior lasing properties, such as a low threshold current density, a high side-mode suppression ratio, and so on.

The schematic structure of the BIG-DR laser is shown in Fig. 1. In the fabrication, recently developed island-type mesa process[4] was used in order to obtain flat growth condition for waveguide over the active and passive regions. The corrugation was formed on the entire surface of waveguide. The active region width of buried heterostructure was 3 μ m.

Figure 2 shows a typical I-L curve and lasing spectra at various current levels. The output power of 7mW and the front to rear output power ratio of 1.6:1 were obtained. As can be seen in the right side of Fig. 2, the side-mode suppression ratio (SMSR) reached to quite a high value of 38dB at the output power level of 6mW ($I=3I_{th}$).

Figure 3 shows the temperature dependences of the threshold current and the lasing wavelength of another sample. The lowest CW threshold current of 25mA (threshold current denstity J_{th} was about 2KA/cm^2) and the front to rear power ratio of 2.1:1 were obtained. The temperature coefficient of the lasing wavelenth and the characteristic temperature of threshold current T_0 were 0.1nm/deg and 53K at $I=1.2I_{th}$, respectively. A fixed single-mode temperature range of larger than 55degrees was obtained, which indicates that this laser is operating in DR mode rather than DBR mode.

88CH2609-8/88/0000/0010$1.00 1988IEEE

In this structre, it is important to adjust the propagation constants between active and passive region. The design theory will be given elsewhere [5].

The authors would like to appreciate Prof. K. Iga and Assoc. Prof. K. Furuya, Assoc. Prof. M. Asada and Dr. F. Koyama for fruitful discusions and Messers K. S. Lee, M. Aoki, I. Arima for their helps in experiments.

REFERENCES:

(1) Y.Suematsu, S.Arai, and K.Kishino; IEEE J.L.T., LT-1, pp.161-176 (Mar. 1983)
(2) M.Kitamura, M.Yamaguchi, S.Murata, I.Mito, and K.Kobayashi, Intl' conf. on Integrated optics and optical fiber Commun. (IOOC'85&ECOC'85), Venice, Italy, (Oct.1985)
(3) Y.Tohmori, K.Komori, S.Arai, and Y.Suematsu; Electron. Lett., vol.21, no.17, pp.743-745, (Aug. 1985)
(4) I.H.Choi, K.Komori, S.Arai, Y.Suematsu, K.S.Lee, M.T.Pang; Jpn. J. Appl. Phys., vol,26, No.10, pp.L1593-L1596, (Oct.1987)
(5) K.Komori, S.Arai, Y.Suematsu, M.Aoki, and I.Arima; to be published in Trans. IEIEC of Japan, (Apr. 1988)

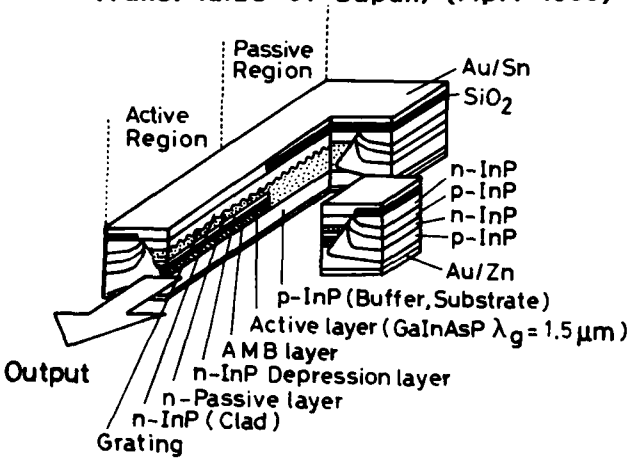

Fig.1 Structure of BH-BIG-DR lasers

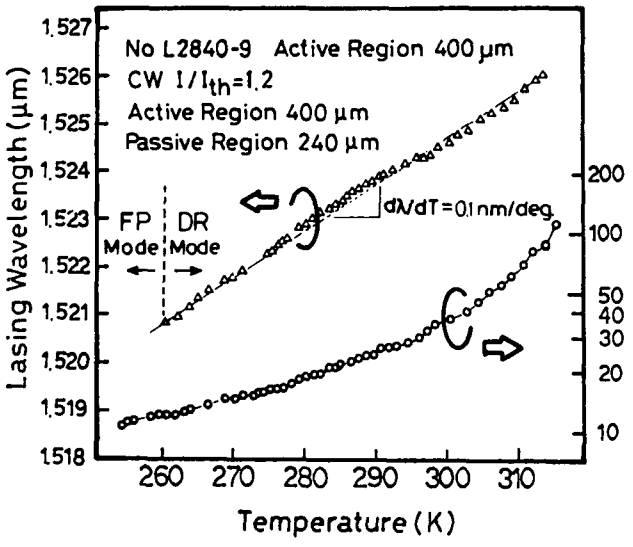

Fig.3 Temperature dependence of lasing spectrum and threshold current

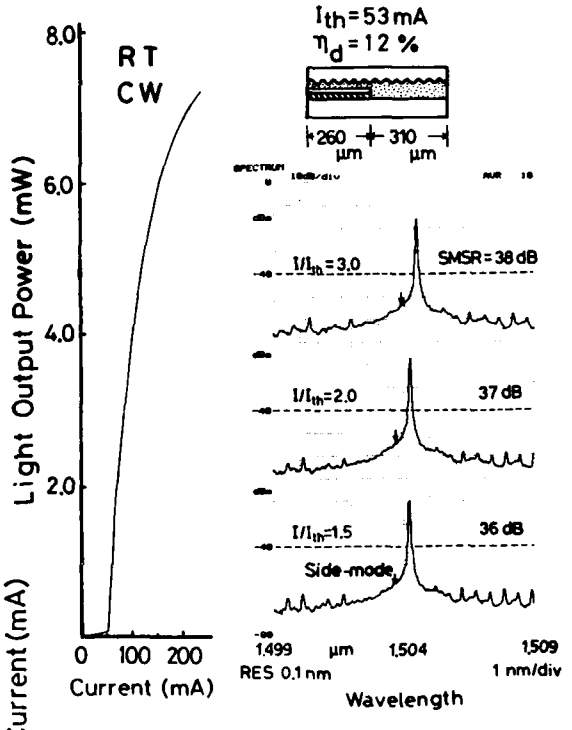

Fig.2 I-L characteristics and lasing spectrum of a BH-BIG-DR laser

A—6

DBR Laser with Non-Dynamic Plasma Grating Formed by Focused Ion Beam Implanted Dopants

M. M. Boenke, M. C. Wu and S. Wang
Department of Electrical Engineering and Computer Science, University of California, Berkeley, Berkeley, California 94720

W. M. Clark Jr., E. H. Stevens and M. W. Utlaut
Hughes Research Laboratories, Malibu, California 90265

A new type of distributed Bragg reflector (DBR) GaAlAs/GaAs laser is experimentally demonstrated in which the grating is based on a non-dynamic implementation of the plasma effect made possible by focused ion beam (FIB) implantation of dopants.

Gratings in DFB and DBR lasers are usually formed by etching the guide material at some multiple of the Bragg wavelength and regrowing over it to create a periodic change in the effective index of the waveguide. Dynamic gratings utilizing the plasma effect formed by the interference of two or more laser beams have also been used extensively.[1] An increase in excited carriers is created where the beams interfere constructively causing an increase in gain. The imaginary part of the index increases proportionately, which, through the Kramers-Kronig relation causes a decrease in the real part of the index. The recent development of FIB technology has made new fabrication techniques possible such as submicron ion implantation patterning,[2] disordering of superlattice material to form laser waveguides[3] and micromachining of semiconductor laser mirrors.[4]

In the FIB-DBR laser presented here, the fine resolution capability of the FIB is used to write 1000Å stripes of dopants at twice the Bragg wavelength. The carriers tend to diffuse away from areas of higher dopant concentration, uncovering space charge and creating fields which oppose this diffusion current. This results in a fluctuation in the carrier density similar to that formed in a dynamic plasma grating. Simultaneous solution of Poisson's equation and charge continuity has been carried out to find the steady state carrier distribution. Figure 1a shows this distribution for a Si^{++} implant in GaAs at 100KeV annealed at 950°C for 2.5 seconds. The concentration across the peaks of these implants is shown in Figure 1b.

The FIB-DBR structure is shown in Figure 2. Part of a large optical cavity GaAlAs/GaAs ridge laser is etched down to the guiding layer to form a passive cavity. Stripes of Si^{++} are implanted across the passive waveguide spaced by .2288Å. Single mode operation was observed from 20°C to 40°C as shown in Figure 3. A characteristic shift of about .8Å/°C is observed in the DBR mode. Also, directional surface emission, as expected from second order gratings, is shown in Figure 4.

FIB gratings offer new flexibility in semiconductor laser fabrication. They are not limited to parallel lines as are, for example, holographically exposed gratings. Curved or chirped gratings are possible simply by reprogramming the controlling computer. They could be buried under an active waveguide without exposing the wafer to masking materials or atmosphere in an MBE or CBE machine with FIB attached, resulting in cleaner wafers and more reliable devices. Also, due to their localized nature, they are ideal as components in integrated optoelectronic devices as on-chip or off-chip couplers. FIB gratings represent an effective application of the fine resolution available with this new technology to semiconductor laser fabrication.

—

1. A. Miller, D. A. B. Miller, and S. D. Smith, *Advances in Physics*, 30(6):697, 1981.
2. D. B. Rensch, D. S. Mathews, M. W. Utlaut, M. D. Courtney, and W. M. Clark, Jr., *IEEE Trans. Elect. Dev.*, **ED-34**(11):2232, 1987
3. K. Ishida, K. Matsui, T. Fukunaga, J. Kobayashi, T. Morita, E. Miyauchi, and H. Nakashima, *Appl. Phys. Lett.*, **51**(2):109, 1987
4. R. K. DeFreez, J. Puretz, R. A. Elliott, J. Orloff, and L. W. Swanson, *Elect. Lett.*, 22(17):919, 1986

88CH2609-8/88/0000/0012$1.00 1988IEEE

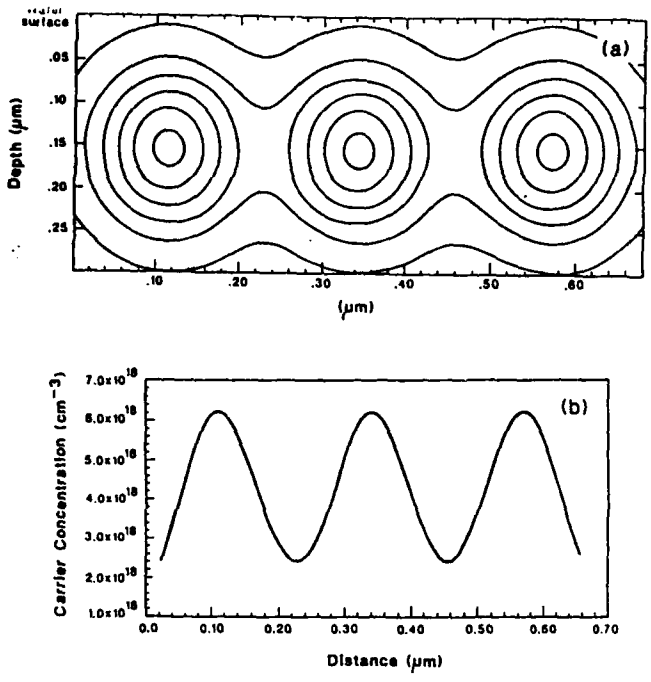

Figure 1 a) Computer simulation of the FIB-implanted stripes of Si in GaAs after a 950°C 2.5 second anneal. Contours of constant carrier concentration decrease in steps of 1×10^{18} cm^{-3} from peaks of 6.3×10^{18} cm^{-3}. b) Free carrier concentration plotted across the peaks of figure 1a at a depth of .154 μm.

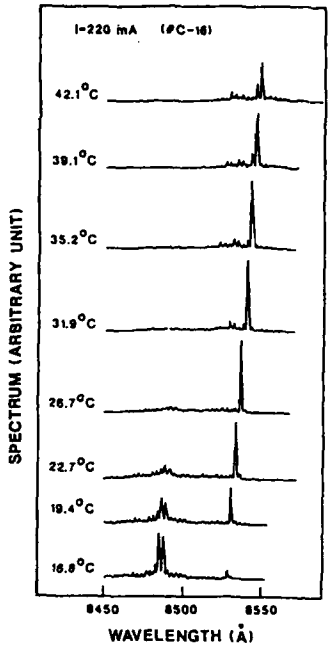

Figure 3 Spectra of the FIB-DBR as a function of temperature. Good side mode suppression is observed from 20°C to 40°C. The DBR mode shifts by .8Å/°C.

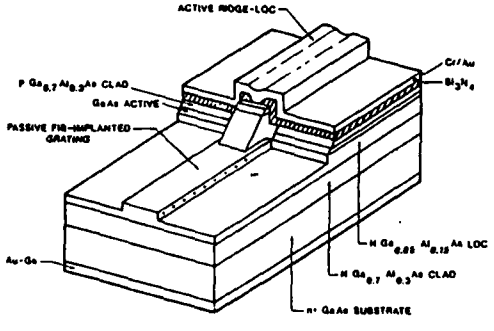

Figure 2 Schematic diagram of the FIB-DBR. The active region is a large optical cavity buried heterostructure ridge waveguide. The passive section is etched down to the waveguide below the active region so that the FIB grating can be directly implanted into the waveguide.

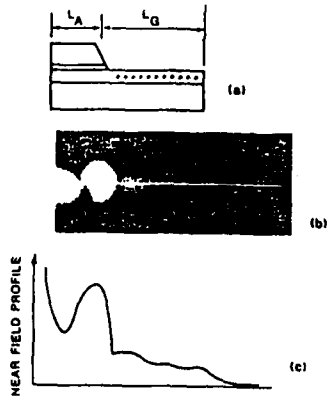

Figure 4 Surface light emission of the FIB-DBR. a) Schematic cross section to scale with measurements. b) Streak camera picture of near field. c) Intensity profile along center of guide. As expected, peaks of intensity are seen at each facet and at the cavity interface; of interest is the light observed above the grating region which falls off roughly exponentially.

A—7

Nanosecond Wavelength Selection with 10-dB Net Gain in a Subthreshold DFB Laser Amplifier

E.L. Goldstein, H. Kobrinski, M.P. Vecchi, and R.M. Bulley

Bell Communications Research, Morristown, New Jersey 07960

We report the first demonstration to date of wavelength selection at GHz rates by operating a subthreshold DFB laser as an injection-current-tunable, amplifying, wavelength demultiplexer.

Multiwavelength optical network proposals increasingly require both tunable sources and tunable filters that can select among tens or hundreds of incident wavelength-multiplexed channels. Coherent detection can be used for the latter task, as can electromechanically tuned fiber [1] and bulk [2] resonators. Alternatively, one can obtain very rapidly tunable filtering by exploiting resonant amplification in DFB structures biased below threshold. Recent experiments with such devices have generated measurements of static selectivity [3,4], gain [5,6], and tuning range [7]. However, the dynamic properties have not been explored. We here report fast-tuning experiments that demonstrate injection-current tuning times of 1 ns, dynamic tunability exceeding 0.1 nm/mA, and noise sufficiently low to yield error rates $< 10^{-9}$ at 1 Gb/s in the amplified, demultiplexed signal.

Experiments were performed on a commercially available 1.5μm BH DFB with a first-order grating incorporating no $\lambda/4$-shift, an AR-coated input facet, and a cleaved, uncoated output facet. The device was placed in the experimental arrangement of Fig. 1 and was excited using similar DFB sources.

Fast-tuning behavior was studied by adding to the device's $0.96I_{th}$ bias current a tuning-current squarewave $\Delta I_a = 1.2$ mA peak-to-peak, producing two resonant amplifier wavelengths separated by $\Delta\lambda = 0.23$ nm. The incident signal from TX A was modulated at 1 Gb/s and temperature-tuned to match one of the amplifier's two resonant wavelengths. Figure 2(a) shows the risetime of the amplifier tuning current; Fig. 2(b) shows the risetime of the resulting optical signal detected by the fast APD receiver. As shown, the time required for the amplifier to select the desired wavelength is ≈ 1 ns, in agreement with expectations based on the carrier lifetime.

To verify that fast wavelength-selective amplification can be performed without incurring intolerable noise penalties, TX A and TX B, temperature tuned to yield $\Delta\lambda = 0.23$ nm, were intensity-modulated with the fixed binary patterns of Fig. 3(a), and the DFB amplifier was current-tuned with the indicated 20-ns squarewave. The receiver output (Fig. 3(b)) yielded error rates $< 10^{-9}$, showing that tuning the amplifier during a single bit period resulted in no loss of pattern integrity.

In addition to the dynamic properties described above, static selectivity, gain, and tunability were measured using lock-in detection to remove the amplified-spontaneous-emission background. Minimum channel-separation, determined by crosstalk, was measured with the sources pseudorandom-modulated at 1 Gb/s and with the DFB amplifier current adjusted to yield resonant amplification of TX B. The interfering source, TX A, was slowly temperature-tuned while monitoring the error rate of the selected, amplified channel B. Figure 4 shows error rate as a function of channel separation and crosstalk for amplifier output power $P_{out} = -26$ dBm. As shown, $\Delta\lambda > 0.2$ nm sufficed to produce error rates $< 10^{-9}$. Static net gain as a function of incident TX B wavelength is shown for various amplifier bias-current settings in Fig. 5. Net gain, measured by comparing amplifier input power and output power with the optical interference filter removed, includes total input and output coupling losses of 3.8 ± 0.5 dB. The results, summarized in Fig. 6, show static tuning at a rate of 0.17 nm/mA with a 3-dB optical bandwidth of 0.1-0.2 nm and a maximum net gain > 10 dB.

In conclusion, we have measured nanosecond wavelength-selection times in current-tuned DFB optical amplifiers with net gain > 10 dB and dynamic wavelength selectivity better than 0.2 nm for 1 Gb/s data channels. Additional device properties and their system implications will be described.

References

[1] I.P. Kaminow et al., *Electron. Lett.*, vol.23, pp.1102-1103, 1987.
[2] A. Frenkel and C. Lin, *Proc. Optical Fiber Commun. Conf.* (New Orleans), 1987, paper WO3.
[3] H. Kawaguchi et al., *Appl. Phys. Lett.*, vol.50, pp.66-67, 1987.
[4] T. Numai et al., *Electron. Lett.*, vol.24, pp.236-237, 1988.
[5] H. Nakajima, in *Proc. 13th Eur. Conf. Opt. Commun.* (Helsinki), 1987, pp.121-124.
[6] H. Inoue and S. Tsuji, *Appl. Phys. Lett.*, vol.51, pp.1577-1579, 1987.
[7] K. Magari et al., *Appl. Phys. Lett.*, vol.51, pp.1974-1976, 1987.

88CH2609-8/88/0000/0014$1.00 1988IEEE

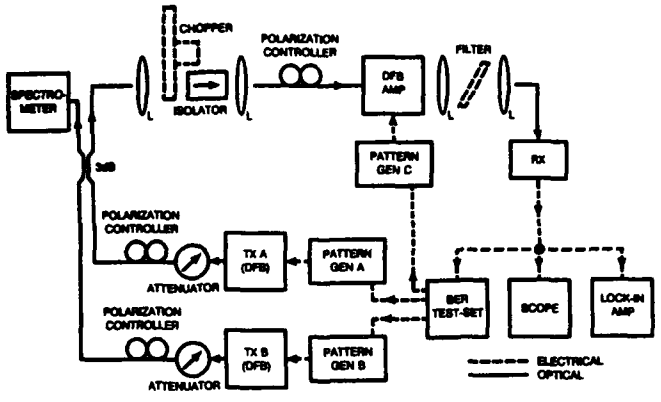

Fig.1. Experimental set-up.

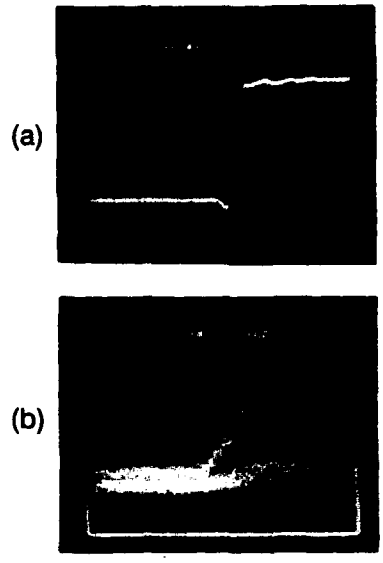

Fig.2. Wavelength-selection-time measurement. (a) DFB amplifier tuning-current waveform showing risetime < 200 ps. (b) Receiver output waveform showing wavelength-selection risetime ≈ 1 ns. Upper trace of (b) is due to marks in the incident bitstream; lower trace is due to spaces.

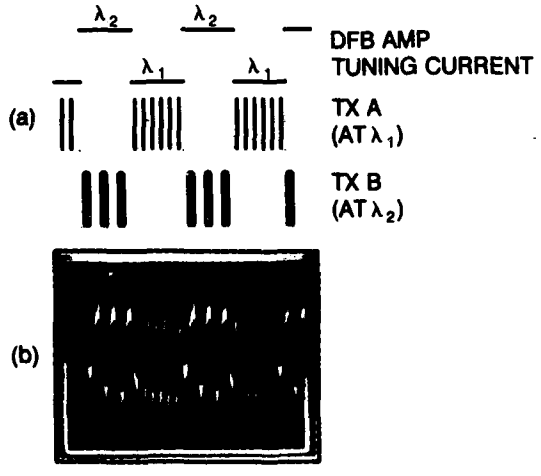

Fig.3. Modulating signals (a) and receiver output voltage (b) showing wavelength selection at 10-ns intervals with measured error rates < 10^{-9}. Pulse duration for the TX A sequence was 0.83 ns.

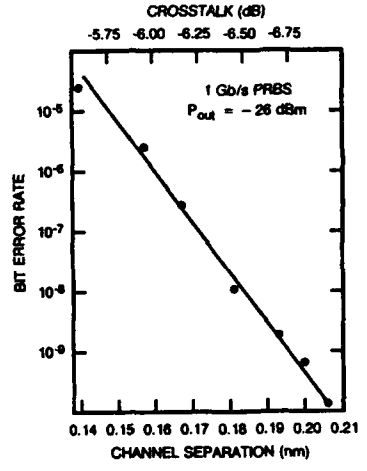

Fig.4. Measured BER vs. channel separation. Source bias points were fixed such that amplifier output power $P_{out} = -26$ dBm when tuned individually to TX A and TX B.

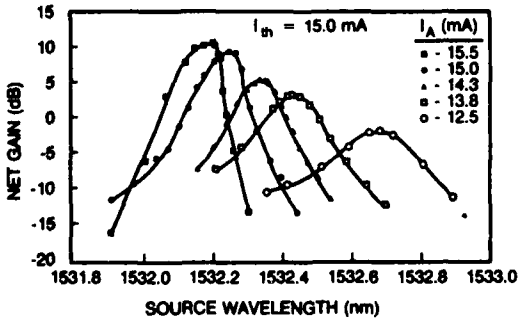

Fig.5. Measured net optical gain vs. incident wavelength under static tuning conditions.

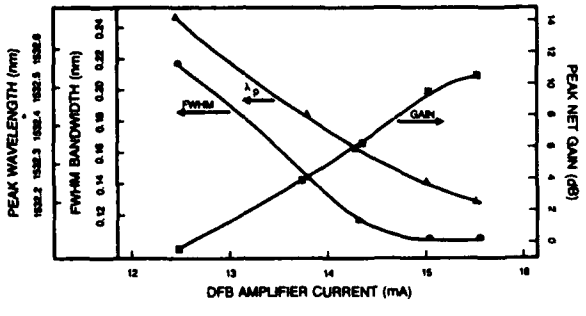

Fig.6. Summary of measured dc tunability, selectivity, and gain.

Session B: Phase Locked Arrays

B—1

Two Solutions that Achieve High-Power ($\geq$200mW) Diffraction-Limited-Beam, Array Operation: 1) Out-of-Phase Coupled Positive Index Guides, and 2) Closely Spaced Antiguides

D. Botez, L. Mawst, T.J. Roth, P. Hayashida and G. Peterson
TRW Space & Technology Group
One Space Park, M5/1065, Redondo Beach, CA 90278

Progress in diffraction-limited arrays has been slow. The fundamental-mode beam of evanescently-coupled devices invariably broadens at powers $\gtrsim$40 mW, because of gain spatial hole burning (SHB).[1] Y-junction coupled devices,[2] while immune to gain SHB, have beams 3.5-4 times the diffraction limit due to weak coupling. Here we present two solutions for high-power, diffraction-limited operation: 1) devices operating in array modes stable against gain SHB; and 2) devices immune to gain SHB, yet strongly coupled.

High-order modes of evanescently coupled devices have been shown theoretically[1] and experimentally[3] to be stable against gain SHB. We developed two array structures (Figs. 1a & 2a) that select and maintain operation in the out-of-phase mode to high drive levels. The first device consists of 10 evanescently-coupled elements that are further coupled via X-type junctions. (The device cross-section is like that in Ref. 3.) Each X-junction is made of two Y-junctions and a short interconnecting region. When fields are in phase in two adjacent waveguides they excite the fundamental mode in the interconnecting region; which, in turn, suffers high losses at the 2nd Y-junction ($\theta > 3°$ and $\Delta n_{eff} = 7 \times 10^{-3}$). When fields are out of phase in two adjacent waveguides they excite the first-order mode in the interconnecting region; which, by virtue of its null, suffers little loss at the 2nd Y-junction. Thus an array of X-junctions strongly favors out-of-phase mode oscillation. The nearest mode (L=9) is discriminated against since its field adds in phase between elements 5 and 6 and thus it suffers losses in the central X-junction. Thresholds are ~300 mA. Diffraction-limited-beam patterns are maintained to ~3 x threshold and 230 mW total power (Fig. 1b). The beam lobewidths remain under 1.5 x diffraction limit to 6.3 x threshold and 300 mW total power.

The 2nd device is a 9/10-element array of large-optical-cavity (LOC) lasers fabricated by a two-step MOCVD growth. Strong index-guiding ($\Delta n_{eff} = 10^{-2}$) is accomplished by periodically varying the thickness of an $Al_{0.2}Ga_{0.8}As$ guide layer above the active layer. Longitudinally the array has two (coupled) sets of noncollinear waveguides that cause strong scattering losses for fundamental lateral modes. The structure favors out-of-phase oscillation of coupled <u>first-order</u> lateral modes. Threshold currents are ~300 mA. The lateral far-field patterns (Fig. 2b) are virtually diffraction-limited to 5.3 x threshold and 145 mW/uncoated facet. For both devices single-lobe patterns can be simply obtained by using a phase-corrector coating[4] or plate.

In order to achieve a device that has both strong optical-mode confinement as well as strong interelement coupling we have developed an array of closely spaced antiguides. The structure is a 10-element uniform array fabricated by MOCVD, and LPE over channels (Fig. 3a). The effective-index profile (Fig. 3b) is composed of ten antiguides of $\sim 5 \times 10^{-2}$ index step. Lasing in the positive-index regions between antiguides is prevented due to a small confinement factor ($\Gamma \sim 0.03$) (Fig. 3c). While a single antiguide (one element of the array) has high radiation losses (~90 cm^{-1}), ten closely spaced antiguides have negligible radiation loss, since radiation is trapped between antiguides and then fed back in the antiguides. Interelement coupling is leaky-wave coupling.[5] The array modes with least field at the array edges, the fundamental and the out-of-phase modes, have negligible radiation losses (3-5 cm^{-1}). Discrimination between adjacent array modes (4-5 cm^{-1}) is much stronger than in arrays of evanescently-coupled guides. Threshold currents are ~280 mA, and the maximum cw power is 200 mW. Diffraction-limited, fundamental-mode operation is achieved to 200 mW (~166 in the fundamental mode) (Fig. 3d).

88CH2609-8/88/0000/0018$1.00 1988IEEE

In conclusion, we have developed several array types that operate diffraction-limited to powers 4-5 times higher than previously obtained from 10-element arrays.

1. G.H.B. Thompson and J.E. Whiteaway, Electron. Lett., 23, 445 (1987).
2. D.F. Welch et al, Appl. Phys. Lett., 49, 1632 (1986).
3. D. Botez et al, Appl. Phys. Lett., 52, 266 (1988).
4. D.E. Ackley, D. Botez and B. Bogner, RCA Review, 44, 625 (1983).
5. D.E. Ackley and R.W.H. Engelmann, Appl. Phys. Lett., 39, 27 (1981).

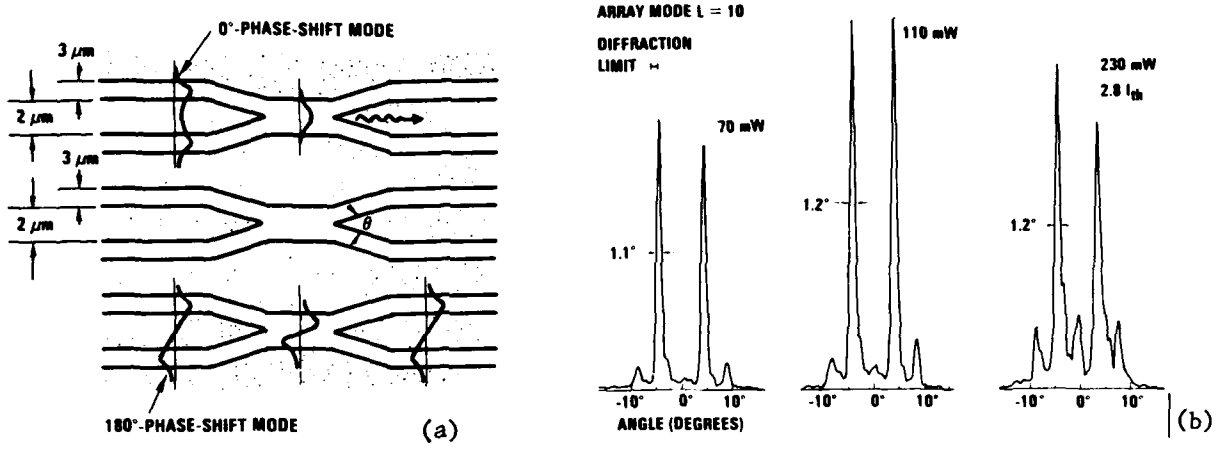

Fig. 1. X-junction array: (a) Top view; (b) Far-field patterns.

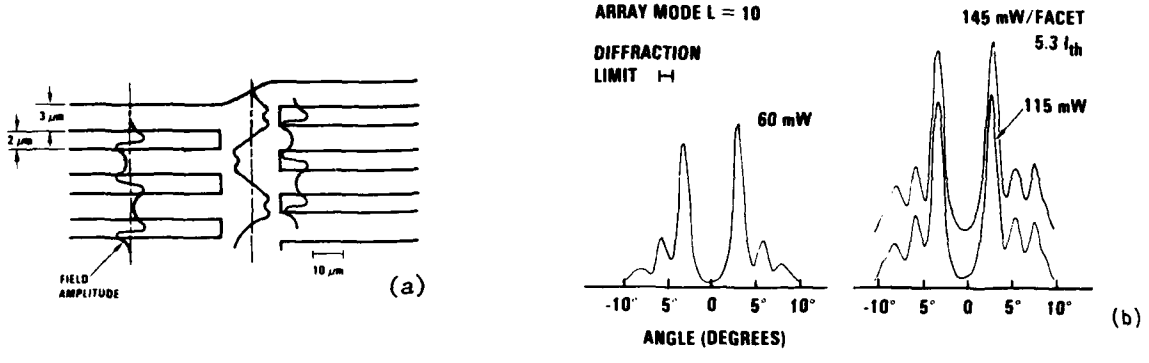

Fig. 2 Array operating in coupled first-order modes: (a) Top view; (b) far-field patterns.

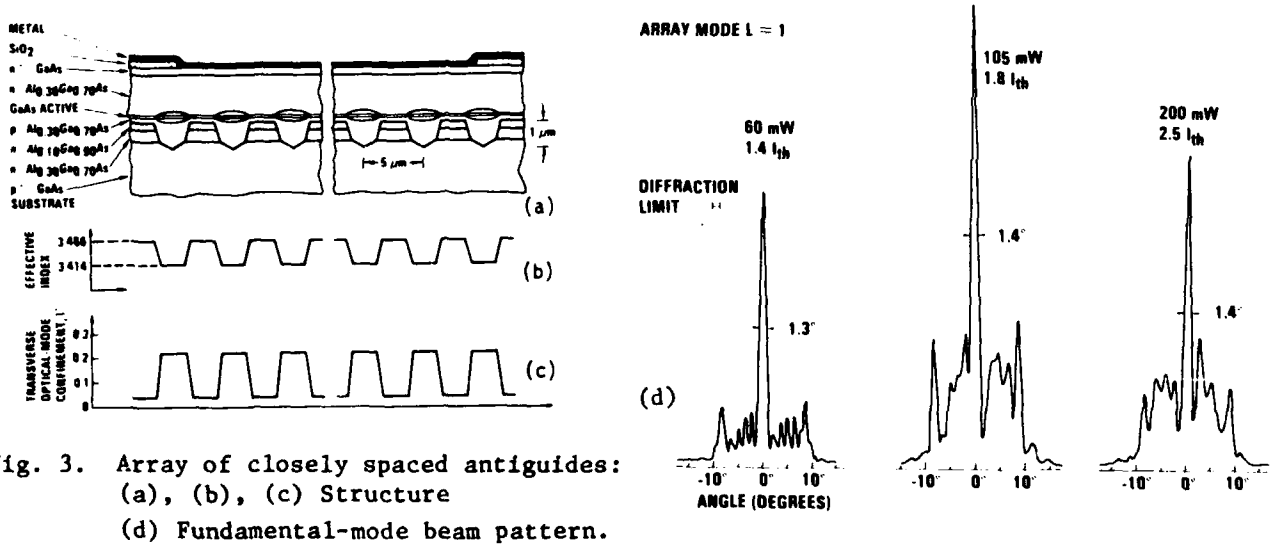

Fig. 3. Array of closely spaced antiguides:
(a), (b), (c) Structure
(d) Fundamental-mode beam pattern.

Coherent Arrays of InGaAsP/InP Buried-Heterostructure Lasers

D. Yap, J. N. Walpole, and Z. L. Liau
Lincoln Laboratory, Massachusetts Institute of Technology
Lexington, MA 02173-0073

Coherent arrays of InGaAsP/InP buried-heterostructure (BH) lasers are reported. These arrays are coupled by Y-junctions [1] or diffraction sections [2]. In contrast to previously reported coherent InGaAsP/InP arrays [3-7], the present arrays are strongly index-guided and have the potential for low threshold currents and stable, single-lobe outputs at high powers. The arrays were fabricated by a new technique which combines dry etching and mass transport [8] and which permits the achievement of sharply defined Y-junctions for low-loss coupling as well as a novel etched-mirror structure for efficient diffraction coupling. A novel method for improving the fill factor of the BH laser arrays by the incorporation of cylindrical output mirrors [9] is also reported.

A schematic illustration of the Y-junction-coupled array structure is shown in Figure 1. In fabricating the arrays, rectangular-shaped mesas are first formed in the LPE-grown double-heterostructure wafers by ion-beam-assisted etching. Next, the active regions are undercut to the desired width by selective wet-chemical etching. Finally, the active regions are buried by mass transport of the InP. The use of the dry-etching technique is crucial to the fabrication of this array structure, since narrow grooves with vertical sidewalls can be formed without regard for the crystallographic orientation. This permits the fabrication of the relatively closely spaced stripes and the sharply defined Y junctions. Figure 2 shows a diffraction-coupled array structure after mass transport. The diffraction-coupled arrays are fabricated by the same procedure as the Y-junction-coupled arrays. The structure shown has a novel mirror with a set of curves which resembles a scalloped shape. These curves are located halfway between the stripes to direct the light efficiently from one stripe into the adjacent stripes, and thus improve the coupling. A single photomask is used to define the laser stripes and mirrors, which are etched and smoothed by mass transport in the same fabrication steps.

The fabricated 8-stripe arrays of both types have room-temperature threshold currents between 150 and 350 mA and output powers as high as 100 mW per facet under pulsed excitation. Figure 3 shows the far-field pattern in the junction plane of a diffraction-coupled array which has a 200-μm-long cavity with a coupling section at one end which is only 30 μm long. The output was taken from the other end, which has a cleaved mirror. Similar far-field patterns were observed for the Y-junction-coupled arrays. The presence of the strong and narrow lobes in the far-field pattern shown is an indication of the strong coupling which has been achieved despite the large stripe spacing of 8 μm. The lobe spacing of 9° is consistent with this stripe spacing. The full-width-at-half-maximum lobe widths are as narrow as 3°. The far-field patterns for some arrays show a second set of lobes which appear at higher powers. Examination of the emission spectra of the individual stripes of those arrays shows that there are several sets of as many as 5 stripes which are locked and lase at the same longitudinal mode, although those stripes may not emit with equal intensities. Further improvements in material uniformity and array fabrication are needed to achieve coherent emission from a larger number of stripes which also is stable with current.

In order to achieve a single-lobed far-field pattern, the fill factor of the array can be increased by fabricating curved mirrors which are located in front of each stripe. These curved mirrors function as an array of cylindrical lenses which reduce the beam divergence in the junction plane of each stripe. Figure 4 shows the far-field pattern of a diffraction-coupled array which has such curved output mirrors. Note that the number of lobes in the far-field pattern is greatly reduced as compared to the pattern shown in Figure 3. With more optimal design of the curved mirrors, it should be possible to obtain single-lobed far-field patterns.

This work was supported by the Department of the Air Force.

88CH2609-8/88/0000/0020$1.00 1988IEEE

1. D. Welch, W. Streifer, P.S. Cross, and D.R. Scifres, IEEE J. Quantum Electron. QE-23, 752 (1987).
2. J. Katz, S. Margalit, and A. Yariv, Appl. Phys. Lett. 42, 554 (1983).
3. T.R. Chen, K.L. Yu, B. Chang, A. Hasson, S. Margalit, and A. Yariv, Appl. Phys. Lett. 43, 136 (1983).
4. N.K. Dutta, L.A. Koszi, B.P. Segner, and S.G. Napholtz, Appl. Phys. Lett. 48, 312 (1986).
5. E. Kapon, Z. Rav-Noy, S. Margalit, and A. Yariv, J. Lightwave Tech. LT-4, 919 (1986).
6. M. Razeghi, R. Blondeau, M. Krakowski, B. deCremoux, J.P. Duchemin, F. Lozes, M. Martinot, and M.A. Bensoussan, Appl. Phys. Lett. 50, 230 (1987).
7. D. Botez, T. Pham, and D. Tran, Electron. Lett. 23, 417 (1987).
8. D. Yap, Z.L. Liau, D.Z. Tsang, and J.N. Walpole, Appl. Phys. Lett., 25 April 1988 issue.
9. J.N. Walpole, Z.L. Liau, L.J. Missaggia, and D. Yap, Appl. Phys. Lett. 50, 1219 (1987).

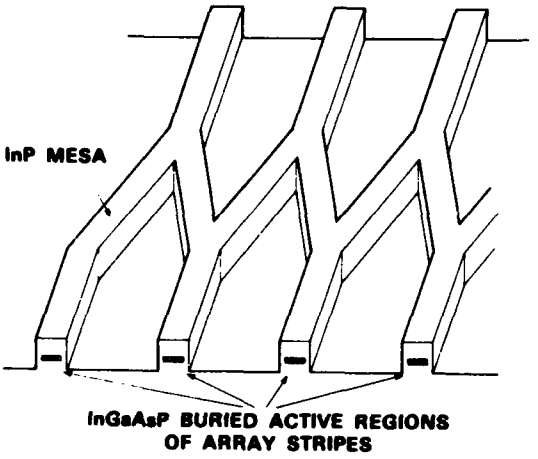

Figure 1. Schematic illustration of a Y-junction-coupled laser array.

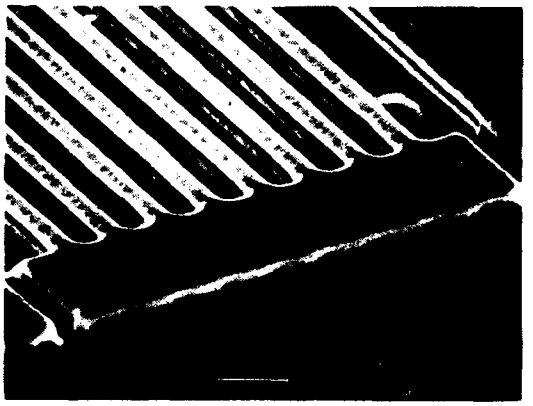

Figure 2. SEM photograph of a diffraction-coupled array structure after mass transport.

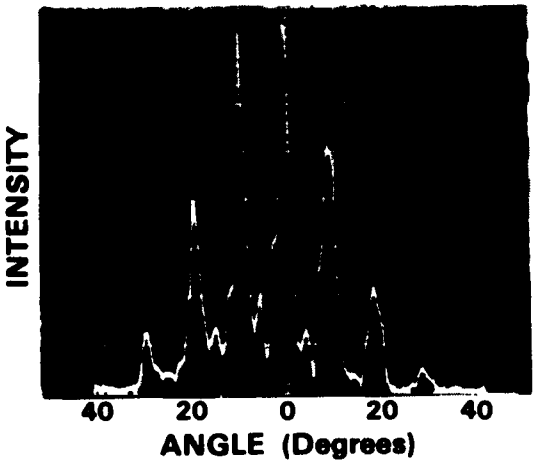

Figure 3. Far-field pattern of a diffraction-coupled array which has a cleaved output mirror.

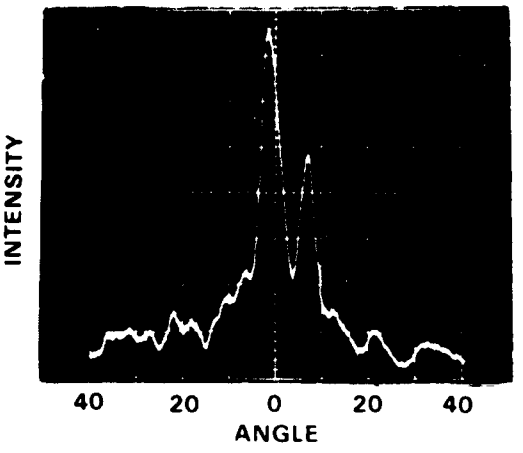

Figure 4. Far-field pattern of a diffraction-coupled array which has an array of cylindrical output mirrors.

B—3

A Phase-Locked "Y" Coupled Index-Guided Visible Light (660 nm) Semiconductor Laser Array

A. VALSTER, J. OPSCHOOR, R. DRENTEN, C. v.d. POEL
Philips Research Labs, Eindhoven, The Netherlands.
J.P. ANDRÉ
Laboratoires d'Electronique et de Physique appliquée
Limeil-Brevannes, France.

Semiconductor laser arrays are attractive for high output power applications. Recently, the first AlGaInP/GaInP visible light (660 nm) laser diode array has been published by Valster et.al (1).This 3 ridge waveguide laser array did not operate in a diffraction limited beam because of absence of any phase coupling between the three waveguides. However, applications like optical recording and laser beam printing require a stable, diffraction limited beam. Here we demonstrate for the first time a visible light emitting phase-locked index-guided laser array.Far-field patterns of a three by two 'Y'-coupled ridge waveguide laser array will be shown.

The AlGaInP/GaInP double heterostructure lasers are grown by OM-VPE at atmospheric pressure.The source materials and most of the growth conditions are the same as those described in a previous paper (2).The ridge type laser array is made by successive selective etching of the GaAs cap layer and the AlGaInP cladding layer.Photoresist with a stripewidth of 3.5 μm seperated by 1.5 μm wide windows is used as the etching mask.

The pulsed threshold currents Ith of the three by two 'Y'-coupled laser arrays are typically in the range of 270-340 mA (cavity lenght is about 250 um).The near- and far-field patterns of the front- and rear facet of such an array at three different output powers and two different pulse widths are shown in figure 1.In figure 2 are plotted the spectrally resolved NF and FF patterns of the same array. As is clearly shown, the pulse width has a big impact on the supermode selection of the array.At short pulse times a pure π phase supermode is selected as can be concluded from the NF and FF patterns.It should be noted that this result is unexpected according to the theory proposed by Streifer et.al (3).At longer pulse times a second supermode starts to lase.This supermode is a superposition of the lowest and highest eigenmode of a parallel 3 waveguide structure.These results will be discussed.

A parallel 3 stripe array without 'Y'-coupling showed similar thresholds as mentioned above, however, with a highest order supermode.Also the efficiency at the front- and rear- facet of the 3-2 'Y'-junction is equal.Both results indicate that the 'Y'-shaped coupling region introduces only very small losses.

In conclusion, a phase-locked 'Y' coupled ridge waveguide visible light emmiting semiconductor laser array is demonstrated for the first time.At short pulse widths an unexpected pure out of phase supermode has been shown.

88CH2609-8/88/0000/0022$1.00 1988IEEE

References :

1.A.Valster, J.P.André, E.Dupont-Nivet, G.M.Martin: Electron. Lett. 1988, to be published.
2.J.P.André, E.Dupont-Nivet, D.Moroni, J.N.Patillon, M. Erman, T.Ngo: J.Cryst.Growth,1986,77,pp.354-359.
3.W.Streifer, D.F.Welch, P.S.Cross, D.R.Scifres: IEEE J. Quantum Electron.,1987,pp.744-751.

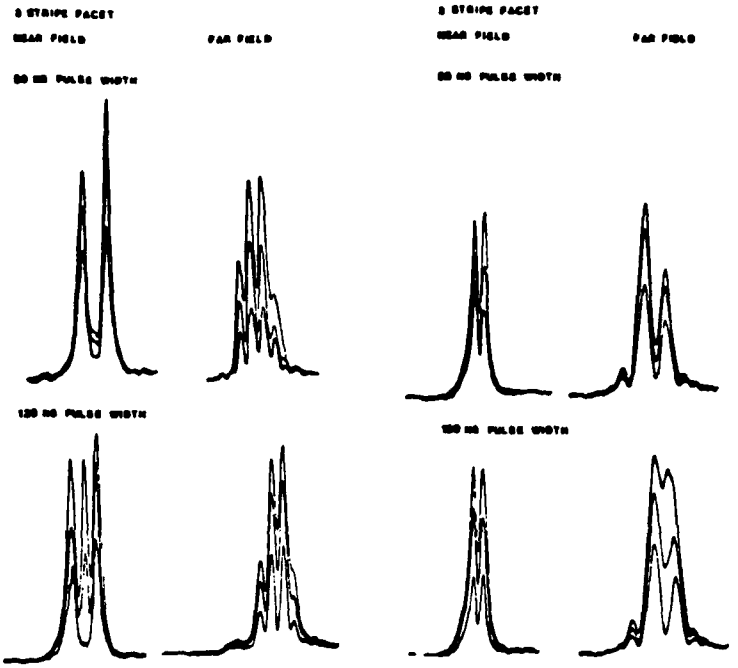

Fig.1 Total NF and FF patterns of the front- and rear-facet of a 3-2 'Y'-coupled ridge waveguide AlGaInP laser array at two different pulse-widths.The laser drive currents are 310 mA,330 mA and 350 mA,respectively.

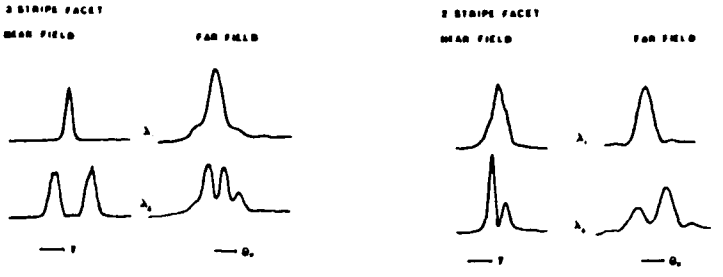

Fig.2 Spectrally resolved NF and FF patterns.The laser drive current is 350 mA and the pulse-width 120 ns.

B—4

Diffraction-Coupled-Output Lasers For High Optical Powers

Siamak Forouhar, Robert J. Lang, Jim Cser and Joseph Katz
Jet Propulsion Laboratory, Pasadena, CA 91109

Paul Gavrilovic, Jeannie Williams, Wolfgang Stutius and Aland Chin
Polaroid Corporation, Cambridge MA 02139

In this paper we demonstrate high-power arrays and broad area lasers with passive diffraction regions at the output facets. The diffraction region takes the form of a long nonabsorbing window. Both arrays and stripe-contact lasers exhibit much narrower far fields than ordinary broad area lasers fabricated from the same wafer.

High-power sources of coherent optical radiation are required for such applications as free-space optical communications, optical radars, solid-state laser pumping and optical data storage. Arrays of lasers have yielded the highest CW powers to date but require more complicated structures [1,2] to insure fundamental lateral mode operation. In one such structure, the diffraction coupled array (DCA), the array is terminated at each end by a section of broad area laser (no array), which allows the elements of the array to couple via diffraction [3]. In this work, we demonstrate a diffraction coupled array which uses a passive window to phase lock the individual elements.

Wide-stripe lasers have been shown to yield narrow single-lobed far fields only rarely [4,5]. Typical wide-stripe lasers possess an irregular near field pattern and emit a broad, unstable far field pattern. We have fabricated wide-stripe lasers as well with long passive windows. The window acts as a spatial filter and reduces high-order spatial frequencies in the near field pattern.

The laser structures are shown in figure 1. The devices (and ordinary broad-area lasers, for comparison) were formed on a large optical cavity GaAlAs wafer. The windows were formed by etching away the upper cladding and active layers and replacing them with SiO. Channels were also etched between the elements of the arrays.

Figure 2 shows the far field patterns for the two diffraction-coupled structures and a normal broad area laser for comparison. (The broad area lasers and windowed broad area lasers were fabricated simultaneously on the same wafer). The far field angles for the diffraction coupled structures are both quite narrow, about 2^{o}, compared to the broad area laser's $5\text{-}15^{o}$. Thus, use of a passive window in a high-power laser structure causes a significant improvement in the optical properties of the output beam.

References:

1. E. Kapon, C. Lindsey, J. Katz, S. Margalit and A. Yariv, Appl. Phys. Lett. vol. 45, p. 200, 1984.
2. D. Welch, D. Scifres, P. Cross, H. King, W. Streifer, R. D. Burnham, J. Yaeli and T. Paoli, Appl. Phys. Lett. vol. 47, p. 1134, 1985.
3. J. Katz, S. Margalit and A. Yariv, Appl. Phys. Lett. vol. 42, p. 554, 1983.
4. W. T. Tsang, Appl. Phys. Lett. vol. 40, p. 217, 1982.
5. A. Larsson, M. Mittelstein, Y. Arakawa and A. Yariv, Elect. Lett. vol. 22, p. 79, 1981.

88CH2609-8/88/0000/0024$1.00 1988IEEE

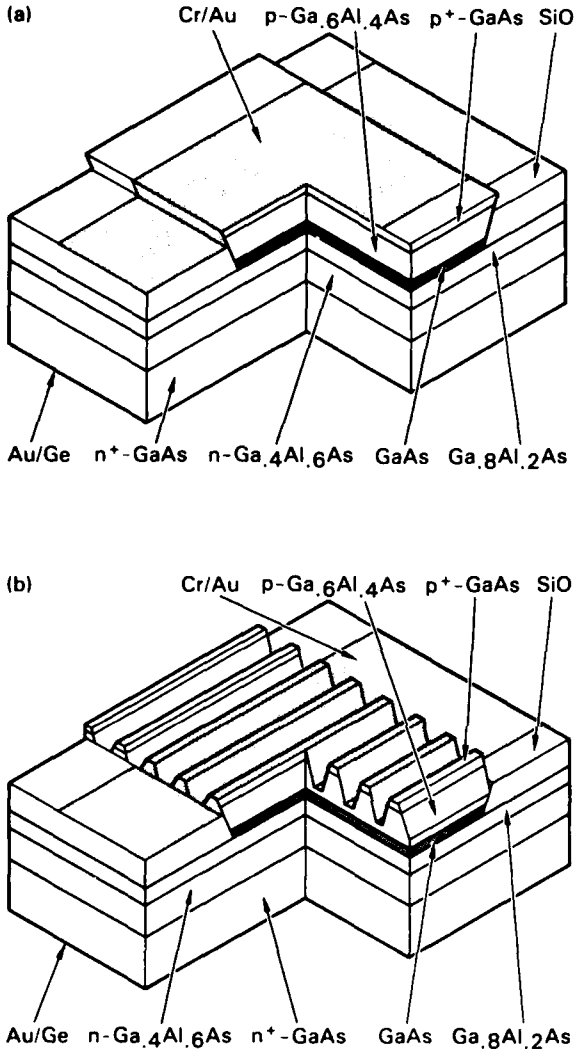

Figure 1: (a) Schematic of a broad area laser with a window region at each end. (b) Schematic of a diffraction coupled array.

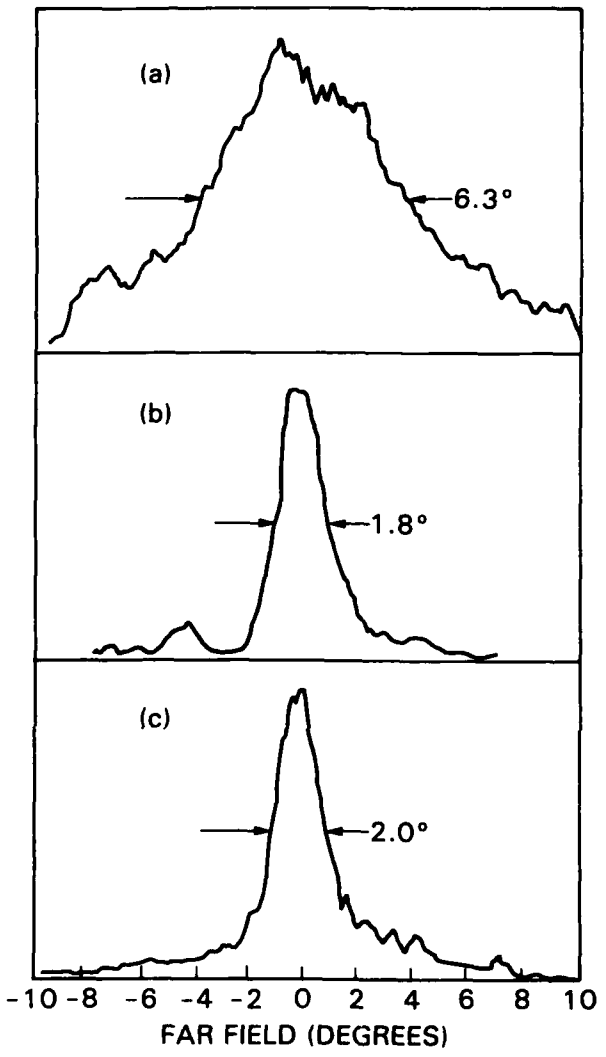

Figure 2: Far field angle (FWHM) for (a) an ordinary broad area laser (100 μm x 300 μm); (b) a diffraction-coupled array (50 μm x 300 μm, 5 elements; 70 μm windows); (c) a broad-area window laser (100 μm x 300 μm, 80 μm windows).

B—5

Spatial Mode Structure of Broad Area Quantum Well Semiconductor Lasers

C. J. Chang-Hasnain, E. Kapon, and R. Bhat
Bell Communications Research
331 Newman Springs Road, Red Bank, NJ 07701

We have identified mechanisms of degradation of the spatial coherence in broad area (BA) quantum well (QW) lasers grown by organometallic chemical vapor deposition (OMCVD). Broad area diode lasers have been recently reconsidered as an approach to high power, coherent injection lasers.[1,2] These lasers, however, typically exhibit imperfect spatial coherence. Using spectrally resolved near field measurements, we show that, conventional BA lasers, grown on (100) substrates, usually exhibit filamentary behavior. Broad area lasers grown on off-(100) substrates, on the other hand, are free from filaments. In these well behaved BA lasers, degradation of the spatial coherence at high currents is due to the appearance of higher order lateral modes. We also show that index-guided and gain-guided BA lasers differ significantly in their spatial mode structure.

Single QW, graded index separate confinement heterostructure (GRIN-SCH) GaAs/GaAlAs laser structure was used in this study. The heterostructure included a 70 Å GaAs QW at the center of 0.3 μm thick $Al_xGa_{1-x}As$ (x=0.2 - 0.7) GRIN region and was grown simultaneously on (100) and 6°-off-(100) oriented n^+-GaAs substrates. Both 50 μm wide oxide stripe gain-guided lasers and ridge-waveguide index-guided lasers were fabricated from the wafers. The lasers were tested under pulsed operation (300 ns @ 20 kHz).

The gain-guided BA lasers grown on (100) substrate have an average threshold current of 62 mA with 57% quantum efficiency for 310 μm long cavities. Similar gain-guided BA lasers grown on 6°-off-(100) substrate have a lower average threshold, 49 mA, and a higher quantum efficiency, 62%. Studies of the spectrally resolved near field of both types of lasers revealed that most of the BA lasers grown on the (100) substrates exhibit filamentary behavior. On the other hand, the majority of the BA lasers grown on 6° off (100) substrate are free from filamentation, indicating excellent uniformity of this laser material. Thus, these well behaved lasers were used to study the spatial mode characteristics.

Fig. 1(a) shows the spectrally resolved near field patterns of a typical gain-guided BA laser on 6°-off-(100) substrate at 1.1 I_{th} and 1.4 I_{th}. Near threshold, the laser operates at the fundamental lateral mode and has a single longitudinal mode. At higher currents, the higher order lateral modes appear successively at different longitudinal mode frequencies. Near threshold, the far field pattern is single lobed and diffraction limited, with a full width half maximum (FWHM) of 4° [Fig. 1(b)]. It remains single lobed at higher currents, but becomes broader due to the appearance of the higher order lateral modes.

The index-guided BA lasers (with 390 μm long cavities) grown on the 6° off (100) substrate exhibit a lower average threshold, 40 mA, and a similar quantum efficiency as their gain-guided counterparts. Their modal behavior, however, is significantly different from that of the gain-guided BA lasers, as shown in Fig. 2(a). Near threshold, the index-guided BA laser emits a single higher order (the ninth) lateral mode. The far field pattern [Fig. 2(b)] at 1.1 I_{th} is double lobed with lobe separation of 7.6°, which agrees well with the Fourier transform of the ninth lateral mode. At higher currents, the far field broadens due to the onset of higher order lateral modes.

Our study shows that BA lasers free from filamentation can be obtained using OMCVD growth on off-(100) oriented substrates. The degradation in the spatial coherence of these devices at higher pumping levels arises from excitation of higher order lateral modes. Index-guided BA lasers have lower threshold currents than gain-guided BA lasers. However, gain-guided BA lasers tend to lase in the fundamental mode near threshold, whereas index-guided BA lasers tend to operate at a higher order lateral mode. Incorporation of designs for lateral mode discrimination in such well behaved BA lasers should lead to the realization of coherent high power diode lasers.

88CH2609-8/88/0000/0026$1.00 1988IEEE

REFERENCES

1. A. Larsson, M. Mittelstein, Y. Arakawa, and A. Yariv, Electronics Lett., *22*, 79, 1986.
2. M. Sakamoto, and Y. Kato, Appl. Phys. Lett., *50*, 869,187.

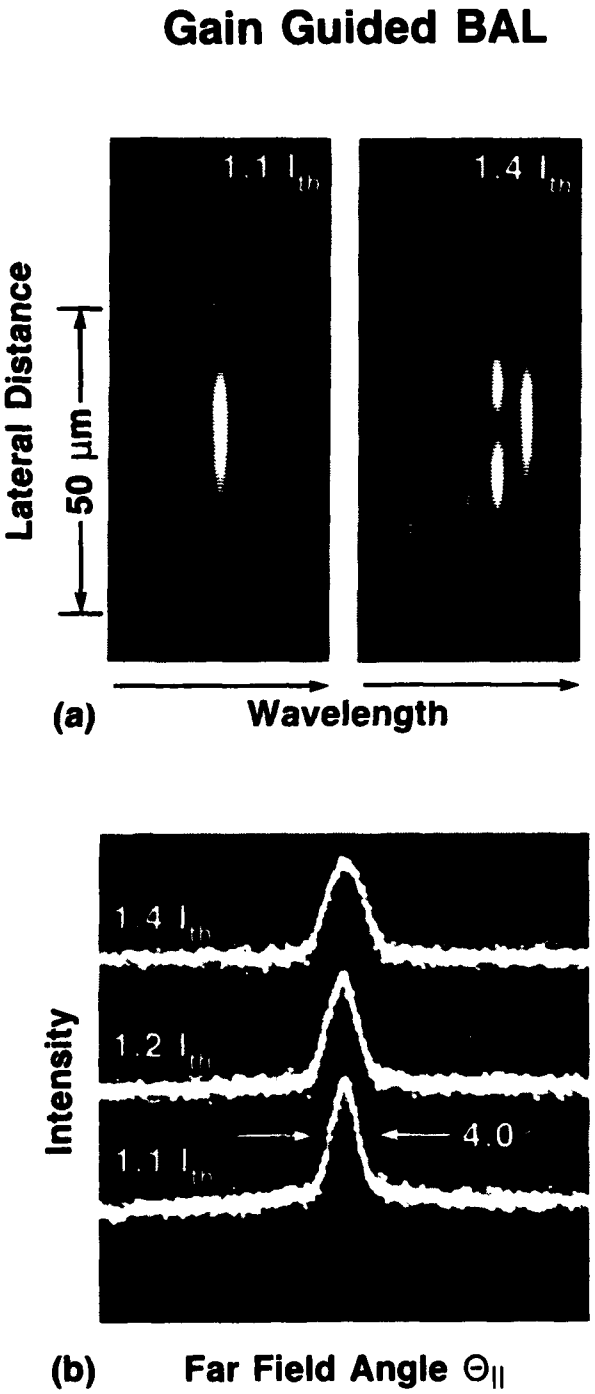

Fig. 1. (a) Spectrally resolved lateral near field and (b) far field patterns of a typical 50 μm gain-guided BA laser.

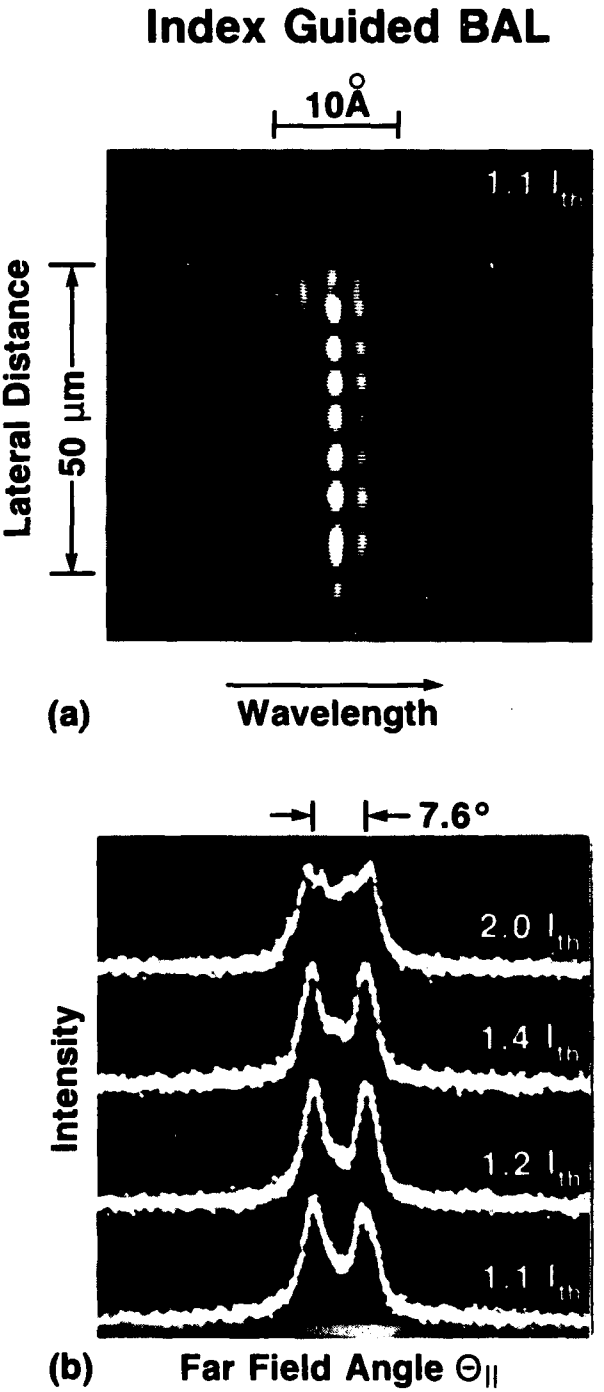

Fig. 2. (a) Spectrally resolved lateral near field and (b) far field patterns of a typical 50 μm index-guided BA laser.

B—6

Power Scaling Laser Diodes Using Phase Conjugates Master Oscillator Power Amplifier Systems

R.R. Craig, R.R. Stephens, R.C. Lind, H.W. Yen, W.W. Ng,A.A. Narayanan, W.P. Brown, W.W. Chow, and C.R. Giuliano

Hughes Research Laboratories
Malibu, Ca

We have performed experimental and theoretical investigations on scaling semiconductor lasers to higher powers with good beam quality and single frequency operation by the use of large area diode amplifiers and optical phase conjugation.

Obtaining high power from laser diodes inevitably involves expanding the output aperture larger than conventional single mode geometries. This results in a degradation in the spectral and spatial properties of the beam. We have demonstrated diffraction limited single frequency performance from a large aperture in a phase conjugate master oscillator power amplifier (PC MOPA) geometry.

Previously[1] we have described a 2-pass phase conjugate master oscillator power amplifier (PC MOPA) system used for power scaling of lasers with single frequency, diffraction limited performance. In this paper we will describe experimental results on a new 4-pass amplifier geometry which more readily allows efficient heat sinking and scaling to multiple amplifier elements in two dimensions. Also by using a broad-area instead of a striped amplifier element side lobes in the far field have been eliminated.

The geometry used in the 4-pass PC MOPA experiments is shown in Fig. 1. The master oscillator is a GaAs/GaAlAs buried heterostructure laser which operates in a single spectral and spatial mode. The beam from the MO is reshaped and focused for the first two passes in the amplifier. The amplifier is an MOCVD grown double-heterostructure design 75μm wide and 500μm long with a high reflectivity (98%) coating on the back facet and anti-reflection (<0.1%) coating on the front facet. The power coupled from the MO to the PA was estimated to be 2mW. After passes 1 and 2 the amplified beam is phase conjugated using a $BaTiO_3$ crystal in a self-pumped internal ring geometry. The beam intensity profile incident on the conjugator is shown in Fig. 2a. This is an image of the amplifier facet and indicates the intensity profile after the first two passes in the system. The conjugate beam returns to the amplifier for passes 3 and 4 and is then coupled out of the system. The far field pattern of the outcoupled beam is shown in Fig. 2b. It is single lobed with a divergence angle approximately 1.1 times the diffraction limit for a 75μm aperture indicating that the phase conjugate arm of the system has corrected phase errors present in the amplifier and the optical system. These initial experiments wee performed using isolation components that were not optimized for the wavelength of operation. For this reason it was necessary to limit the amplifier current density to a relatively low value (1kA/cm^2) in order to avoid feedback to the MO. Under these conditions the output power was limited to 20mW. We are currently performing experiments with improved isolation. The results of these experiments will be presented.

We have also developed a wave-optical model to investigate the behavior of the 4-pass PC MOPA. In particular, we have shown the conditions under which the phase conjugator can correct for or prevent the formation of filaments in the power amplifier.

[1]"Phase conjugate master oscillator-power amplifier using $BaTiO_3$ and AlGaAs semiconductor diode lasers", R.R. Stephens, R.C. Lind, and C.R. Giuliano, Applied Physics Letters, 50(11), 647-9.

88CH2609-8/88/0000/0028$1.00 1988IEEE

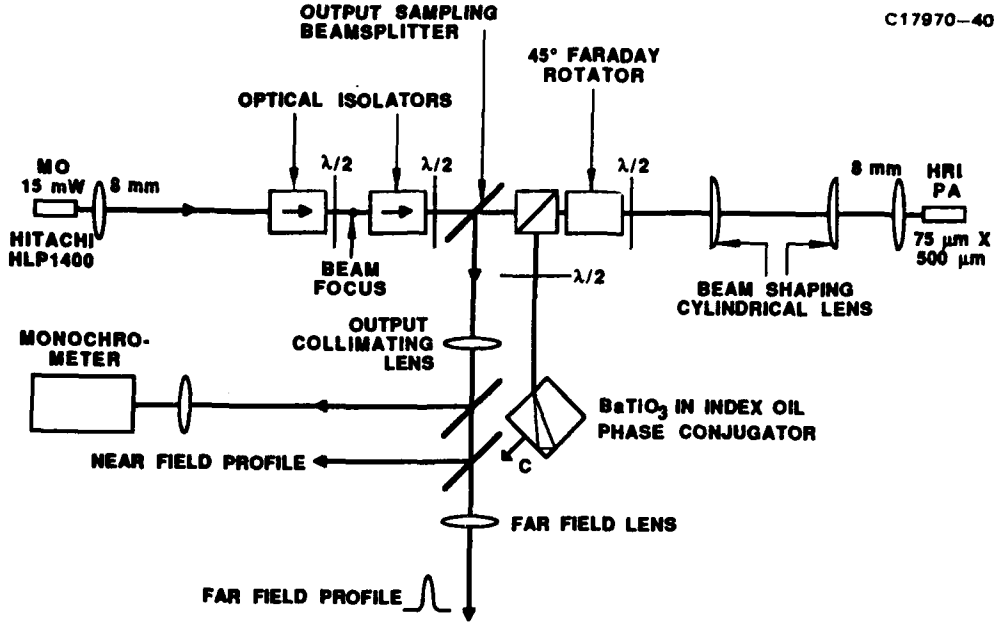

Figure 1. 4-Pass PC MOPA Geometry.

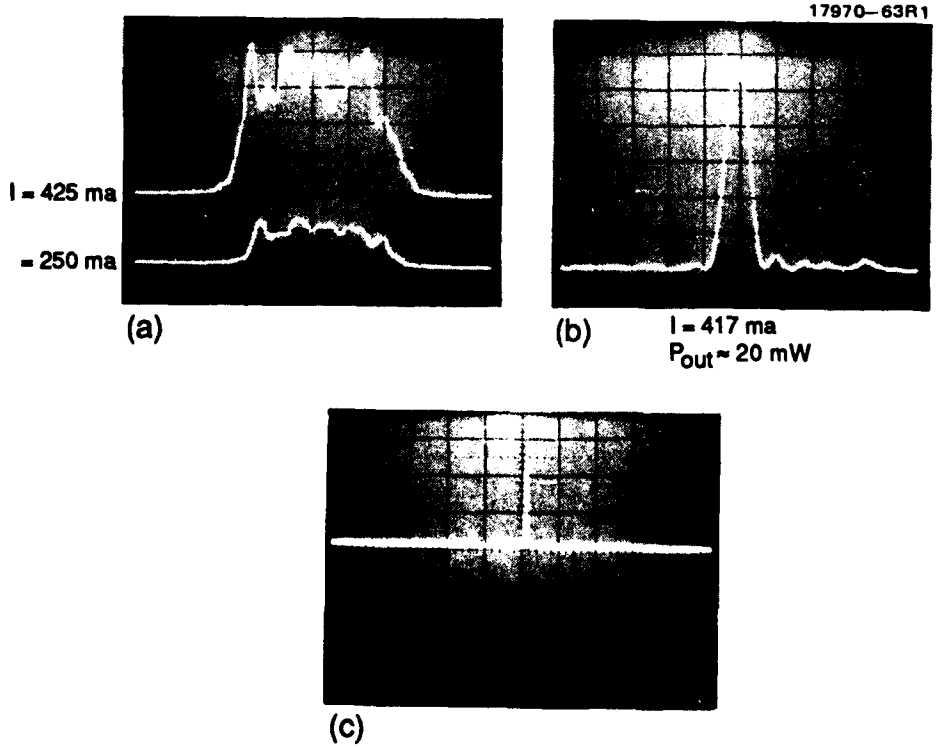

Figure 2. (a) Amplifier near-field intensity after two passes, (b) 4-pass far field pattern, and (c) optical spectrum.

Session C: Quantum Wells I

C—1

Effects of Bandfilling on the Threshold Current of GaAs/AlGaAs Multi Quantum Well Lasers

Radhakrishnan Nagarajan, and Takeshi Kamiya
Department of Electronic Engineering, University of Tokyo,
7-3-1, Hongo, Bunkyo-ku, Tokyo, 113 JAPAN

Atsushi Kurobe
Toshiba Research and Development Center, Toshiba Corporation,
1, Komukai-Toshiba-cho, Saiwai-ku, Kawasaki, 210 JAPAN

In this paper we present an improved model for Multi Quantum Well (MQW) laser operation, carefully considering the bandfilling processes, and test its validity using experimental data for threshold current dependence on the cavity length and the number of wells.

Existing models for MQW laser operation are not always quantitatively accurate in evaluating its bandfilling characteristics thus leading to an excessively optimistic prediction of threshold current reduction. Recently, anomalous cavity length dependence of the threshold current in Graded Index Separate Confinement Heterostructure Single Quantum Well (GRIN SCH SQW) laser was reported and explained in light of the increasingly important non-radiative current mechanisms present at high carrier densities in short cavity lasers [1].

In experiments done by us using low threshold (5 to 7 mA for uncoated lasers) MQW lasers (Fig. 1) [2], with ungraded SCH we observed a similar trend for the case of a single quantum well but a substantially different behaviour for lasers with two or more quantum wells. To compute more accurately the effects of bandfilling on the threshold current of MQW lasers we devised an improved model which includes the effects of band non-parabolicity, energy dependent spectral linewidth, revised band offsets at the heterojunction interface, L-valley scattering, carrier occupation of barrier and waveguide regions and Auger process.

Fig. 2 shows the variation of the conduction band fermi level or the bandfilling process, for various injection levels computed using our model compared with a previously used model [1]. Considering both the effects of finite well height and the carrier scattering to the unconfined states of the quantum well, barrier and waveguide regions which are located at a lower energy level than the L-valley, the fermi level in our model does not rise as fast. This subsequently affects the gain function of the MQW laser and the current contribution of the various non-radiative processes.

As shown in Fig. 3, the threshold current for SQW devices remain largely constant for a range of cavity lengths then suddenly increasing at lengths of about 200 to 300 μm. The non-radiative Auger mechanism and the carrier overflow out of the quantum well are largely responsible for this. The L-valley current and the leakage current out of the SCH via the cladding layers, are not as significant as previously reported [1,3]. For the case of three wells (Fig. 4) the threshold current is no longer constant but increases with increasing cavity length (as in the case for conventional Double Heterostructure lasers) because here the radiative current mechanism becomes dominant. The optimum cavity length is also reduced to about 80 μm. In lasers with a larger number of wells the enhancement of the optical confinement factor reduces the carrier density required at threshold thereby significantly reducing the effect of non-radiative current mechanisms which have a stronger carrier density dependence.

In summary, the good agreement between our predictions and the experimentally observed MQW laser threshold current variation with cavity length and well number indicates the validity of our model for a large range of carrier densities.

[1]. A. R. Reisinger, P. S. Zory, and R. G. Waters, IEEE J. of Quantum Electron., QE-23(6), 993, 1987.
[2]. A. Kurobe, H. Furuyama, S. Naritsuka, Y. Kokubun, and M. Nakamura, Electron. Lett., 22(21), 1117, 1986.
[3]. A. Sugimura, IEEE J. of Quantum Electron., QE-20(4), 336, 1984.

88CH2609-8/88/0000/0032$1.00 1988IEEE

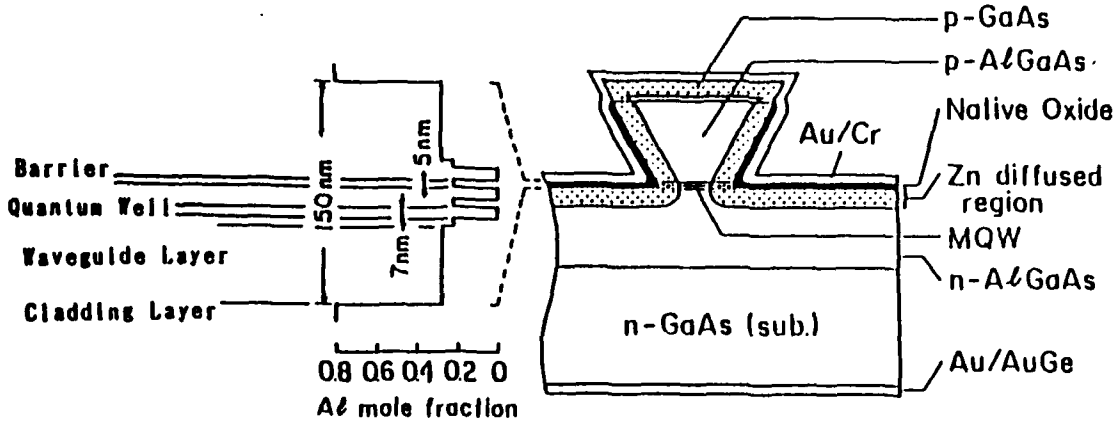

Fig 1. Structure of the low threshold laser used in the experiments.

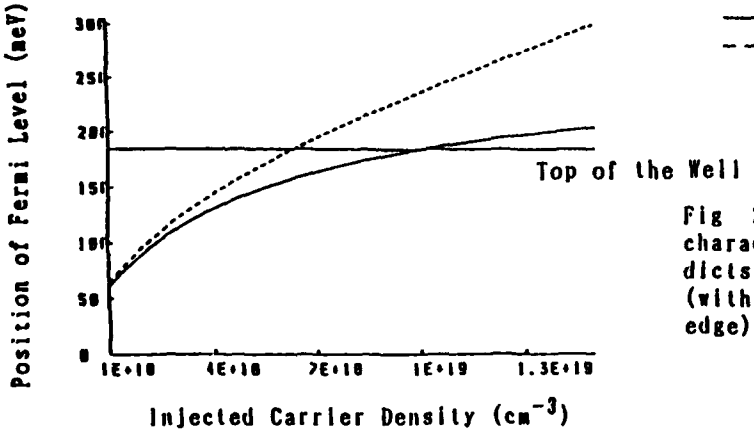

Fig 2. Comparison of the bandfilling characteristics. The previous model predicts a much higher fermi level than ours (with respect to the conduction band edge).

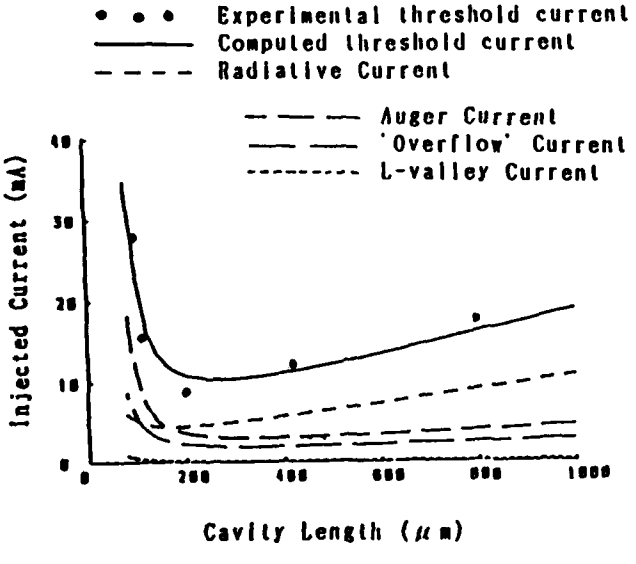

Fig 3. Threshold current for the case of a single quantum well. L-valley current is not significant.

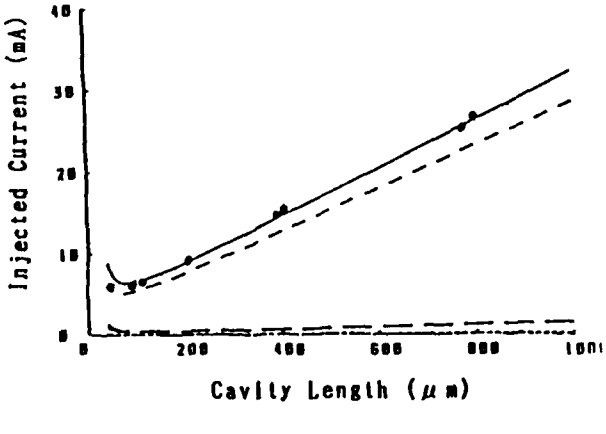

Fig 4. Threshold current for the case of three quantum wells. Radiative current component becomes dominant.

C—2

Temperature Dependence of Threshold Current For GaAs Quantum Well Diode Lasers

P.S. Zory[†], S.R. Chinn[*], A. R. Reisinger[*]

[†]University of Florida - Electrical Engineering Dept.
Gainesville, Florida 32611

[*]General Electric - Electronics Laboratory
Syracuse, New York 13221

Objective: To demonstrate that the anomalous temperature behavior observed at threshold for GaAs quantum well diode lasers has been successfully modeled for the first time.

Background: Published theoretical work[1,2] on the temperature dependence of threshold for GaAs quantum well diode lasers indicates that T_o should increase as device temperature increases above room temperature. Experimental data however[3], as shown in Figure 1, indicates that the opposite is true. The effect gets more pronounced as cavity length decreases and for short (high threshold gain) devices, a discontinuous change occurs in T_o at some critical temperature. Coincident with this T_o change is a threshold wavelength shift which, for the device shown in Figure 1, is about 50 nm.

Techniques: A model for GRIN-SCH-SQW (graded index, separate confinement heterostructure, single quantum well) diode lasers has been developed which utilizes the standard philosophy of solving for carrier energy levels in the GRIN-SCH-SQW potential well. Incorporated into the model are the effects of band non-parabolicity, thermal population of 'X' and 'L' indirect minima, intraband scattering and band-gap renormalization. Also included are the carrier loss mechanisms due to leakage over the confining potential barriers and Auger recombination.

Results: The model predicts, in semi-quantitative fashion, all of the anomalous characteristics observed experimentally.

Impact: This work demonstrates that quantitative modeling of GaAs GRIN-SCH-SQW lasers requires the incorporation of non-radiative carrier loss mechanisms and intra-band scattering. One of the interesting lessons learned from exercising the model is that for a typical structure with quantum well thickness in the 50 Å to 100 Å range, the temperature dependence of threshold current is strongly influenced by quantum well thickness whereas threshold current density is not.

References:

1. N.K. Dutta, Electron Lett. 18, pp.451-453, 1982.
2. P. Blood, S. Colak and A.I. Kucharska, Appl. Phys. Lett. 52(8), pp.599-601, 1988.
3. P.S. Zory, A.R. Reisinger, R.G. Waters, L.J. Mawst, C.A.Zmundzinski, M.A. Emanuel, M.E. Givens and J.J. Coleman, Appl. Phys. Lett 49(1), pp.16-18, 1986.

88CH2609-8/88/0000/0034$1.00 1988IEEE

Threshold Current (I_t) vs. Temperature (T)

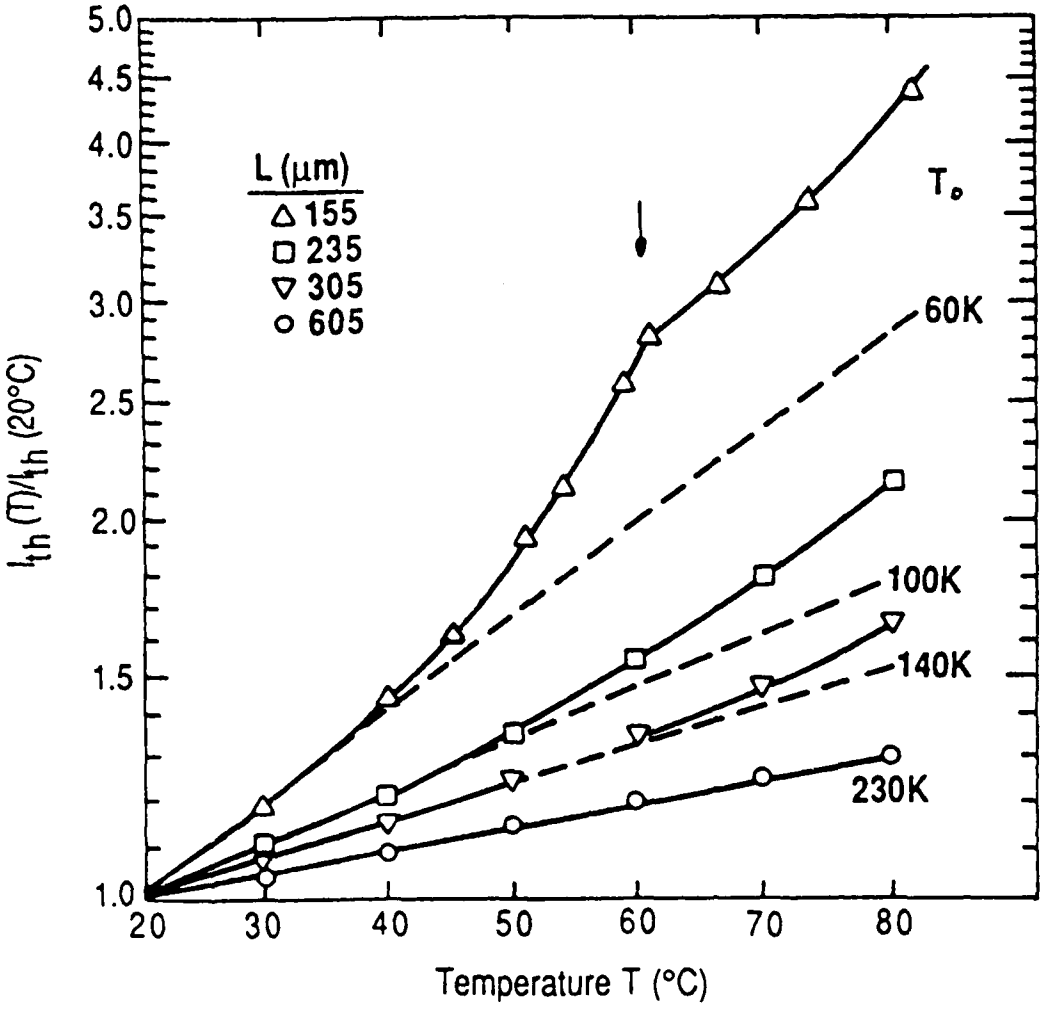

Figure 1. Measured values of short pulse $I_t(T)/I_t(20\,^{o}C)$ plotted against heat sink temperature T for various length, 60 micron stripe width, GRIN-SCH-SQW lasers. The T_o parameters for each length are listed on the right-hand side of the figure. The arrow indicates the location of the T_o discontinuity for the 155 micron long laser.

C—3

Explanation of Low T_0 Values in Short-Wavelength GaAs/AlGaAs Quantum Well Lasers

P. Blood, A.I. Kucharska and E.D. Fletcher

Philips Research Laboratories, Redhill, Surrey RH1 5HA, U.K.

The objective of this paper is to show that the strong temperature sensitivity of threshold current observed in many short-wavelength GaAs/AlGaAs quantum well lasers is due mainly to non-radiative recombination in the barriers.

One of the supposed advantages of quantum wells in lasers is that the temperature dependence of the threshold current (I_{th}) should be weaker than for bulk materials, yet this has rarely been observed, even in short-wavelength devices[1]. Spectral broadening does not account for the observed behaviour of I_{th} as a function of temperature[1] and recombination associated with the L minimum in the wells, and recombination in the barrier regions have been offered in explanation[2].

We have made pulsed measurements on lasers with 25Å GaAs wells and $Al_{0.35}Ga_{0.65}As$ barriers grown by molecular beam epitaxy. Above about 300K, I_{th} increases exponentially with increasing temperature, indicating a thermally-activated recombination process. Spontaneous emission spectra (Figure 1), observed through a narrow window in the top contact of a quantum well laser, have a high energy peak at the known band gap energy of the barriers. While this provides direct evidence for the presence of carriers in the barriers, the associated radiative current is less than 1% of the spontaneous current in the well. However we observe that the overall threshold current at 300K increases when the barrier material has a low radiative efficiency and we conclude that non-radiative recombination in the barriers is responsible for the thermally activated component in $I_{th}(T)$.

We have incorporated the effects of radiative and non-radiative recombination in the barriers and non-radiative recombination from the L minimum in the wells in a model of the optical gain of quantum well lasers which also includes band mixing and spectral broadening[3]. Figure 2 shows that the calculated threshold current varies linearly with T both with and without the inclusion of spectral broadening processes[1]. Inclusion of spectral broadening gives a $T_0 \simeq 414$ K at room temperature, whereas non-radiative recombination in the barriers produces an exponential increase in I_{th}. Our experimental data of $I_{th}(T)$ can be reproduced with a non-radiative

88CH2609-8/88/0000/0036$1.00 1988IEEE

lifetime of 3 ns, giving $T_o \approx 110K$. Similar lifetime values have been reported in the literature for AlGaAs of this composition. Non-radiative recombination via the L minimum in the wells makes only a small contribution to the current even for lifetimes as short as 1 ns.

E.S.M. Tsui has participated in the spectroscopic studies of barrier recombination, and we have benefitted from discussions with A.R. Adams. The structures were grown by K. Woodbridge, and we thank R. Eppenga for providing the calculated in-plane dispersion for the quantum wells.

References

(1) P. Blood, S. Colak and A.I. Kucharska, Appl. Phys. Lett. 52(1988) 599.
(2) A. Sugimura, IEEE J. Quantum Electron QE-20 (1984) 336.
J. Nagle, S. Hersee, M. Krakowski, T. Weil and C. Weisbuch, Appl. Phys. Lett. 49 (1986) 1325.
(3) P. Blood, S. Colak and A.I. Kucharska. To be published in IEEE J. Quantum Electron, August 1988.

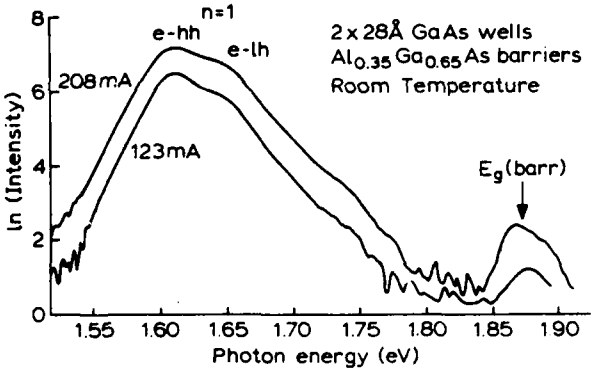

Figure 1
Spontaneous emission spectra observed through a contact window from a quantum well laser. The arrow indicates the energy gap of the barrier material.

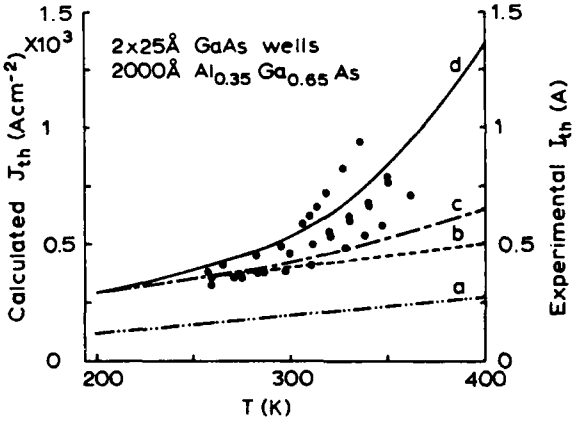

Figure 2
Calculated temperature dependence of threshold current density of a 2-well laser with 2000 Å of barrier material for: (a) ideal case (dotted); (b) broadened (dashed); (c) including radiative recombination in the barriers (dash-dotted); and (d) including non-radiative recombination via the L minimum in both wells and barriers (full curve). The experimental points (threshold current; RH scale) correspond to measurements on three separate 2-well lasers with similar structures.

C—4

Theoretical Gain of Strained-Layer Semiconductor Lasers

Tow C. Chong and Clifton G. Fonstad
Department of Electrical Engineering and Computer Science and
Center for Materials Science and Engineering
Massachusetts Institute of Technology
Cambridge, Massachusetts 02139. (617)253-4620

We present a density matrix approach to analyze the linear gain in strained-layer semiconductor lasers for both the conventional double heterostructure (DH) and the quantum well (QW) structures.

There is increasing interest in novel laser structures consisting of strained active layer which have shown extremely low threshold[1] and unique polarization properties[2]. Although there have been some theoretical efforts addressing the effect of externally applied uniaxial stress on the optical gain of semiconductor lasers[3,4], a general approach similar to that developed for ordinary unstrained lasers and capable of providing a full account of the lasing properties of strained-layer DH and QW lasers has not yet been available. Such understanding can provide important physical insight into controlling the optical gain through the use of strained-layer structures.

We analyze the gain of strained-layer semiconductor lasers based on the density-matrix method taking into account the stress-induced modification of the valence bands and the transition dipole moments. The wave functions for the valence-band states for an arbitrary wave vector at the Γ point in the presence of strain are first derived from diagonalization of the strain Hamiltonian using the original wave functions obtained from the $\mathbf{k} \cdot \mathbf{p}$ method. These wave functions, which are shown to be in general a linear mixing of the atomic p-functions of both spins, are then used to obtain the dipole moment matrix elements at the band edges which are found to be in agreement with the selection rules obtained using the angular momentum representation of the valence-band state quantized in the direction perpendicular to the junction plane.

The results show that the gain difference between the TE and TM polarization in strained layers arises not from the stress-induced anisotropy of the valence bands[4] but rather from the ordering of the two stress-decoupled twofold degenerate valence bands, depending on the direction of the biaxial strain, as well as the dipole moment selection rules associated with them. This leads to the concept of controlling the lasing polarization of strained-layer lasers by modifying the band edge positions of the valence bands through the use of the quantum-size effect. Fig.1 and Fig.2 show the gain spectra of GaAs strained-layer QW (80Å) lasers for a tensile stress and a compressive stress, respectively. The magnitude of the strain is 0.25% which is typical of that encountered in GaAs lasers grown on Si. For comparison, the case for the bulk DH lasers with identical strain is also shown. It is evident from Fig.1 that the originally favored TM mode gain for a tensile strain is suppressed by the incorporation of QWs. However the anisotropy of the valence bands is significant in that the density-of-state effective masses of the valence bands become smaller compared with that of the isotropic heavy hole band in the case with no stress, thus resulting in a smaller carrier density required to reach zero gain in strained-layer lasers. This effect is seen in Figures 3 and 4 where the carrier density dependence of the maximum linear gain is shown for the bulk DH lasers and the QW lasers, respectively. Thus the use of strained active layers and the incorporation of QWs can result in significant improvement of laser threshold performance.

The above analyse are important to the design of low-threshold strained-layer lasers and to the analysis of polarization switching utilizing internal strain in the lasers.

1. S.E. Fischer et al, Appl. Phys. Lett., 50, 714 (1987).
2. S. Sakai et al, IEEE. J. Quantum Electron., QE-23, 1080 (1987).
3. N.B. Patel et al, IEEE. J. Quantum Electron., QE-9, 338 (1973)
4. N.K. Dutta, J. Appl. Phys., 55, 285 (1984).

* Supported by the National Science Foundation, Grant No. ECS 84-13178

88CH2609-8/88/0000/0038$1.00 1988IEEE

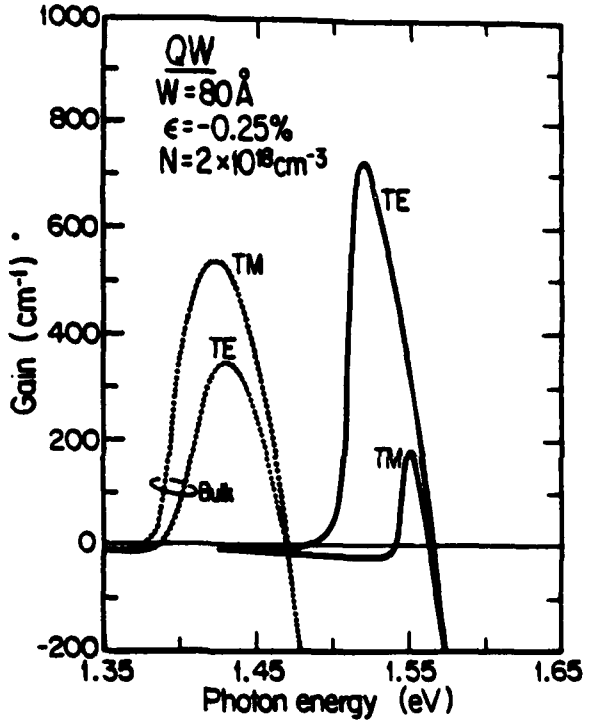

Fig.1

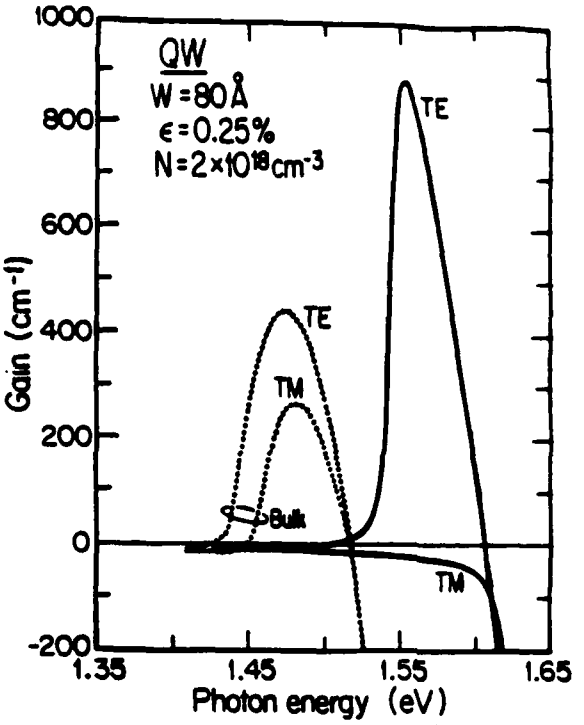

Fig.2

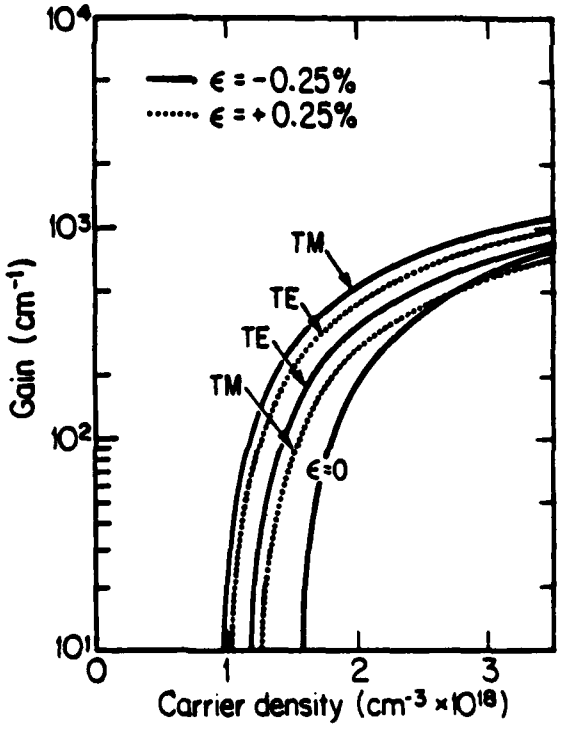

Fig. 3

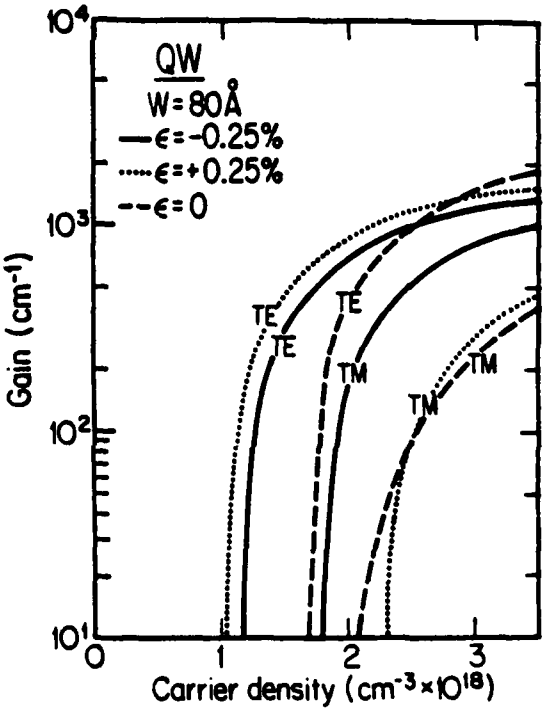

Fig.4

C—5

Spontaneous Emission Factor and Waveguiding in GaAs/AlGaAs MQW Lasers

S.Hausser, W.Idler, M.H.Pilkuhn
4. Physikalisches Institut, Universität Stuttgart, Pfaffenwaldring 57, D-7000 Stuttgart 80, FRG
G.Weimann, W.Schlapp
Forschungsinstitut der Deutschen Bundespost, Am Kavalleriesand 3, D-6100 Darmstadt, FRG

We present a quantitative analysis of the spontaneous emission factor and the waveguiding mechanisms in gain guided GaAs/AlGaAs MQW lasers.

The spontaneous emission factor K in gain guided lasers, introduced by Petermann, is determined by the strength of the gain guiding relative to the index antiguiding. The index antiguiding is due to a reduction of the real refractive index of the active layer by the injected carriers. In "conventional" 3D gain guided lasers the K-factor is of the order of 20-30, leading to double lobed lateral far fields with a half width of 40^{o}, an astigmatism of about 40μm and a spectral multi mode emission with about 20 longitudinal modes.

We measured the lateral near- and far fields of gain guided multi quantum well lasers, in order to determine the influence of the multi quantum well active layer on the lateral waveguiding in these lasers. Furthermore, the carrier induced reduction of the real refractive index of these lasers was determined by measuring the shift of the laser modes with increasing injection current, and longitudinal mode spectra were measured to test the predicted changes in the mode spectra. The lasers investigated are MBE grown GaAs/AlGaAs oxide stripe multi quantum well lasers /1/ with a stripe width of 5.5μm and 5 quantum wells with $L_z \approx 7.5$nm. The width of the barriers is $L_b = 2.5$nm.

The lateral near field measurements yield results which are identical to the case of conventional 3D lasers. The far field measurements, however, show big differences between quantum well and conventional 3D lasers (fig.1). The far field of the MQW lasers is single lobed and exhibits a half width of only 7.5^{o}. From the near and far fields the K-factor can be calculated easily. The surprising result is a low K-factor of K=3 for the MQW lasers, in contrast to the much larger values of K=20-30 in conventional 3D lasers. This means that in quantum well lasers the ratio of index antiguiding to gain guiding is much smaller than in conventional 3D lasers. This conclusion is supported by the carrier induced refractive index change, which is determined from the shift of the laser modes with increasing injection current. The observed change in the real part of the refractive index of -0.06 is similar to conventional 3D lasers. On the other hand, the gain in quantum well lasers is much stronger than in conventional 3D lasers.

The small K-factor of the MQW lasers has two important consequences. First, the astigmatism of the quantum well lasers becomes even stronger than for conventional 3D lasers. Calculations using the model by Mamine /2/ yield values as large as 200μm. The second consequence concerns the longitudinal mode spectra of the MQW lasers. The theory by Streifer et al. /3/ predicts that the half

88CH2609-8/88/0000/0040$1.00 1988IEEE

width of the envelope of the mode spectra is directly proportional to the K-factor. Thus the MQW lasers should have narrower mode spectra than conventional lasers. This prediction was tested by measuring the mode spectra of the lasers. The result is in excellent agreement with the theoretical prediction (fig.2): At an output power of about 6mW the MQW lasers exhibit a nearly single longitudinal mode with a side mode suppression ratio of 1/10. Thus this behaviour of quantum well lasers is due to the altered lateral waveguiding in these lasers.

In conclusion, near- and far field measurements on GaAs MQW lasers show that the K-factor of these lasers is reduced by a factor of 10 compared to conventional 3D lasers. This reflects the high peak value of the gain profile, leading to a stronger gain guiding in these lasers. The consequences are a larger astigmatism of quantum well lasers and nearly single longitudinal mode operation.

/1/ G.Weimann, W.Schlapp, Physica **129B**, 459 (1985)

/2/ T.Mamine, J. Appl. Phys. **54**, 2103 (1982)

/3/ W.Streifer, D.R.Scifres, R.D.Burnham, Appl. Phys. Let. **40**, 305 (1982)

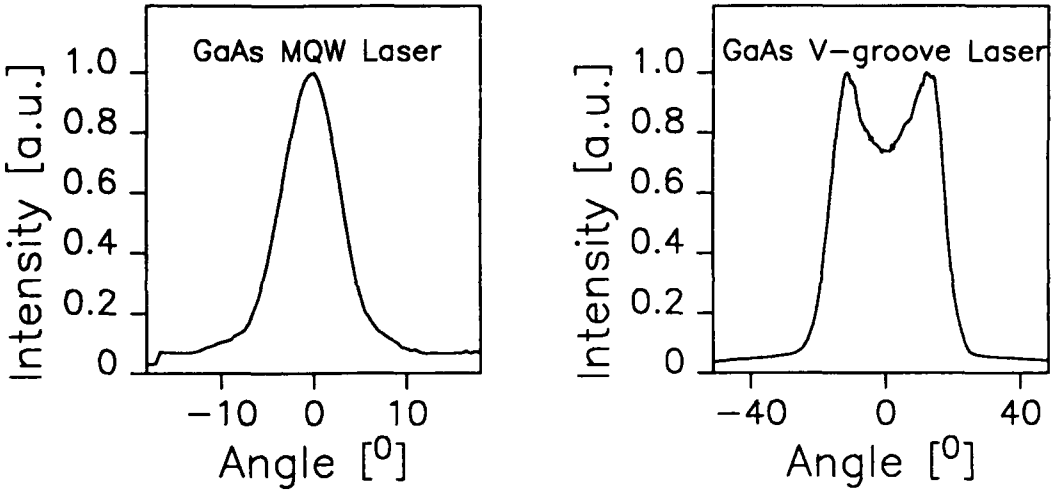

fig.1: far fields of a MQW laser and a 3D V-groove laser

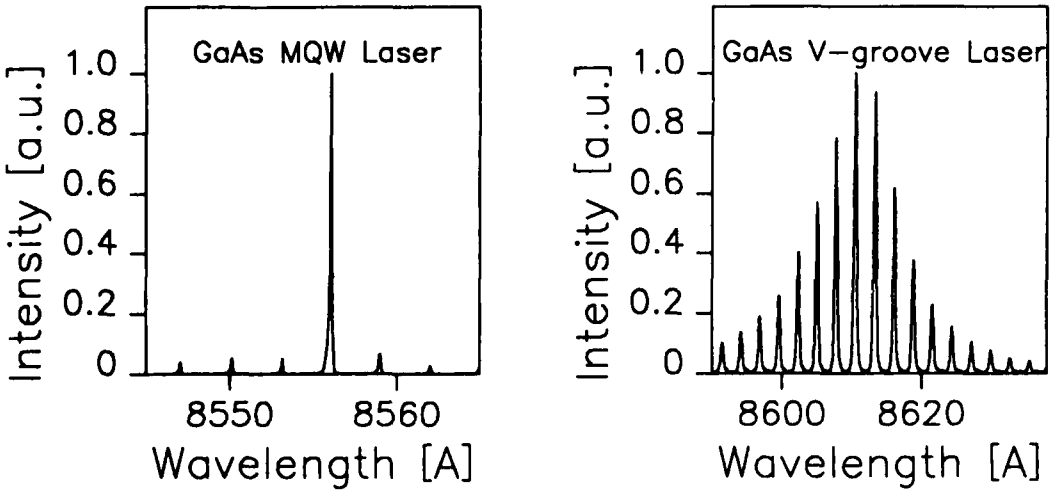

fig.2: mode spectra of MQW and 3D V-groove lasers at 6mW output power

C—6

Reduction of the Interfacial Recombination Velocity in GaAs/AlGaAs Quantum Well Structures by Superlattice Buffer Layers

H.Iwata,H.Yokoyama,M.Sugimoto,N.Hamao,and K.Onabe
Opto-Electronics Research Laboratories,NEC Corporation
4-1-1,Miyazaki,Miyamae-ku,Kawasaki,Japan 213

It is well known that the introduction of superlattice (SL) buffer layers remarkably improves the luminescence efficiency of a GaAs/AlGaAs quantum well (QW) and reduce the threshold current of QW laser diodes (LDs) grown by MBE. This improvement was presumed to be due to either the interface smoothing or impurity trapping effect of the SL buffer layers.[1] This paper reports the quantitative study on the effect of SL buffer layers on the QW optical quality.

Figure 1 shows the changes with the number of growth runs in the threshold current density J_{th} of separate-confinement heterostructure (SCH) single quantum well (SQW) LDs with alloy and SL guide layers. As shown in this figure, J_{th} of SQW-LDs with alloy guide layers decreases remarkably with the number of growth runs. The J_{th} reduction by SL guide layers is particularly conspicuous in the devices obtained in the earlier runs. This strong dependence on the number of growth runs suggests that impurity incorporation is somehow involved in the J_{th} reduction.

Shown in Fig.2 is the recombination lifetimes τ of DH and QW structures with different GaAs layer thickness d, which were obtained through the time-resolved photoluminescence (PL) measurement using picosecond light pulses from AlGaInP visible LD.[2] The PL decay times τ_{PL} are seen to depend strongly on the layer thickness d. Figure 3 shows a $1/\tau$ versus 1/d plot, in which we set the value τ equal to twice τ_{PL} because bimolecular recombination was dominant in our measurement. The value of the GaAs bulk nonradiative recombination lifetime τ_{nr}^{b} and the interfacial recombination velocity of the interfaces S_1+S_2 can be deduced from this plot through the following expression,[3]

$$1/\tau = 1/\tau_r + 1/\tau_{nr}^{b} + (S_1+S_2)/d\,, \qquad (1)$$

where τ_r, τ_{nr}^{b}, S_1, S_2 are the GaAs bulk radiative and nonradiative recombination lifetime and the interfacial recombination velocities at the first and second interface respectively. The estimated values for τ_{nr}^{b} and S_1+S_2 are 68nsec and 330cm/sec respectively. These estimated values indicates that the interfacial recombination dominates the property of DH structures with thin GaAs layer, especially QW structures.

We also measured the recombination lifetime τ of the QW structure with 10nm GaAs well and SL barrier, which consisted of 33 couples of 2nm GaAs and 1nm AlAs. The value of τ is 63nsec, which is about ten times as long as that of the QW structure with alloy barriers as shown in Fig.2. The interfacial recombination velocity S_1+S_2 of this sample is estimated less than 16cm/sec.

88CH2609-8/88/0000/0042$1.00 1988IEEE

This clearly indicates that the major effect of the SL buffer layers is to reduce the nonradiative recombination at the QW interfaces.

The drastic reduction in the interfacial nonradiative recombination accounts for the remarkable decrease in J_{th} in devices with the SL buffer layers. The mechanism of the interfacial recombination reduction by the SL buffer layers is not yet clear. However, the strong run number dependence of J_{th} suggests that impurity trapping is a likely mechanism.

(1) P.M.Petroff, R.C.Miller, A.C.Gossard, and W.Wiegmann, Appl. Phys. Lett. 44, 217 (1984).

(2) H.Yokoyama, H.Iwata, K.Onabe, and T.Suzuki, to be published in April 1988 issue of Rev. Sci. Instrum.

(3) P.Dawson and K.Woodbridge, Appl. Phys. Lett.4 5, 1227 (1984).

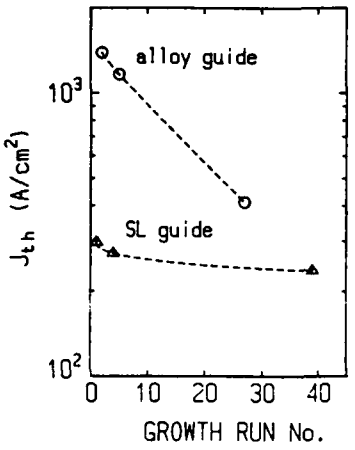

Fig.1 The changes of J_{th} of SCH-SQW LDs with alloy and SL guide layers during growth run.

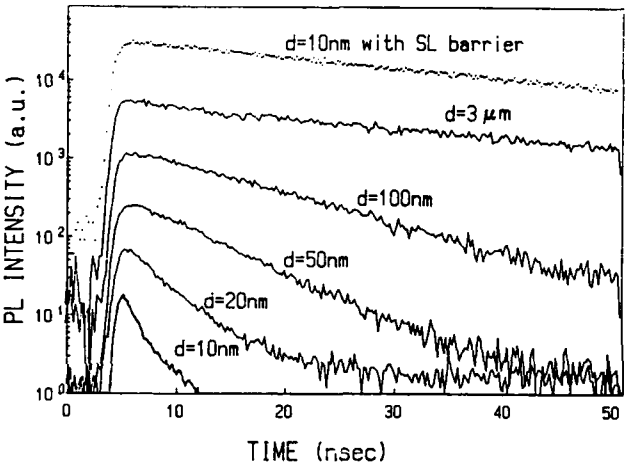

Fig.2 PL time decay of DH structures with alloy barriers for different GaAs layer thicknesses d, covering QWs. The dotted line is PL time decay of a QW with SL barriers.

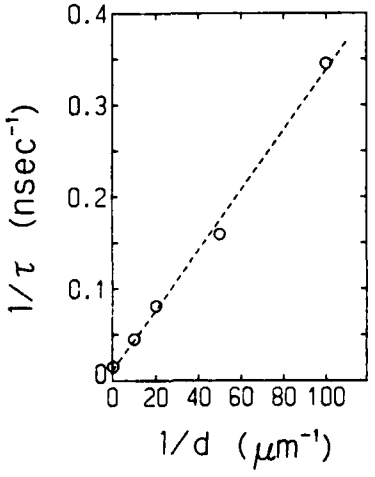

Fig.3 $1/\tau$ versus 1/d plot. The interfacial velocity S_1+S_2 is estimated to be 330cm/sec.

Session D: High Speed Modulation

D—1

High Speed (13 GHz) 1.5 μm Self-Aligned Constricted Mesa DFB Lasers Grown Entirely by MOCVD

Yuzo Hirayama, Hideto Furuyama, Motoyasu Morinaga, Nobuo Suzuki, Yutaka Uematsu, Kazuhiro Eguchi and Masaru Nakamura

Toshiba Research and Development Center
1 Komukai,Toshiba-cho,Saiwai-ku,Kawasaki 210,Japan

Objective High speed 1.5μm InGaAsP/InP DFB lasers are required for use in long haul multigigabit optical communication systems.
Background Very high speed 1.3μm Fabry Perot lasers with constricted mesa (CM) structure have been reported.(1),(2) In DFB lasers emitting at 1.5μm, however, more than 10GHz bandwidth has not been achieved.
Techniques A new self-aligning (SA) process for 1.5μm SA-CM DFB lasers was developed to reduce parasitic capacitance uniformly in a wafer. Figure 1 shows the fabrication procedure. (a)First, an InGaAsP active layer and a corrugated waveguide layer were patterned in a stripe with dual channels. (b)Next, an InP cladding layer and a contact layer were successively over-grown and a mesa was formed. (c)Finally, selective undercut etching of the side quaternary regions was performed. Each layer thickness could be controlled with an accuracy of ±5% by a low pressure MOCVD. Laser chips were mounted on the end of microstrip line.
Results The controllability of the widths of lateral confining InP regions were dramatically improved by the self-aligning process. Stray InP junction capacitance was only 1.62pF with a small standard deviation of 0.08pF for 250μm cavity length. Smith chart plot of measured impedance for 0.045GHz-20GHz frequencies was shown in Fig.2. Inductance and resistance were 0.4nH and 4.2Ω respectively. Figure 3 shows I-L characteristics of SA-CM DFB laser. Threshold current was 16mA. As shown in the inset, the lasing wavelength was 1.51μm and side mode suppression ratio was more than 30dB. Small signal frequency responses for different output powers are shown in Fig.4. A 3dB bandwidth of 11GHz was obtained at an output power of 8mW. This is the widest value that has ever been reported for 1.5μm DFB lasers.(3) At higher powers, 13GHz bandwidth (detector limit) was observed. The ultimate frequency response of 1.5μm single mode lasers will be discussed in comparison with 1.3μm lasers and multimode lasers.
Impact Frequency responses to 13GHz of 1.5μm DFB laser was obtained for the first time using a newly developed self-aligning process and MOCVD growth.

References
(1)J.E.Bowers et al.,IEEE J.Quantum Electron.,QE-22,833(1986)
(2)R.Olshansky et al.,ibid.,QE-23,1410(1987)
(3)M.Yamaguchi et al.,OFC88,New Orleans,paper THK4(1988)

88CH2609-8/88/0000/0046$1.00 1988IEEE

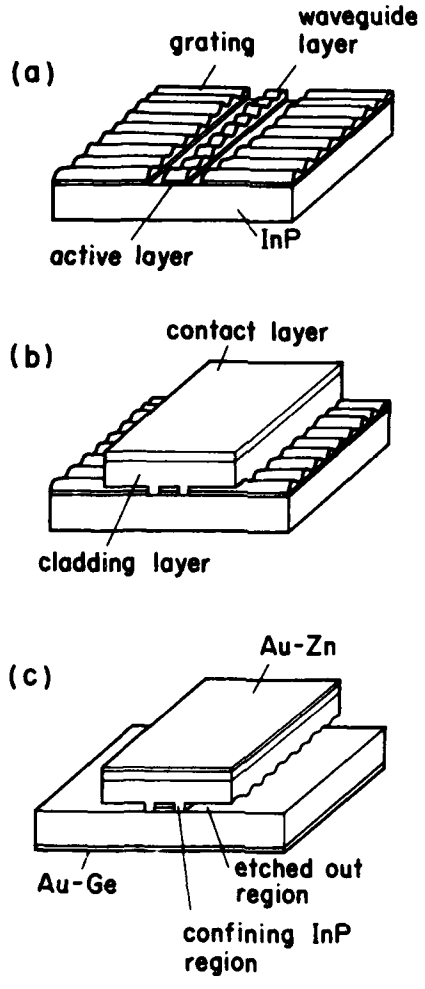

Fig.1 Self-aligned fabrication procedure for SA-CM DFB lasers.

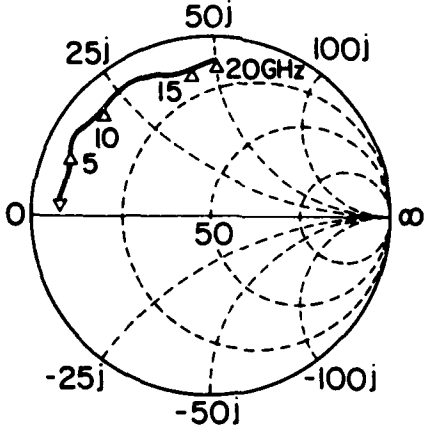

Fig.2 Smith chart plot of measured impedance.

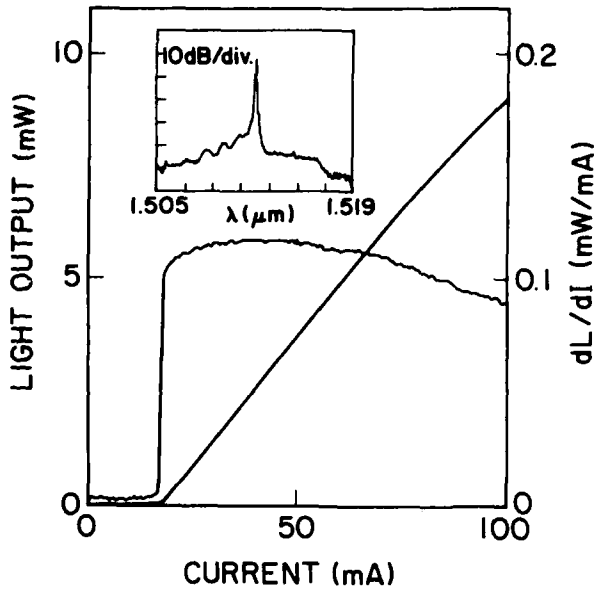

Fig.3 I-L characteristics of SA-CM DFB laser. Lasing spectrum is also shown in the inset.

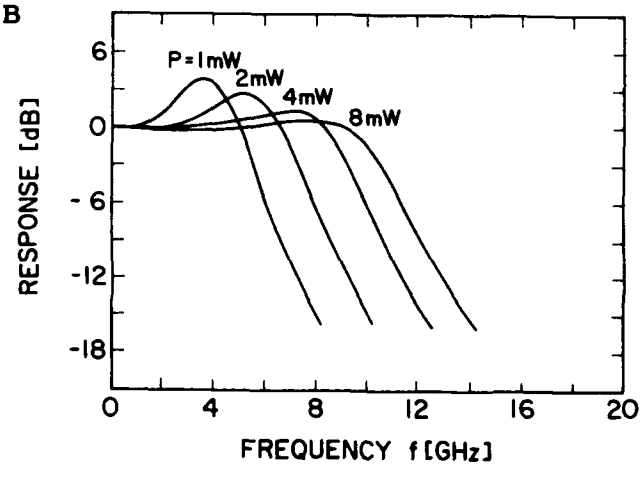

Fig.4 Small signal frequency responses for different output powers.

D—2

Low-Threshold and Wide-Bandwidth 1.3 μm InGaAsP Buried Crescent Lasers with Co-Doped Semi-Insulating Current Blocking Layers

W. H. Cheng, K. D. Buehring, J. Pooladdej, S. Y. Huang, D. Wolf, A. Appelbaum, and D. Renner
Rockwell International Corporation, Lightwave Systems Division, Dallas, Texas 75207
K. L. Hess and S. W. Zehr
Rockwell International Corporation, Science Center, Thousand Oaks, California 91360

Co-doped semi-insulating (SI) InP layers have been grown for the first time by low-pressure metalorganic chemical vapor deposition (LPMOCVD) for use as a current blocking layer for 1.3-μm InGaAsP buried crescent lasers. Lasers with this Co-doped InP blocking layers have CW threshold currents as low as 8 mA at room temperature. This is the lowest threshold current yet reported for an InGaAsP laser with an SI current blocking layer.

Semiconductor lasers with SI current confinement layers have demonstrated the potential for achieving both high-speed and high-power operation, because SI layers offer high resistivity and low parasitic capacitance. High-resistivity Fe-doped SI InP grown by MOCVD has shown great promise for use as a current blocking layer in long wavelength lasers. However, heavy Fe doping in MOCVD grown InP layers causes FeP_2 precipitates (1) which may degrade laser performance. Alternative transition metals such as Cr, Co, Mn, and Ti have been studied as dopants in InP for obtaining SI properties for high performance long wavelength optoelectronic devices and integrated circuits.

Fig. 1 shows a schematic cross-section of the 1.3-μm InGaAsP semi-insulating buried crescent (SIBC) laser, which is fabricated by a hybrid growth technique. The Co-doped SI blocking layer is first grown about 4.5 μm thick on an n-InP substrate by LPMOCVD using triethylindium (TEI), phosphine (PH_3), and cobaltnitrosyltricarbonyl ($Co(NO)(CO)_3$) as reactant gases. In the second growth stage, four layers are grown by liquid phase epitaxy (LPE). The layers are an n-InP buffer layer, an undoped InGaAsP active layer, a P-InP cladding layer, and a p-InGaAs cap layer. Details on Co-doped LPMOCVD growth are given in reference (2).

The CW light-current characteristic at 23°C and the corresponding far-field patterns parallel to the epitaxy layers of a SIBC laser are shown in Fig. 2. The laser is mounted P-side up and has a 275-μm-long cavity with uncoated as-cleaved facets. It has a threshold current of 8 mA and a total differential quantum efficiency of 60% at low current. The maximum CW power output is 30 mW/facet. The device operates in a stable single transverse mode over the full output power range.

Fig. 3 shows the temperature dependence of the CW light-current characteristics. The laser exhibits a characteristic temperature To of 60K between 25°C and 70°C, and CW operation up to 100°C with optical power of 6 mW.

Fig. 4 shows the small-signal frequency repsonse of the SIBC laser measured at various output power levels. A 3-dB modulation bandwidth of 8 GHz was obtained at 12 mW.

In conclusion, we have demonstrated a high-performance 1.3-μm InGaAsP laser structure with a Co-doped SI blocking layer. Lasers have CW threshold currents as low as 8 mA at 23°C, high-temperature cperation up to 100°C, high-power output of 30 mW/facet, and 3-dB bandwidth of 8 GHz. These results indicate that this Co-doped SI layer grown by LPMOCVD is effective for current blocking.

88CH2609-8/88/0000/0048$1.00 1988IEEE

References:

1. N. A. Smith, I. R. Harris, B. Cockayne, and W. Macewan, J. Cryst. Growth 68, 517 (1984).
2.) K. L. Hess, S. W. Zehr, W. H. Cheng, J. Pooladdej, K. D. Buehring, and D. Wolf, ICMOVPEIV, May 16-20, 1988, Hakone, Japan (to be presented).

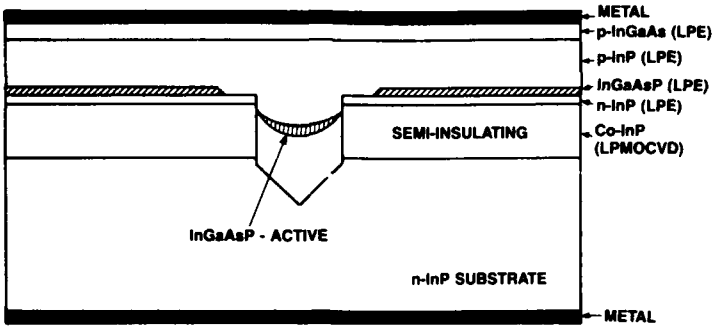

Fig. 1 Schematic cross-section of a 1.3 μm SIBC laser.

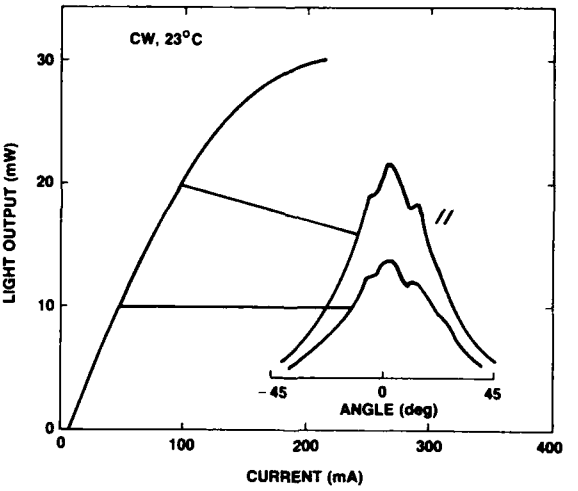

Fig. 2 Light-current characteristic at 23°C for CW operation.

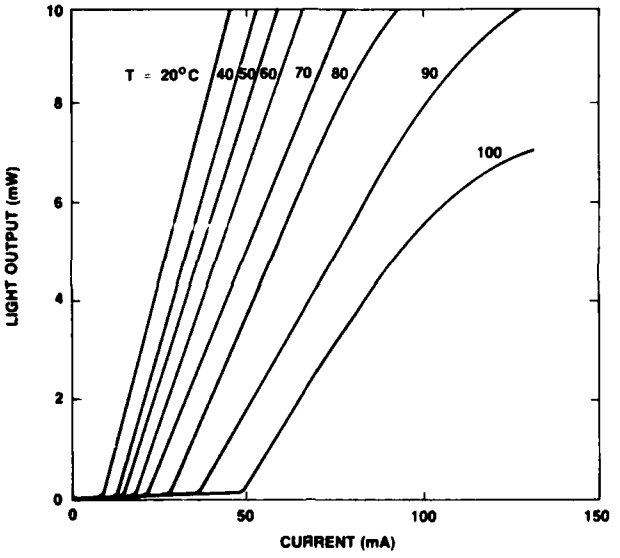

Fig. 3 CW light-current characteristic at various temperatures.

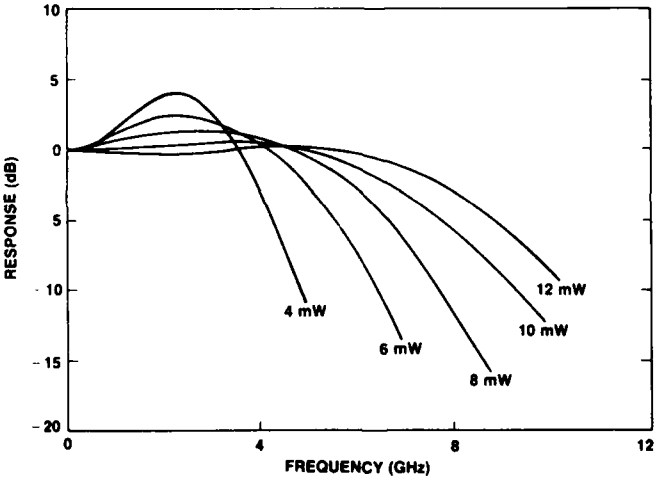

Fig. 3 Small-signal modulation characteristics at various optical power levels.

D—3

High Speed 1.3 μm InGaAsP Distributed Feedback Lasers

T. Cella
R. L. Brown
Y. Twu
J. L. Zilko
N. K. Dutta

AT&T Bell Laboratories
Murray Hill, New Jersey 07974

We report the fabrication and performance characteristics of double channel planar buried heterostructure lasers that utilize semi-insulating InP grown by metal-organic vapour phase growth technique for current confinement. The schematic of the device is shown in Fig. 1. The fabrication involves the following steps. First, a holographically patterned grating (Λ ~ 2000Å) is etched into the InP substrate using wet chemical etching. Four layers are then grown over the grating. They are an n-InGaAsP waveguide layer (λ ~ 1.1 μm), an undoped InGaAsP active layer (λ ~ 1.3 μm), a p-InP layer and a p-InGaAsP contact layer. Two channels are etched using a photolithographically patterned SiO_2 mask and wet chemical etching. The final active layer width between the two channels is 1.5 μm and the active layer thickness is 0.2 μm. With the SiO_2 mask still in place, Fe doped semi-insulating InP is grown, in the channels only, using metal-organic vapor phase growth technique. The wafer is then processed to produce the laser structure shown in Fig. 1. The cavity length is 250μm.

The lasers have thresholds currents in the 20 to 30 mA range and operate in a single frequency to output powers of 20 mW. Side mode suppression ratios of greater than 30 dB has been observed under large signal modulation at 8 Gb/s.

Small signal response of the device was measured at various bias currents. The measured response, using a sinewave modulation, is shown in Fig. 2. Bandwidths (3 dB) up to 14.0 GHz have been achieved suggesting that this device is suitable for high data rate fiberoptic transmission systems.

88CH2609-8/88/0000/0050$1.00 1988IEEE

Measurements of frequency chirp under high speed modulation is presented which show that the chirp increases with increasing data rate and is larger for laser biased below threshold than if it is biased above threshold.

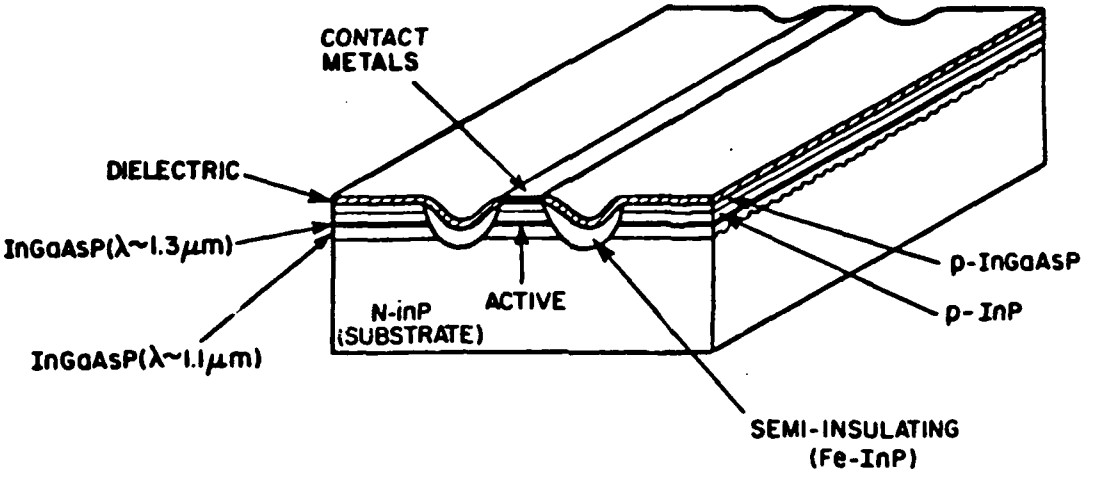

Fig.1: Laser structure

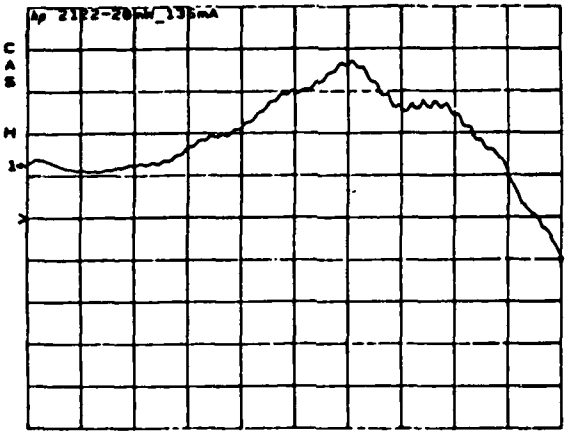

FREQUENCY (GHz): 1.5 GHz/div.

Fig. 2: Measured small signal bandwidth at 20 mW

D—4

Wideband Modulation of Semiconductor Lasers for Microwave-Multiplexed Lightwave Systems

by Robert Olshansky, Vincent Lanzisera and Paul Hill
GTE Laboratories, 40 Sylvan Road, Waltham, MA 02254

Microwave-modulation of high speed semiconductor lasers is an important new approach to realization of very wideband optical communication systems[1-5]. To achieve optimal performance lasers should be operated so that relative intensity noise (RIN) and second and third order intermodulation products (IMPs) lie below the receiver's thermal noise. This paper analyzes these three noise sources and develops the design rules for microwave modulation of semiconductor lasers. Results are presented for a 120 channel FM system operating over the 3-8 GHz band and a 20 channel FSK system operating over the 2-6 GHz band[5].

The carrier to noise ratio in channel i (CNR_i) is given as

$$CNR_i = (m_i I)^2 /2 \{ NF\ kT\ B/R + (RIN_i)\ I^2\ B + N_2\ IM_2^2 + N_3\ IM_3^2 \}$$

where m_i is the modulation depth in channel i, I is th DC photocurrent, and the three terms in the denominator represent, respectively, thermal noise of the wideband amplifier, laser RIN in channel i, and the cumulative noise in channel i due to N_2 second and N_3 third order IMPs.

Modulation Depth: Because the N microwave carriers have random phase relations the total modulation index $M = \Sigma m_i$ can exceed unity. The rms index $M_{rms} = \sqrt{\{ \Sigma\, m_i^2 \}}$ is the more appropriate measure of modulation depth. A 120 channel FM video experiment has been conducted where M=3 and $M_{rms} = 0.28$.

Relative Intensity Noise: High speed lasers biased at 5 mW can typically achieve RINs of less than -135 dB/Hz in the 2-8 GHz band. The RIN lies below the thermal noise of a wideband amplifier if the DC photocurrent is below 30 μA, as shown in Fig.(1).

Intermodulation Products: Within each information channel there are $N^2/2$ third order IMPs. As shown in Fig. (1) the cumulative effect is many dB below the thermal noise floor. Second order IMPs are signifcantly larger. They can be avoided completely by restricting the transmission

88CH2609-8/88/0000/0052$1.00 1988IEEE

bandwidth to one octave. Design rules will be described which allow the use of bandwidths of two octaves (2-8 GHz).

Figures (2) and (3), respectively, show results achieved for a 120 channel FM video tranmssion system occupying 3-8 GHz and for twenty 100 Mb/s FSK channels[5] operating in the 2-6 GHz band. These results demonstrate important new applications of high speed semiconductor lasers.

References: [1] R. Olshansky, ECOC '87, [2] Darcie et al, JLT LT-5, 1103,1987, [3] R. Olshansky and V. Lanzisera, Electron Lett. 23, 1196, 1987, [4] W. Way et al, JLT LT-5, 307, 1987, [5] P. Hill and R. Olshansky, CLEO '88.

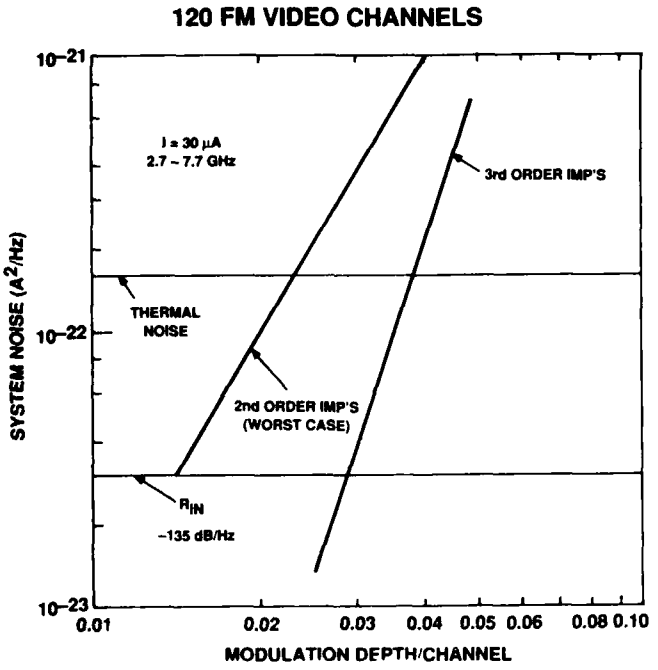

Fig 1. Noise vs modulation depth for 120 channel FM video transmission.

Fig 2. CNR and SNR versus m for 120 channel transmission system.

Fig 3. BER vs. modulation depth for twenty 100 Mb/s FSK channels tramsitted over 12 km.

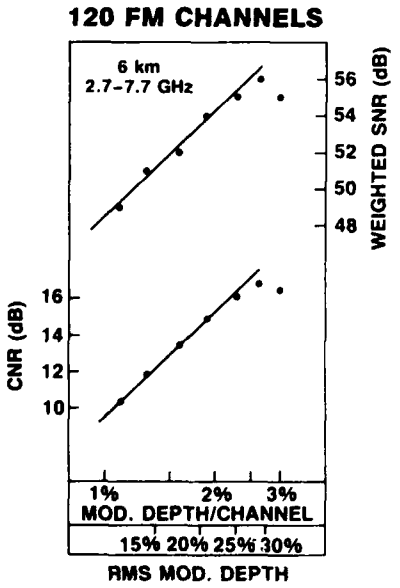

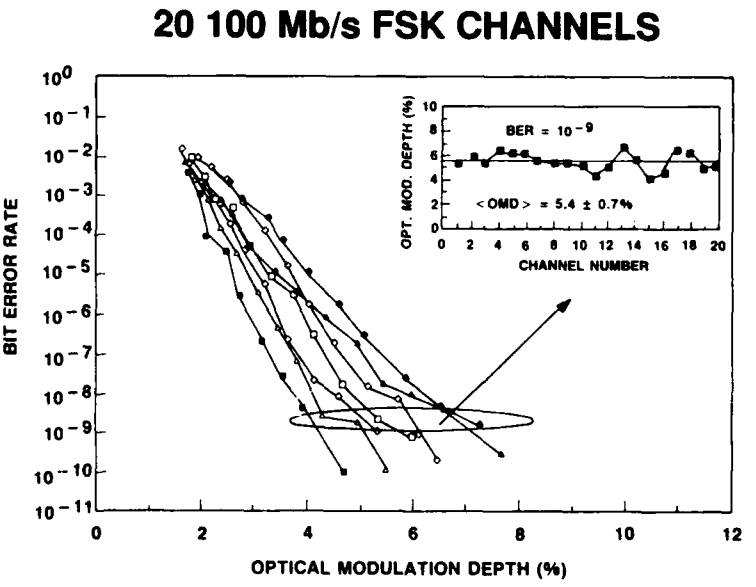

D—5

Ternary Optical Signalling Experiment for Gbit/s Systems Using Two Electrical Drive Levels

R.F. O'Dowd and D.M. Byrne, Department of Electronic Engineering, University College, Merrion Street, Dublin 2, Ireland. Tlx 93704

1. Demonstration of ternary system by controlled gain switching at gigabit/second rates using only two 1.3 µm laser drive levels as predicted in authors previous theoretical study [1].

2. To achieve the 100 Gbit/s goal [2] a combination of optical MUX with multi-level signalling may provide the ultimate solution to the transmitter limitation. We provide experimental verification of three-level optical PCM suited to optical MUX for multi-gigabit/s transmission.

3. Dynamic modeling [1] has predicted a technique to electrically control relaxation oscillations and generate Gbit/s three-level optical data to facilitate a factor 1.58 baud rate reduction. Furthermore, only two electrical drive levels were involved indicating simpler laser circuitry.
An experiment is described which verifies the theory, proving capability to control drive pulse duration with sufficient precision. This was 30 ps for the selected 1.3 µm BH laser.

4. Reliable translation from two electrical to three optical levels was implemented. The 2.5 GHz laser resonance was driven by GaAs logic and a MESFET interface (described). Streams of electrical 470 ps level-2 pulses with 230 to 400 ps level-1 pulses produced 3-level shortened optical data without pattern effects. The traces correspond with the signals predicted by the model for both a 2 level only system and the 3 level system. Estimated maximum wavelength shift was 0.1 nm. Operation was well within the facet damage limit.

5. This is the first demonstration of a three level PCM system based on two level gain switching. By applying the technique to an advanced laser with high resonance frequency and including optical tdm [3,4], which the short duty cycle data stream suits, the 100 Gbit/s goal is within reach.

6. References:

[1] D.M. Byrne and R.F. O'Dowd. "Two and Three level Optical PCM Transmitter Design for Multigigabit Systems Using a Relaxation Oscillation Technique". IEEE Vol.LT-5, 10 pp 1412 -25.

[2] C.K. Kao. "10^{12} bit/s Optoelectronics Technology". IEEE Proc. Vol. 133, J, No.3 pp 230 - 6, June 1986.

[3] G. Eisenstein et al. "Optical Time-Division Multiplexed Transmission System Experiment at 8 Gbit/s". Electronics Lett. Vol. 23, No.21 pp 1115 - 6, 8 Oct 1987.

[4] K. Habara and K. Kikuchi. "PCM of a Gain Switched LD and its Application to a High Speed Electrooptical Time Multiplexer". IEEE J. Lightwave Tech. Vol. LT-5, 10 pp 1426 - 32, Oct 1987.

88CH2609-8/88/0000/0054$1.00 1988IEEE

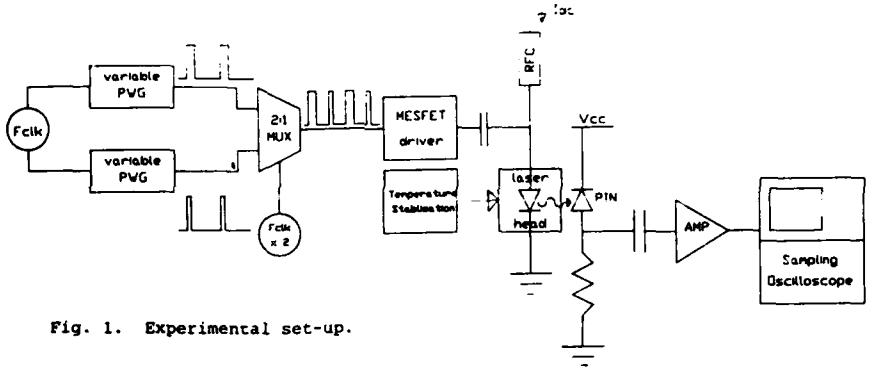

Fig. 1. Experimental set-up.

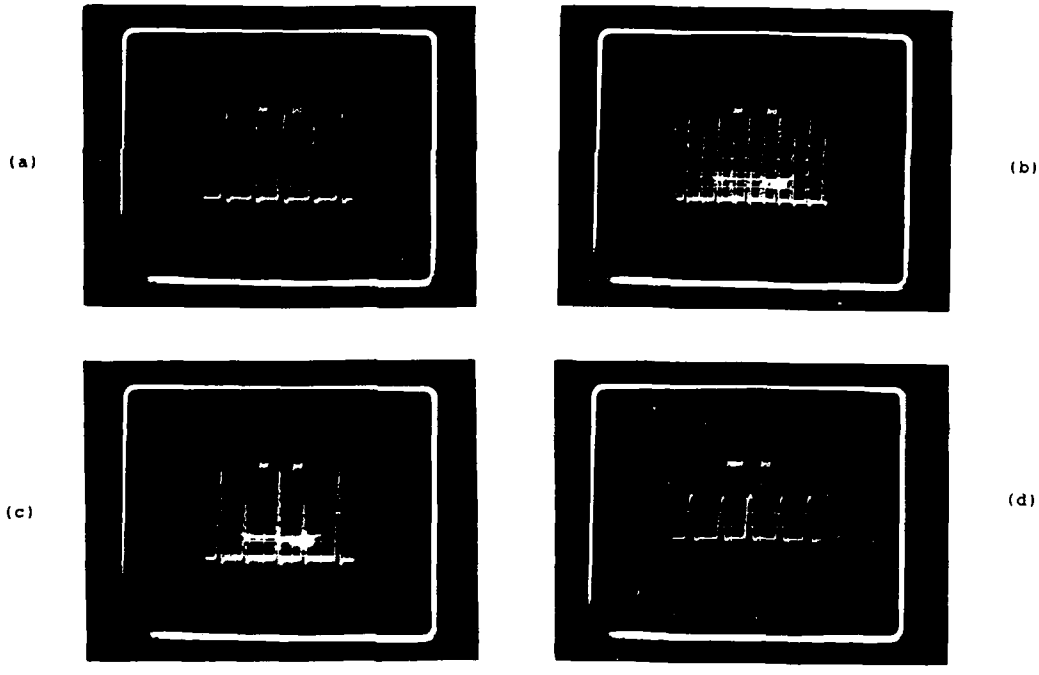

Fig. 2. Measured effect on optical output of varying electrical drive pulse duration using a 470 ps level-2 multiplexed with (a) 350 ps level-1 pulse, (b) 310 ps level-1 pulse, (c) 280 ps level-1 pulse, (d) electrical drive sequence for optimum conditions using $t_{on}(1)$ = 280 p with $t_{on}(2)$ = 470 ps

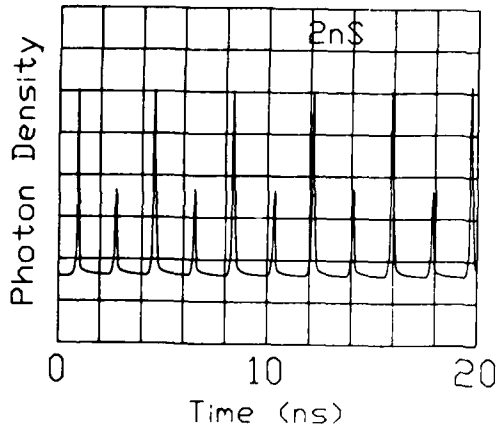

Fig. 3. Theoretically predicted photon density versus time corresponding to Fig. 2(c) showing good agreement.

Table 1: Laser diode parameters

Parameters	Values
I_{th}	45 mA
n_t	1×10^{24} m^{-3}
e.V	8.46×10^{-26} Am^{3}s
Γ	0.3
A	2.1×10^{-12} m^3/s
τ_{pA}	2.0 ps
τ_{sp}	3.0 ns
β	8×10^{-5}

Table 1. Data used in computer model [1] to generate Fig. 3

D—6

Generation of Short Optical Pulses From Laser Diodes with a Compound Multifrequency External Cavity

H. IZADPANAH
Bell Communications Research
435 South Street, Morristown, NJ 07960

We demonstrate Picosecond Optical Pulse (POP) generation from semiconductor laser diodes operating in a novel external fiber cavity in which the cavity length and its end reflectivity are easily adjustable.

One method of obtaining short optical pulses from lasers, via mode-locking or otherwise, is to impose a coupled external cavity. Lensed, single-mode fiber cavities with partially reflecting ends have been employed successfully for mode-locking and pulse generation[1,2]. In this paper, we present a novel approach to generate POPs from laser diodes operating in an external fiber cavity whose reflectivity is continuously variable between 0% and 100%.

The proposed cavity arrangement is based on the use of a looped directional coupler. For illustration a 2x2 fiber optic directional coupler of zero excess loss with coupling coefficient K has been assumed. A closed loop of length L_l is formed by connecting the coupler's output ports shown schematically in Fig. 1(a). When a pulse from the laser is launched into the coupler, its power splits into two propagating waves that counter-rotate around the loop. After one loop-delay time, both waves return to the coupling region where further power exchange takes place between the two guides. As a result, a fraction of the original pulse power is returned to the input port, providing a *virtual reflector* or a partially reflecting *mirror* positioned at coupling region MM'. Employing standard coupled mode theory[3] for a fused biconnical taper fiber optic directional coupler, we have calculated the magnitude of the reflected field Er, the reflected power Pr, the output field Eo, and the output power Po as a function of coupling lenght shown in Fig. 1(b). It is seen that the magnitude of reflected power Pr is adjustable between 0% to 100% and is controlled by the coupling length KL. The value of KL can be adjusted mechanically for a passive coupler, or electrically for an active electrooptic directional coupler switch. In the above configuration, the coupling region MM' between the two fibers acts as a discontinuity region for the circulating laser pulse. Then the fibers on either side can act as independent resonant cavities accommodating different sets of standing-waves depicted in Figure 1(c). Once the applied modulating frequency f_m is made equal to any of the several possible cavity resonances, fundamental or harmonics, the laser is selectively locked to the relevant feedback required for POP generation[2]. The loop delay time, i.e. the value of f_m, can be adjusted by either changing the required loop fiber length or by switching the loop into different pass lengths via additional fiber delay lines[4].

In the experiment, a lensed fiber 135 cm long was used for L_c connected to the coupler's 18 cm long arm. A loop 37 cm long was formed by interconnecting the coupler's output arms. An InGaAsP/InP BH laser with high/low reflectivity facets was used and biased at 85% of its threshold with a sinusoidal drive current for modulation. The detector was a pig-tailed InGaAs p-i-n photodiode. Some recorded POP waveforms at the resonant frequencies of fundamentals at (a) f_{1mc} = 130 MHz, (b) f_{2c} = 73.6 MHz, and (c) f_{ml} = 538 MHz, and harmonics at (d) $5\times f_{1mc}$ = 652 MHz, and (e) $5\times f_{2c}$ = 365 MHz shown in Fig. 2.

In conclusion, we have proposed and experimentally demonstrated the generation of discrete multi-frequency of POPs from laser diodes when synchronized to the resonant frequencies of a compound external cavity. The new arrangement exhibits a rich variety of resonant frequencies and permits the cavity length and its end reflectivity to be readily adjusted.

[1] Eisenstein, G., et al; Electron. Lett. 21, 173(1985).
[2] Izadpanah, H.; Electron. Lett. 24, 137(1988).
[3] Yariv, A., and Yeh, P., ; Optical Waves in Crystals, J. Wiley (1984).
[4] Macdonald, R. I.; J. Lightwave Techn. LT-5, No. 6, 856(1987).

88CH2609-8/88/0000/0056$1.00 1988IEEE

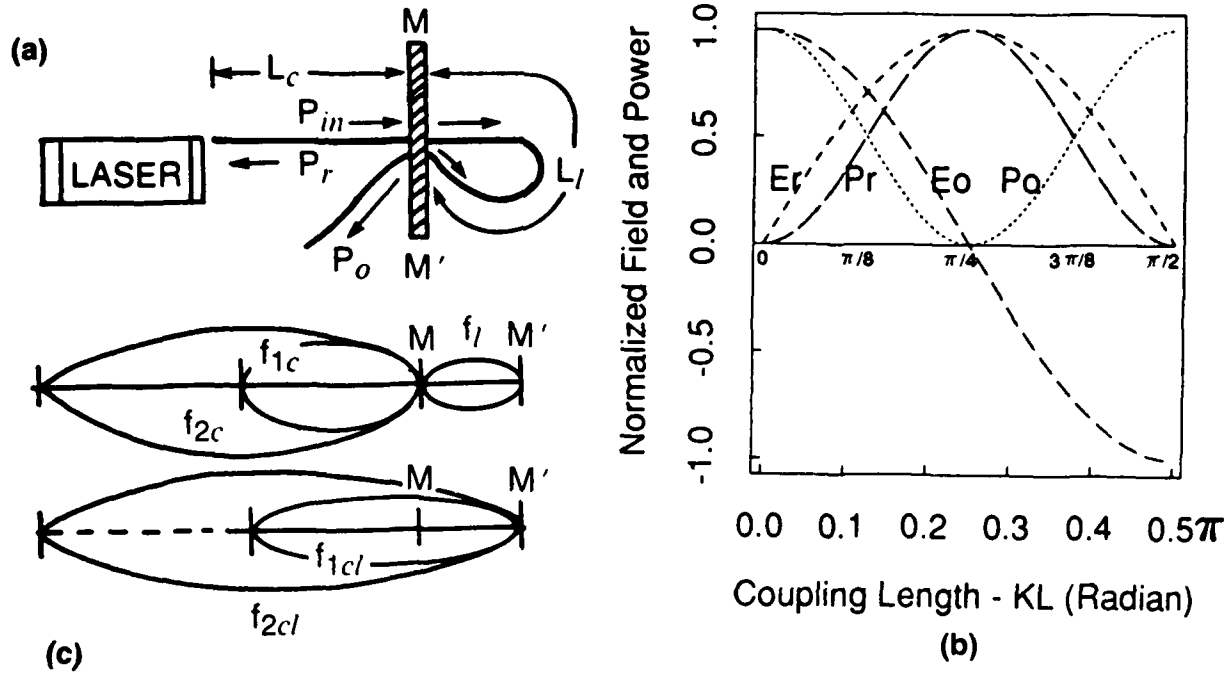

Fig. 1. Compound fiber external cavity/laser structure (a), calculated reflected and output fields and powers (b), and some of the possible standing-wave resonances (c).

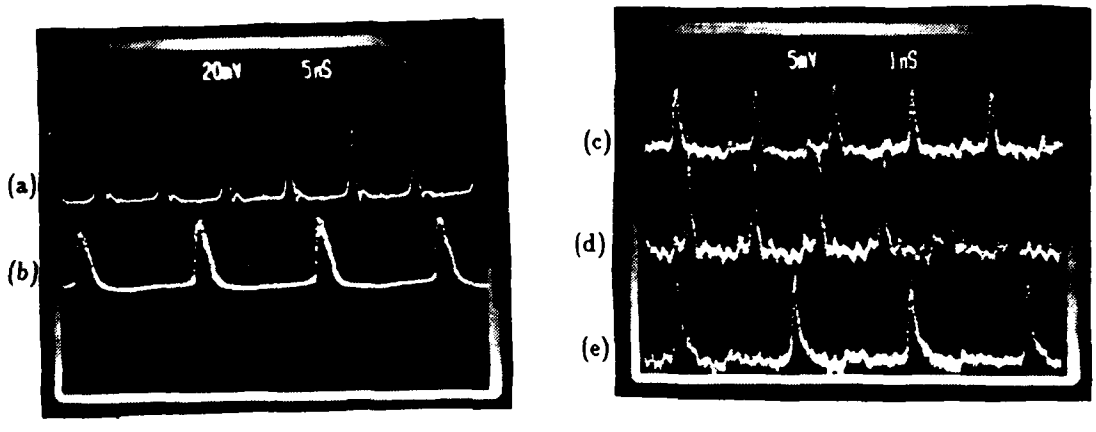

Fig. 2. Recorded waveforms of POPs at some fundamentals (a), (b), (c), and harmonic resonant frequencies (d), and (e).

TUESDAY, August 30, 1988

Session E: Visible and Infrared

E—1

CW Operation of Mode-Stabilized AlGaInP Visible Light (λ_L = 646nm) Semiconductor Laser Diodes with a MQW Active Layer

Seiji KAWATA. Kenichi KOBAYASHI. Hiroaki FUJII. Isao HINO*
Akiko GOMYO. Hitoshi HOTTA and Tohru SUZUKI
Opto-Electronics Research Laboratories. NEC Corporation
4-1-1. Miyazaki. Miyamae-ku. Kawasaki-shi. 213. Japan
*Compound Semiconductor Device Division. NEC Corporation
1753. Shimonumabe. Nakahara-ku. Kawasaki-shi. 211. Japan

$(Al_xGa_{1-x})_{0.5}In_{0.5}P$ is an extremely attractive material for 600nm-band semiconductor laser diodes(LDs). In this alloy system. there are two methods to shorten the lasing wavelength. One is increasing the amount of aluminum for an active layer. So far. LDs operating at 662nm(298K)[1] and 584nm(77K)[2] were reported. The other method is employing a (multi-)quantum-well ((M)QW)-structure for an active-layer. CW operation was reported only for a gain-guided-MQW LD[3] with a 668nm wavelength. This paper reports first mode-stabilized short-wavelength(646nm) AlGaInP LDs with an MQW active layer.

Laser wafers were grown by three-step low-pressure metalorganic vapor phase epitaxy. In Fig.1. the laser structure and the band energy diagram are shown. The active layer consists of eight 35Å thick $Ga_{0.5}In_{0.5}P$ wells. separated by 40Å thick $(Al_{0.5}Ga_{0.5})_{0.5}In_{0.5}P$ barriers. To stabilize the transverse-mode. mesa stripes. formed by selective chemical etching. were buried by a GaAs light absorbing layer. A 40Å thick $(Al_{0.15}Ga_{0.85})_{0.5}In_{0.5}P$ etching stopper was inserted between p-cladding layers. in order to make mesa-etching much easier and more controllable.

Room temperature(25°C) CW operation was achieved with 55mA(4.4kA/cm²) typical threshold current. The 19mW maximum light output power was obtained for LDs with as-cleaved mirror-facets. as shown in Fig.2. The lasing spectrum at 5mW output power is shown in Fig.3. The lasing wavelength was 646nm. This is 17nm(which corresponds to 50meV in photon energy) shorter than the wavelength for conventional DH lasers with a 0.05μm thick $Ga_{0.5}In_{0.5}P$ active layer grown under the same condition as the present MQW laser. The merit is a direct result of employing an MQW structure. Figure 4 shows the far field pattern. Fundamental transverse-mode operation has been achieved. at least up to 15mW. Beam divergence angles. parallel and perpendicular to the junction plane. were 7° and 33°. respectively.

88CH2609-8/88/0000/0060$1.00 1988IEEE

References
1) K. Kobayashi. et al.,Electron.Lett.21(24),pp1162-1163(1985)
2) I. Hino, et al.,Appl. Phys. Lett..46(1),pp7-9(1985)
3) M. Ikeda. et al.. Appl. Phys. Lett., 50(16),pp1033-1034(1987)

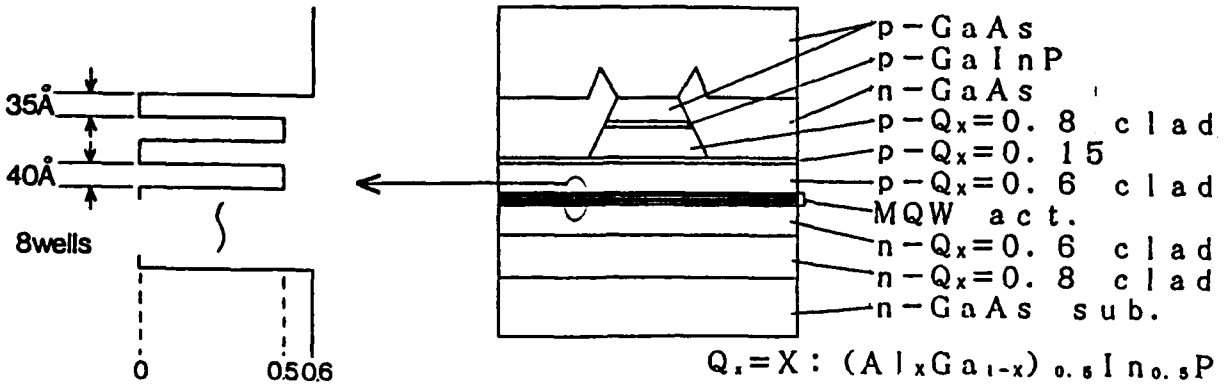

Fig.1. Cross-sectional view and band diagram of an AlGaInP transverse-mode stabilized laser with an MQW active layer

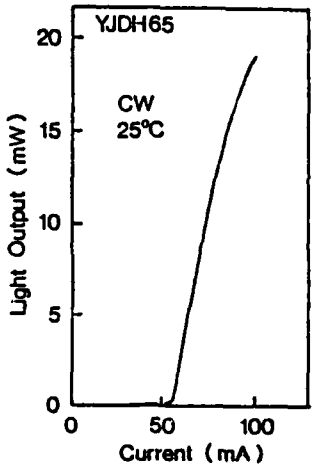

Fig.2. CW light-output vs. injection-current characteristics at 25°C

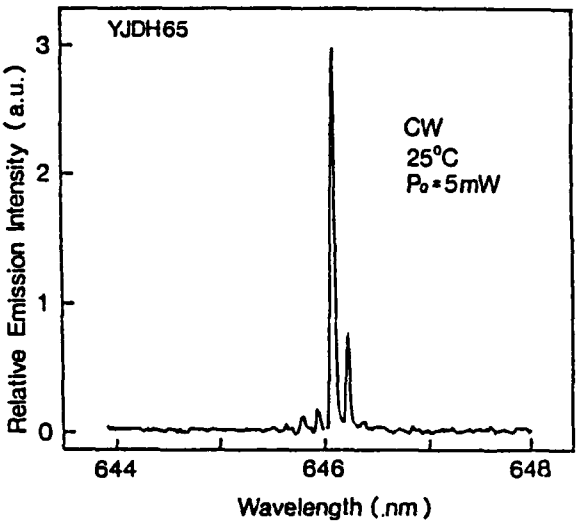

Fig.3. CW emission spectrum at 25°C

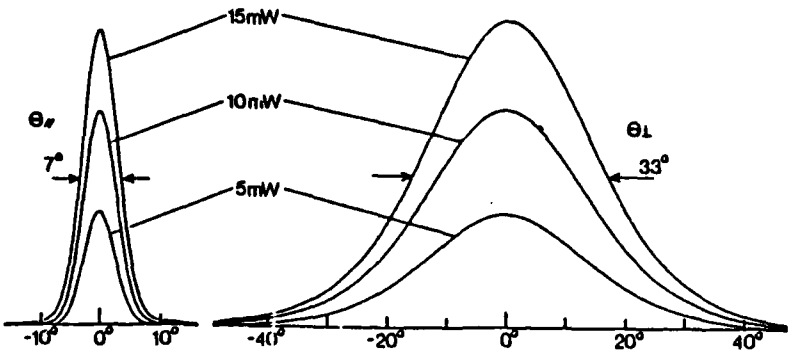

Fig.4. Typical CW far-field pattern

E—2

Highly Reliable InGaP/InGaAlP Visible Inner Stripe Lasers with 667nm Lasing Wavelength

Masayuki Ishikawa, Hajime Okuda, Hideo Shiozawa,
Kazuhiko Itaya, Gen-ichi Hatakoshi, Yukio Watanabe,
Koichi Nitta and Yutaka Uematsu

Research and Development Center, Toshiba Corporation,
1, Komukai Toshiba-cho Saiwai-ku, Kawasaki 210, Japan

1)Objective: The objective of this paper is to realize highly reliable InGaP/InGaAlP visible inner stripe (IS) lasers with optimized Al composition x, carrier concentration and thickness h of cladding layers and optimized thickness d of active layer.

2)Brief background: InGaP/InGaAlP visible lasers are promising light source for use in optical disks, laser beam printers and barcode readers. Room temperature cw operation was reported with gain-guided lasers grown by metalorganic chemical vapor deposition (MOCVD) [1]-[3]. Taking acount of practical applications, highly reliable InGaP/InGaAlP visible inner stripe lasers are indispensable.

3)Technique: We have optimized InGaP/InGaAlP inner stripe lasers by using computer simulation.

4)Results: Figure 1 shows the schematic structure of InGaP/InGaAlP inner stripe laser fabricated by two step MOCVD. The stripe width is 7μm and the cavity length is 300μm. Figure 2 shows relative threshold current density J_{th} and characteristic temperature T_0 versus Al composition x of $In_{0.5}(Ga_{1-x}Al_x)_{0.5}P$ cladding layers. It is found that J_{th} decreases and T_0 increases as x increases. In the region of x>0.7, it is difficult to obtain high carrier concentration of p-cladding layer because Zn is used for p dopant. In the region of x=0.7, the optimized p-carrier concentration was 4×10^{17} cm^{-3} which corresponded to maximum temperature of 80-90 °C for cw operation. So x=0.7 is considered to be the most suitable for cladding layer. Figure 3 shows the results of computer simulation of the threshold current versus cladding layer thickness as the parameter of active layer thickness. It is found that cladding layer thickness giving the lowest threshold current varies with the active layer thickness. The threshold current of 65-70mA was obtained experimentally in the region of 0.05-0.06μm active layer thickness and 0.8 μm cladding layer thickness. Temperature dependence of I-L curve is shown in Fig.4. The maximum temperature for cw operation was 90°C. Figure 5 shows the degradation rate of the lasers with and without Al_2O_3 facet coating. Facet coating is very effective to suppress the gradual degradation. Figure 6 shows the aging characteristics of lasers with facet coating at 60°C, 3mW. Lasers tested have all been operating for about 1000h without significant degradation. In the case of 50°C, 3mW, lasers have been stably operating for more than 2500h.

5)Impact: It is very new that optimized IS lasers with InGaAlP cladding layers have been realized and lasers tested at 60°C, 3mW have all been operating for about 1000h without significant degradation.

6)References: [1] M.Ishikawa et al.,Appl.Phys.Lett.48,207(1986).
[2] M.Ikeda et al.,Appl.Phys.Lett.51,1572(1986).
[3] A.Gomyo et al.,Electron.Lett.23,85(1987).

88CH2609-8/88/0000/0062$1.00 1988IEEE

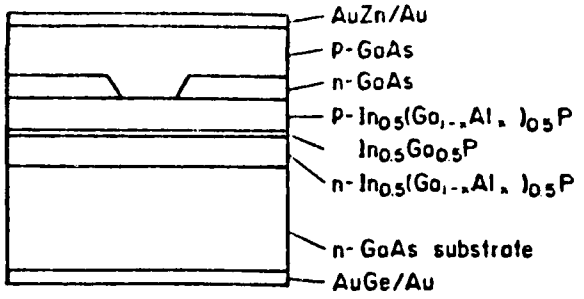

Fig.1 Shcematic structure of IS laser

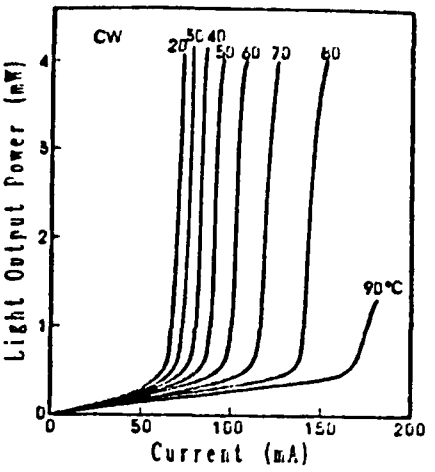

Fig.4 Temperature dependence of I-L curve

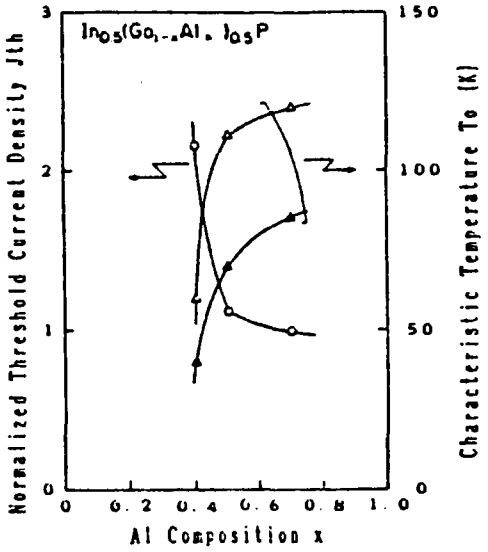

Fig.2 Threshold current and characteristic temperature versus Al composition

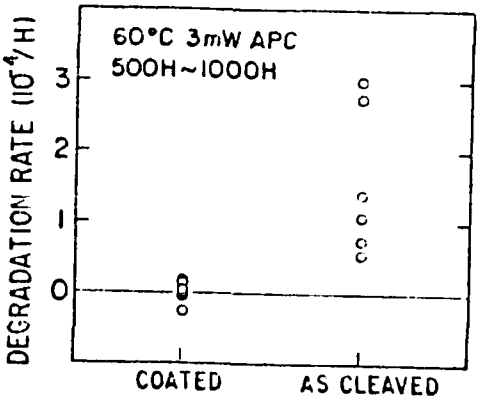

Fig.5 Facet coating effect on degradation rate.

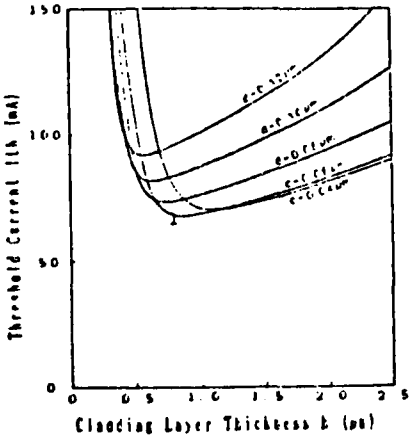

Fig.3 Threshold current versus p-cladding layer thickness

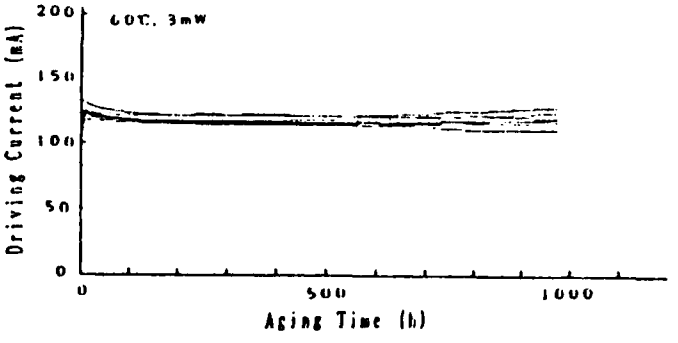

Fig.6 Aging characteristics of 60 C,3mW

E—3

660nm GaInAsP/AlGaAs DFB Lasers Grown on GaAs by LPE

Katsumi KISHINO and Te-Ho CHONG
Dept.of Electrical and Electronics Eng., Sophia University
7-1, Kioi-cho, Chiyoda-ku, Tokyo 102, Japan

Visible light distributed feedback (DFB) semiconductor lasers with as much shorter emission wavelength as possible are very attractive as light sources for optical information processing and measurement. Quite recently, DFB lasers emitting at 760-770nm have been fabricated using AlGaAs compound[1]-[2]. However DFB lasers emitting at the wavelength less than 700nm was not realized. We report the first successful lasing operation of the visible light GaInAsP/AlGaAs DFB laser emitting at 660nm in wavelength. The DFB mode oscillation in single longitudinal mode was observed in the temperature range from 22°C to -24°C, with the smaller wavelength shift of 0.04nm/deg.

Figure 1 shows a cross-sectional SEM photograph of the GaInAsP/AlGaAs DFB laser prepared by two-step liquid phase epitaxy (LPE). In the first step of LPE, n-$Al_{0.7}Ga_{0.3}As$ cladding $Ga_{0.52}In_{0.48}As_{0.03}P_{0.97}$ active($\sim$0.15μm), $Al_{0.7}Ga_{0.3}As$ barrier($\sim$0.16μm) and p-$Ga_{0.51}In_{0.49}P$ guiding($\sim$0.2μm) layers were successively grown on a n-type (100)GaAs substrate. The growth condition for the GaInAsP/AlGaAs DH laser is discribed in detail in ref.[3]. A third-order grating with 2910 Å period was formed along <01$\bar{1}$> crystal direction on the p-GaInP guiding layer, by use of holographic photolithography using a 325 nm line of He-Cd laser and then wet etching. In the second step of LPE, p-$Al_{0.7}Ga_{0.3}As$ cladding, p-GaAs cap layers were grown on the corrugated GaInP. To supress the deformation of grating, the epitaxial growth was done at lower temperature of 680°C and with higher cooling rate of 5 °C/min. One-side cleaved facet of the DFB laser was coated with an Si_3N_4(n=1.84) film to about $\lambda/4$ thickness ($\sim$87nm) by RF sputtering, reducing the reflectivity as small as 2%.

Figure 2 shows an example of lasing spectra for various pulsed current levels observed for the oxide stripe DFB laser 12μm wide, 260μm long, at 22°C. Single longitudinal mode lasing was maintained in the current range up to 1.25 times the threshold, with the maximum light output of 5mW. From the lasing wavelength of 660.3nm and the grating period of Λ=2910 Å, the equivalent refractive index of the DFB structure was evaluated to be 3.40.

Figure 3 shows the temperature dependence of the threshold current and the lasing wavelength. The DFB mode oscillation was observed in the temperature range from 22°C to -24°C. The lasing wavelength varied with temperature by 0.04nm/deg, which was much smaller than that for the gain shift observed in a conventional GaInAsP/AlGaAs DH laser, of 0.17nm/deg[3]. At -4°C, the DFB lasing wavelength matched to the gain peak wavelength, where the threshold current was minimum at $\sim$700mA.

In summary, GaInAsP/AlGaAs DFB lasers with third order grating emitting at 660nm was fabricated by two step LPE for the first time.

88CH2609-8/88/0000/0064$1.00 1988IEEE

References
[1] T.OHATA, K.HONDA, S.HIRATA, K.TAMAMURA, H.ISHIKAWA, K.MIYAHARA, Y.MORI, C.KOJIMA: J. Crystal Growth, 77,637,1986.
[2] Y.NAKANO, Y.LUO, K.TADA: Electron Lett. Vol.23,1343,1987.
[3] K.KISHINO, A.HARADA, Y.KANEKO: IEEE J.Quantum Electron.,QE-23,180,1987.

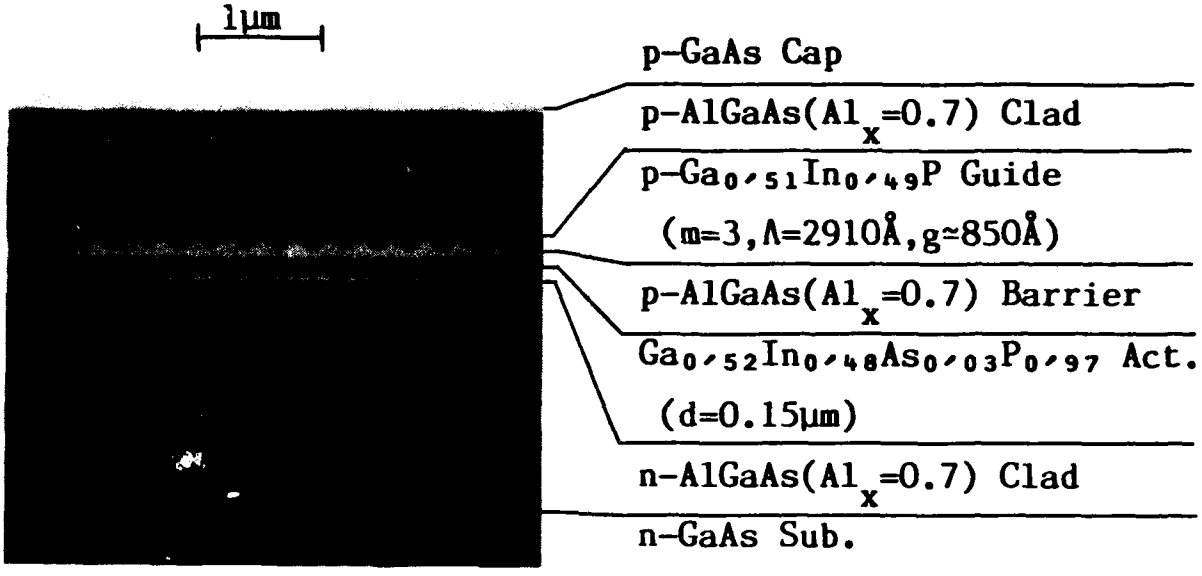

Fig.1 A cross-sectional SEM photograph of the GaInAsP/AlGaAs DFB laser.

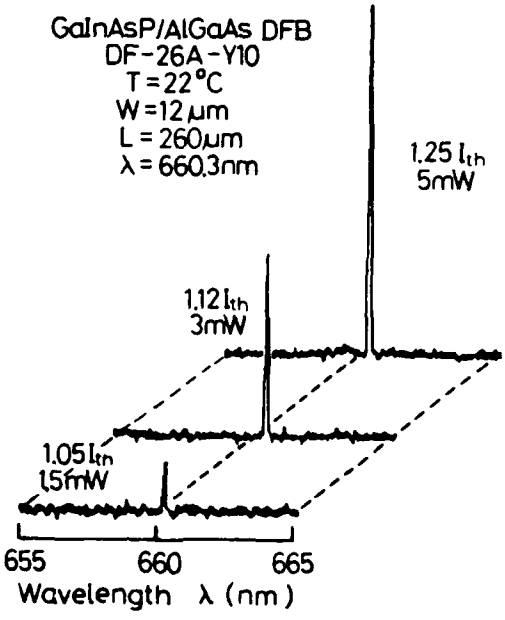

Fig.2 Dependence of lasing spectrum at 22°C on injection current.

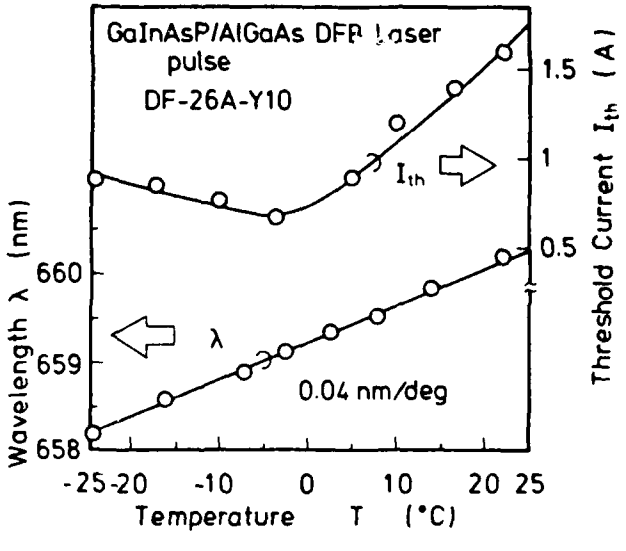

Fig.3 Dependence of lasing wavelength and threthold current on heatsink temperature.

E—4

GaInAsSb/AlGaAsSb Double Heterostructure Lasers Operating at Mid-Infrared Wavelengths

J. L. Zyskind, C. Caneau*, T. E. Glover†, J. W. Sulhoff, C. A. Burrus,
J. C. Centanni, A. G. Dentai and M. A. Pollack
AT&T Bell Laboratories
Crawford Hill Laboratory
Holmdel, NJ 07733

Ultra-low-loss optical fiber telecommunications systems operating in the mid-infrared will require efficient, low threshold room temperature diode lasers operating at wavelengths greater than 2 μm. Room temperature pulsed operation of simple GaInAsSb/AlGaAsSb double heterostructure lasers grown by liquid phase epitaxy (LPE) on GaSb substrates has been demonstrated at 2.2 μm[1] and threshold current densities as low as 3.5 kA/cm^2 have been reported.[2]

Substantial improvements in the performance of broad-area GaInAsSb-based lasers grown by LPE were achieved through better optical confinement. Lower threshold current densities and higher quantum efficiency were achieved by adding more Al to the AlGaAsSb confining layers to decrease their refractive indices. Because of the low solubility of As in the Al-Ga-As-Sb growth solutions, the lattice constants of these Al-rich layers are positively mismatched relative to the substrate and to the active layer by more than 0.2%. To avoid performance degradation associated with this interface strain, thin intermediate cladding layers ($Al_{0.34}Ga_{0.66}As_{0.04}Sb_{0.96}$) were grown between the active layer and the two Al-rich cladding layers ($Al_{0.40}Ga_{0.60}As_{0.04}Sb_{0.96}$). This structure is shown in Figure 1.

The modified double heterostructure lasers exhibited broad area threshold current densities as low as 1.7 kA/cm^2 at room temperature.[3] We have studied the characteristics of these lasers as a function of temperature. The external quantum efficiencies range from 9-10% per facet at 80K to 2.5% per facet at room temperature (Figure 2) and the characteristic temperature, T_O, for the thresholds is 61K.

The threshold current densities of these lasers are much lower and the quantum efficiencies higher than those predicted[4] using theoretical estimates of the Auger coefficients. We will compare these results to the earlier predictions and discuss the prospects, in light of these data, for the operation of lasers with GaInAsSb active layers at even longer wavelengths.

[1] A. E. Bochkarev, L. M. Dolginov, A. E. Drakin, L. V. Druzhina, P. G. Eliseev, and B. N. Sverdlov, Sov. J. Quantum Electron., *15*, 869 (1985) and C. Caneau, A. K. Srivastava, J. L. Zyskind, J. W. Sulhoff, A. G. Dentai and M. A. Pollack Electron. Lett., *21*, 815 (1985).

[2] C. Caneau, A. K. Srivastava, A. G. Dentai, J. L. Zyskind, C. A. Burrus and M. A. Pollack, Electron. Lett., *22*, 992 (1986) and references therein.

[3] C. Caneau, J. L. Zyskind, J. W. Sulhoff, T. E. Glover, J. Centanni, C. A. Burrus, A. G. Dentai and M. A. Pollack, Appl. Phys. Lett., *51*, 764 (1987).

[4] A. Sugimura, IEEE J. Quantum Electron., *QE-18*, 352 (1982).

*Presently at Bell Communications Research, Red Bank, NJ
†Presently at Department of Physics, Univ. of California at Berkeley

88CH2609-8/88/0000/0066$1.00 1988IEEE

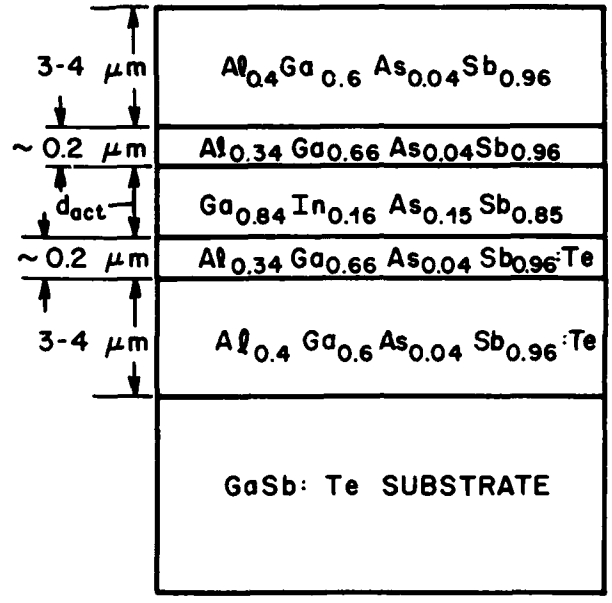

FIGURE 1 - Modified Double Heterostructure

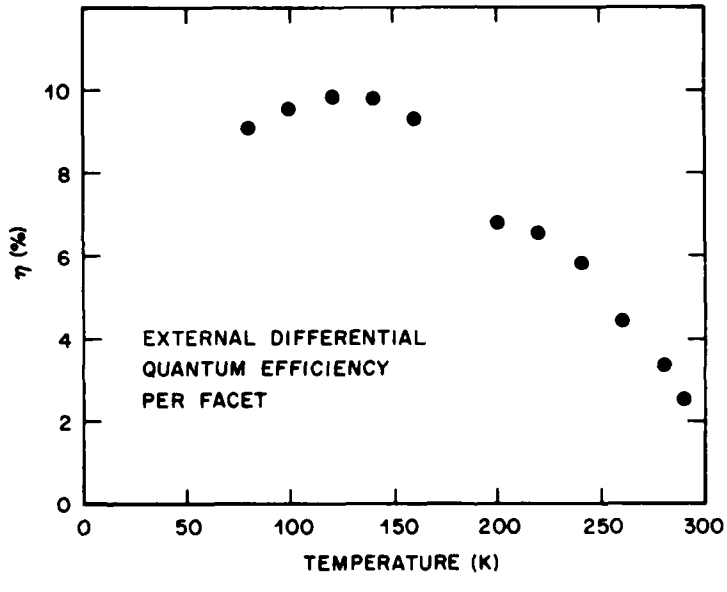

FIGURE 2 - Quantum Efficiency As A Function Of Temperature

E—5

PbEuTe Laser with 4-6 μm Wavelength Developed Using Hot-Wall Epitaxy

H. Ebe, Y. Nishijima, and K. Shinohara
Infrared Devices Laboratory, Fujitsu Laboratories Ltd.
10-1 Morinosato Wakamiya, Atsugi 243-01, Japan

We developed PbEuTe lasers operating at over 200K with a thermoelectric cooler by using hot-wall epitaxy (HWE).

Lead chalcogenide lasers with wavelengths between 4 μm and 20 μm show promise as light sources in laser gas sensing systems. These conventional lasers operate below 77K using cryogenic coolers. To make such systems compact, however, the laser must operate above 200K and use a thermoelectric cooler.

To raise the laser operation temperature, we used HWE to develop high-quality $Pb_{1-x}Eu_xTe$ thin-film crystals as the laser material. HWE is conventionally used in crystal growth at low substrate temperatures. The PbTe substrate was heated to 300° C in our work.

Controlling the temperature of PbTe, Eu, and Te_2 sources enables the growth of $Pb_{1-x}Eu_xTe$ films with high mobility between 10^3 and 10^4 $cm^2/(vs)$ and carrier concentration between 10^{17} and 10^{18} cm^{-3}.

Using HWE, we fabricated $Pb_{1-x}Eu_xTe$ double-heterojunction lasers with wavelengths between 5.5 μm and 4.0 μm at 77K, which correspond to the contents of active regions between x=0 and x=0.015. Lasers are tunable by controlling the operating temperature. Figure 1 shows the wavelength dependence on the temperature of $Pb_{0.98}Eu_{0.02}Te/PbTe/Pb_{0.98}Eu_{0.02}Te$ DH lasers. The laser operates in pulses with wavelengths between 6.0 μm and 4.1 μm, covering the absorption lines of CO (4.7 μm) and NO (5.3 μm) and corresponding to operating temperatures between 20 K and 220 K. Figure 2 shows the threshold current density vs. the temperature of the laser. The value of the laser at 77K was 0.5K A/cm^2, lower than values for similar infrared PbSnTe lasers. We believe this is because bandstructure of the PbEuTe semiconductor is type I[1], similar to that of AlGaAs, enabling carriers to be contained in the DH laser active region, whereas that of PbSnTe is type I'[2], in which carriers are hard to confine. This low value enabled lasers to operate at extremely high temperatures. The highest temperature in pulse operation was 243K, high enough to operate them using thermoelectric coolers. Figure 3 shows laser light power vs. current pulse. Laser power exceeded 200 μW up to 210K, making the laser applicable as a light source for a gas sensor.

References

1) A. Ishida, S. Matsuura, M. Mizuno, and H. Fujiyasu, Appl. Phys. Lett. 51 (7), 478, (1987)
2) K. Murase, S. Shimomura, S. Takaoka, A. Ishida, and H. Fujiyasu, Superlattices and Microstructures, 1 (2), 177, (1985)

88CH2609-8/88/0000/0068$1.00 1988IEEE

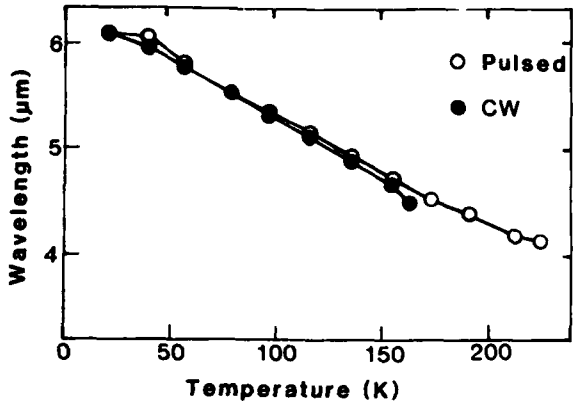

Fig. 1 Wavelength dependence on temperature

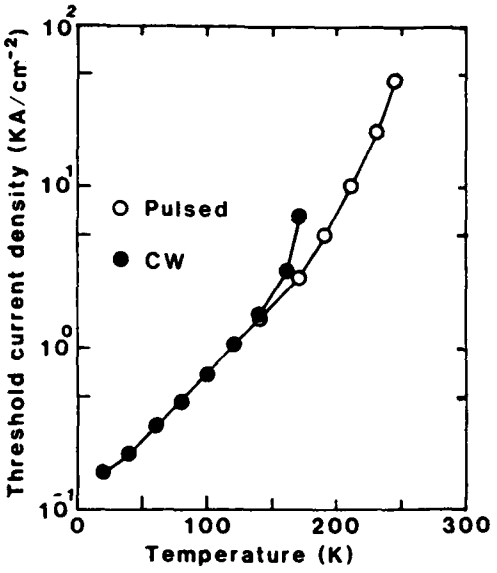

Fig. 2 Threshold current density vs. temperature

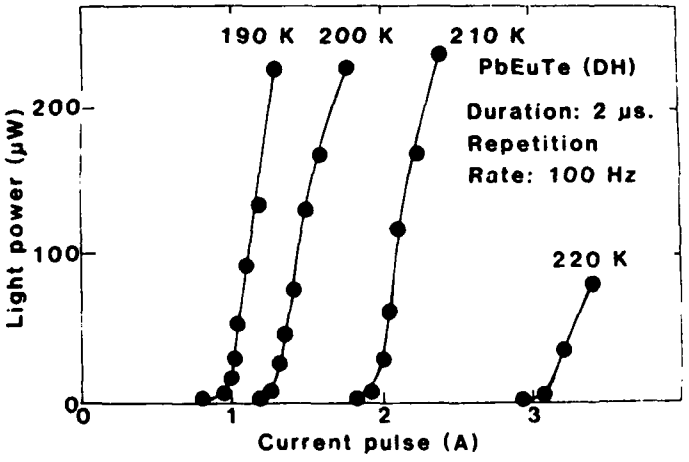

Fig. 3 Light power vs. current pulse of a PbEuTe DH laser, operating with a thermoelectric cooler, at different temperatures.

E—6

PbSnSe Grating Coupled Emission Lasers and Metal Clad Distributed Feedback Lasers

Y. Shani[a)], A. Katzir,
School of Physics and Astronomy, Tel Aviv University, Israel

M. Tacke, H.M. Preier[b)]
Fraunhofer Institut fur Physikalische Messtechnik, Freiburg, W. Germany

a)Present address: AT&T Bell Laboratories, Murray Hill, NJ 07974
b)Present address: Spectra Physics, Laser Analytics Division, Bedford, MA 01730

Summary:

Lead salt lasers are commonly used as tunable radiation sources for ultrahigh resolution spectroscopy and for infrared heterodyne detection. In these applications, a low divergence far field pattern and a cw single mode operation are desired.

Lead salt injection lasers with cleaved Fabry Perot (FP) resonators emit widely divergent beams of ~80° perpendicular to the layers [1]. High power lenses or mirrors are therefore required to collimate their radiation. This wide far field distribution can be reduced by coupling the radiation through a broader waveguide region. Grating Coupled Emission (GCE) lasers are useful for that purpose [2].

The FP lasers suffer also from multimode emission and mode hopping which limit their performance. The common and preferable way to obtain control of these longitudinal modes is by using Distributed Feedback (DFB) and Distributed Bragg Reflector (DBR) lasers. These corrugated lasers had already been demonstrated with lead salts, but it was only lately that cw operation, of DBR lasers, above 77K was achieved [3].

The devices: GCE and DFB lasers are described in Fig. 1 and 2, respectively. They were $Pb_{1-x}Sn_xSe/Pb_{1-x-y}Eu_ySn_xSe$ double heterostructure stripe geometry diode lasers grown by molecular beam epitaxy. See Ref. [3] for more details.

The GCE lasers were based on the DBR structure. They had an active injected region and a passive corrugated region with a periodicity of 1.56 μm, in order to provide second order Bragg reflection. These lasers were mounted upside down, with the substrate facing the cold stud, in order to be able to detect the radiation (from the grating region) which was emitted in the perpendicular direction.

The DFB lasers had a periodic constant of 0.78 μm. These lasers had a thin top cladding layer, and a metal contact layer which was put directly on top of the gratings. They were cleaved at one facet and sawed at the other, in order to suppress the competitive FP modes.

The GCE lasers had a multimode emission with a spectral width of ~0.1 μm. They operated in cw mode up to 60K and had a narrow far field pattern (perpendicular to the gratings), ~5° for multimode emission and ~2° for single mode operation, see Fig. 3. These results are in reasonable agreement with the theoretical values - 1° for single mode, when taking into account the experimental error of 1°.

The DFB lasers operated in cw mode up to 90K and in the pulse mode up to 100K. They were unique in their low tuning rate with injection current, 4 cm^{-1}/A , and in that they withstood high cw injection currents, 2A, without damage. The lasers had at a certain heat sink temperature a continuous tuning single mode spectrum, see Fig. 4, while at other temperatures, 'central wavelength', around which the mode are concentrated, were obtained.

Here we report the first lead salt GCE lasers. These devices, with the low divergence far field pattern, may be useful especially for coupling the laser light to optical fibers. Our DFB lasers, with the low tuning rate and the high cw operation temperatures (above 77K), may be useful for heterodyne detection where a small wavelength dependence on temperature or current fluctuation is required.

The authors wish to thank Dr. Norton for growing the epitaxial layers.

88CH2609-8/88/0000/0070$1.00 1988IEEE

References:

[1] Y. Shani, A. Hardy, E. Kapon and A. Katzir, IEEE J. Quantum Electron. *QE-20*, 1267-1270 (1984).

[2] R. D. Scifres, R. D. Burnham and W. Streifer, Appl. Phys. Lett. *26*, 48-50 (1975).

[3] Y. Shani, A. Katzir, K.-H. Bachem, P. Norton, M. Tacke and H.M. Preier, Appl. Phys. Lett. *48*, 1178-1180 (1986).

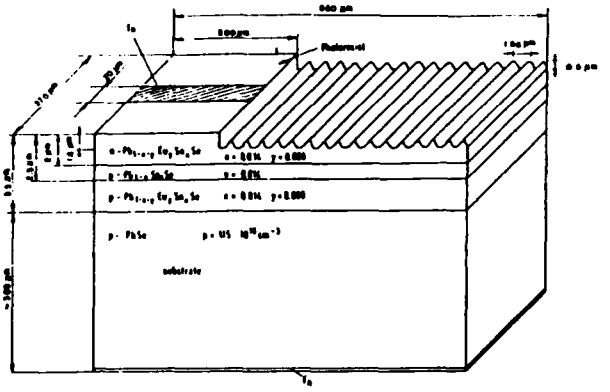

Fig. 1. Schematic description of the grating coupled emission lasers.

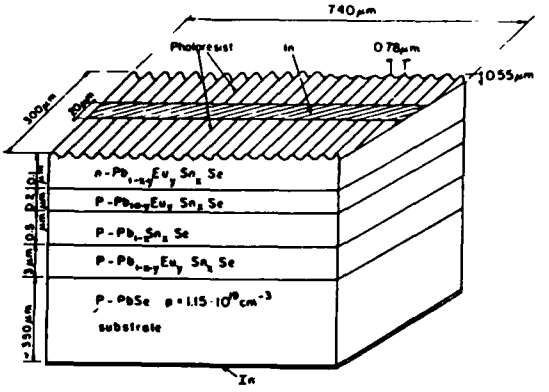

Fig. 2. Schematic description of the distributed feedback lasers.

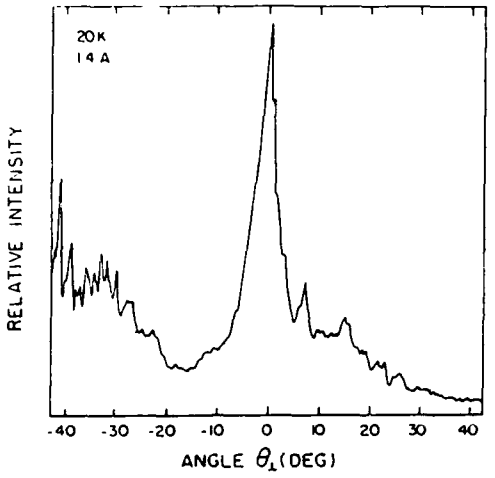

Fig. 3. The far field pattern, perpendicular to the grating section of the GCE laser.

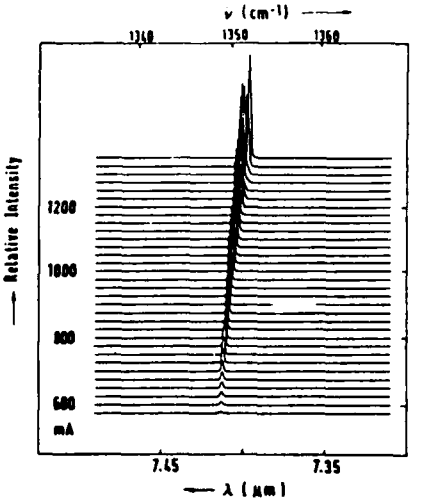

Fig. 4. The emission of the DFB laser, operated cw mode, as a function of the injection current (25 mA steps) at 60K.

Session F: Quantum Wells II

F—1

Patterned Quantum Well Semiconductor Lasers and Laser Arrays Grown by Molecular Beam Epitaxy

E. Kapon, C. P. Yun, J. P. Harbison, D. M. Hwang and N. G. Stoffel
Bell Communications Research
Red Bank, NJ 07701

We report the fabrication and the characterization of low-threshold GaAs/AlGaAs patterned quantum well (PQW) lasers grown by molecular beam epitaxy (MBE) on grooved GaAs substrates. The nonplanarity of the substrate gives rise to lateral variations in the thickness of the quantum well (QW) active region, which in turn results in lateral patterning of the effective bandgap [1]. This bandgap patterning provides the lateral carrier confinement required for low-threshold and high-efficiency laser operation.

GaAs/AlGaAs PQW lasers were fabricated by growing a graded index, separate confinement heterostructure (GRIN-SCH) QW laser structure on grooved GaAs substrate using MBE. The resulting structure is depicted schematically in Fig. 1. A ~1μm wide, 70Å thick QW stripe which is laterally bounded by thinner (~40Å) QW sections is formed at the center of the structure. The higher effective bandgap of the thinner QW sections provides lateral carrier confinement to the 1μm wide, thicker QW active region. This carrier confinement resulted in very low threshold currents, as low as 1.8 mA for uncoated devices (see Fig. 2), which is the lowest value reported thus far in the literature for uncoated semiconductor lasers. The differential efficiency was 63 percent. High yield of low threshold lasers was achieved (see Fig. 3). The PQW lasers exhibit single lobe far fields and a few longitudinal modes at a few mW output power, which indicate real-index waveguiding.

Arrays of PQW lasers were prepared by growing a similar GaAs/AlGaAs GRIN-SCH on a periodically corrugated GaAs substate (3.5μm period). The PQW arrays were pumped using 50μm wide oxide stripe contacts. The threshold current was ~60mA, or ~4mA per laser. The arrays were not phase locked, as indicated by their spectrally resolved near-field patterns (Fig. 4), because of the strong index waveguiding of their elements.

Our results show that very low threshold, effectively-buried QW lasers can be obtained by using a simple single MBE growth on grooved substrates. Still lower thresholds should be obtained by optimizing the laser structure and applying high-reflection mirror coatings [2]. Such PQW laser configurations are particularly attractive for fabricating quantum wire and quantum box semiconductor lasers.

We wish to thank L. T. Florez for assistance in the MBE growth.

References:

1. E. Kapon, C. P. Yun, J. P. Harbison and N. G. Stoffel, Appl. Phys. Lett. *52*, 607 (1988).
2. K. Y. Lau, P. Derry and A. Yariv, Appl. Phys. Lett. *52*, 88 (1988).

88CH2609-8/88/0000/0074$1.00 1988IEEF

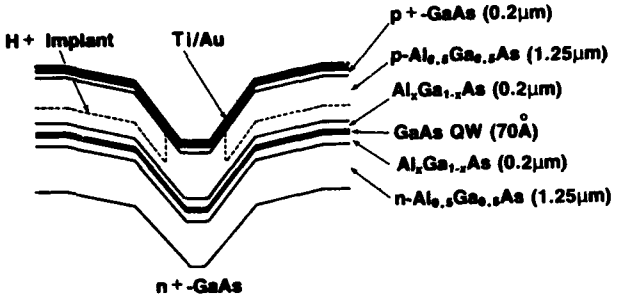

Fig. 1: Schematic cross section of a patterned QW laser grown by MBE.

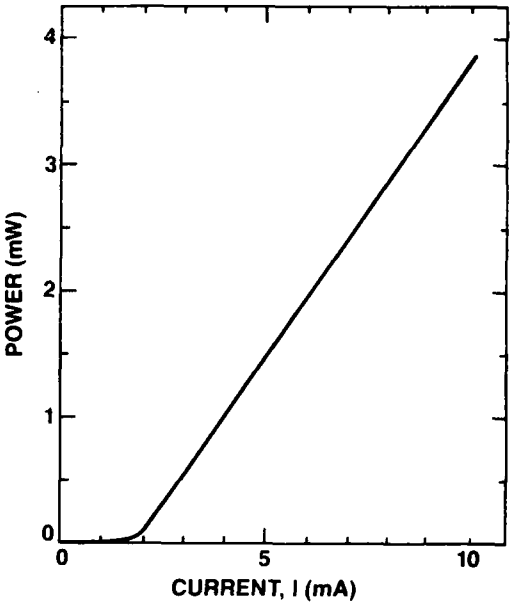

Fig. 2: Light versus current characteristic of a patterned QW laser grown by MBE. Cavity length is 350μm (Pulsed operation, uncoated facets).

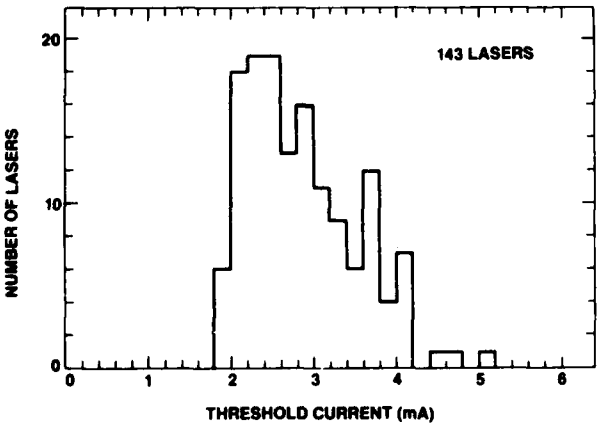

Fig. 3: Threshold current distribution of 143 patterned QW lasers grown by MBE. Cavity lengths are 250–350 μm (Pulsed operation, uncoated facets).

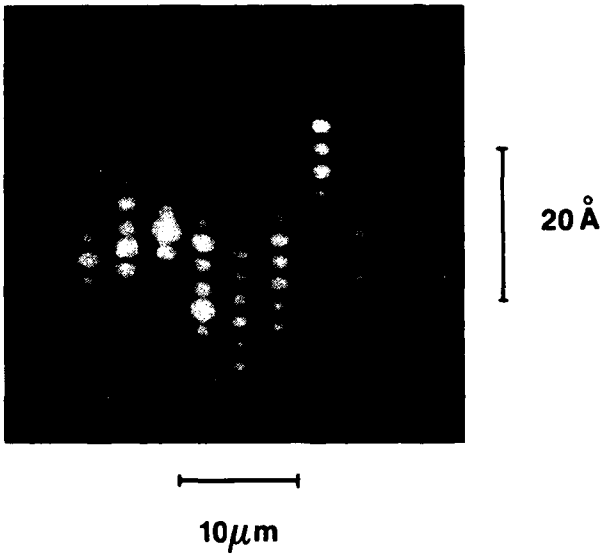

Fig. 4: Spectrally resolved near field of part of a patterned QW laser array grown by MBE. The lasing wavelength is ~8450Å. I=65 mA.

F—2

High Efficiency AlGaAs/GaAs Single-Quantum-Well Laser Diode with Short Period (GaInAs) (GaAs) Strained Superlattice Buffer Layer

K. IMANAKA, F.SATO, H.IMAMOTO, and M.Shimura
Central R&D Laboratory, OMRON Tateisi Electronics Co.,
Nagaokakyo City, Kyoto 617 JAPAN

I. OBJECTIVE

A strained superlattice buffer layer is proposed to the lattice-matched AlGaAs/GaAs quantum-well heterostructure in order to improve the laser characteristics.

II. BACKGROUND

A lattice-matched (AlGaAs)(GaAs) superlattice buffer layer (SLB) has been used widely in the AlGaAs/GaAs quantum well laser diode to improve the laser quality by the capture of defects[1]. However, the SLB is not effective to an internal stress caused by the difference in the thermal expansion coefficients between the AlGaAs epi-layers and the GaAs substrate when the Al composition in cladding layers is increased($x > 0.7$). A strained superlattice buffer layer (SSLB), which has been used widely in GaAs/Si hetero-epitaxial system [2], seems to be effective in such a problem. From these point of view, we have introduced the SSLB followed by the SLB to the AlGaAs/GaAs SQW laser diode grown by MBE.

III. EXPERIMENTS (LASER STRUCTURE)

A cross-sectional structure of laser and buffer layers is shown in Fig.1 schematically. A 3 μm-wide polyimide buried ridge waveguide (PBR) [3] GRIN-SCH-SQW laser structure has been adopted in this experiment. The SSLB and the SLB were composed of 50 pairs of $(In_{0.15}Ga_{0.85}As)_2(GaAs)_5$ short period superlattice and 5 pairs of $(Al_{0.7}Ga_{0.3}As)_{50}(GaAs)_{50}$, respectively, where subscripts indicate the number of monolayer; much attention has been paid to the InGaAs layer growth to avoid the problem of critical layer thickness[4].

IV. RESULTS (LASER CHARACTERISTICS)

First, room temperature photoluminescence measurements on the laser wafers with both of the SSLB and the SLB, and with the SLB alone have been made. The former showed more than 5 times higher peak intensity than the latter. Figure 2 shows a typical power output versus injected current under cw operation at 25°C in the 675 μm-long PBR laser emitting at 770 nm without facet coatings. Power output is almost linear over 50mW with high differential quantum efficiency of 80 %. In fig.3, $1/\eta_d$ is depicted as a function of cavity length to show the cavity loss α according to the equation shown in the inset of the figure. Very small α value of 3 cm^{-1} has been observed in such a narrow ridge waveguide laser which is applicable to the practical use. This cavity loss originates mainly in the fluctuation of the ridge width.

V. CONCLUSION

A high quantum yield ($\eta_d > 50\%$ even at 3mm long cavity), a small cavity loss ($\alpha \sim 3\ cm^{-1}$), and a high power operation have been achieved in a 3 μm-wide ridge waveguide 770 nm GRIN-SCH-SQW laser diode. These improvements are due to the introduction of strained superlattice buffer layer which relaxes the internal stress.

[1]T. Fujii et al: J.Vac.Sci.Technol., B3, 776(1985). [2]S. Sakai et al: Appl. Phys.Lett., 48, 413(1986).

[3]F.Sato et al: J. Appl. Phys., 63, 964 (1988). [4]T.G.Andersson et al: Appl.Phys.Lett., 51, 752(1987).

88CH2609-8/88/0000/0076$1.00 1988IEEE

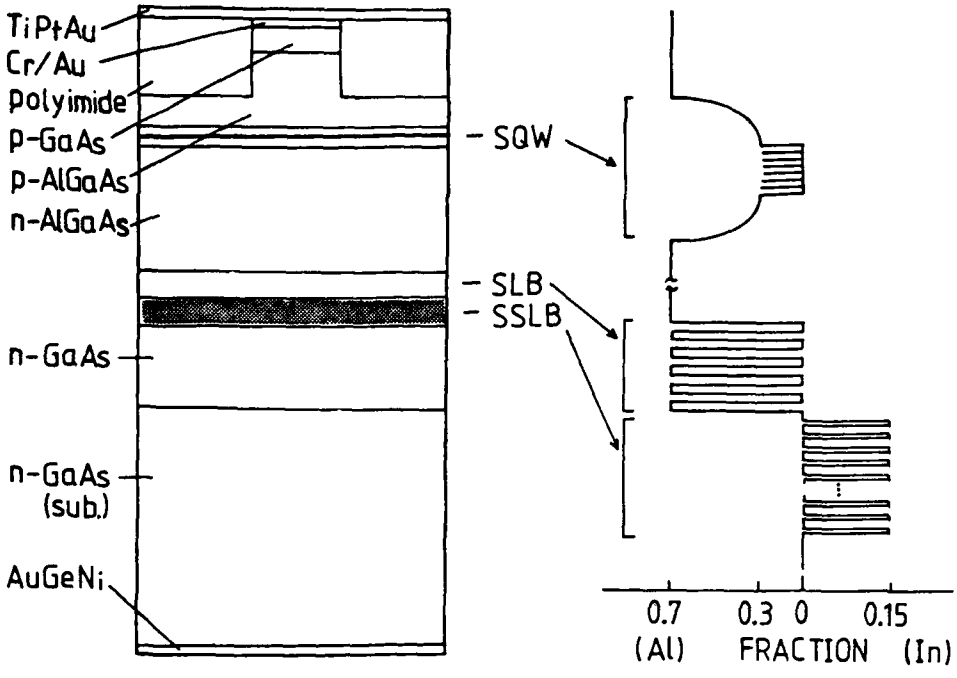

Fig.1 Cross section of the polyimide buried ridge GRIN-SCH-SQW laser and the superlattice buffer (SLB) and strained superlattice buffer (SSLB) layers.

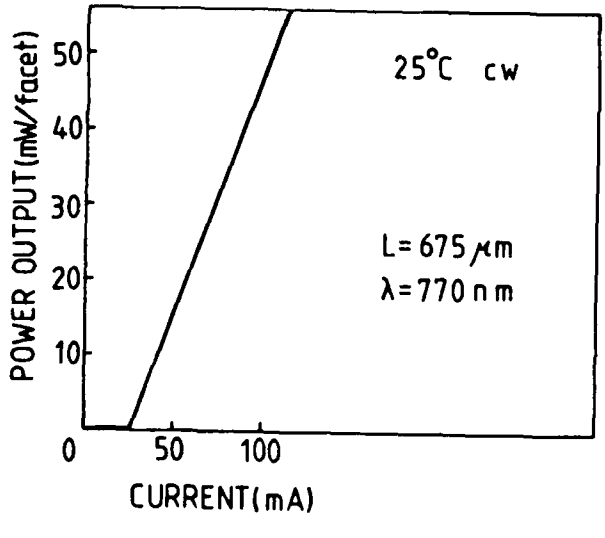

Fig.2 Laser power output versus injected current characteristicsunder cw operation at 25°C.

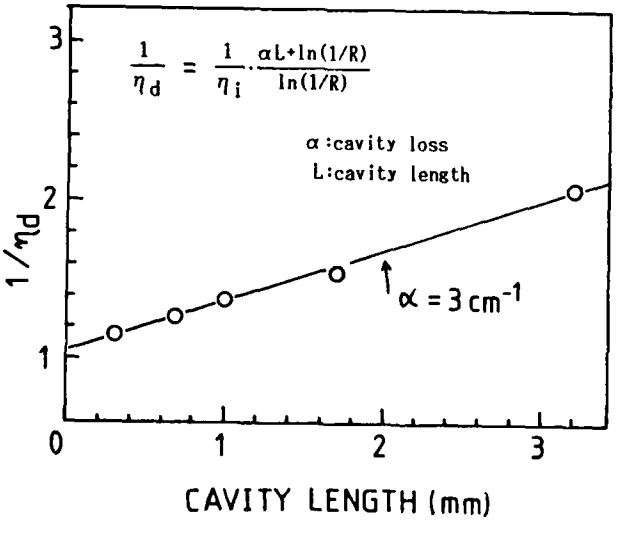

Fig.3 Differential quantum efficiency η_d as a function of cavity length L.

F—3

Entirely MOVPE Grown GaAs/AlGaAs Quantum Well Buried Heterostructure Laser Diodes with Oxygen-Doped Semi-Insulating Blocking Layers

J. Temmyo, M. Okayasu, A. Kozen, Y. Hasumi and S. Uehara
NTT Opto-electronics Laboratories
3-1, Morinosato Wakamiya, Atsugi-Shi, Kanagawa, 243-01 Japan

ABSTRACT

Buried heterostructure (BH) lasers[1] have the advantages of low threshold current as well as surface flatness for optoelectronic integration. Using a combination of molecular beam epitaxy (MBE) /liquid phase epitaxy (LPE) techniques, GaAs/AlGaAs single quantum well (SQW) BH lasers with low threshold currents have been realized[2]. This paper reports the characteristics of high quality SQW laser structures and fully planar GaAs/AlGaAs BH laser diodes with semi-insulating blocking layers entirely grown by low-pressure metalorganic vapor phase epitaxy (LP-MOVPE).

Epitaxial layers were grown at low-pressures of 40-76 Torr and at growth temperatures of 650-750°C with a substrate rotation of 10 rpm. Our MOVPE system has a very low "dead volume" run-vent manifold with automatic pressure balancing and leak-tight gas lines (the leak rate of less than 2×10^{-9} atom.cc/s for the total system). Trimethylgallium (TMG), trimethylaluminum (TMA), and arsine were used as source materials. Bis(methylcyclopentadienyl)magnesium, hydrogen selenide, and oxygen diluted in nitrogen were employed as p-, n-type, and semi-insulating dopants, respectively.

First, GaAs/AlGaAs SQW laser structures with a graded refractive index separate confinement heterostructure (GRIN-SCH) with various buffer layers were grown on (001) n^+-GaAs substrates with GaAs QW layer thicknesses of 30-300 Å. The graded layers are 0.2 μm each and graded aluminum mole fraction typically is from 0.6 to 0.2. Three kinds of buffer layers were inserted between the GaAs n^+-layer and AlGaAs clad layer--5 periods GaAs/AlGaAs superlattice (SL) buffer, graded (GR) buffer, and no buffer layers--and tested. No variation in lasing threshold currents was observed in contrast with MBE grown laser structures , indicating that the MOVPE grown epitaxial layers are of high quality (Fig.1). The lowest threshold current density of 165 A/cm^2 for 500 μm cavity length was obtained for clad layer aluminum content, x_c, of 0.75 (Fig.2).

Next, in order to obtain BH lasers with semi-insulating blocking layers, selective burying growth in an AlGaAs system and oxygen-doped highly-resistive AlGaAs growth were tried. Higher aluminum content degrades the selectivity and polycrystal covers the entire SiO_2 mask at x=0.65 due to the large bonding energy between the aluminum and oxygen (Fig.3). In an actual selective growth with narrow SiO_2 stripes (typically 5-10 μm wide) almost perfect selectivity is obtained for aluminum content up to 0.5. The burying growth modes in the grooved laser epitaxial layers for three kinds of mesas were examined and the distinctive growths with various facets were clarified (Fig.4). It was found that very little growth occurred on the {111} B and {110} planes. The SiO_2 overhang length is crucial in determining the flatness of the regrowth surface. LP-MOVPE is useful for planar selective burying growth in contrast with MBE. Semi-insulating AlGaAs with resistivity up to 10^6 Ω cm is obtained using oxygen doping due to the formation of a midgap deep level at 0.76 eV (Fig.5). Higher temperature growth increases the efficiency of oxygen doping in the AlGaAs system.

By using the above-mentioned growth techniques, fully planar GaAs/AlGaAs SQW BH lasers with semi-insulating blocking layers were fabricated. Dependences of threshold currents on active layer widths at various regrowth temperatures, T_s, are shown in Fig.6, together with those of ridge waveguide lasers and high-mesa ridge lasers. The lowest threshod current of BH lasers is 19 mA with external differential quantum efficiency of 50% and a maximum pulsed operation power up to 100 mW/facet. Threshold current dependences of the 650°C regrowth lasers were found to be comparable with those of high-mesa lasers. Even at 750°C, oxygen diffusion into the active layer was not observed by SIMS analysis, suggesting that damage and/or contamination at the sidewalls of the active layer may exist. This indicates that in-situ cleaning similar to LPE melt-back technique may be necessary for LP-MOVPE regrowth .

In summary, high quality SQW laser epitaxial layers and fully planar BH lasers with semi-insulating blocking layers were fabricated by using LP-MOVPE.

REFERENCES:

1) T. Tsukada, J. Appl. Phys. 45, 4899 (1974).

2) W. T. Tsang, R. A. Logan, and J. A. Ditzenberger, Electron. Lett. 19, 845 (1982)

11th IEEE International Semiconductor Laser Conference 1988, Boston, MA

88CH2609-8/88/0000/0078$1.00 1988IEEE

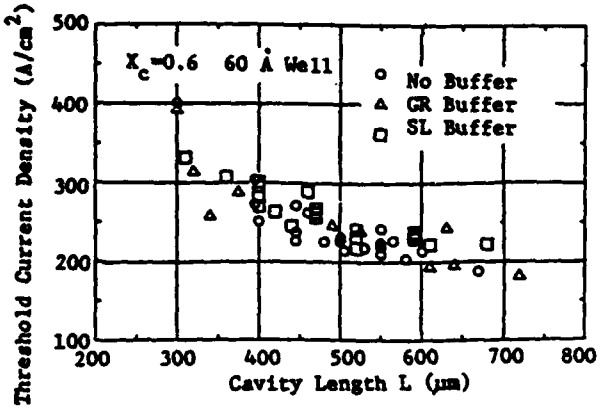

Fig.1 Broad area threshold current densities as a function of cavity length for GRIN-SCH SQW lasers with different buffer layers.

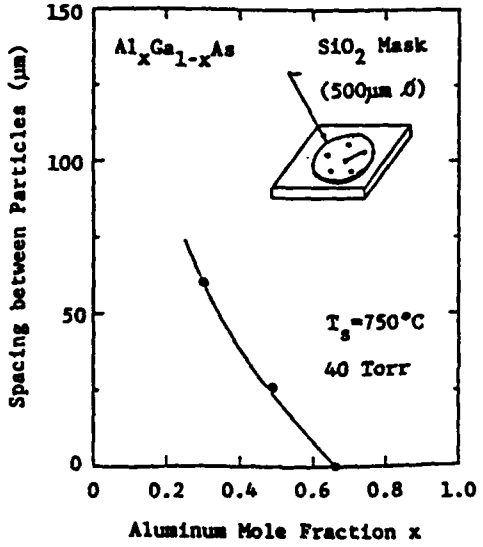

Fig.3 Relationship between aluminum mole fraction and spacing between polycrystal particles deposited on the circular SiO_2 mask pattern shown in the figure.

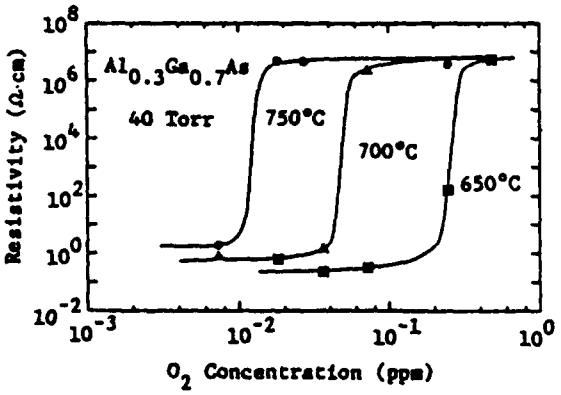

Fig.5 Relationship between oxygen concentration in the gas phase and AlGaAs resistivity with parameters of growth temperature.

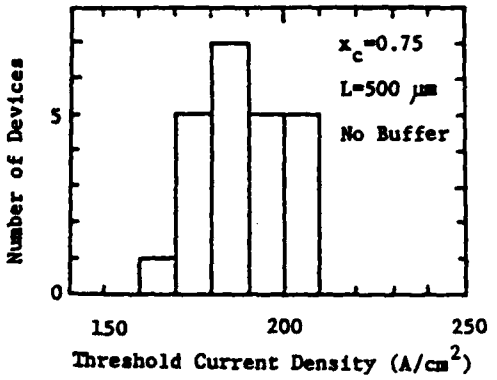

Fig.2 Distribution of threshold current density of GRIN-SCH SQW lasers.

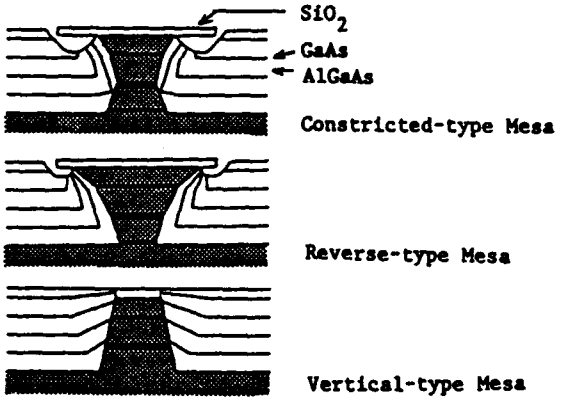

Fig.4 Detailed schematic drawing of the ⟨110⟩ cross section of selectively grown AlGaAs layers in etched grooves of an actual laser epitaxial wafer. Four thin GaAs layers were sandwitched as marker layers.

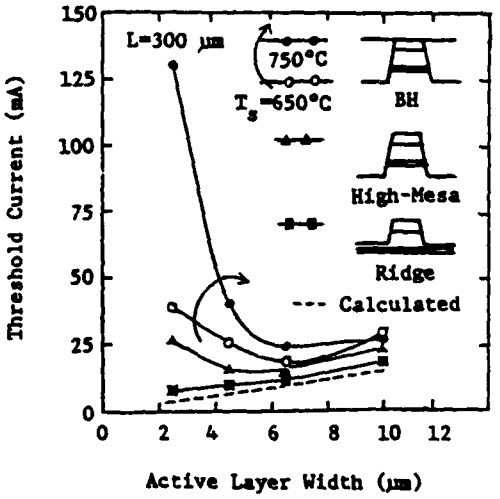

Fig.6 Lasing threshold current as a function of active layer widths of BH, ridge waveguide, and high-mesa ridge lasers. Similar vertical sidewall mesa structures were used for each laser and were formed by dry-etching technique. Threshold current density of laser wafers used was 0.55 kA/cm^2.

F—4

Low Threshold AlGaAs/GaAs SCH Single Quantum Well Lasers Grown by LPE

Zh.I.Alferov, S.A.Gurevich, V.P.Khvostikov, V.R.Larionov, E.L.Portnoy, F.N.Timofeev

A.F.Ioffe Physico-Technical Institute, Academy of Sciences of the USSR, Leningrad

Low threshold ($\lesssim$10 mA) diode lasers are usually fabricated on single or multiple quantum well SCH structures prepared by MBE or MOCVD techniques. In this paper we present low threshold (I_{th} = 4.3 mA, η = 63%) AlGaAs/GaAs SCH single quantum well (SQW) ridge-waveguide lasers, grown by the low temperature LPE method. In this LPE method the starting temperature was $\simeq 600^{\circ}$C, which allowed us to obtain high quality heterostructure material with heterojunction abruptness of about 20 Å [1]. In the laser structures SQW active layer thickness d was varied in d=100-200 Å range. The threshold current density of a broad contact lasers was 200-300 A/cm^2. The 4 μm wide ridge-waveguide laser structure (Fig.1) was formed by photolithography and selective chemical etching. Lasers with cavity length L > 100 μm were obtained by conventional cleaving, while lasers with 30 μm < L < 100 μm had the both mirrors microcleaved.

Fig.2 displays the experimental dependence of threshold current (I_{th}) and threshold current density (J_{th}) on cavity length. In $1/L \to 0$ limit the threshold current density was found to be 640 A/cm^2, which should be compared with 300 A/cm^2 for long cavity broad contact lasers. This increase of I_{th} is attributed, in accordance to [2], to lateral current spreading in ridge structure. As seen from Fig.2, I_{th} vs L is a weak dependence with minimum $I_{th} \simeq$ 10 mA at L=50-100 μm. This means that even at $J \simeq 3$ kA/cm^2 electrical confinement is sufficient. For L=50-100 um (d $\simeq$ 200 Å) the nonradiative recombination in SQW is also negligible, which is evident from the comparison of experimental data and calculated dependences of external efficiency η on L (Fig.3, calculations are made with different values of the internal efficiency η_i=1.0; 0.8; 0.6). Fig.4 shows typical 300 K CW L/I characteristics. Short-cavity laser with a reflective coated rear mirror has the threshold current 4.3 mA and one side (front mirror) efficiency 63%. In a considerable output power range (3-10 mW) short cavity lasers ($L \lesssim 100$ μm) operated in single longitudinal and fundamental transverse mode under CW and pulse pumping.

In conclusion, the low temperature LPE has been successfully applied to fabrication of low threshold, high efficiency SCH SQW AlGaAs/GaAs lasers.

1. Zh.I.Alferov et al. Pis'ma v Zh.Tekhn.Fiz.,v.12,N.18,pp.1089-1093 (1986).
2. A.Shimizu, T.Hara, IEEE J. of Quant.Electr. v.QE-23, N.3,p.293-302 (1987).

88CH2609-8/88/0000/0080$1.00 1988IEEE

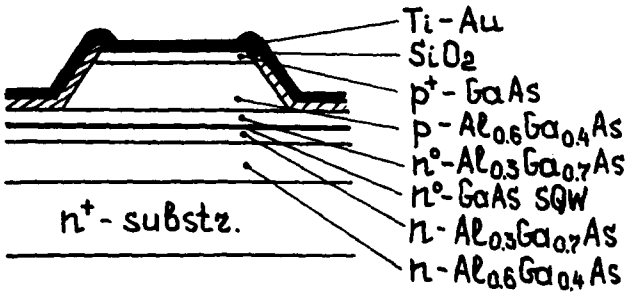

Fig. 1

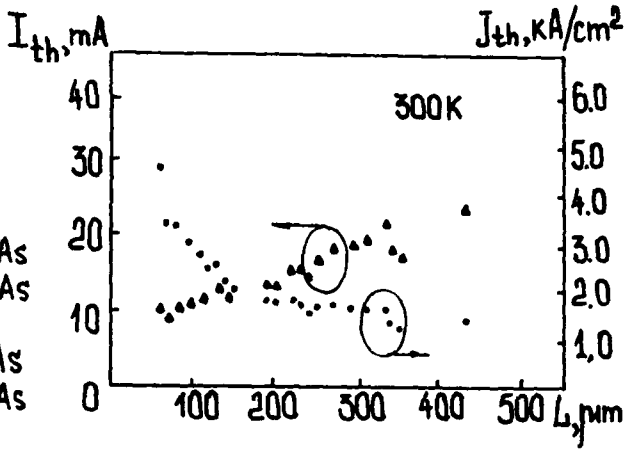

Fig. 2

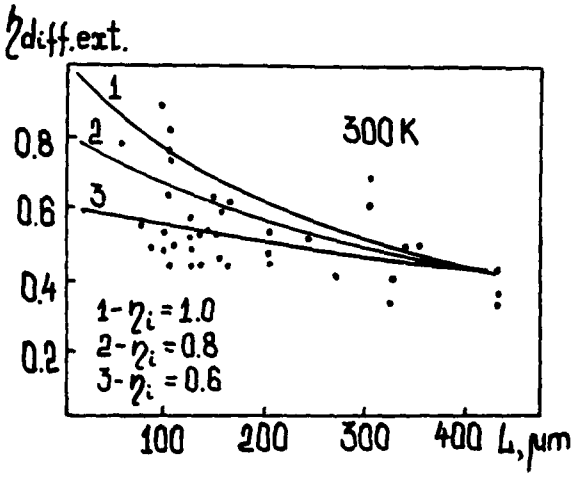

Fig. 3

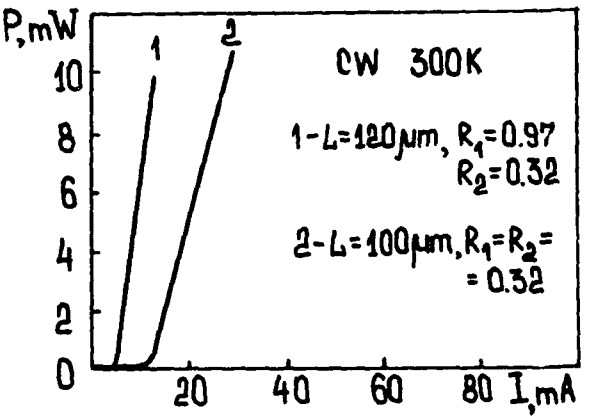

Fig. 4

F—5

Extremely Low Threshold Current in a Potential Controlled Laser

Minoru YAMADA and Keiichi OMI
Department of Electrical and Computer Engineering
Faculty of Technology, Kanazawa University
Kodatsuno, Kanazawa, 920 JAPAN

Reduction of the threshold current in semiconductor injection lasers is a basic problem for developing the devices. We have proposed a new structure of the injection laser called a Potential Controlled (POCO) laser giving very low threshold current[1]. In this paper, the optimum configuration of the POCO laser is theoretically examined and a very low threshold current less than 100 μA is theoretically predicted.

Operating mechanism of the POCO laser is illustrated in Fig.1. The lasing gain is proportional to the difference between transition probability of the optical emission and that of the optical absorption. In case of conventional lasers, energy distributions of the electrons and the holes are determined under the electrical neutral condition, and there remains the optical absorption as shown in Fig.1(a). However, if the number of the holes in the valence band is increased by pulling down the quasi-Fermi level μ_v as shown in Fig.1(b), the optical absorption decreases, resulting in reduction of the threshold current.

This idea is realized in a structure shown in Fig.2, where the intrinsic active (quantum-well) layer (1) is sandwiched with heavily doped potential control layers (2). A large number of the holes are supported from the potential control layers. Our structure is very close to the so called Modulation-Doped MQW lasers proposed by Uomi et. al [2] except the number of the wells.

The lasing gain and the injection current are theoretically analyzed by taking into account both the optical field distribution and the charge distribution. A calculated characteristic of the lasing gain v.s. the injection current density is shown in Fig.3. The model is an $Al_xGa_{1-x}As$ system and the layer thicknesses and the aluminum compositions are L_1 = 4nm, x_1 = 0.0, L_2 = 12nm, X_2 = 0.8, L_3= 60nm, x_3 = 0.3 and x_4 = 1.0. The heavier the acceptor is doped in the potential control layers, the larger the lasing gain becomes.

Variation of the threshold current I_{th} with the cavity length ℓ is shown in Fig.4, where the stripe width is put as W = 3 μm, the guiding loss is α_i = 5 cm^{-1}, and the mirror reflectivity R is set as the parameters. The lowest threshold current is 89μA for $N_A = 10^{19} cm^{-3}$ or 72μA for $N_A = 10^{20} cm^{-3}$.

The threshold current obtained in this paper is much smaller than that in

88CH2609-8/88/0000/0082$1.00 1988IEEE

other lasers.

References

[1] M.Yamada, K.Omi, Y.Nashida and M.Gamo; Trans. of IEICE, E70, pp.178-180, (March, 1987)

[2] K.Uomi, T.Ohtoshi and N.Chinone ; Tenth IEEE International Semiconductor Laser Conf., Kanazawa, (Oct. 1986)

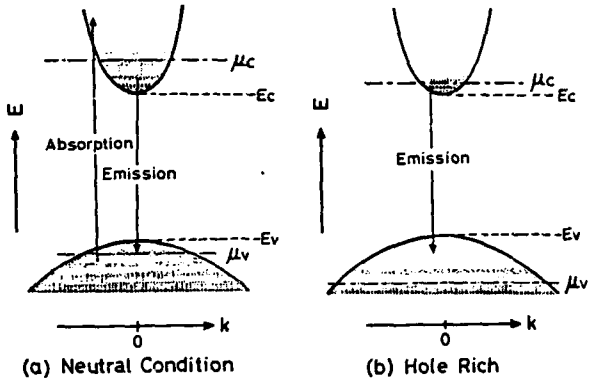

Fig.1 Electron transitions under neutral condition and hole rich condition

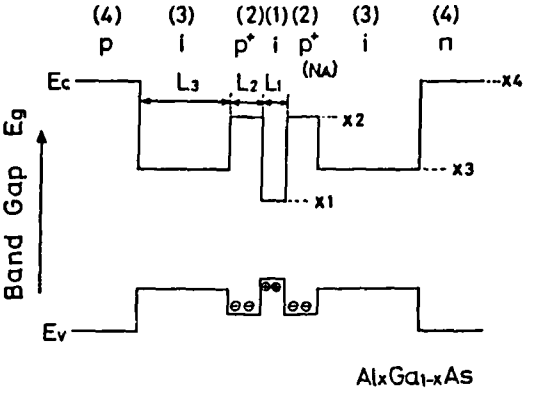

Fig.2 Band-Gap Profile of the Potential Controlled Laser

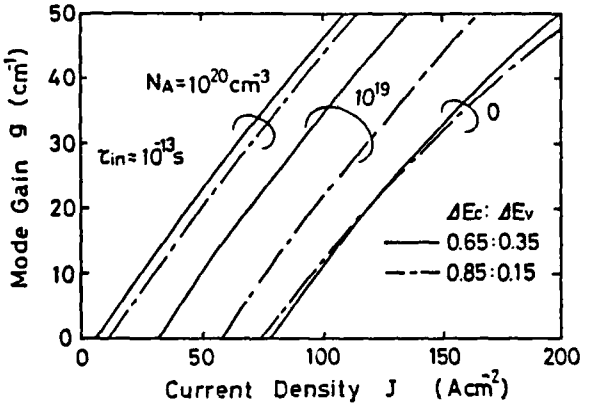

Fig.3 Lasing Gain v.s. Injection Current Density

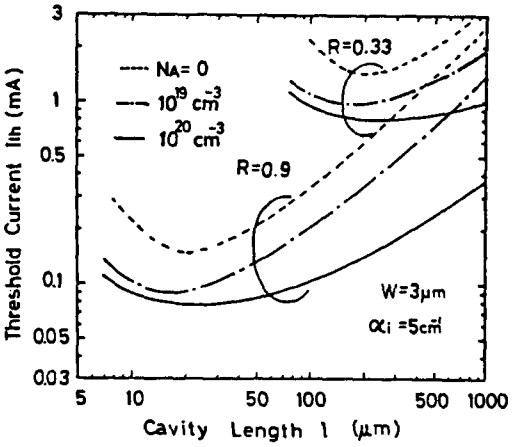

Fig.4 Variation of the Threshold Current with the Cavity Length

F—6

Impact of Well Coupling on the Spontaneous Emission Properties of Multiple Quantum Well Structures

M. Krahl[a], D. Bimberg[a], J. Christen[a], D.E. Mars[b], J.N. Miller[b]

[a]Institut für Festkörperphysik, Technische Universität Berlin, Hardenbergstr. 36, 1000 Berlin 12, Germany

[b]Hewlett Packard Labs, 3500 Deer Creek Road, Palo Alto, CA 94304, U.S.A.

Light emitters based on two-dimensional structures such as Quantum Well (QW) lasers and light emitting diodes are in many respects superior to three-dimensional light emitting devices[1,2]. The altered density of states and the strong enhancement of radiative mono- and bimolecular recombination coefficients present the main causes[3]. Two quite different QW laser structures are presently used, the Multiple Quantum Well (MQW) Laser, pioneered by Tsang[1], using a sequence of wells coupled by narrow barriers as active part and the Graded Refractive Index Separate Confinement Heterostructure - Single Quantum Well (GRINSCH-SQW) Laser introduced by Tsang and later by Hersee[2]. Presently no investigations of the consequences of coupling of wells exist, although it might be of fundamental importance for the emission properties of such devices.

It is the purpose of the present work to present a systematic investigation of the large impact well coupling has on the spontaneous emission properties of MQW structures. We will show that our results are of largest importance for laser gain profiles. Detailed investigations of the barrier width L_B dependence of the luminescence in the temperature range between 1.5 K and 300 K for GaAs/AlGaAs MQW structures are presented. For a constant well width L_Z = 5.1 nm L_B is varied in small steps within the whole range between the limit of uncoupled wells (L_B = 18.1 nm) and true superlattices (SL) (strongly coupled wells: L_B = 0.57 nm). So the effects of increasing coupling of wells can be studied in detail. Coupling results in a low energy shift of the excitonic luminescence lines. In particular the light/heavy hole splitting decreases with increasing coupling and converges to zero, visualizing directly a transition from two- to three-dimensional behaviour. In addition we find that the coupling dramatically suppresses Gaussian line broadening due to interface roughness. More important for devices operating at room temperature we observe a pronounced spectral narrowing with increasing barrier width L_B at 300 K (Fig. 1).

88CH2609-8/88/0000/0084$1.00 1988IEEE

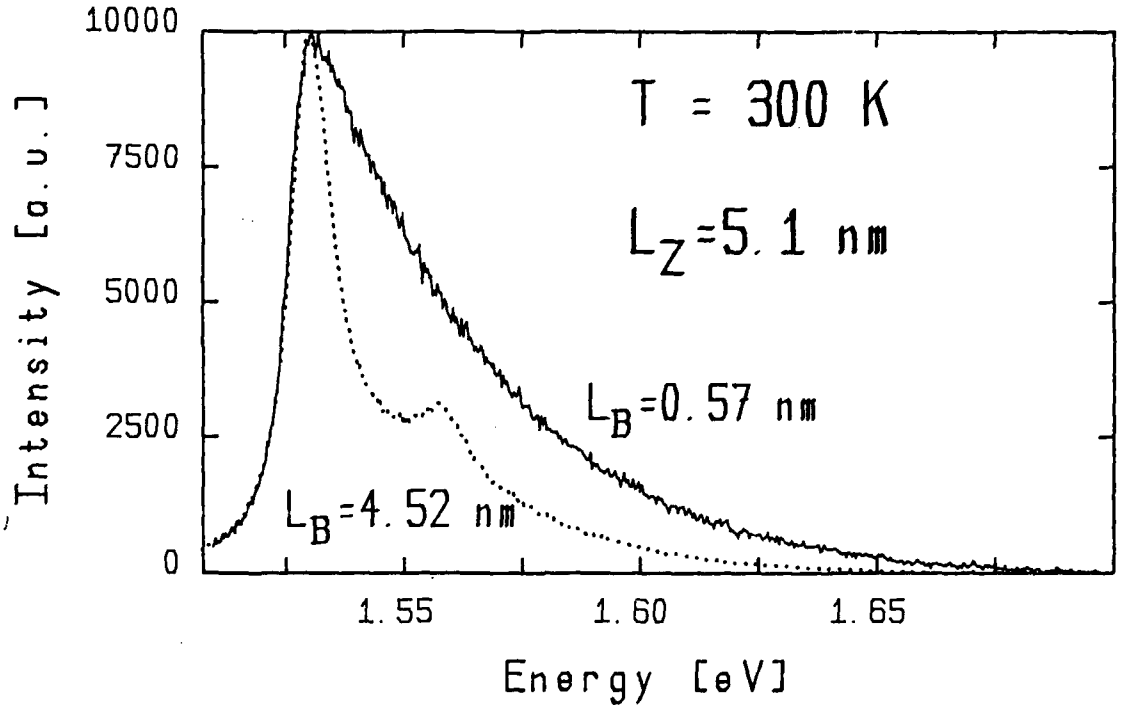

Fig. 1: Photoluminescence lineshape at 300 K for two samples with L_Z = 5.1 nm and different barrierwidths : L_B = 4.52 nm and L_B = 0.57 nm respectively. For comparison the latter one is shifted by 57 meV to higher energy.

All observations are perfectly described by our model of electronic states in SL's - the LCWO model (Linear Combination of Well Orbitals). Based on this model the resulting density of states for interband transitions given by a arcos-function is adapted to calculate luminescence lineshapes of realistic MQW structures: The full theory includes for the first time the excitonic density of states and interface roughness induced effects. The consideration of both components is shown to be essential to interprete correctly the luminescence lineshape and therefore to calculate the resulting gain profile. At room temperature coupling of wells results in a decrease of the excitonic enhancement, a property typical for uncoupled QW's. This decrease explains the observed increase of the luminescence linewidth.

References

/1/ W.T. Tsang, Appl. Phys. Lett. 39, 786 (1981)

/2/ W.T. Tsang, Appl. Phys. Lett. 39, 134 (1981)
S.D.Hersee, M.Bally, P.Assenat, B.de Cremoux, and J.P.Duchemin, Electron. Lett. 18, 870, 1982

/3/ E.H. Böttcher, K. Ketterer, D. Bimberg, G. Weimann and W. Schlapp, Appl. Phys. Lett. 50, 1074 (1987)

Session G: Mode Locking and Fast Switching

G—1

Modulation Frequency Dependence of Active Mode Locking of Semiconductor Lasers

J. E. Bowers, Y. G. Weh, A. Mar, P. A. Morton, and S. W. Corzine

University of California
Department of Electrical and Computer Engineering
Santa Barbara, CA 93106

Summary

The objective of this work is to examine the transient characteristics of high speed semiconductor lasers mode locked at very high rates and with very short electrical pulses. In particular, numerical calculations based on a traveling wave set of rate equations for the electron and photon densities are compared to extensive experimental measurements of pulse shapes for mode locking at frequencies from 1 to 16 GHz.

Mode locking of lasers has been used to obtain very short pulses. Although the gain bandwidth of semiconductors is similar to that of dyes and color centers, the pulsewidths obtainable from semiconductor lasers have unfortunately been several orders of magnitude larger than the pulse widths (under 50 fs) that have been obtained with dye and color center lasers (in particular, color center based soliton lasers). Several authors have found that a lower limit of 5 ps pulse width can be produced from actively mode locked lasers[1,2]. Recently, we found that subpicosecond pulses of width 0.56 ps or larger could be generated by using large bandwidth semiconductor lasers driven by large amplitude, short electrical pulses[3].

We report here experimental measurements of the dependence of pulsewidth on modulation frequency (Fig.1) for the laser configuration shown in Fig. 2. The laser is antireflection coated on one facet and high reflection coated (60%) on the other facet. The laser[4] has very low capacitance (<1 pF) and had a bandwidth before coating of 15 GHz. The GRINROD is antireflection coated on both ends. The external cavity length is set for a resonant frequency of 2 GHz. The laser is biased close to threshold and modulated with a microwave signal which is many times the size of the dc bias current. The modulation frequency is set at various harmonics of the fundamental cavity length for the measurement in Fig. 1. It can be seen that much shorter pulses can be achieved at higher modulation frequencies, corresponding to shorter electrical drive pulses. Similar results were seen with several other lasers. No degradation of the laser or its light-current characteristic were observed before or after the mode locking experiments.

We compare these measurements to extensive calculations of the active mode locking process using a traveling wave formulation of the rate equations for the electron and photon population. Unlike previous theoretical formulations of active mode locking calculated primarily in the frequency domain with small signal modulation[5], we use numerical integration in the time domain to allow for large signal modulation with spatially dependent saturation of the gain. One example of these calculations is the dependence of pulse width on modulation frequency, which is shown in Fig. 1 and compared to recent experimental results. The theoretical limit on pulsewidth is well below 0.5 ps, and is limited by dispersion in the cavity and the spectral width of the gain curve, which are not included in the calculations shown here. Cavity dispersion is included in the computer program and its limitations will be described in the paper. Fig. 3 compares the experimentally measured shape of the autocorrelation

88CH2609-8/88/0000/0088$1.00 1988IEEE

with the calculated result. The agreement is good, with the primary differences in the height of the wings of the autocorrelation.

These experimental results show an order of magnitude decrease from earlier results in the pulsewidths obtainable from active mode locking. The theoretical calculations confirm that subpicosecond pulses are possible with purely active mode locking, unlike many earlier calculations. Experiment and theory suggest using shorter electrical pulses (higher frequency modulation) to obtain even shorter optical pulses.

References

[1] G. Eisenstein, R. Tucker, U. Koren, and S. Korotky, J. Quantum Electron. QE-22, 142(1986).
[2] J. Kuhl, M. Serenyi, and E.O. Gobel, Optics Lett. 12, 334 (1987).
[3] S. W. Corzine, J. E. Bowers, G. Przybylek, U. Koren, B. I. Miller, and C. E. Soccolich, Appl. Phys. Lett. 52, 348(1988).
[4] J. E. Bowers, U. Koren, B. I. Miller, C. Soccolich and W. Jan, Electron. Lett., 23 1263(1987).
[5] For example, H. Haus, Jpn. J. Appl. Phys. 20, 1007(1981).

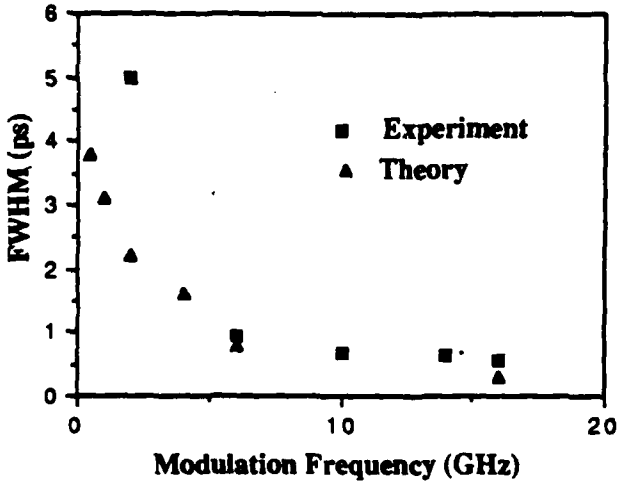

Figure 1. Dependence of minimum pulsewidth on modulation frequency for various harmonics of a 2 GHz cavity.

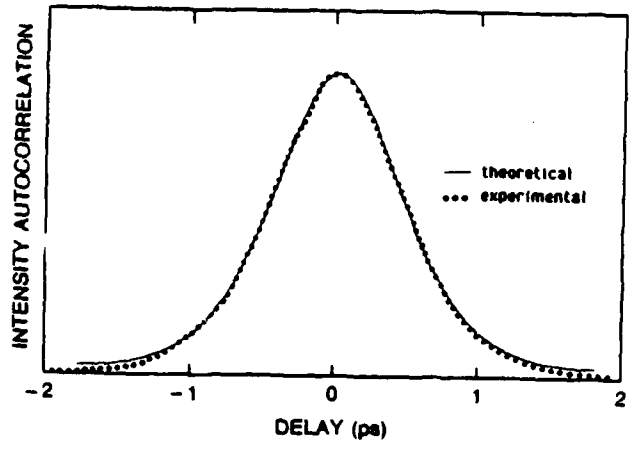

Figure 3. Comparison of measured and calculated pulse shapes for the autocorrelation of the actively mode locked laser output.

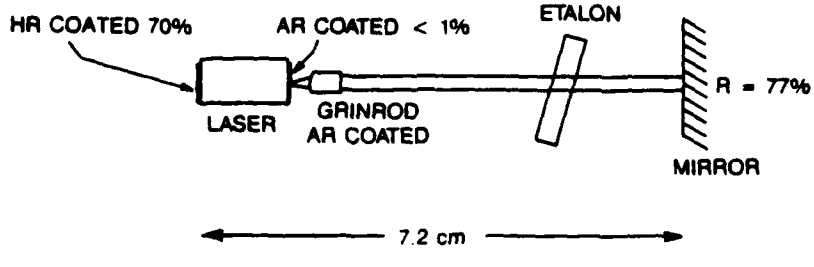

Figure 2. Schematic diagram of an actively mode locked semiconductor laser. The cavity length was

G—2

Gain Dynamics in InGaAsP Traveling-Wave Optical Amplifiers by Amplification of High Repetition Rate Picosecond Pulses

P. B. Hansen*, G. Eisenstein, R. S. Tucker, J. M. Wiesenfeld and G. Raybon

AT&T Bell Laboratories
Crawfords Hill Laboratory
Holmdel, NJ 07733
(201) 949-7211

Picosecond pulse amplification experiments have been carried out to study the dynamic effects of optical amplifiers on the characteristics of multi-gigabit per second pulse-code-modulated systems.

The use of optical amplifiers in multi-gigabit per second transmission and switching systems requires knowledge of their gain characteristics under high repetition rate picosecond optical pulse excitations. We address the issues of pulse distortion and gain compression (or saturation) due to carrier depletion during amplification of a pulse and its subsequent recovery. The magnitude and characteristic time constants involved are examined. Recent publications have described gain dynamics in GaAs amplifiers on a time scale of 0.1-5 ps [1] and pulse distortion in InGaAsP amplifiers injected by high energy pulses from a color center laser [2]. We present results on the gain dynamics for amplification of pulses in a 1.3 μm amplifier [3] on a time scale of 10-500 ps. The pulses used are generated by semiconductor lasers and represent realistic conditions of high-speed transmission and switching systems with respect to pulse energy, width and repetition rate. That is, pulses with energies less than ~100 fJ, width of 10-30 ps and repetition rates in the GHz range.

A schematic of the experimental set-up is shown in Fig.1. Two external cavity lasers are actively mode-locked and generate ~20 ps pulses at a repetition rate of 1.0 GHz. The two pulse trains are combined in a fiber directional coupler. Laser #1 generates the pump pulse, whereas the pulse from laser #2 being much weaker is used as a probe. The maximum energies of the two pulses out of the fiber near the input facet of the amplifier are 93 fJ and 1.9 fJ. The delay between the pulses can be varied by a variable microwave phase shifter inserted in the RF signal line of the second laser. The gain is measured using a lock-in amplifier while chopping the appropriate external cavity laser.

The measured gain as a function of the derived facet output power is shown in Fig.2 (a 4.5 dB output coupling loss was assumed). The saturation level of the amplifier defined as the average output power at which the gain is compressed by 1 dB is ~9.5 dBm in the case of CW injection and drops to ~5.1 dBm for 27 ps 1 GHz pulses. The corresponding output pulse energy is 3.2 pJ per pulse.

The gain recovery is measured as the relative delay between the pump and the probe pulse is varied. As can be seen in Fig.3, the gain is compressed by as much as 2.3 dB 20 ps after the pump pulse and it recovers with a time constant of only ~100 ps. The magnitude of the gain compression and the recovery time constants determine the range of power and bit rates for which amplification without degradation of the system performance is possible.

REFERENCES

[1] M. P. Kesler, and E. P. Ippen, Appl. Phys. Lett., *51*, 1765, (1987).
[2] I. W. Marshall, and D. M. Spirit, Proc. CLEO 88, Paper TuM64, Anaheim Ca, April 1988.
[3] G. Eisenstein, B. C. Johnson and G. Raybon, Electron. Lett., *23*, 1020, (1987)

---

* Permanent address: Electromagnetics Institute, Technical Univ. of Denmark, DK-2800 Lyngby, Denmark.

88CH2609-8/88/0000/0090$1.00 1988IEEE

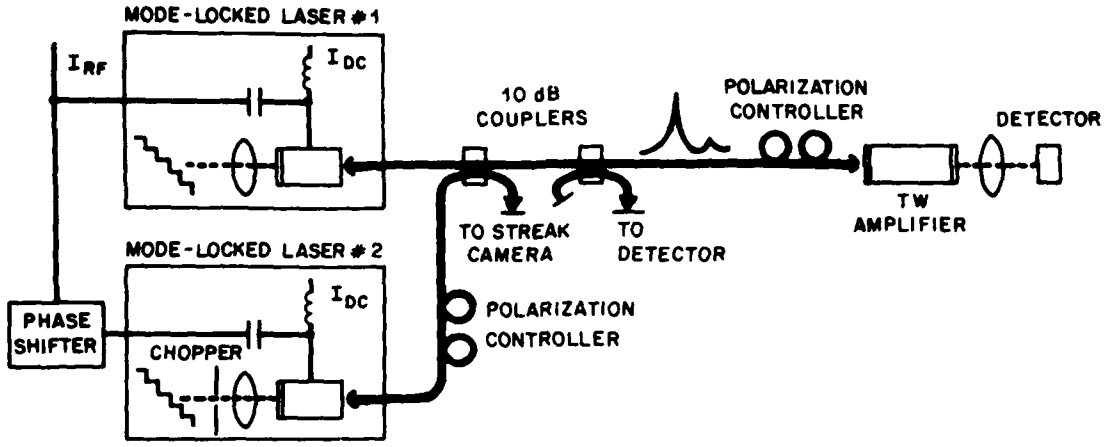

FIGURE 1 SCHEMATIC OF THE EXPERIMENTAL SET-UP

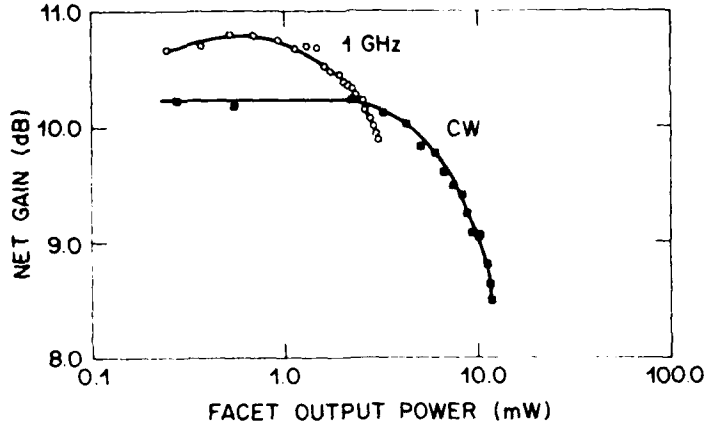

FIGURE 2 NET GAIN VERSUS FACET OUTPUT POWER FOR A CW SIGNAL AND A 1 GHz PULSE TRAIN.

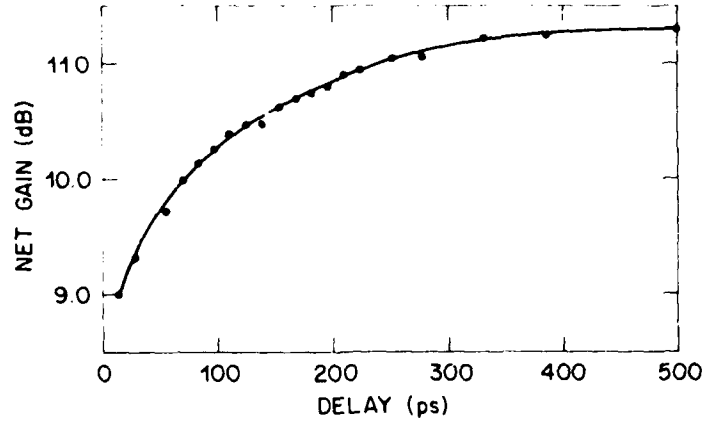

FIGURE 3 NET GAIN VERSUS DELAY BETWEEN PUMP AND PROBE.

G—3

Subpicosecond Temporal and Spectral Gain Dynamics in GaAlAs Laser Amplifiers

Morris P. Kesler and Erich P. Ippen
Department of Electrical Engineering and Computer Science and
Research Laboratory of Electronics, Massachusetts Institute of Technology,
Cambridge, MA 02139

The objective of this work is to study subpicosecond temporal and spectral dynamics of gain in diode laser amplifiers.

Gain nonlinearities become increasingly important when diode lasers are modulated at high rates and when they are used as amplifiers in multiplexed systems. Several groups are attempting to characterize these nonlinearities in the frequency domain by four-wave mixing. We have undertaken, instead, to study them directly, in the time domain, with ultrashort pulses.

We have previously reported on experiments which utilized 90 fs optical pulses to both stimulate and measure gain saturation dynamics in GaAs diode amplifiers[1]. In this paper, we extend this work by using a tunable probe technique to observe these gain dynamics at wavelengths throughout the bandwidth of the amplifier. This technique, similar to that used previously to study spectral dynamics in dye molecules, uses up-conversion gating to achieve subpicosecond time resolution at the probe wavelengths.

Typical gain saturation data obtained in the laser amplifier for three wavelengths are shown in Figure 1 for a saturating pulse wavelength of 808 nm. The data at all three probe wavelengths show a transient gain depletion, caused by the passage of the pump pulse, and subsequent recovery. Rapid, partial recovery occurs within 2 picoseconds, with complete recovery, brought about by recovery of the population inversion, occurring on a much longer (nsec) timescale. Similar data were obtained with a pump-probe wavelength separation of 30 nm.

This series of studies gives the ability to distinguish among the possible causes of the gain nonlinearities, and can also yield information on group velocity dispersion in the devices. The data obtained show no spectral hole feature and indicate gain depletion over much of the amplifier bandwidth, consistent with the mechanism of dynamic carrier heating. The fact that the signal is observed over a large wavelength separation indicates that group velocity dispersion is not sufficient at these wavelengths to obscure it. This work, to our knowledge, represents the first subpicosecond, time-resolved, non-degenerate four-wave mixing measurements in diode laser amplifiers.

REFERENCES

[1] M. P. Kesler and E. P. Ippen, Appl. Phys. Lett., **51**, 1765 (1987).

88CH2609-8/88/0000/0092$1.00 1988IEEE

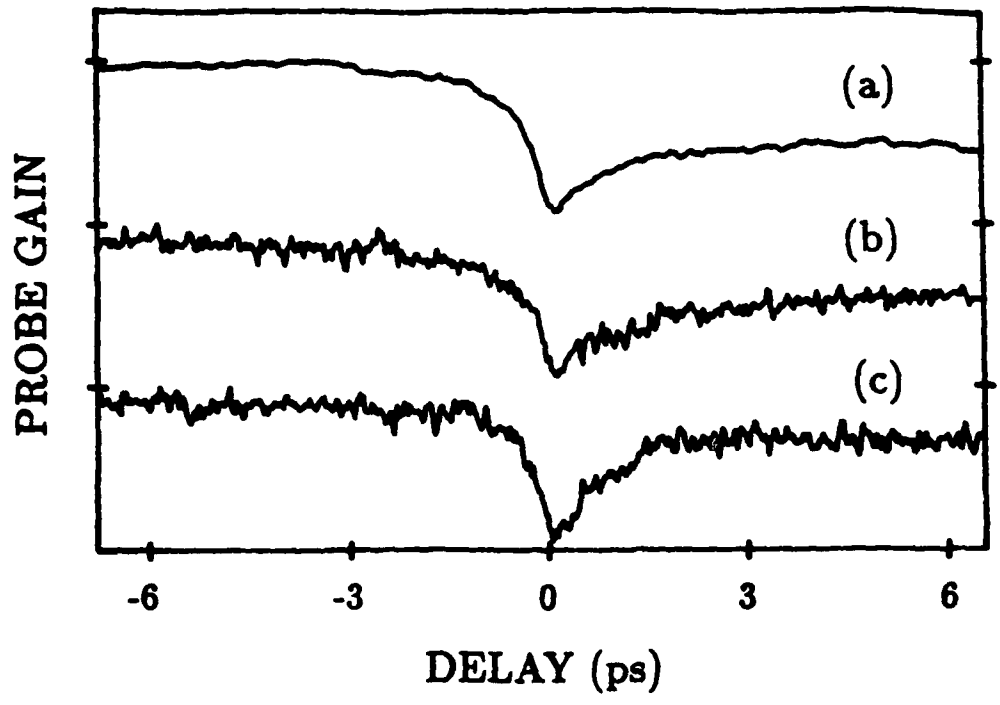

Figure 1. Gain saturation data obtained in the laser amplifier. The pumping wavelength was 808 nm, and the gated probe transmission was measured at wavelengths of 808 nm (a), 818 nm (b), and 826 nm (c). The peak transmission has been normalized to unity, and the three curves have been offset for clarity. The maximum gain depletion was approximately 10% in all cases.

G—4

Gain Switched High Repetition Rate Picosecond Pulse (< 10 ps) Generated from a 1.3 μm Short Cavity V-grooved InGaAsP Laser Diode

H. F. Liu, M. Fukazawa, T. Kamiya, Y. Kawai*
Department of Electronic Engineering, University of Tokyo
7-3-1, Hongo, Bunkyo-ku, Tokyo, 113, JAPAN
*Research Laboratory, OKI Electric Industry Co. Ltd.,
550-5 Higashi-Asakawa, Hachioji, Tokyo, 193, JAPAN

Generation of picosecond optical pulse is of great importance for optical information processing and communication system. Gain switching, among others, is the simpliest generation method. Up to date, optical pulse as short as 1.8ps and 2ps have been successfully generated at relatively low repetition rate both by means of optical pumping and electrical pumping[1,2]. However, except the appearance of some substructure within the pulse[3], they are lacking in reproducibility. And at high repetition rate, pulse width less than 10ps seems to be difficult to achieve. In this paper, we report a direct streak-camera observation of the shortest pulse generated at 100 MHz by means of electrical pumping from a short cavity V-grooved P-substrate (VIPS) InGaAsP laser diode.

Structure of the 1.3μm InGaAsP VIPS laser diode is shown in Fig.1, where P-substrate was advantageously used, because it is suitable for high power output (> 100mW) and for efficient injection of the pumping current[4]. By cleaving, laser diode with cavity length of 95μm was successfully prepared, threshold current of which was 19.6mA. Biasing the device below threshold, we pumped it with a strong current pulse (FWHM = 130ps, V_{p-p}=16v), which is obtained from a 100 MHz comb generator. Generated optical pulses were observed by a streak camera. As we changed D.C bias from 0mA to I_{th}, we found, as shown in Fig.2, the laser pulse gradually decreased and reached minimum around $0.6I_{th}$ and after that, it increased significantly. For comparison, experimental data of a 140μm LD is also shown (by □), which showed similar but a little different tendency. Directly measured shortest pulse width is 12.5ps, which is shown in Fig.3. However, because the resolution of the streak camera we uesd is 10ps, we can deduce, by deconvolving this resolution and trigger jitter, the actual pulse width obtained should be 7.6ps. This is the shortest pulse ever generated from 1.3μm semiconductor laser at high repetition rate by gain switching scheme. Because the laser diode was substantially oscillating with multimodes under current modulation, we performed the theoretical analysis with a set of multimode rate equations, where gain saturation effect was taken into account($\varepsilon = 10^{-17}cm^3$). The calculated FWHM at different photon lifetimes are shown in Fig.4. Curve a), which corresponds to the photon lifetime of 0.5ps, shows quite good agreement with the experimental resluts of Fig.2. To further reduce the pulse width, antireflection coating is effective. This effect together with the experimental determination of the gain saturation parameter are under investigation.

In summary, we found, multimode laser diode with high injection efficiency, like VIPS LD, is suitable for short pulse generation. Optical pulse less than 10 ps was successfully generated from a short cavity VIPS laser diode. By performing antireflection coating, we expect optical pulse can be reduced further.

88CH2609-8/88/0000/0094$1.00 1988IEEE

References:
[1]. Y. Arakawa, T. Sogawa, M. Nishioka, M. Tanaka and H. Sakaki, Appl. Phys. Lett., 51, pp. 1295-1297, 1987
[2]. D. Bimberg, K. Ketterer, E. H. Bottcher and E. Scholl, Int. J. Electron., Vol. 60, pp. 23-45, 1986
[3]. K. Y. Lau, Appl. Phys. Lett., 52, pp. 257-259, 1988
[4]. S. Oshiba, H. Horikawa, A. Matoba, M. Kawahara and Y. Kawai, 10th IEEE International Semiconductor Laser Conference, Paper K-1, 1986

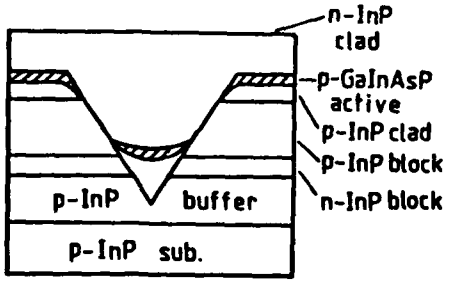

Fig. 1. Device structure of the 1.3μm InGaAsP VIPS laser diode

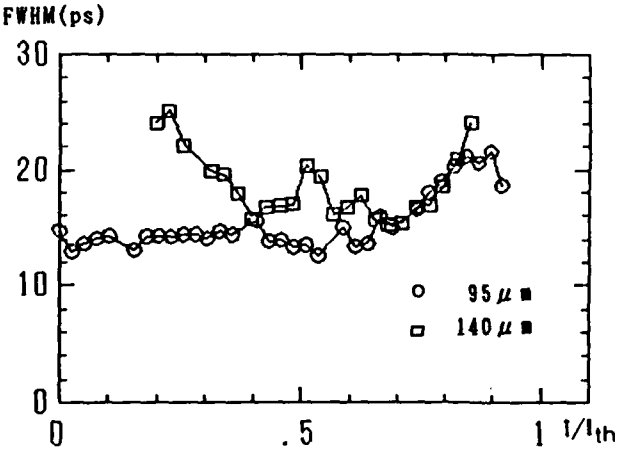

Fig. 2. D.C. bias dependence of the pulse width obtained from a 95μm VISP laser diode (without deconvolving the resolution of *streak camera and trigger jitter*). For comparison, data of a 140μm LD is also shown(□).

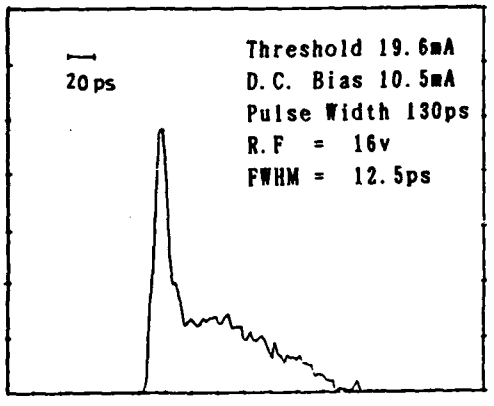

Fig. 3. Straek camera observation of the shortest optical pulse. By deconvolving the resolution of the streak camera (10ps) and trigger jitter, actual pulse width should be 7.6ps.

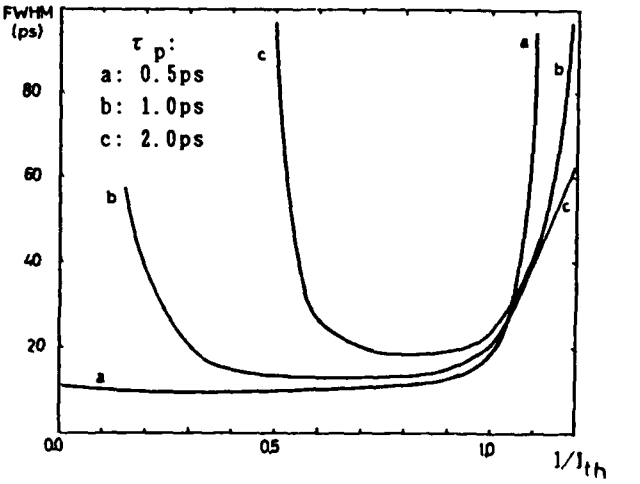

Fig. 4. Calculated D.C. bais dependence of the pulse width with different photon lifetimes. τ_p=0.5ps corresponds to a LD of about 95μm and τ_p=1ps corresponds to a 140μm LD.

G—5

Evaluation of Single Mode Property of DFB Lasers by Gain Switched Ultra Short Pulse Operation

H. Ishikawa, K. Kamite, K. Kihara, H. Sudo, M. [illegible]ano and H. Imai

Fujitsu Laboratories Ltd., 10-1 Morinosato Wakamiya, Atsugi, Japan

The objective of this paper is to investigate a DFB laser structure and the design that give dynamical single mode operation under very high speed modulation.

Under giga-bit range modulation it is a serious problem that even DFB lasers often exhibit mode partition and cause a floor in the bit-error measurement [1]. Here, we have investigated the single mode property of several types of DFB laser using gain switched ultra short pulse operation [2], because it gives the largest overshoot of gain above the threshold level, thereby causing a poor side mode suppression ratio (SMSR)in lasers with small threshold gain diffrence between modes. We also performed bit-error measurement and examined the correlation between SMSR.

We fabricated two types of asymmetric reflectivity DFB lasers different in facet reflectivity and a $\lambda/4$ shifted DFB laser as listed Table 1, all emitting at 1.3 μm. We used a mesa to reduce the parasitic capacitance of the BH strucutre and obtained 3 dB bandwidth exceeding 11 GHz for all of these three types of lasers. We applied a 200 mA comb shaped pulse train with pulse width of 70 ps and repetition rate of 1 GHz. Gain switched pulses of the half width of 17 to 25 ps were obtained. Fig.1 shows an example of an autocorrelation trace. An exmple of a spectrum under this operating condition is shown in Fig.2.

Fig.3 and Fig.4 show the measured SMSR under gain switched operation as a function of detuning. We used samples whose SMSR is above 30 dB under DC operation. Asymmetric reflectivity lasers with 5 % reflectivity exhibited small SMSR due to Fabry-Perot modes, while lasers with low reflectivity exhibited high SMSR. The rather small SMSR observed in several $\lambda/4$ shifted lasers was due to TM mode. We further performed the bit-error rate measurement using a -160 ps/nm dispersion fiber at 1.8 Gb/s RZ modulation. 100 % error free transmission was achieved for asymmetric reflectivity lasers with below 1% reflectivity. In several $\lambda/4$ shifted lasers we observed a floor at 10^{-10} due to TE-TM mode competition, nevertheless their SMSRs are large. This is due to the larger mode spacing between TE and TM mode than that between modes in an asymmetric reflectivity laser. The effect of fiber dispersion is pronounced in $\lambda/4$ shifted laser.

In the asymmetric reflectivity laser, reduction of the facet reflectivity attained large SMSR under gain switched operation and error free transmission. In the $\lambda/4$ shifted DFB laser, careful design of its waveguide or an incorporation of strong TM mode suppression mechanism was confirmed to be necessary to attain 100 % error free transmission.

[1] S. Sasaki et al. Paper WQ34, presented at OFC'88, New Orleans
[2] K. Kamite at al. Paper THK3, presented at OFC'88, New Orleans

88CH2609-8/88/0000/0096$1.00 1988IEEE

Table 1.
Samples used in the experiment

Laser structure		I_{th}(mA)	η (mW/mA)	κ L	Single mode CW output(mW)
Asymmetric reflectivity DFB laser	5% -as cleaved	10-15	0.25-0.35	0.5-1.0	40-60
	below 1% -as cleaved	15	0.25-0.35	0.5-1.0	40-60
$\lambda/4$ shifted DFB laser	both facets below 1 %	15-20	0.20-0.30	1.3	40

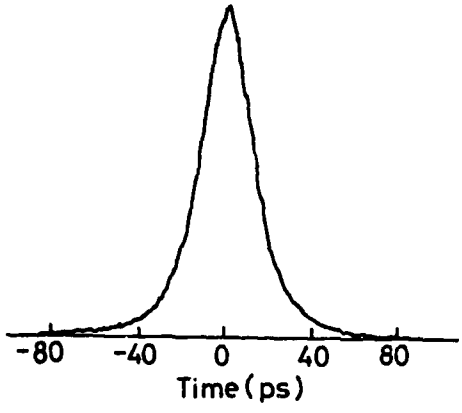

Fig.1 Autocorrelation trace. This trace gives pulse width of 19 ps.

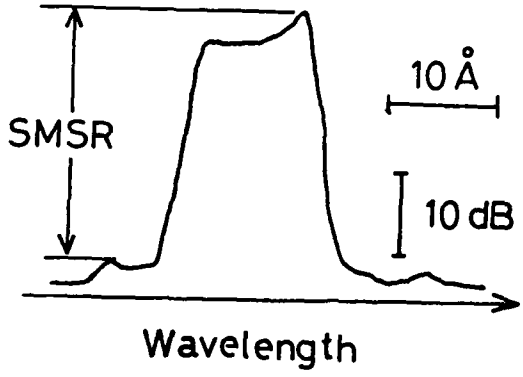

Fig.2 An example of a spectrum under gain switched operation. Large chirp indicates large gain overshoot.

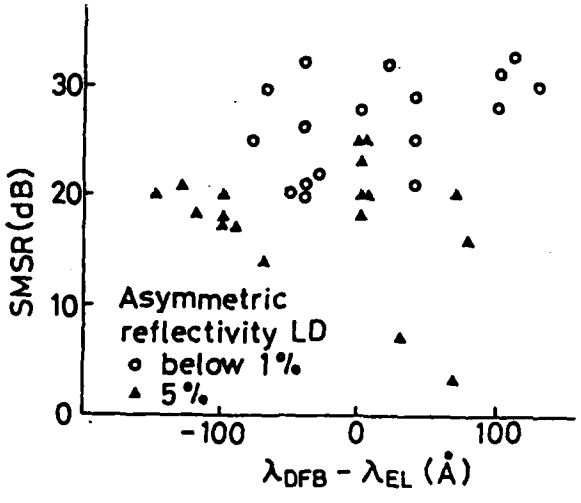

Fig.3 Side mode suppression ratio of asymmetric reflectivity laser.

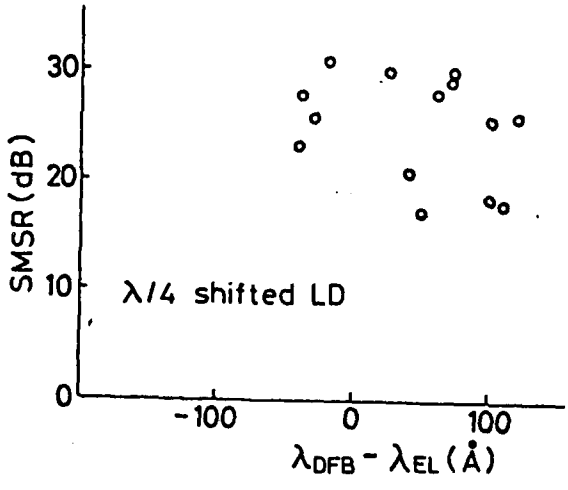

Fig.4 Side mode suppression ratio of $\lambda/4$ shifted laser.

Session H: Single Mode DFB & DBR Devices II

H—1

Current Tailoring for Lowering Linewidth Floor

T. Ikegami, M. Fukuda and H. Yasaka

NTT Opto-electronics Labs
Atsugi-shi, Kanagawa 243-01, Japan

The floor in the linewidth and output power relation has been observed with conventional solitary DFB lasers. A suggestion on the phenomenon has been proposed, that is, 1/f noise [1], threshold gain difference between the lasing main-mode and nonlasing sub-mode [2], and the Gaussian lineshape instead of Lorentzian lineshape [3] etc, however, the cause is still inexplicable. We found that intensity of spontaneous emission or sub-mode increased when the floor appeared or the rebroadening of the linewidth occured, and the floor could be lowered in some extent by changing the current distribution along the stripe electrode of DFB lasers for reducing residual carriers.

Figure 1 shows the linewidth, the intensity ratio of the main-mode to the sub-mode observed with a DFB laser having the cavity length of 300 μm, κL of 1.5 and the both-cleaved structure. At the high output power, the linewidth floor is observed as already reported, and moreover, the intensity of the sub-mode are found to slow down the reduction with the inverse power. The lineshape remains to be Lorentzian. At the high excitation, the suppression of carriers becomes broken and the stabilization of the gain or the field intensity is degraded due to spatial hole-burning along the lasing axis.

In order to control the spatial hole-burning, a three terminal DFB laser with separated 100 μm length electrodes, κL of 2 and a both-cleaved structure is used. The current Is is supplied to two terminals at the cleaved sides, and the current Ic is supplied to the center terminal. Ic and Is are independently adjusted each other. Figure 2 shows that the linewidth and the intensity of the sub-mode Isub change with the ratio of the center current Ic to the total current (Ic + Is) under the constant output power of 6 mW. In the figure, the arrow indicates the uniform excitation, and the linewidth and Isub can be reduced by increasing the center current Ic. In the three-terminal DFB laser, the carrier densities in the vicinity of the cleaved ends are higher than that at the center due to the non-uniform field distribution under the uniform and high excitation, then the above adjustment of the current distribution can improve the linewidth. By tailoring the current distribution, the linewidth floor can be lowered to the values shown by the straight line of the linewidth vs. inverse power curve in Fig. 3.

88CH2609-8/88/0000/0100$1.00 1988IEEE

References:
1. K. Kikuchi and T. Okoshi, Electron Lett., 21, p.1011(1985).
2. S. Takano, S. Murata, I. Mito, and K. Kobayashi, in Tech. Dig., 1st Optoelectronic Conf., Paper D2-5(1986).
3. K. Kobayashi and I. Mito, in Tech. Dig., OFC/IOOC,Paper WC1(1987).

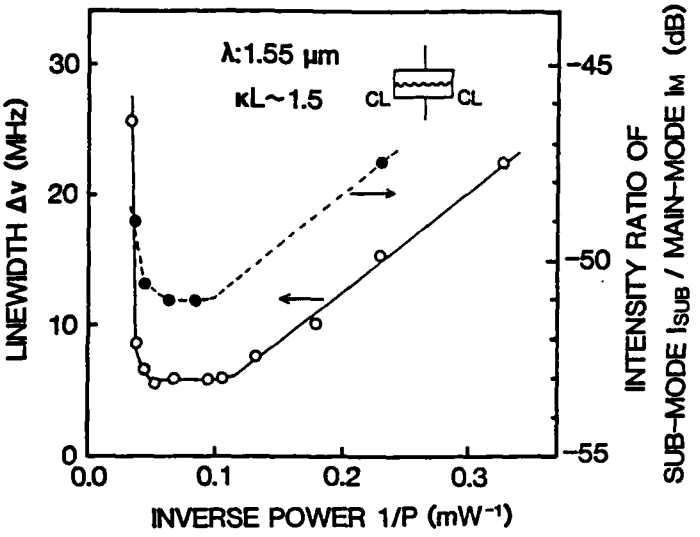

Figure 1: Linewidth floor of a solitary DFB laser

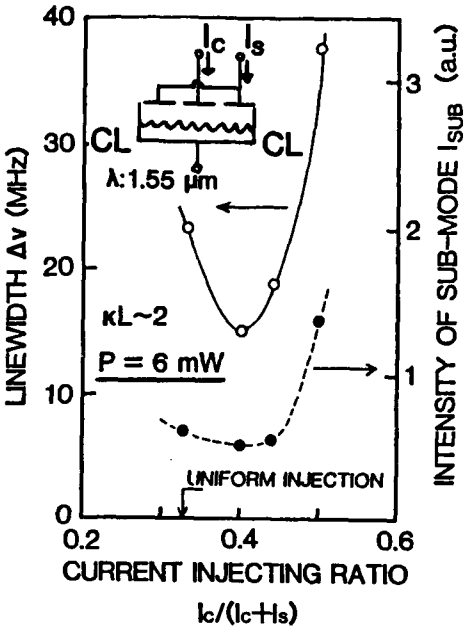

Figure 2: Linewidth & intensity of sub mode vs. current injection ratio under constant power operation

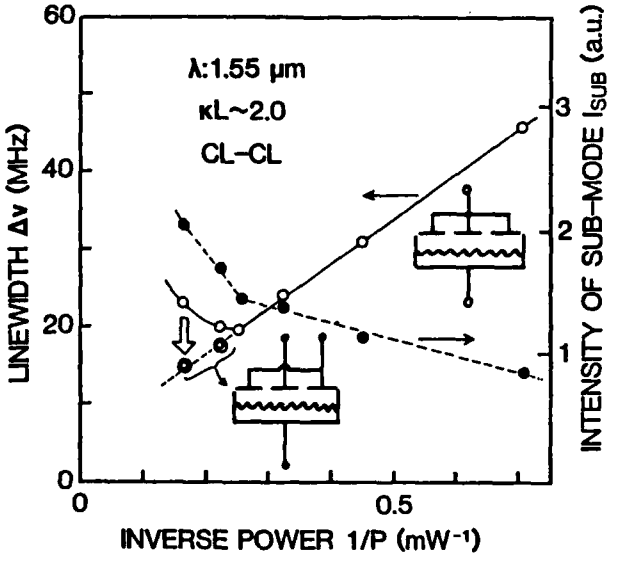

Figure 3: Improvement of linewidth floor by current tailoring

H—2

Effects of Longitudinal Spatial Hole Burning on the Characterisitics of Phase-Shifted DFB Lasers—Calculation Considering Longitudinal Gain Distribution

Yoshiaki NAKANO, Osamu KAMATANI, and Kunio TADA
Department of Electronic Engineering, University of Tokyo
7-3-1 Hongo, Bunkyo-ku, Tokyo, 113, JAPAN

In the cavity of distributed feedback (DFB) lasers, optical intensity distribution along the laser axis is apt to become nonuniform, and is strongly dependent on the normalized coupling coefficient κL.[1] This will induce axial nonuniformity in carrier density to result in what is called "longitudinal spatial hole burning."[2] Due to this phenomenon the laser characteristics such as oscillation wavelength and single mode selectivity change with increasing injection current. This may be a substantial problem preventing high power operation of the lasers.

Soda et al. pointed out through their numerical analysis that, in order to suppress this effect and to keep stable single longitudinal mode operation in quarter wave shifted (QWS) DFB lasers, κL should be controlled to 1.25 at which the intensity distribution along the axis becomes almost uniform.[2] Their analysis successfully explained the two mode nature of QWS DFB lasers with high κL, yet failed to explain experimentally observed "blue shifts" of oscillation wavelength at high κL. We thought that this discrepancy might arise from their constant gain approximation along the axis, and carried out a numerical analysis including the effect of the longitudinal gain distribution.

We started with the coupled mode equations and the steady state rate equations as usual. Local gain was approximated as a linear function of local carrier density. Inclusion of this axial coordinate dependent gain parameter into the coupled mode equations characterizes our analysis. Because of the axial index and gain distributions we could not obtain analytical solutions for the coupled mode equations. Instead, the numerical method described in Ref.[3] was employed. Although a complicated double iteration scheme was needed in obtaining self-consistent optical intensity profile and carrier density profile along the axis for an oscillating mode, our algorithm did not double the cpu time required for the case of the constant gain approximation.

Figure 1 shows the normalized oscillation frequency δL as functions of injection level calculated for QWS DFB lasers with several κL. Like the previous work, the "blue shift" of oscillation frequency caused by current injection diminishes with increasing κL when $\kappa L < 1.2$. However, unlike before, it again increases when $\kappa L > 1.2$, and no "red shift" is observed. This is consistent with experimental results.[4] In terms of frequency stability, the optimum κL is understood as 1.2 which is slightly different from the optimum value of 1.25 in the foregoing work. Even with κL of 1.2, a considerable frequency shift remains.

On the other hand, if we use the modulated stripe width (MSW) structure[3,5] having an axial index distribution as shown in Fig.2 instead of QWS, oscillation frequency shift can be reduced by a factor of 10 as observed in Fig.1. This is one of the facts showing its superiority over QWS.

Figures 3 and 4 illustrate single mode selectivity expressed in terms of the normalized threshold gain difference ΔgL and its shifts from the values at threshold. Our calculation found out that the constant gain approximation overestimates and exaggerates the shifts of ΔgL. From Fig.3 we understand that the above MSW structure has slightly lower single mode selectivity than QWS, yet the absolute value itself is sufficient for achieving large side mode suppression ratio. In addition, injection current strengthens the single mode selectivity of the MSW while lessens that of QWS as shown in Fig.4. This tendency becomes notable at high κL where the single mode selectivity of the MSW will exceed that of QWS.

In conclusion, we here pointed out that in DFB lasers the spatial gain profile along the axis that the previous work neglected plays an important role in determining the oscillation

88CH2609-8/88/0000/0102$1.00 1988IEEE

characteristics. We also showed some advantages of MSW over QWS structures.

1) H. Kogelnik and C. V. Shank, J. Appl. Phys. **43**, 2327 (1972)

2) H. Soda et al., IEEE J. Quantum Electron. **QE-23**, 804 (1987)

3) K. Tada et al., Electron. Lett. **20**, 82 (1984)

4) M. Yamaguchi et al., Paper of Technical Group on Optical and Quantum Electron., Inst. of Electron. and Commun. Engrs. of Jpn., OQE86-150 (1986)

5) Y. Nakano and K. Tada, Appl. Phys. Lett. **51**, 387 (1987)

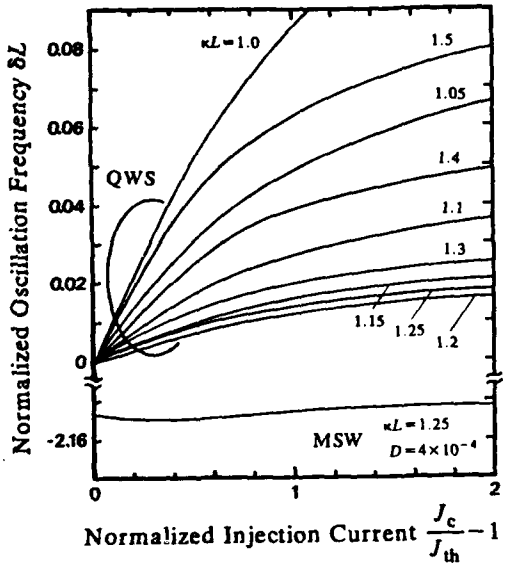

Fig.1. Dependence of normalized oscillation frequency on normalized injection current (J_c : injection current density, J_{th} : threshold current density).

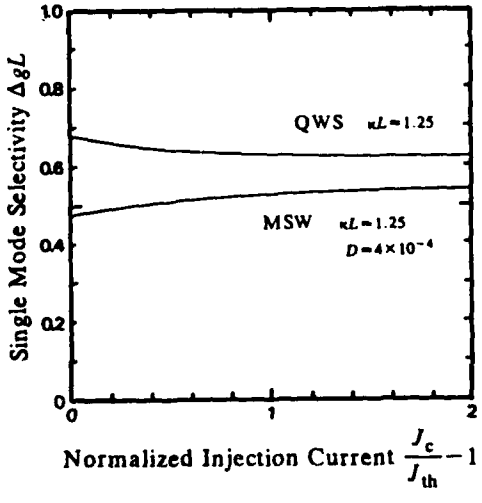

Fig.3. Single mode selectivity as functions of normalized injection current.

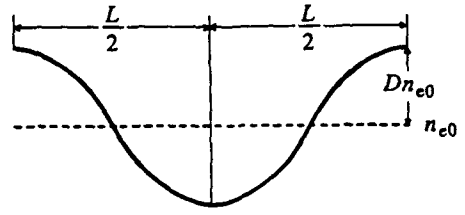

Fig.2. Longitudinal (cosine) distribution of refractive index to be implemented by stripe width modulation (L : cavity length, n_{e0} : average effective index of refraction, D : relative amplitude of the index modulation).

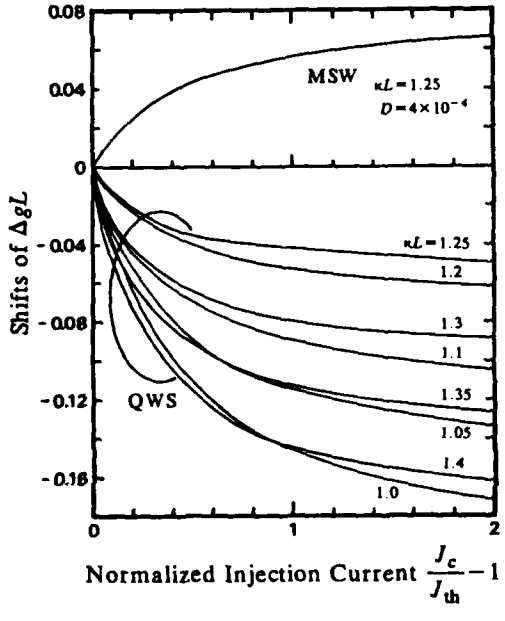

Fig.4. Change of single mode selectivity from the value at threshold ($J_c/J_{th}-1=0$)

H—3

The Influence of Longitudinal Mode Spatial Hole Burning on the Linewidth and Spectrum of λ/4-Phase Shifted DFB Laser

J.E.A. Whiteaway, G.H.B. Thompson, C.J. Armistead, A.J. Collar
S.J. Clements and M. Gibbon

STC Technology Ltd, London Road, Harlow, Essex, CM17 9NA, UK

In order to optimise the performance of λ/4-phase shifted DFB lasers it is necessary to allow for longitudinal mode spatial hole burning.

The presence of injected carriers in the active layer of a laser depresses the refractive index. The interaction of the photon distribution with the carrier distribution therefore gives rise to longitudinal spatial hole burning in single frequency laser structures incorporating a grating[1]. All aspects of the laser performance above threshold are influenced by this non-linear mechanism. It can, for example, lead to hopping between longitudinal modes with increasing output power.

A computer model has been set up that enables laser structures composed of arbitrary series combinations of grating and planar sections to be analysed. Longitudinal mode spatial hole burning is taken into account and multi-longitudinal mode operation can be simulated. The longitudinal mode intensity, carrier density and refractive index distributions are predicted as a function of drive current above threshold. In addition the linewidth is estimated in a self-consistent manner by simulating the injection of spontaneous emission at many points along the device cavity. This also allows the spontaneous emission spectrum radiated from each end of the device to be predicted above and below threshold.

Detailed measurements have been made of the cw spectra emitted by λ/4-phase shifted DFB lasers, and the linewidth has been measured using the delayed self-homodyne technique.

The model has been used to produce plots enabling the threshold current, efficiency, linewidth-power product and single mode output power of λ/4-phase shifted DFB lasers to be traded-off against one another as K and L are varied, see Figure 1.

Spectral measurements have shown clear evidence of hole burning as predicted by the model. For example for high KL product devices the lasing mode moved to longer wavelengths relative to the side modes at the stopband edges as the drive current is increased. The measured linewidth varied approximately inversely with the output power, but with a non-zero offset at high power see Figure 2. The effect on the linewidth of changes in effective grating reflectivity and in the spontaneous emission distribution along the cavity as hole burning takes place will be examined.

In summary a comprehensive model of single frequency laser operation in the presence of longitudinal hole burning has been used to interpret the first detailed measurements of spectral changes with increasing output power. The measured dependence of linewidth on inverse output power has a non-zero offset which can be explained by detailed modelling of the linewidth in the presence of hole burning.

REFERENCES

1. H. Soda, H. Ishikawa and H. Imai, Electron. Lett., 22(20), 1049, 1986.
2. C.H. Henry, IEEE Jnl. Quantum Electron., QE-18(2), 259, 1982.
3. K. Kojima, K. Kyuma and T. Nakayama, Jnl. Lightwave Tech., LT-3(5), 1048, 1985.

88CH2609-8/88/0000/0104$1.00 1988IEEE

Map of Linewidth x Power Product in κ L v/s L Plane for $\lambda/4$ DFB Lasers

Figure 1.

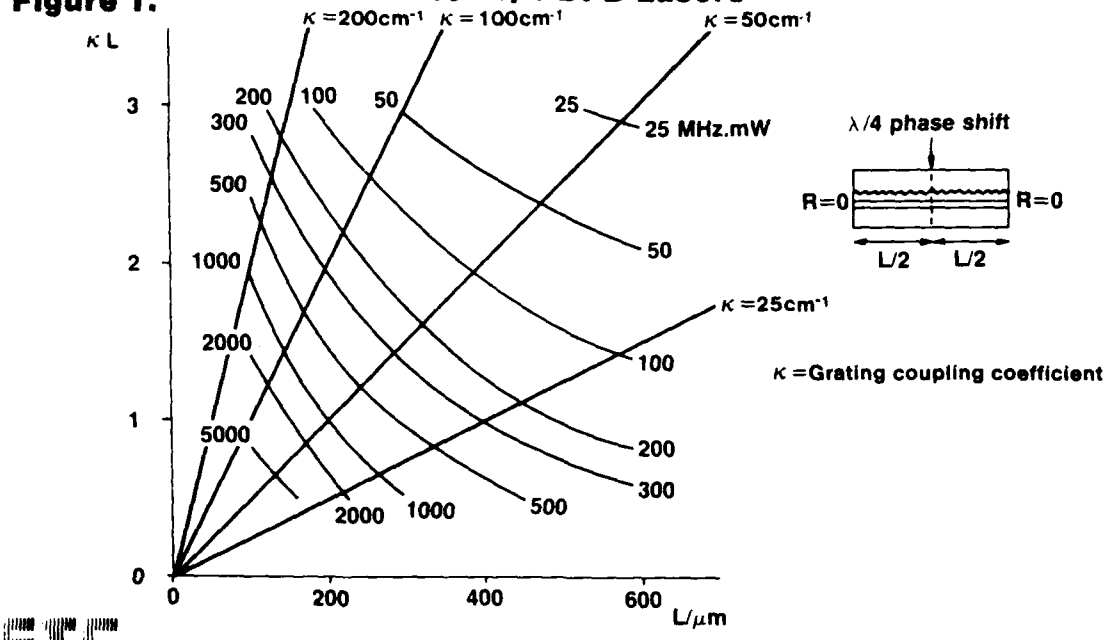

STC TECHNOLOGY LTD

Measured Dependence of Linewidth on Inverse Current in Excess of Threshold for $\lambda/4$-phase Shifted DFB Laser

Figure 2.

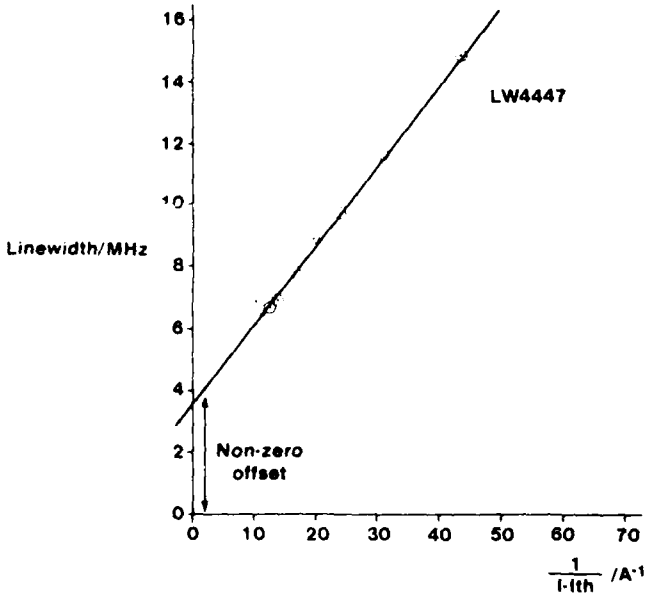

STC TECHNOLOGY LTD

H—4

Axially Homogenized Internal Field in DFB lasers with Two λ/8 Phase Shifters

Jun-ichi KINOSHITA and Kenji MATSUMOTO

Electron Device Engineering Laboratory, TOSHIBA Corp.
Shinsugitacho 8, Isogo-ku, Yokohama 235 Japan

A new DFB laser structure, which achieves single longitudinal mode (SLM) operation with very high yield, is required as a light source in long-span and high bit-rate optical transmission systems.

A recent study has suggested that spatial hole-burning along the laser axis (z-HB) must be suppressed to obtain stable SLM operation above the threshold.[1] This phenomenon originates in an axially inhomogeneous internal field distribution. Also a large threshold gain difference between the main and next submode ($\Delta \alpha L$) must be required. Therefore, DFB lasers with a large $\Delta \alpha L$ value and an axially homogeneous optical intensity distribution should be targeted.

We proposed a new DFB laser structure which has two $\lambda/8$ phase-shifters spaced with a distance of $2\Delta L$ ($2\times \lambda/8$ structure). For this model and conventional single shifted models, the yields of lasers with a large $\Delta \alpha L$ value and with a homogeneous internal field distribution were calculated by changing facet phases and normalized coupling coefficient (κL). Also, axial intensity distributions were calculated as a function of $\Delta L/L$ (L;the cavity length).

Yield maps of DFB lasers satisfying the following conditions are illustrated in Fig.1.

$$\Delta \alpha L \geqq 0.05, \quad FR \geqq 0.60$$

where FR(Field ratio) is defined as minimum/maximum in the axial intensity distribution (FR=1.0 means a completely homogeneous distribution). The maps correspond to structures with:

(a) a $\lambda/4$ phase shifter at the cavity center,
(b) a $\lambda/8$ phase shifter at the center,
(c) two $\lambda/8$ shifters which are L/3 apart.

The results demonstrated that the new structure has a greater design margins for the facet reflectivities (r) and for the κL value than the conventional single shifted structures. In Fig.2, axial intensity distributions of $2\times \lambda/8$ structures are shown as a function of $\Delta L/L$ (where $\Delta L/L=0$ corresponds to the conventional $\lambda/4$ shifted structure). This figure shows that the optical field concentrated on the $\lambda/4$ shifter is dispersed into the two splitting $\lambda/8$ shifters, flattening the whole distribution, as $\Delta L/L$ increases.

In conclusion, a new $2\times \lambda/8$ shifted DFB structure is found to be effective to homogenize its internal field distribution along the axis and has greater margins of r and κL. This will contribute greatly to obtaining SLM DFB lasers with higher yields and suppressing unfavorable z-HB effects.

[1] Soda et.al.,IEEE QE J.of Quantum Electron., QE-23(6), p.804, (1987)

88CH2609-8/88/0000/0106$1.00 1988IEEE

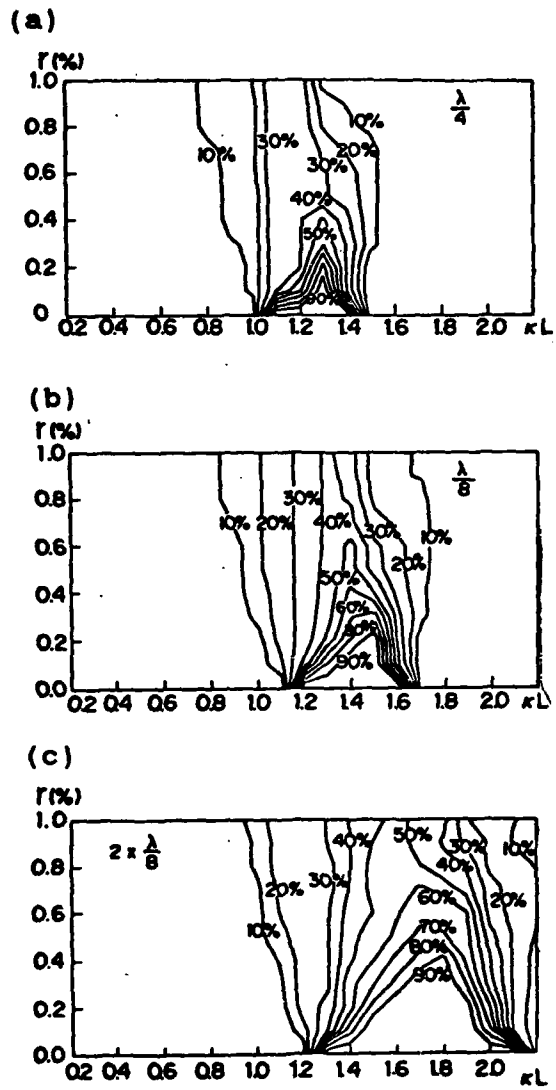

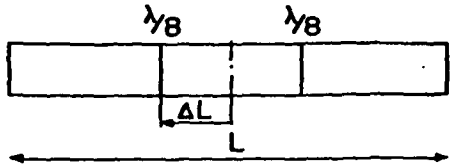

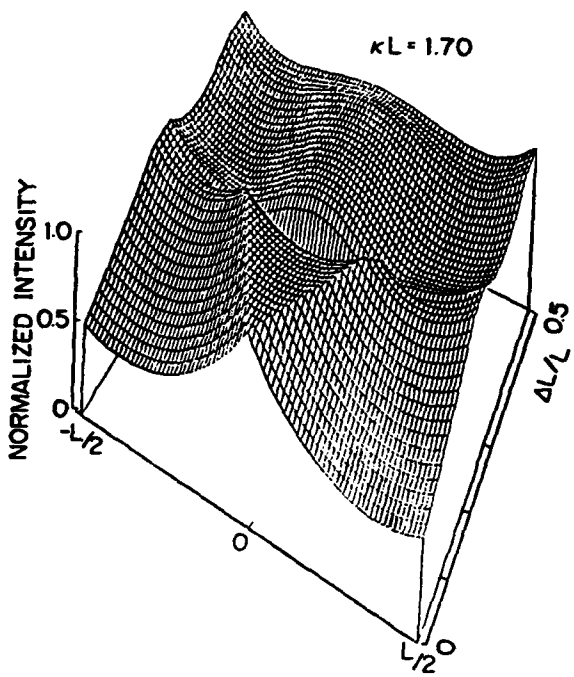

Fig.1 Yield maps of DFB lasers satisfying $\Delta \alpha L \geq 0.05$, $FR \geq 0.60$
(a) a $\lambda/4$ phase shifter at the center,
(b) a $\lambda/8$ phase shifter at the center,
(c) two $\lambda/8$ shifters which are L/3 apart.
r:both facet reflectivity,
κ L:normalized coupling coefficient

Fig.2 Axial intensity distributions of 2× $\lambda/8$ structures (as a function of Δ L/L)

Session I: Grating Laser Dynamics & Stabilization

I—1

Dynamic Longitudinal Mode Stability in Quarter Wave Shifted DFB Lasers

S.TSUJI, M.OKAI, H.NAKANO and N.CHINONE
Central Research Laboratory, Hitachi, Ltd.
Kokubunji, Tokyo 185, Japan
and
M.CHOY
Bell Communications Research
Red Bank, NJ 07701, U.S.A.

Stable single mode operation of semiconductor lasers are of great interest for multi-giga bit long-span optical fiber communications.[1] Especially, quarter wave shifted (QWS-) DFB lasers are expected to be one of the most attractive light sources, because of their large threshold gain difference between a main mode and sub modes.

In this paper, mode competitions in QWS-DFB lasers are investigated comparing with conventional DFB lasers with antisymmetric facet reflectivity (RAS-DFB). The QWS-DFB lasers are found to sustain single longitudinal mode operation even if they are driven in gain switching modes.

The lasers used in this experiments are based on a BH structure, which gives stable transverse mode excitation inside the cavity.[2] These lasers were fabricated through second step LPE on InP substrates with first order corrugations. For QWS-DFB, the phase jump position was made at the center of the cavity, and the measured κL was 2. Both of the facets of QWS-DFB were coated with SiN films to reduce facet reflectivity. CW mode stability of the QWS-DFB lasers were firstly investigated in regarding to their facet condition. The lasers were driven up to 4 times threshold, and the mode stability were investigated. Longitudinal mode jump was observed for the lasers with relatively large reflectivity as shown in Fig.1. That can be explained by the phase change due to hole burnings.[3] However the effect of the hole burning can be small for the low reflectivity lasers, which was theoretically confirmed. According to Fig.1, the facet reflectivity should be controlled to less than 0.8% and these devices were used for dynamic experiments.

DFB lasers were driven with rectangular current pulses (750MHz, 40mAp-p) and bias current were controlled so that lasers oscillated in only the first cycle of resonance frequency. Time averaged spectra were measured as shown in Fig.2. Relatively flat shape of the main mode shows the linear charping. As sub modes have peak at their shorter wavelength side, the gain over shoot at the leading edge was the cause of the mode competition, which could be well explained by the two mode rate equation. Threshold gain differece $\Delta\alpha th$ between main mode and sub modes was measured at 0.9Ith. According to the reduction in $\Delta\alpha th$, main mode-sub mode intensity difference at gain switched pulses decrease as shown in Fig.3. The measured $\Delta\alpha th$ of QWS-DFB lasers was larger than 10 cm^{-1}, and the stable single mode operation was obtained. The measurement on photon statics also showed the mode stability.

Dynamic single mode stability of QWS-DFB lasers is firstly confirmed using gain switching drive.

88CH2609-8/88/0000/0110$1.00 1988IEEE

We would like to thank to S.Hattori and M.Hirao of Komoro Works, Hitachi and S.Sasaki of C.R.L., Hitachi for their assistance in laser fabrication and useful discussions.

Reference [1]S.Fujita, OFC'88 PD16, 1988 [2]S.Tsuji, IEEE/OSA LT5,p822,1987 [3]H.Soda, SLC'86, 1986

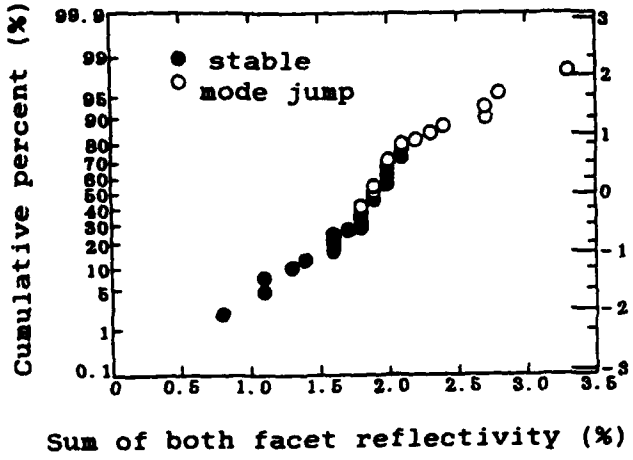

Fig.1. CW longitudinal mode stability vs. facet reflectivity in QWS-DFB laser

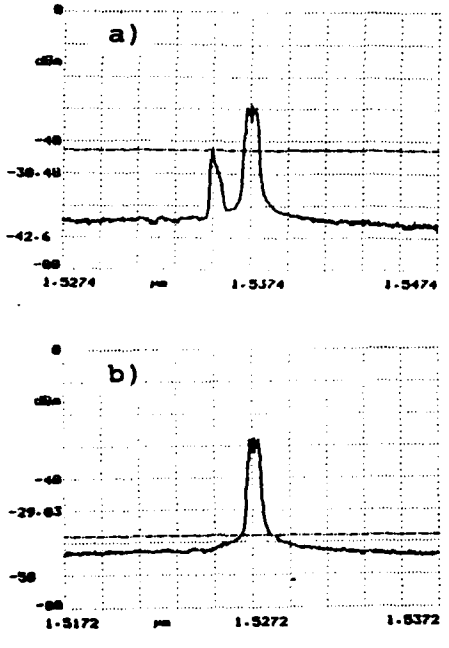

Fig.2. Average spectra under gain switched modulation
a)conventional RAS-DFB
b)QWS-DFB

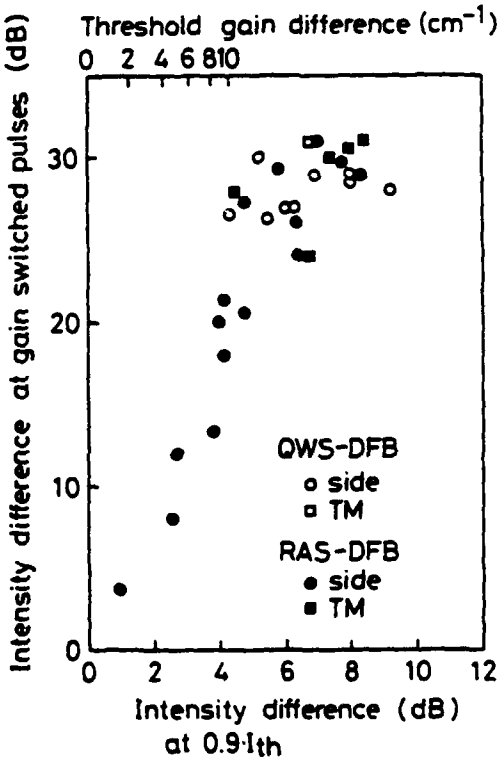

Fig.3. Measured relation between threshold gain difference and peak intensity difference at gain switched pulse

I—2

Experimental Verification of a Beat-Frequency Fluctuation Model

R.J.S.PEDERSEN, Electromagnetics Institute, Technical University of Denmark, DK-2800, Lyngby, Denmark,
G. JACOBSEN, Telecommunication Research Laboratory, Lyngsø Allé 2, DK-2970 Hørsholm, Denmark.
I. GARRETT, British Telecom Research Laboratories, Martlesham Heath, Ipswich, Suffolk, U.K.

Objective: Experimental verification of a theoretical model for the frequency fluctuation probability density function of single mode semiconductor lasers.

Background: Weakly coherent systems are likely to be the dominant type of coherent systems due to the relatively easy engineering of transmitter and local oscillator modules. In examining the performance of this kind of systems it is necessary to include the influence of laser phase noise. This can be done using the frequency equivalent of the random phase noise process [1] (eqn. 5). The scope of the present work is to verify experimentally the theoretical model for the random frequency process originating from the laser phase noise.

Experiment: The experimental setup is shown in fig.1. The phase noise signal is generated by beating a DFB-laser (linewidth app. 40 MHz) with an external cavity laser (negligible linewidth). By measuring the statistics of the output voltage from the frequency discriminator the statistics of the instantaneous frequency at the output of the IF-filter can be found (fig.1). In this setup we measure the cumulative density function (cdf) of frequency deviation from a nominal center frequency $f - f_0 = \Delta f$ by integrating the relative time the frequency is below the threshold frequency f. We measure the cdf(Δf) for three different IF-filters in order to verify the influence of the IF-filter, and for one filter (fig.2) we measure the cdf(Δf) for three positions of the mean beat frequency in order to verify the influence of signal position within the filter.

Results: In fig.3 $\log_{10}(cdf)$ is shown versus Δf for three positions of the beat signal within the IF-filter. The experimental points are compared with theoretical fits. The theoretical cdf(Δf) can be written as

$$cdf(\Delta f) = \frac{1}{2} + \frac{1}{2} erf(\Delta f \sqrt{\frac{\pi}{\Delta \nu B}}) \tag{1}$$

The fitting parameter is the product of beat signal linewidth ($\Delta\nu$) and IF-bandwidth B. The IF-bandwidths are calculated as the normalized lowpass equivalent [2]

$$B = \int_0^\infty \left| \frac{H(f - f_0) + H(f + f_0)}{2H(f_0)} \right|^2 df \tag{2}$$

where H(f) is the complex frequency transfer function of the IF-filter. In table 1 the measured results are compared with theoretical predictions for three IF-bandwidths and for three positions of the beat signal within one of the IF-filters. The measured results are given with some uncertainty from determination of linewidth, measurement of IF-filter characteristic and the fitting of theoretical curves. The theoretical model of frequency fluctuation statistics is shown to give a very good description of the laser phase noise influence.

Acknowledgements: We thank the Danish Telecommunications Research Laboratory and the Director of Research of British Telecommunications plc for permission to publish this work. One of us (RJSP) thank the Danish Technical Research Council for financial support. We thank Peter Smythe for suggestion of the data acquisition method, R. Lobbett and R. Wyatt for stimulating discussions.

[1] I.Garrett and G.Jacobsen,'Statistics of laser frequency fluctuations in coherent receivers', Electron. Lett., Vol. 22, pp 168-170, 1986.

[2] I.Garrett, G.Jacobsen and R.J.S.Pedersen, 'Filtered Laser Beat-frequency Fluctuations', To be published.

88CH2609-8/88/0000/0112$1.00 1988IEEE

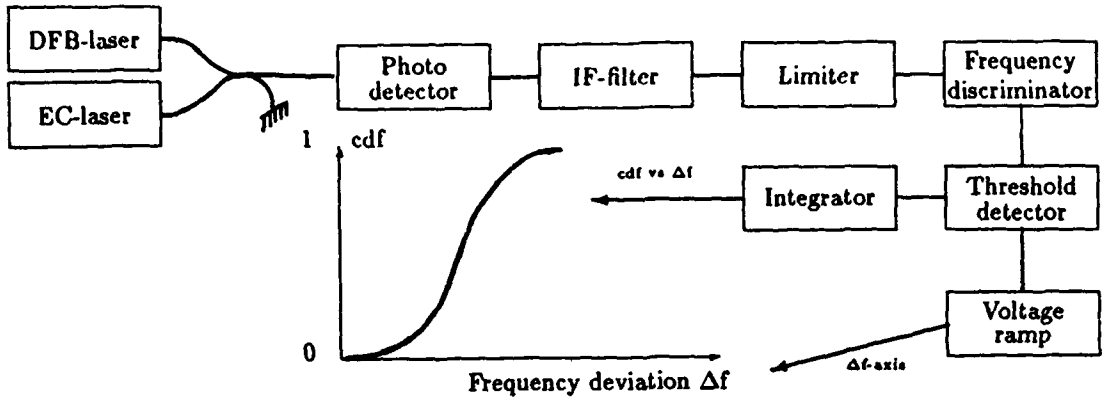

Fig. 1 : Schematic diagram of experimental setup.

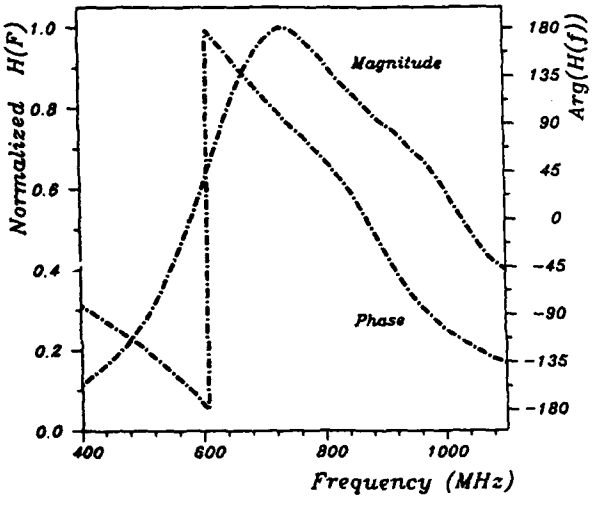

Fig. 2 : Magnitude and phase of IF-filter number 3.

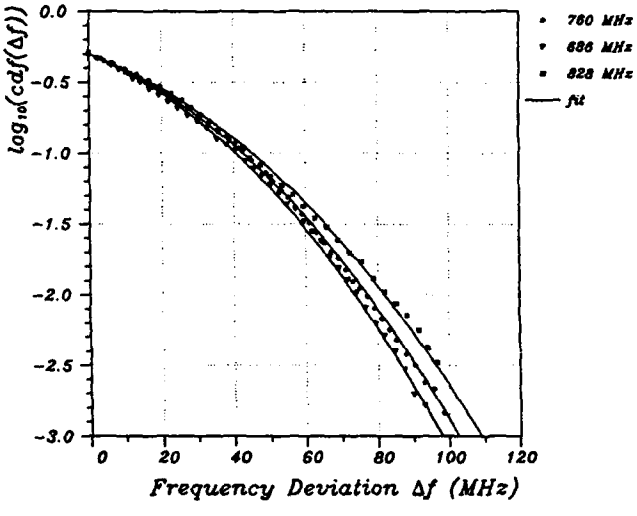

Fig. 3 : Experimental points compared with theoretical fits. The curves correspond to f_0 equal to 686,760 and 828 MHz respectively.

	Center frequency f_0					
	686 MHz		760 MHz		828 MHz	
IF-filter	*Calculated*	*Measured*	*Calculated*	*Measured*	*Calculated*	*Measured*
1	-	-	99 MHz	101±7 MHz	-	-
2	-	-	153 MHz	148±10 MHz	-	-
3	163 MHz	158±11 MHz	167 MHz	174±12 MHz	207 MHz	196±13 MHz

Table 1 : Comparison between measured and calculated (eqn. (1),(2)) results.

I—3

FM Characteristics of Multi-Electrode DFB and DBR Lasers[1]

X. PAN, *Electromagnetics Institute, Technical University of Denmark, DK-2800 Lyngby, Denmark,*
H. OLESEN and B. TROMBORG, *Telecommunication Research Laboratory, Lyngsø Allé 2, DK-2970 Hørsholm, Denmark.*

We present the first theoretical study of the FM response of multi-electrode DFB and DBR lasers, when the current to the passive section(s) is modulated.

Multi-electrode lasers are currently under development in many laboratories, and several experimental results have been reported. An attractive feature of devices with passive sections is the possibility of getting a high FM response, which is uniform in modulation frequency from DC up to several hundred MHz [1]. The cut-off frequency is roughly determined by the carrier lifetime in the passive section. The static tuning properties of multi-electrode DFB and DBR lasers have recently been analysed by the authors [2],[3], but to our knowledge the modulation characteristics have not previously been analysed.

One example of a multi-electrode laser is the phase-tunable DFB laser [1],[2] shown in Fig. 1. From our transmission line model for compound cavity lasers [4] we can derive the following rate equation for the photon number $I_p(t)$ and the phase $\phi(t)$ of the electric field

$$\frac{1}{2}\frac{d}{dt}\ln I_p(t) + j\frac{d\phi}{dt} = \frac{1}{1+\tau f_D}\left\{\frac{1}{2}(1+j\alpha)G_N\Delta N(t) + f_D\frac{\partial \ln r_R}{\partial N_2}\Delta N_2(t)\right\} \tag{1}$$

where τ is the round-trip time in the phase control (PC) section, f_D is the (complex) round-trip frequency for the DFB section, α is the linewidth enhancement factor, G_N is the differential gain, r_R is the effective reflectivity of the PC section seen from the interface, and $\Delta N(t)$ and $\Delta N_2(t)$ are the deviations of carrier densities from the steady-state values in the DFB and PC sections, respectively. The PC current is modulated with an amplitude $\Delta I_{PC}(t)$ so that

$$\frac{d}{dt}\Delta N_2(t) = \frac{1}{eV_2}\Delta I_{PC}(t) - \frac{1}{\tau_s}\Delta N_2(t) \tag{2}$$

Here, e is the electron charge, V_2 is the waveguide volume of the PC section, and τ_s is the differential carrier lifetime. The small-signal FM response can then be calculated from (1) and (2) and the usual rate equation for the carrier density in the active section. Eq. (1) shows that there are two contributions to the FM: 1) a direct contribution ($\sim \Delta N_2(t)$), which is carrier lifetime limited, corresponding to modulation of DC operating point, and 2) a 'dynamic' contribution ($\sim \Delta N(t)$), which persists up to several GHz and corresponds to an indirect modulation of the carrier density in the active section. The direct part acts as a driving term for the indirect modulation part.

Fig. 2 shows the static frequency tuning characteristics [2]. Four regions of continuous tuning separated by discrete mode jumps across the Bragg frequency are observed, and both positive, zero and negative slopes are present on the curves. The slopes indicate the low-frequency FM efficiency, which can be expected. Generally, the magnitude of the slope decreases for increasing injection level, because Auger recombination limits the efficiency at high injection. On the other hand, the carrier lifetime decreases with increasing injection, which makes the direct FM contribution extend to higher frequencies. This is clearly seen in Figs. 3a-b, which show the magnitude and phase of the FM response for three different bias points in Fig. 2. At 5 mA the DC response and cut-off frequency is 8 GHz/mA and 190 MHz, respectively, and at 100 mA the corresponding values are 1.1 GHz/mA and 1.6 GHz. At 17.7 mA the static characteristic is near a minimum and the dynamic part of the FM is dominant. In the region above 1 GHz, a clear relaxation resonance peak is observed and intricate 'interference'

[1]This work was supported by the EEC under Contract No. ST2J-0171-2-DK

88CH2609-8/88/0000/0114$1.00 1988IEEE

effects occur between the two FM contributions. The phase delay is 0 at low frequencies (if the static curve has a positive slope) and changes smoothly, except in the vicinity of the resonance peak. In direct modulation of an active section the FM response is usually dominated by thermal effects at low frequencies, which leads to a non-uniform structure. The present response is uniform over a large range and should be easy to equalize further up to several GHz [5]. The presence of the resonance peak is a new result, which has not been reported experimentally, but below 1 GHz there is an excellent agreement with experiments. Here, we have only presented results for the phase-tunable DFB laser, but calculations on 2- and 3-section DBR lasers show qualitatively very similar results.

In summary, we have given a simple theory for the FM response of multi-electrode DFB and DBR lasers. Our results indicate that these devices can be very promising as FSK transmitters in coherent transmission systems, if the operating point is carefully selected.

References

1. S. Murata et al., Electron. Lett., vol. 23, pp. 12-14, Jan. 1987.
2. H. Olesen et al., to appear in IEEE J. Quantum Electron., vol. QE-24, 1988.
3. X. Pan et al., submitted for publication.
4. B. Tromborg et al., IEEE J. Quantum Electron., vol. QE-23, pp. 1875-1889, Nov. 1987.
5. O. Nilsson et al., Electron. Lett., vol. 23, pp. 1371-1372, Dec. 1987.

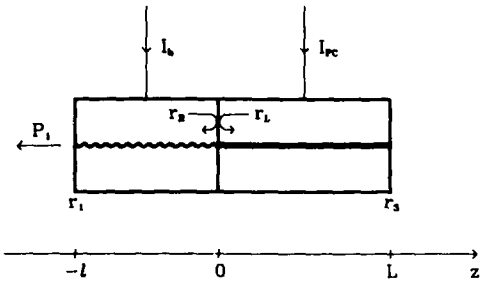

Fig. 1. Phase tunable DFB laser with an active DFB section and a passive phase control (PC) section. l = 350 μm, L = 200 μm, $r_1^2 = r_3^2 = 32$ %.

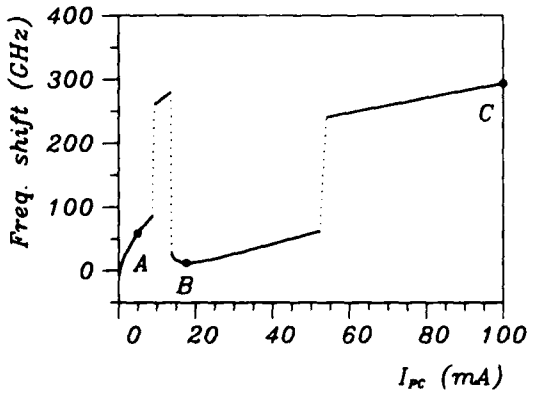

Fig. 2. Frequency shift versus PC current. The points A, B and C refer to the PC bias currents used in Fig. 3.

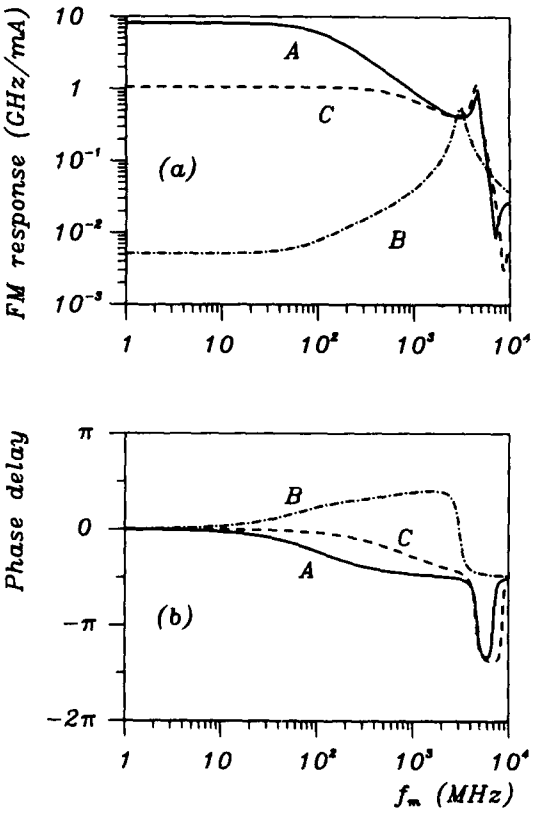

Fig. 3. FM response at 3 different PC bias currents, a) magnitude, b) phase. f_m is the modulation frequency. The bias current I_b is 30 mA, and the threshold currents at A, B and C are 17.5 mA, 16.3 mA and 21.8 mA, respectively [2].

I—4

InGaAsP DFB Lasers Frequency-Locked to an Absolute Reference

Y. C. Chung
R. W. Tkach

AT&T Bell Laboratories
Crawford Hill Laboratory
Holmdel, New Jersey 07733

Semiconductor lasers frequency-locked to an absolute reference in the 1.3 and 1.5-μm wavelength regions are needed in many applications of coherent optical communication systems. However, most of the previous reports on frequency-locked semiconductor lasers are limited to GaAlAs lasers operating at about 0.8 μm. This is mainly due to the difficulties of finding any useful atomic or molecular absorption lines at longer wavelengths. A few experiments have been reported at longer wavelengths, which used molecular absorption lines of NH_3 [1] or HF [2] as their references.

Molecular transition lines are not ideally suited for use as references in optical communication systems, due to their complex and weak absorption spectra. By comparison, atomic spectra offer a relatively small number of strong lines which can be easily identified, facilitating their use as optical references. However, there is no useful atomic transition at longer wavelengths originating from the ground state. This problem can be solved by using the optogalvanic signals corresponding to transitions from excited atomic states. This effect is convenient for our application due to its high signal-to-noise ratio and simplicity of the experimental system.

By using the optogalvanic effect corresponding to the Ar $2p_{10}$ - $3d_6$ transition, we have locked the frequency of an InGaAsP DFB laser at 1.2960 μm. A block diagram of the experimental setup is shown in Fig. 1. Since this technique utilizes an electronic transition of the Ar atom, its line spectrum is very simple and clear. Thus, this transition can be an excellent frequency discriminator.

Fig. 2 shows the trace of the error signal. The peak-to-peak frequency fluctuation in the free-running condition was estimated to be 650 MHz. With the servo-loop closed, the frequency stability was improved to 4.1 MHz. This stability was maintained over several days in normal laboratory conditions. Also, similar results have been obtained at 1.5339 μm using the Kr $2p_{10}$-$3d_3$ transition.

In conclusion, an InGaAsP DFB laser has been frequency-locked to an Ar $2p_{10}$ - $3d_6$ transition at 1.2960 μm by using optogalvanic effect. To our knowledge, this represents the first demonstration of the frequency-locking of a 1.3-μm laser to an atomic transition line. In contrast to molecular spectra, atomic spectra are relatively simple, strong, and easily identified. Thus, atomic transition lines are readily suited for the use as optical references in coherent communication systems.

REFERENCES

1. T. Yanagawa, S. Saito, S. Machida, Y. Yamamoto, and Y. Noguchi: "Frequency stabilization of an InGaAsP distributed feedback laser to an NH_3 absorption line at 15137 A with an external frequency modulator," Appl. Phys. Lett., vol. 47, pp. 1036-1038, 1985

2. S. Yamaguchi and M. Suzuki: "Frequency locking of an InGaAsP semiconductor laser to the first overtone vibration-rotation lines of hydrogen fluoride," Appl. Phys. Lett., vol. 41, pp. 1034-1036, 1982

88CH2609-8/88/0000/0116$1.00 1988IEEE

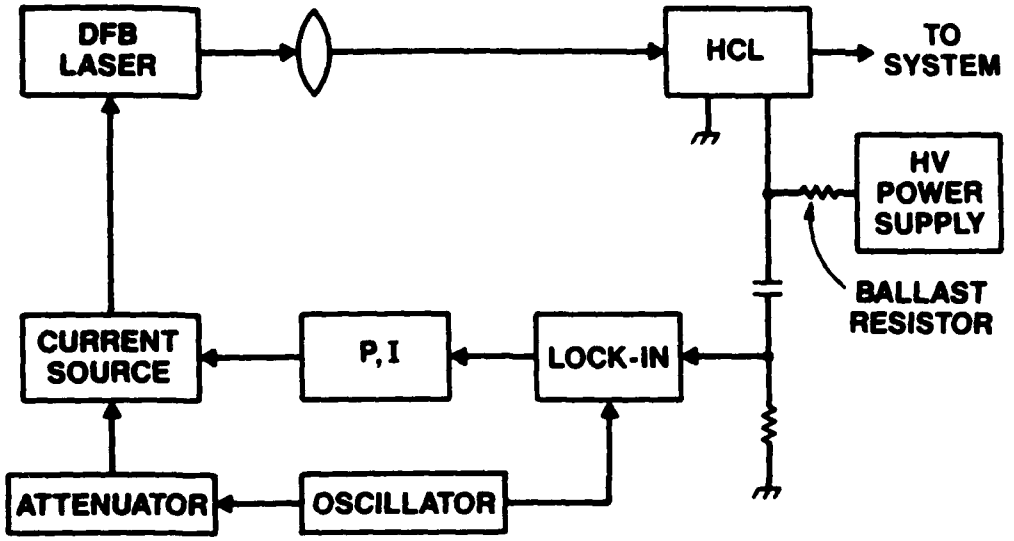

Figure 1. Experimental setup. HCL represents the hollow cathode lamp. P and I are a proportional amplifier and an integrator, respectively.

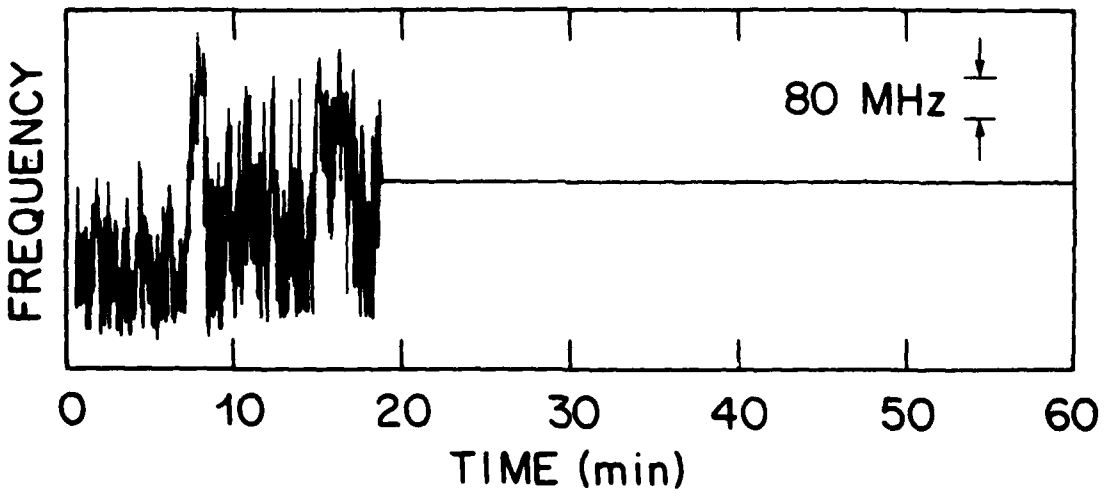

Figure 2. Trace of error signal. In the free-running condition, the frequency stability was 650 MHz. When the servo-loop was closed, the stability was improved to 4.1 MHz.

WEDNESDAY, August 30, 1988

Session J: Tunable Lasers

J—1

High Performance Tunable 1.5 μm InGaAs/InGaAsP Multiple-Quantum-Well Distributed-Bragg-Reflector Lasers

by
T. L. Koch, U. Koren, and B. I. Miller

AT&T Bell Laboratories
Holmdel, New Jersey 07733

Tunable semiconductor lasers[1-3] are expected to play a major role in both high-speed direct detection wavelength-division-multiplexed (WDM) systems and coherent heterodyne detection systems. Here we describe the structure and properties of multi-section tunable dynamic-single-mode multiple-quantum-well (MQW) distributed-Bragg-reflector (DBR) lasers operating at 1.5 μm. These lasers display low threshold, excellent differential quantum efficiency, large tuning range, with both low chirp under high-speed direct modulation and narrow linewidth under CW operation.

Figure 1 shows the longitudinal structure of both two and three-section lasers. These devices were grown entirely by atmospheric pressure metal-organic chemical-vapor deposition (MOCVD), and the lateral laser structure is the SIPBH geometry[4], providing low capacitance Fe-doped InP current blocking for high-speed operation. For MQW devices[5] the active (gain) layer consists of four 80 Å thick InGaAs wells with 100 Å thick barriers of 1.3 μm λ_g InGaAsP. In the present DBR structure the guide layer beneath the active stack is ~2500Å of 1.3 μm λ_g InGaAsP. The gratings are first order (~2350 Å pitch) formed by conventional holographic means. Isolation grooves allow separate contacting of the various sections. We have explored Bragg region grating coupling constants in the range of 70-140 cm^{-1}.

Figure 2 shows the CW 23°C light-current characteristic of both a ~507 μm total length two-section device with no current to the Bragg section, as well as a ~1250 μm total length three section device with no current to the phase or Bragg sections. For the two section device, the differential efficiency is η_d = 32%/front facet with no coatings applied, although some roll-over occurs at higher powers. This is the highest value we know of for DBR lasers and indicates very good coupling into the Bragg region. Typical thresholds are 17-20 mA, with excellent device yield and uniformity permitting 10 mW output below 100 mA drive in the vast majority of devices. For the three section device shown in Fig. 2, the active, passive, and Bragg section lengths are respectively 390, 550, and 310 μm. The 16% differential quantum efficiency is quite good, considering only 390 out of the total 1250 μm length is pumped. Both the two and three section devices operate in a single longitudinal mode above threshold with side mode suppression well in excess of 30 dB.

The tuning characteristics for the two-section devices are shown in Figure 4 for both a 615 μm and a 298 μm active length device with a maximum total tuning range of 94 Å. In the two-section devices, the wavelength changes in discrete hops with a relatively small continuous tuning between each hop. The longer device has seventeen successive longitudinal modes which are accessible, while the shorter device has nine. The hopping behavior is uniform and reproducible, and a small amount of temperature tuning allows access to all wavelengths throughout the tuning range. For the three section devices the comparable discrete tuning range was 71 Å. The phase tuning electrode provided electronic access to most wavelengths, but some gaps existed due to internal reflections from overly deep isolation grooves.

Figure 4 shows the linewidth data for a two-section device measured by the delayed self-heterodyne technique. At powers as low as 2 mW the linewidth reaches 5.75 MHz. The linewidth remains at this level as the power is increased, even though the light-current behavior and side-mode suppression remain quite ideal to considerably higher powers. We believe the narrow linewidth results both from the MQW gain medium as well as detuning of the Bragg wavelength to values shorter than the gain peak which was evident in the below threshold spectrum. Independent evaluation of the linewidth enhancement factor by FM and IM index measurements under high speed modulation yielded a low value of α ~ -3.5, consistent with the observed linewidth. The longer three-section device also had a minimum linewidth of ~6 MHz, suggesting some limiting mechanism for these structures.

At fixed Bragg current, the SIPBH geometry makes the two-section tunable MQW DBR an excellent dynamic-single-longitudinal-mode source. Figure 5 shows the log-scale spectrum of the single mode under 5 Gb/s NRZ modulation with a 1.4Å width at the 20 dB level. This low chirp also results from the smaller α factor obtained in these devices. We believe the prospects for application of the MQW DBR structure to high-performance continuously tunable lasers is quite good.

88CH2609-8/88/0000/0120$1.00 1988IEEE

[1] Y. Kotaki, M. Matsuda, M. Yano, H. Ishikawa, and H. Imai, Electron. Lett. 23, 327(1987).

[2] S. Murata, I. Mito, and K. Kobayashi, Electron. Lett. 23, 405(1987)

[3] W. T. Tsang, N. A. Olsson, and R. A. Logan, Appl. Phys. Lett. 42, 650(1983).

[4] U. Koren, B. I. Miller, G. Eisenstein, R. S. Tucker, G. Raybon, R. J. Capik, Electron. Lett. 24, 138(1988).

[5] U. Koren, B. I. Miller, Y. K. Su, T. L. Koch, and J. E. Bowers, Appl. Phys. Lett. 51, 1744(1987).

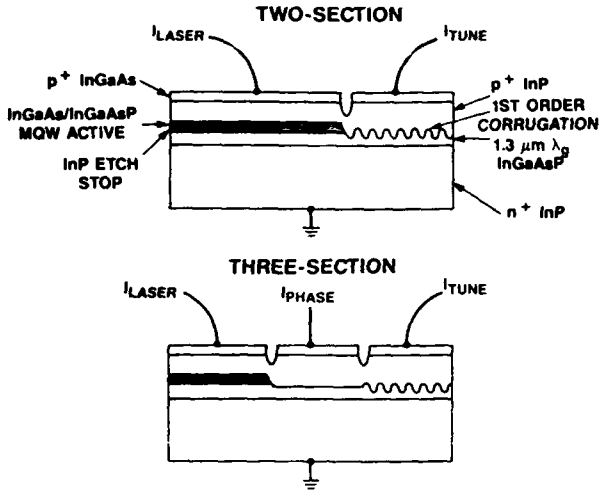

Figure 1. Longitudinal structure of two and three section tunable MQW SIPBH DBR lasers.

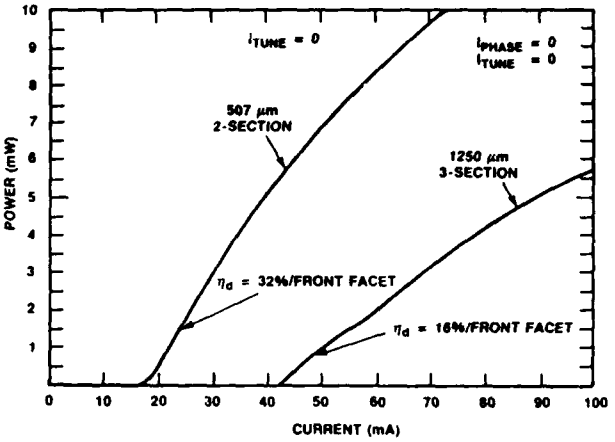

Figure 2. CW light-current characteristic for both a 507 μm total length two-section device and a 1250 μm total length three section device at 23°C with no current to the Bragg or phase sections.

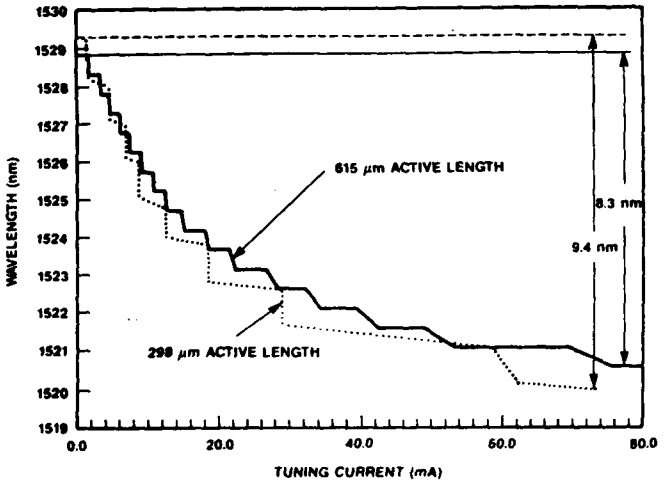

Figure 3. Wavelength vs. Bragg tuning current for two different active length two-section devices. For strong grating devices, continuous tuning between mode jumps is typically <20% of the mode jump spacing; in weaker grating devices we have observed >10Å continuous tuning under proper drive conditions.

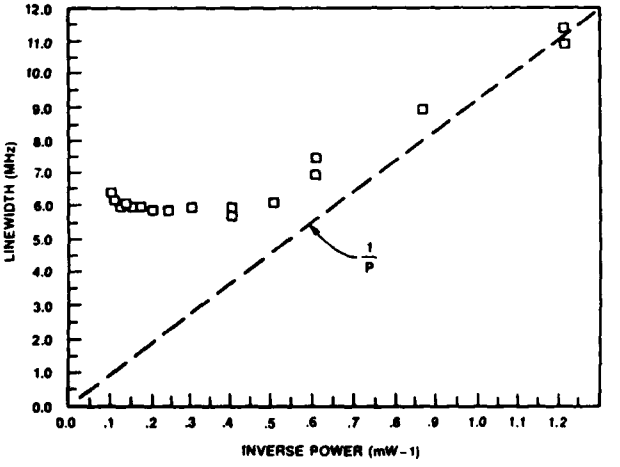

Figure 4. Linewidth vs. inverse optical power measured by delayed self-heterodyne method for two-section device.

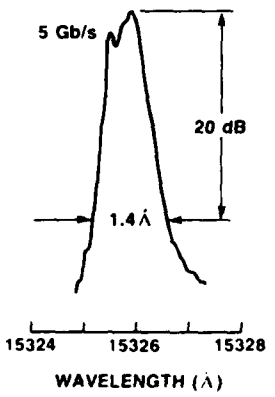

Figure 5. Log-scale spectrum of single longitudinal mode under 5 Gb/s NRZ modulation. Low chirp is due to α value of ~ -3.5.

J—2

1.5 μm Wavelength Tunable DBR Lasers with Large Continuous Tuning Ranges and Narrow Spectral Linewidths

S. MURATA, T. NUMAI, S. TAKANO, I. MITO and K. KOBAYASHI
Opto-Electronics Research Labs., NEC Corporation
4-1-1 Miyazaki, Miyamae-ku, Kawasaki-shi, 213, Japan

Wavelength tunable semiconductor lasers are attractive for use in FDM optical coherent transmission systems. A wavelength tunable distributed Bragg reflector (WT DBR) laser, using the free carrier plasma effect[1-3], is a particularly suitable light source because its continuous tuning range is very large. We have recently reported a 1.5μm three section WT DBR laser with the maximum continuous tuning range of 4.4nm under 1mW light output condition.[4] To improve the continuous tuning range at higher light output, further studies for the device parameters should be required. In this report we describe experimental results of continuous tuning range and linewidth dependence on active section length and on light output level for 1.5μm WT DBR lasers.

In the experiment, we used WT DBR DC-PBH lasers[1] with relatively short phase control (PC) section length (Lp=100μm), because longer PC section gave a smaller gain difference between DBR modes and resulted in a degradation of a single mode stability. The DBR section length Ld was about 600μm. The waveguide layer thickness t was 0.2μm. The lasers were mounted on silicon heat sinks with junction-up configuration and operated under CW conditions. Figure 1 shows the continuous tuning range $\Delta\lambda c$ as a function of the active section length La under 2, 5 and 8mW ligtht output conditions at 20°C. There was an optimum La to achieve the largest $\Delta\lambda c$ when the light output level was fixed. As the light output level increased, the optimum La shifted toward the longer side and $\Delta\lambda c$ decreased. At 5mW, the largest continuous tuning range of 3.4nm (430GHz) was achieved for the laser whose La was 270μm. For shorter active section, $\Delta\lambda c$ was limited by the light output decrease due to the free carrier absorption loss increase in the PC and DBR sections (loss limit). On the other hand, for longer active section, $\Delta\lambda c$ was limited by saturation of the refractive index change in the PC section waveguide layer (refractive index limit). The refractive index limit might be improved by optimizing the PC section waveguide layer thickness (t=0.4-0.5μm), because a largest refractive index change could be obtained.[4] Over 5nm continuous tuning range might be expected under 5mW light output condition.

Figure 2 shows spectral linewidth as a function of the wavelength shift at three light output levels in continuous tuning. The laser (La=270μm) was the same as shown in Fig.1. As the wavelength shift (i.e. the tuning current) increased, the linewidth increased from less than 10MHz to 2-3 times the values

88CH2609-8/88/0000/0122$1.00 1988IEEE

and became saturated. The behavior was nearly the same at different light output levels. At 5mW, less than 17MHz linewidth was achieved under 3.4nm tuning. The linewidth was sufficiently narrow to use in FSK optical heterodyne envelope detection systems.[5] We also measured linewidth as a function of the wavelength shift for the lasers with different lengths (La=180, 320 and 510μm) under fixed light output conditions. Although the longer active section laser tended to have narrower linewidth, the linewidth increase and saturation with tuning were obserbed for all lasers. One of causes for the linewidth increase is probably the absorption loss increase in the PC and DBR sections. However, the linewidth saturation mechanism is not understood at this time.

In conclusion, we have experimentaly confirmed that there was an optimum active section length to obtain largest continuous tuning range under fixed light output condition for 1.5μm WT DBR lasers. The linewidth was maintained less than 17MHz over 3.4nm (430GHz) continuous tuning range at 5mW light output level. The WT DBR laser could be available as a local oscillator in more than several tens of channels FDM optical heterodyne transmission systems.

References

1. S. Murata et al.; Electron. Lett. , 1987, 23, 403
2. Y. Kotaki et al.; ibid, 1987, 23, 325
3. Y. Tohmori et al.; Paper of technical group meeting of IECE, Japan, 1984, OQE84-81, 47
4. I. Mito ; OFC'88 ,ThK1
5. K. Emura et al.; J. Light. Tech., 1987, LT-5, 469

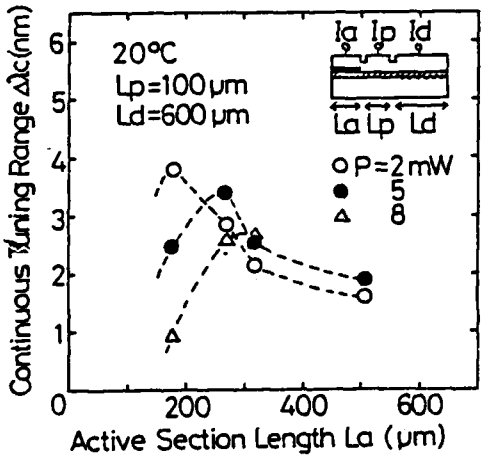

Fig.1 Continuous tuning range $\Delta\lambda c$ as a function of the active section length La

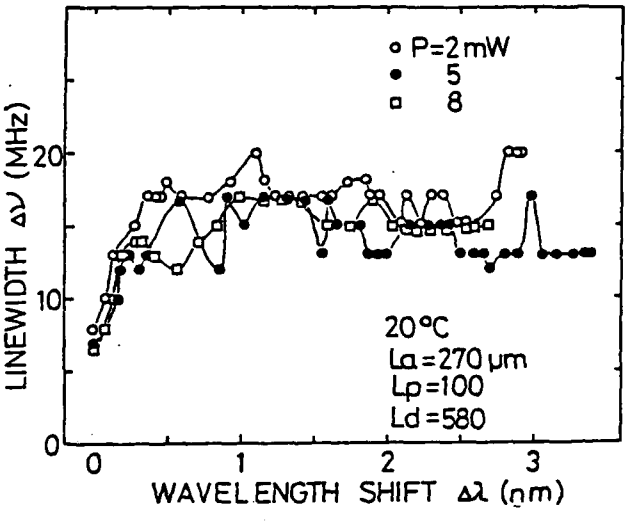

Fig.2 Spectral linewidth $\Delta\upsilon$ as a function of wavelength shift $\Delta\lambda$ in continuous tuning. The lasers are the same as those shown in Fig.1.

J—3

A Tunable Optical-Wavelength Conversion Laser with TM-Polarized Light Input

K. Kondo, M. Kuno, S. Yamakoshi and T. Sakurai*

Optoelectronic Technology Research Corporation
Present address: c/o Fujitsu Laboratories, Atsugi
10-1, Morinosato-Wakamiya, Atsugi 243-01, Japan

*Fujitsu Laboratories, Atsugi

Summary

A tunable wavelength conversion device has been strongly required for photonic switching and optical computing systems[1]. Recently, we have successfully demonstrated a novel wavelength-conversion laser with tunable range of 30Å[2].

The present work represents the input light's polarization dependence of this device and shows a new configuration for optical-wavelength conversion to improve a crosstalk of light input, and also shows the new function of this device as an optical inverter. Fig. 1 shows a schematic structure of our wavelength-conversion laser. This structure is the almost same as a tunable DBR laser except that the active region has a tandem electrode with a saturable absorber to realize differential or bistable characteristics by optical pumping. A train of light pulses at some wavelength excites the saturable absorber to generate a similar train of light pulses with another wavelength, which can be controlled by changing the currents of phase shifter section and DBR section. For optical-wavelength conversion, colinear coupling configuration is very simple and effective, however, it is necessary to avoid a crosstalk of light input. Input power sensitivity of this device strongly depends on the polarization and the wavelength of light input, as shown in Fig.2. The results reflect the resonant cavity characteristics of this device, and the TE sensitivity shows large oscillation. In the case of TM mode, sensitivity is relatively flat, and suitable for practical use. On the other hand, the polarization state of the light output is TE, due to the higher value of its reflectivity at the facet. Therefore, by using TM-polarized light input and polarizer as shown in Fig.3, the optical-wavelength conversion without crosstalk of input light is successfully achieved. Fig.4 is the obtained tunable wavelength conversion. The light input is not detected in the output signal. the wavelength of the light output was successfully controlled from 1.5364μm to 1.5337μm, by changing the currents of phase and DBR sections from 0 to 50mA.

Furthermore, it is important to note that this device can operates as an optical inverter as well as a wavelength converter or memory, when the bias currents of the active part are set above the threshold. As shown in Fig.5, the intensity of TE light output is inversely modulated by the injection of TM light input.

References

1) M. Sakaguchi *et al.*, Tech. Dig. of 1st Optoelectronics Conf., July 1986, Tokyo, C9-3.

2) S. Yamakoshi *et al.*, OFC'88 postdeadline paper, PD10

88CH2609-8/88/0000/0124$1.00 1988IEEE

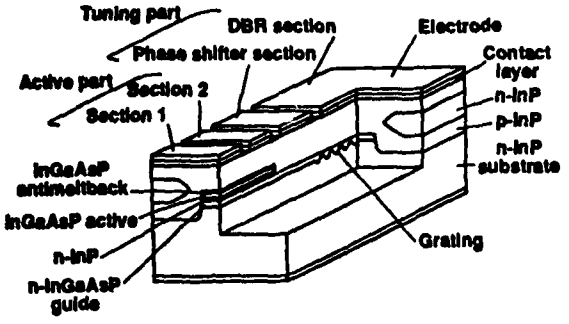

Fig.1 Schematic structure of the device

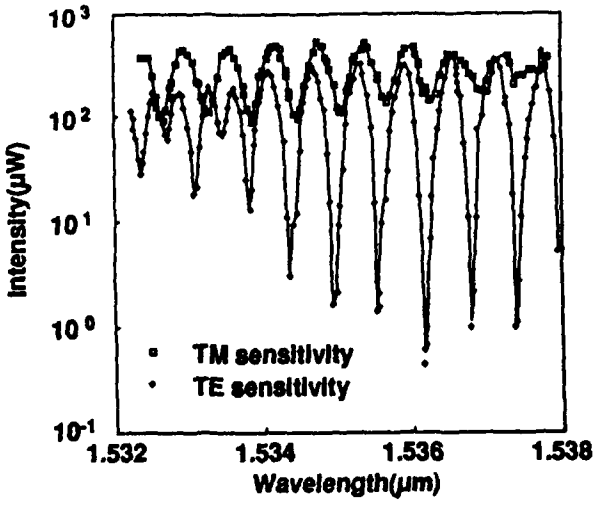

Fig.2 Input power sensitivities of wavelength conversion laser

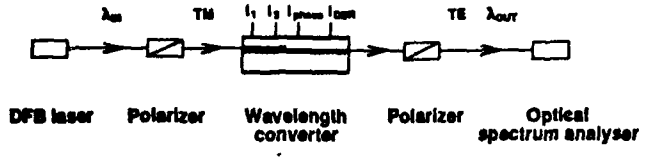

Fig.3 Configuration for optical wavelength conversion

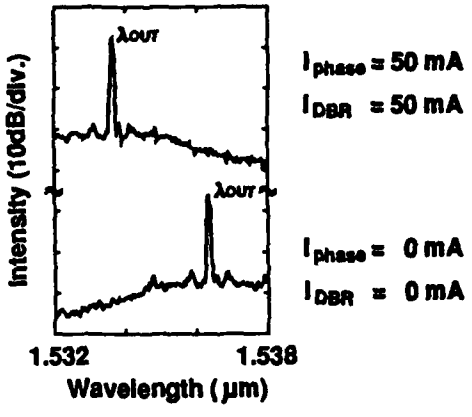

Fig.4 Tunable wavelength conversion with TM-polarized input light at 1.5328 μm

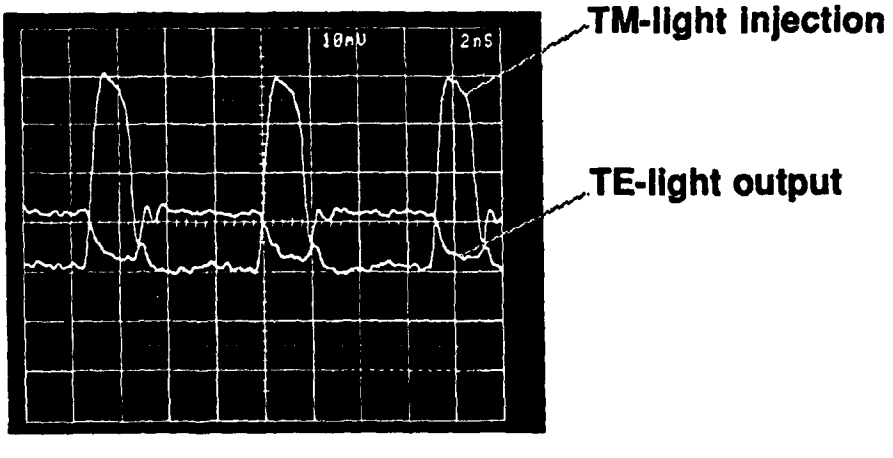

Fig.5 Inverter characteristics of TE-light output by TM-light injection

J—4

Measurement and Analysis of the 'λ-vs-Injection Currents' Characteristics of Continuously Tunable DBR Lasers

P.I. Kuindersma, T. v. Dongen, G.J.A. v.d. Hofstad, W. Dijksterhuis & J.J.M. Binsma
Philips Research Laboratories,P.O. box 80.000, 5600 JA Eindhoven
The Netherlands

We report investigations on wide range Continuous Tuning of DBR lasers, by injection. In our λ_L=1.56 μm CT-DBR lasers the optical Amplification section and the Bragg Reflector section are interconnected by a waveguide, the phase shift Tuning section. Sections R and T have only a λ_{gap} of 1.3 μm.

The principle of operation of CT-DBR lasers is easy to grasp. A pictorial representation of λ-tuning by injection is given in fig.1:
a) selection of mode with round trip phase $2\pi N$ by bias I_R ($\lambda = 2n_R \Lambda_{pitch}$)
b) increase of bias I_T lowers index n_T, yields blue shift of λ and $\lambda < 2n_R \Lambda_{pitch}$
c) increase of bias I_R lowers index n_R, restores the 'local' Bragg condition $\lambda = 2n_R \Lambda_{pitch}$ (with smaller λ and n_R)
d) repeating b,c over and over leads to lower and lower λ for mode N.

The above procedure can also be done continuously: a decreasing λ by a decreasing n_T of the phase shift tuning section, while staying at the Bragg-condition by a simultaneous decrease of n_R of the Bragg reflector section (i.e. $\Delta\phi_R$=0). The most important characteristic of the device then is a set of tuning lines, as shown in fig. 2a, representing the
wavelength λ as a function of-Δn_T (=bias I_T), while retaining $\Delta\phi_R$=0.
Each line corresponds to a particular mode, of round trip phase $2\pi N$. Each point on each line corresponds to single mode operation at the 'local' Bragg-condition ($\lambda = 2n_R \Lambda_{pitch}$).

An experimental characteristic corresponding to fig. 2 is given in fig. 3, showing the (all single mode!) spectra of one of our CT-DBR devices as a function of wavelength. The spectra are arranged in blocks of constant bias I_T on the phase shift tuning section; from block to block I_T is gradually (but stepwise) increased. Within each block of constant I_T the spectra at all possible biases I_R on the Bragg reflector are displayed. By displaying measured spectra in this way, the individual modes of round trip phase $2\pi N$ are easily recognized (assigned). As is their λ-tuning by the bias I_T, while fullfilling the 'local' Bragg condition. In the lowest block, with I_T=0, is seen that the initial bias I_R on the Bragg-reflector determines the selection of the particular mode N to be detuned continuously.

Remarkable in fig. 3 is the repetitive occurrence of apparently forbidden wavelengths for each mode N, limiting the continuous tuning range when staying in the same mode (for this device still ~ 20Å). Wavelength gaps for the various mode do not coincide and overlapping modes still allow a large continuous tuning range (for this device about 45Å).
The wavelength gaps arise from a small reflection on the interface of the optical Amplifier section and the phase shift Tuning section. Gaps occur at wavelengths for which the amplification section round trip phase/π is an odd integer. To first order the index n_A of the amplification section is clamped at threshold. Therefore all modes N would have coinciding wavelength gaps, as indicated in fig. 2b by the

88CH2609-8/88/0000/0126$1.00 1988IEEE

vertical dash-dot lines of odd-integer round trip phase/π in the amplification section (while $\Delta\phi_R$=0)
The wavelength gaps, however, do not coincide due to an increased optical damping upon increased bias on tuning and/or Bragg reflector section. Increased damping leads to an increased gain at threshold and a correspondingly lower n_A. As a consequence the dash-dot lines of constant <u>amplifier</u> round trip phase are tilted towards shorter wavelength at higher bias I_T (fig. 2c). With this tilt the wavelength gaps do no longer coincide and wide range continuous tuning with λ -overlapping modes is regained. More over it is obvious that the stronger the damping effect, the larger the continuous tuning range of the individual mode N.

Experimental λ vs I_T-characteristics (around $\Delta\phi_R$=0) for each CT-DBR device, are used to determine its two terminal input driving conditions (one input for tuning and the other for controlling the output power). Example in fig. 4a, b, c.

Ref.: Y. Kotaki et al, Electron. Lett., 1987, <u>23</u>, pp. 325-327
S. Murata et al, Electron. Lett., 1987, <u>23</u>, pp. 403-405

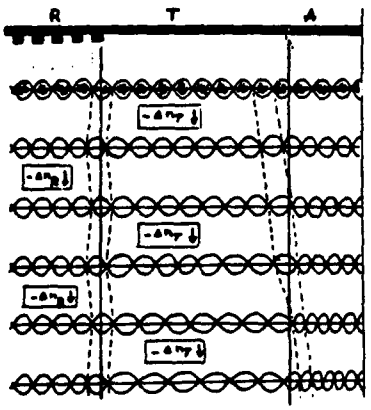

<u>Fig.1</u>: CT-principle

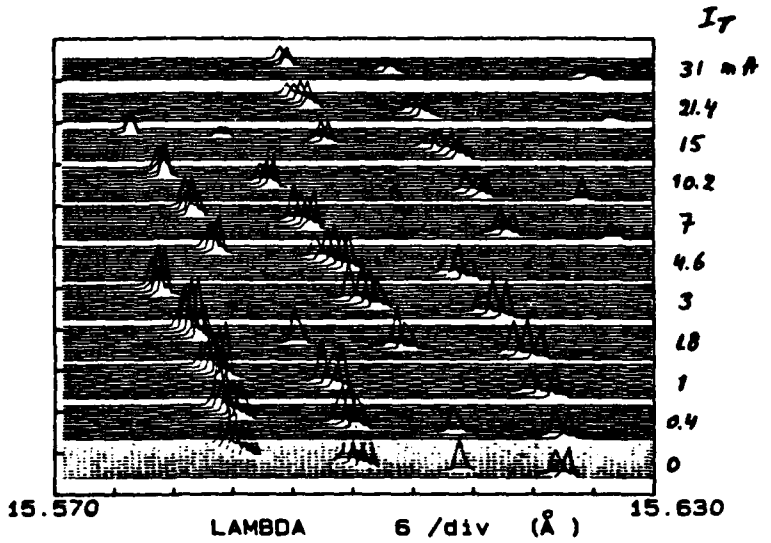

<u>Fig.3</u>: λ vs. I_T characteristic of CT-DBR

In each block I_R = 0 step 5 to 50 mA
(all spectra single mode!)

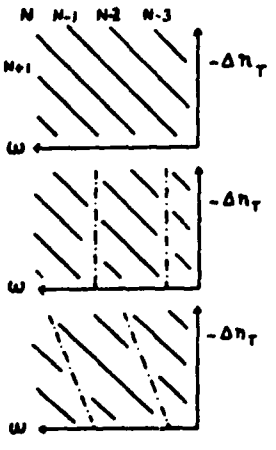

<u>Fig. 2a,b,c.</u>: theory,

λ vs. I_T while $\Delta\phi_R$ = 0
(all points single mode)

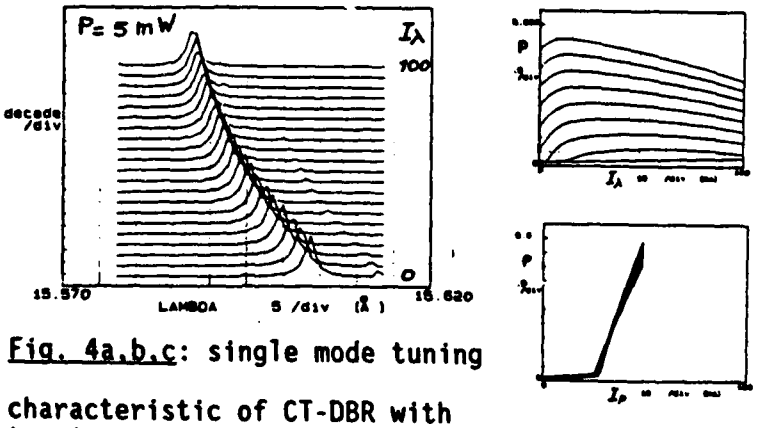

<u>Fig. 4a,b,c</u>: single mode tuning characteristic of CT-DBR with two inputs: I_λ and I_p

J—5

Influence of Isolation Resistance on Spectral Linewidth in Wavelength Tunable DBR Laser

Y.Kotaki and H.Ishikawa
Fujitsu Laboratories Ltd.
10-1 Morinosato-Wakamiya, Atsugi, Japan

The objective of this paper is to investigate a linewidth of a wavelength tunable distributed feedback reflector (DBR) laser, especially on the effect of isolation resistance between active section and phase control section.

A wavelength tunable DBR laser is an indispensable light source for coherent optical communication systems. Therefore it is very important to realize the tunable DBR laser with narrow linewidth.

Fig.1 shows a schematic structure of the wavelength tunable DBR laser.[1],[2] The active layer was an undoped InGaAsP (g=1.54um), the guide layer was an n-InGaAsP (g=1.29um). The isolation between p-electrodes was performed by narrow mesa etching just outside of the waveguide. The resistance between nearest two electrodes was 4.5kohms at applied voltage of 1V.

In order to investigate the influence of isolation resistance on linewidth we loaded an external resistance between the active and the phase-control electrodes. Fig.2 shows the dependence of spectral linewidth on the normalized injected current to the active region taking the external resistor R_0 as a parameter. We used the delayed self-heterodyne technique to measure the linewidth. In this figure the DBR section current I_d was kept constant at 0 mA. The linewidth of the tunable DBR laser strongly depended on the isolation resistance between the active and the phase-control sections. A decrease of the isolation resistance caused the linewidth broadening. This effect was mainly caused by the increase of threshold current due to leakage current from the active section to the phase-control section. Leakage current increased the optical loss in the guide layer and broaden the linewidth. Fig.3 shows the threshold current increase due to the phase-control current. Taking this threshold increase into consideration, we renormalized I_a/I_{th}, and the result is shown in fig.4. In this figure I_{th} depends on I_a. This figure clearly shows a decrease of the dependence of the linewidth on the isolation resistance. This verifies that the increase of I_{th} broadens the linewidth of the tunable laser.

However there still remains a dependence of the linewidth on the isolation resistance. We suppose that this residual dependence is due to the electrical noise generated at active layer by spontaneous emission.[3] It is transmitted to the guide layer at the phase control region through the isolation resistance and broadens the linewidth. The isolation resistance higher than several kohms is needed in order to avoid the linewidth broadening.

References

(1)Y.Kotaki, et al., Electron.Lett., 23, pp.325-327, 1987.
(2)S.Murata, et al., Electron.Lett., 23, pp.403-405, 1987.
(3)P.A.Andrekson, et al., IEEE J.Lightwave Tech., LT-4,pp.804-811, 1986.

88CH2609-8/88/0000/0128$1.00 1988IEEE

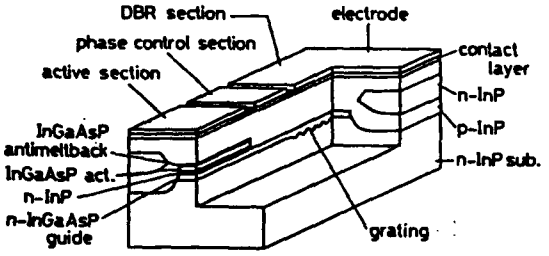

Fig.1 A schematic structure of a wavelength tunable DBR laser.

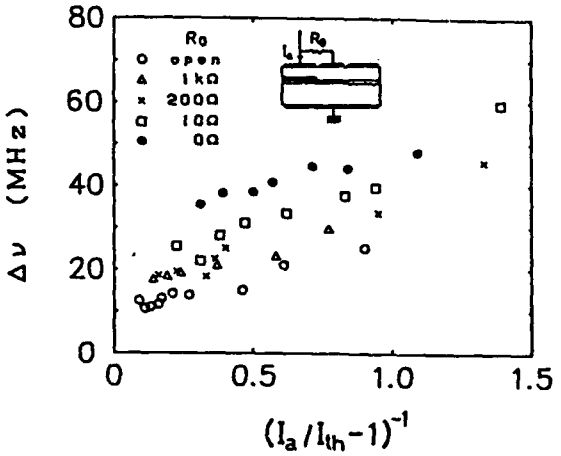

Fig.2 Dependence of spectral linewidth on injected current to active section taking the external resistor R_0 as a parameter.

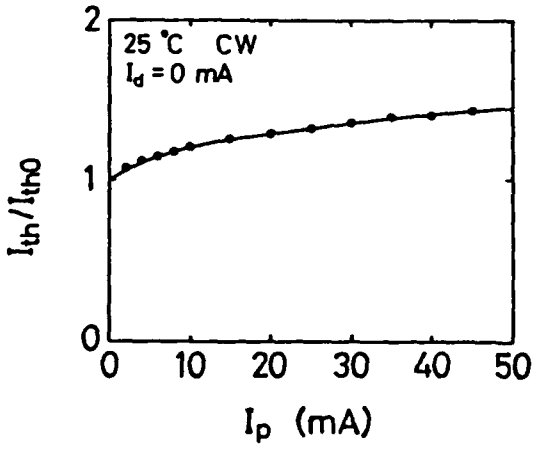

Fig.3 Threshold current increase due to the phase-control current.

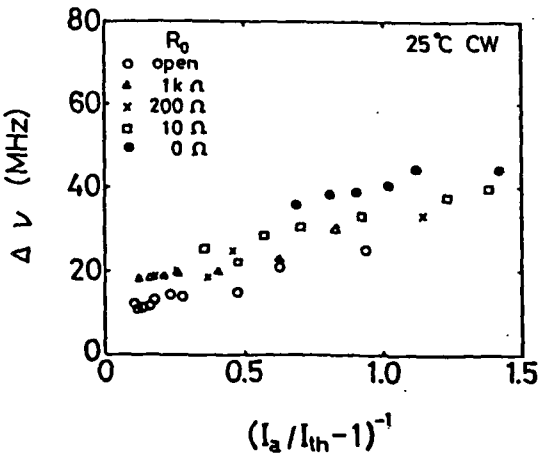

Fig.4 Dependence of the linewidth on renormalized I_a/I_{th}. I_{th} depends on I_a.

J—6

Single- and Multiple-Wavelength Operation of Acousto-Optically Tuned Semiconductor Lasers at 1.3 Microns

G. Coquin and K. W. Cheung

Bell Communications Research, Morristown, New Jersey 07960

M. M. Choy

Bell Communications Research, Red Bank, New Jersey 07701

We report single- and multiple-wavelength tuning of a 1.3μm InGaAsP semiconductor laser over a wavelength range of 0.07μm (70nm) using an acousto-optic tunable filter in an external cavity configuration.

Many optical communication network proposals require tunable-wavelength optical sources. Such devices are extremely attractive for optical instrumentation also. Acousto-optic tunable filter (AOTF) devices [1] have a narrow optical transmission bandwidth with the center wavelength controlled electronically by the drive frequency that is applied to the acoustic transducer. Use of an AOTF to tune a dye laser in the visible spectral range has been reported previously [2]. Recently we have reported fast tuning of semiconductor lasers at 0.85μm[3] and 1.3μm[4] using an AOTF in an external-cavity. We also demonstrated that incorporating a second acousto-optic device inside the laser cavity will compensate for the frequency shift of the optical wave in passing through the AOTF, thus eliminating the frequency chirping[2] of the cavity modes.

We show the basic cavity configuration used for the frequency-compensated tunable laser in Fig. 1. Inside the cavity are an AOTF and an acousto-optic modulator, the latter device serving to correct for the frequency shift of the optical beam by the AOTF. The frequency compensation gives a non-chirping mode of operation of the laser[3], which allows one in principle to achieve linewidths as narrow as those achieved with external cavity grating lasers. We have not yet achieved narrow-linewidth, single-mode operation or continuous tuning due to bandwidth($\approx$3nm) and efficiency($\approx$50%) limitations in the AOTF and imperfect AR coating on the laser. None of these limitations are fundamental, however.

We have also investigated the non-frequency-compensated mode of tuning for the semiconductor laser, i.e. AOTF only. Although this leads to frequency-chirped cavity modes[2], for many applications this mode of operation will be satisfactory. In fact we find that given the performance of the acousto-optic and laser devices available to us, the non-frequency-compensated operation results in better secondary mode suppression than frequency-compensated operation.

In Fig. 2 we show the optical spectrum of the acousto-optically tuned semiconductor laser (AOTSL) at 4 different input frequencies spanning the major portion of the tuning range. These spectra were taken using the non-frequency-compensated mode. Total tuning range is 70nm, but the power output and mode purity are reduced at the extremes of this range. The Fabry-Perot modes of the semiconductor laser are visible in Fig. 2, but secondary mode suppression is more than 30dB over the entire wavelength range shown in the figure.

A particularly interesting feature of the AOTSL is that multiple wavelengths can be selected simutaneously by applying several different frequencies to the AOTF at the same time. In Fig. 3 we show the optical spectrum taken during 2- and 3- wavelength operation of the laser. In multiwavelength operation all of the wavelengths can be tuned individually, at speeds limited only by the access time of the AOTF, which in this case is 3μs. So as not to exceed the maximum power limit of the AOTF, each frequency has reduced RF power input, which leads to reduced optical efficiency and increased optical bandwidth[1]. Thus the multiwavelength spectra in Fig. 3 exhibit poorer secondary mode suppression than the single wavelength spectra of Fig. 2. Also the optical power of *each* mode is extremely sensitive to *all* of the acoustic power inputs, as one would expect when there are competing modes inside the cavity.

In conclusion, we have achieved all-electronic tuning, at a 3μs rate, over a 70nm wavelength range, for a 1.3μm InGaAsP semiconductor laser, using an AOTF as the tuning element. Both single- and multiple-wavelength operation have been demonstrated.

References

[1] YANO,T., and WATANABE,A., *Appl.Optics*, 1976, **15**, pp.2250-2258.
[2] TAYLOR,D.J., HARRIS,S.E., NIEH,S.T.K., and HANSCH,T.W., *Appl.Phys.Lett.*, 1971, **19**, pp.269-271.
[3] COQUIN,G. and CHEUNG,K.W., submitted to *Electon.Lett.*.
[4] CHEUNG,K.W.and COQUIN,G., submitted to CLEO/88.

88CH2609-8/88/0000/0130$1.00 1988IEEE

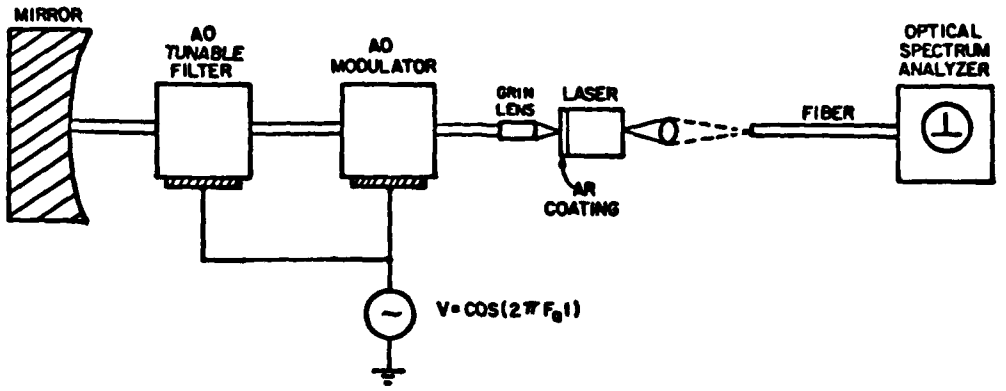

Fig. 1. External cavity configuration for frequency-compensated acousto-optically tuned semiconductor laser. For the non-frequency-compensated version the acousto-optic modulator is not used.

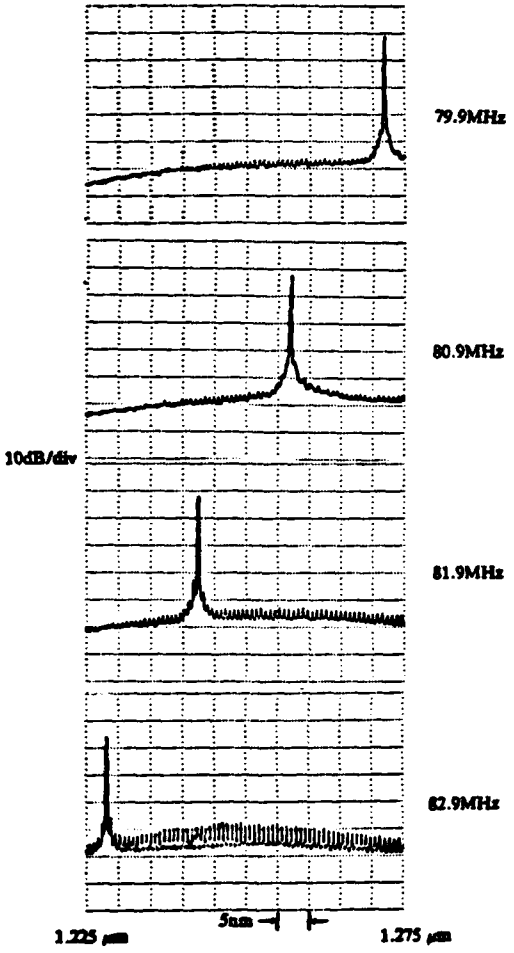

Fig. 2. Optical spectrum analyser traces of output of non-frequency-compensated AOTSL at 4 values of acoustic drive frequency, viz. F_a= 79.9, 80.9, 81.9, and 82.9MHz.

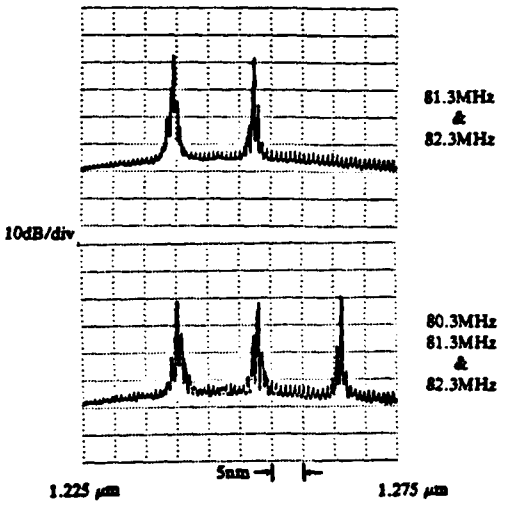

Fig. 3. Optical spectra showing multiple wavelength operation of AOTSL using (a) 2 input frequencies and (b) 3 input frequencies.

Session K: Stabilization, Noise and Bistability

K—1

The Dynamic Characteristics in a Common Cavity with Two Sections Bistable Laser (CCTS Laser)

Wang Qiming Liu Wenxu Zhao Jianhe Wu Ronghan
Institute of Semiconductors, Academica Sinica, Beijing, China

A CCTS Laser behaves a lot of attractive functions, such as,switch, memory, transphasor, shaper etc. in optical domain, which vest the devi--ce with a potentiality in optical communication and optical signal processing.

We have recently investigated on a CCTS laser experimentally and theoretically, in which, stability, optical amplification, Q-switch, static and dynamic characteristics etc. were concerned[1)-(3)].

In this paper, experimental observation is given of dynamic chrac-teristics in a CCTS laser. And a correlation injection is first time used in mode rate eqations to simplify the calculation of an attainable ultrafast pulse and controllable persistent self-sustained pulsation.

The samples in experiment were of GaAs/GaAlAs proton bombarded stri--pe laser. Two gain sections with an absorber in between them constitute the active layer in the laser. The switch on current ranged from 50ma to 100ma. Either 2-terminal or 3-terminal connection can be operated.

In 2-terminal connection, with a square current pulse at low frequ--ency(to avoid heating) applied to the device, the relaxation, self-su--stained pulsation, chaos have been seen in different current regions larger than I_{on}. Noticeable is that in the relaxation, the first pulse is of high power output with the off-side able to drop down to zero, shown in Fig.1. Cutting this first pulse by applied a short duration electric pulse(ns) to the device, an ultrafast light pulse with FWHW less than 10ps(by streak camera) has been attained.

The correlation injection is defined as follows

Mode rate equations are often used to a CCTS laser. For a given structure in 3-terminal connection, the adjustable variables are gene--rally current injected in to gain and absorption region(I_1 and I_2). They are often considered independent, which lead to the solution fle--xible, complicated and the physics blurred. In correlation injection, the designed relation between injected currents is introduced in to the rate equations as an additional condition. In this case, I_1 and I_2 are dependent and controlled. The solution is simplly limited to a given region with a clear physical picture.

88CH2609-8/88/0000/0134$1.00 1988IEEE

Two illustrations are in this paper.

Given in Fig.2, is a calculated persistent self-suatained pul--sation according to correlation injection, where, $Q<0$ is the re--gion for self-sustained pulsation(reference(1)), correlation inje--ction condition $I_2=1-K_1I_1$,(K_1 ranging from 0.01 to 0.1), S_0 photon intensity(a.u) at ON state. In Fig.3a), Time-dependence of I_1, I_2 and S_0. In Fig.3b), calculated attainable ultrafast light pulse.

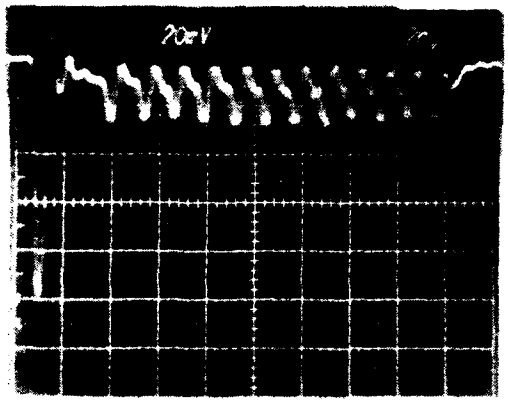

Fig.1

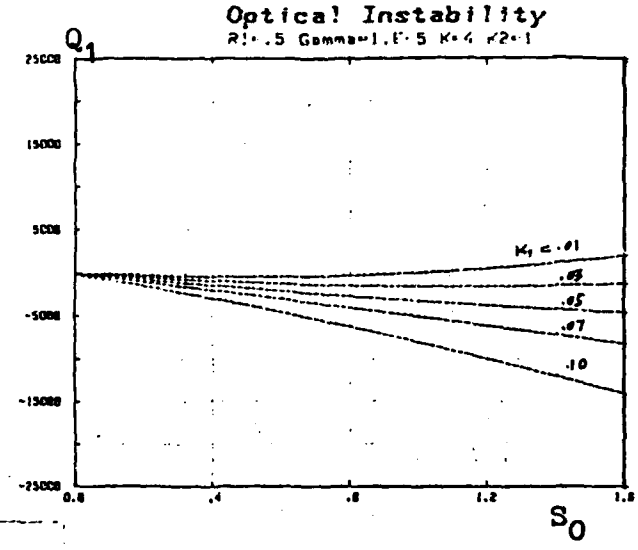

Fig.2

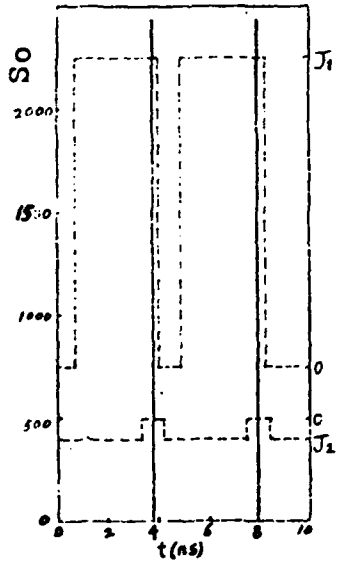

Fig.3a)

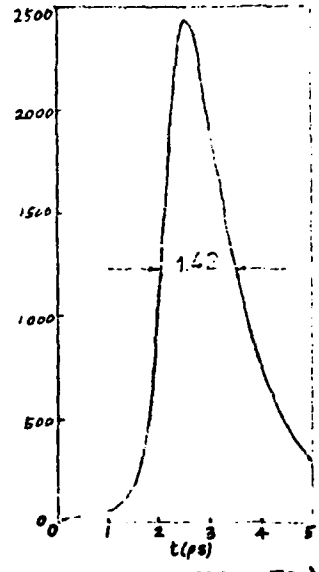

Fig.3b)

Reference

(1) Wang Shou-wu Wang Qiming and Lin Shiming, IEEE J. Quantum Electron. Vol QE-23 pp1033 1987

(2) Chi-ming Wang Jian-meng li, 10th IEEE International Semiconductor Laser Conference pp.144 Kanazawa Japan

(3) Wang Qiming Wu Ronghan Li Jianmeng Wu Hong Chinese J. Semiconductors, Vol 9 pp.110 1988

K—2

Experimental Measurement and Theoretical Explanation of Time Jitter in Pulse Modulated Semiconductor Lasers

P.Spano, A.D'Ottavi, A.Mecozzi, S.Piazzolla, B.Daino

Fondazione Ugo Bordoni, via B. Castiglione 59, 00142 Roma (Italy)

Aim of this work is a systematic investigation of the statistical properties of the turn on time jitter which arises when semiconductor lasers are suddenly switched from below to above threshold by means of a current pulse. The knowledge of such statistical properties can be important in the design of high bit rate intensity modulated communication systems. In fact, as shown below, time jitter can reach values high enough to cause an appreciable degradation of the system performances in terms of bit error rate. Previous experimental works [1] have shown the presence of a non zero time jitter in Distributed Feeedback (DFB) lasers, differently from the case of Fabry-Perot (FP) structures [2]. Numerical simulations, however, have shown that time jitter should be present in both structures and depends critically on the initial biasing state [3].

Our measurements confirm the presence of time jitter also in FP lasers, even if its amount is quite lower than in DFB lasers. However, contrary to what found in [3], our experiment shows that the statistical properties of time jitter depend only on the final state of the system, a fact which we are able to explain also from a theoretical point of view. Our measurements have been performed on a NTT DCPBH DFB laser with I_{th} = 27 mA and emitting at λ = 1.55 μm, and on a NEC DCPBH FP laser with I_{th} = 25 mA and emitting at λ = 1.32 μm. The results are obtained by varying independently the values of the initial biasing current (0÷10 mA) and of the amplitude of the applied current pulse (20÷60 mA). Three different technique are used, which, within the experimental errors, give the same results.

In Fig. 1 we report σ_τ^2, the variance of the distribution of time jitter, as a function of the inverse of the stationary value of the output power in the upper state P_f. Dots refer to the DFB laser and squares to the FP laser. The continuous curve is a plot of the theoretical expression for σ_τ^2 which, generalizing a previous work on Q-switched gas lasers by Haake et al [4], has been derived for the case of strictly single mode semiconductor lasers. This theory, which will be fully explained at the Conference, shows how time jitter is determined only by quantum fluctuations of the photon number into the cavity which take place in the vicinity of threshold. Moreover, it explains that the only parameter which affects the value of σ_τ^2 is just P_f. Theoretical work for the case of multimode lasers is also in progress. Work carried out at the Fondazione Ugo Bordoni under the agreement between the Fondazione Ugo Bordoni and the Italian P.T. Administation.

1. F.T.Arecchi, V.Degiorgio, and B.Querzola, *Phys.Rev.Lett.* **19**, 20, 1168 (1967).
2. P.M.Downey, J.I.E.Bowers, R.S.Tucker, and E.Agyekum, IEEE J. Quantum Electron. QE-**23**,1039 (1987).
3. S.E.Miller, IEEE J. Quantum Electron. **QE-22**,16 (1986).
4. F.Haake, J.W.Haus, and R.Glauber, Phys.Rev.A **23**, 6, 3255 (1981).

88CH2609-8/88/0000/0136$1.00 1988IEEE

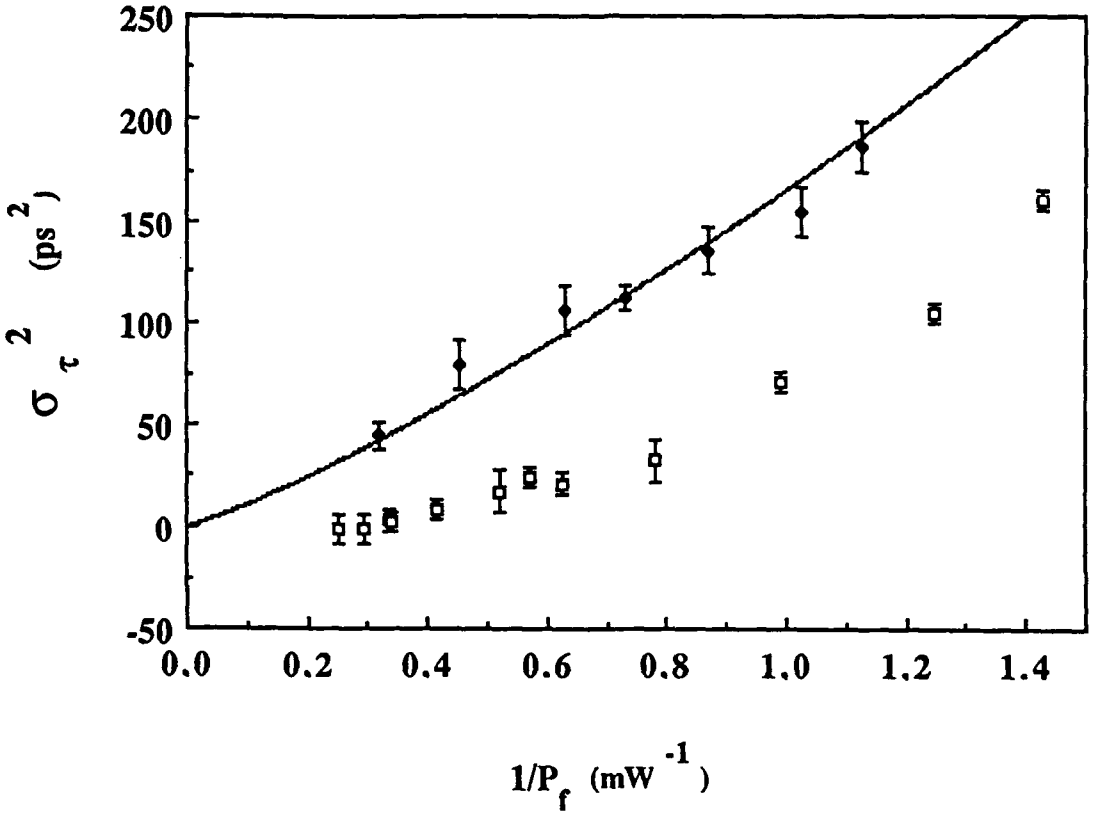

Fig.1 - Variance of the distribution of time jitter vs. the inverse of the stationary value of the output power in the on state. Dots refer to the DFB laser, squares to the FP laser. The continuous curve is a plot of the theoretical behaviour for single mode lasers.

K—3

Reduced Feedback Sensitivity of DFB-Lasers by Design of Grating Shapes

K.Wünstel, H.Schweizer, W.Idler, M.Schilling, K.Dütting, A.Mozer
Standard Elektrik Lorenz AG, Research Centre,
Optoelectronic Components Division, 7000 Stuttgart, FRG

Introduction: Suppression of optical feedback is an essential requirement for single mode lasers in high bit rate optical transmission systems. Generally, optical isolators are applied to prevent external reflections. However, realization of lasers with reduced feedback sensitivity would extremly simplify device assembly and packaging. In a recent theoretical work /1/, DFB-lasers with high coupling coefficients κ were proposed to reduce feedback sensitivity. We have realized devices with such large coupling coefficients applying dry etching for grating design with desired properties. One order of magnitude noise reduction is achieved for DFB-lasers with dry etched gratings compared to conventional ones.

Experimental: InGaAsP/InP DFB-lasers (λ = 1300nm) with κ = 50-70 cm^{-1} were fabricated using wet chemical etching for formation of 2nd order gratings (Fig.1a). For deep, dry etched gratings (Fig.1b), much higher coupling coefficients in the range of 150 cm^{-1} were obtained. Reactive ion beam etching using Ar/O_2 was applied for this purpose. In contrast to wet chemical etching, this dry etching method allows for grating design with a wide variety of grating shapes. Thermal deformation of grating shape was prevented in the LPE-overgrowth process, where planar layers were grown on the extremely deep corrugations /2/. DFB-lasers with threshold currents as low as 10 mA and 11 GHz cut off frequency were fabricated taking advantage of the DC-DCPBH structure /3/.
Feedback sensitivity of the lasers was investigated by means of a short backreflecting fibre link. To suppress back reflection noise from detectors, we took an asymmetric coupler (97%/3%) in conjunction with antireflection coatings of detector and fibre surfaces. The laser noise was measured both optically (Relative Intensity Noise, RIN) with a high sensitivity SEL pin-FET receiver (S = -42 dBm, bandwidth 170 MHz) and electrically (Terminal Electrical Noise, TEN) revealing the same results.

Results: From stopband measurements, κL = 1.5 was determined for lasers of type I (Fig.1a) and κL = 4 for lasers of type II (Fig.1b). Mode spectra at various temperatures are presented in Fig.2 for type II lasers showing a high sidemode suppression >40 dB. Laser noise was measured first without fibre coupling: For lasers with large κL, the intrinsic noise level at threshold is 5 dB reduced compared to lasers with small κL (Fig.3). This effect is well explained by the changed filter function of the grating. For back reflection measurements, variable feedback ratios R of 1%-10% were applied. Drastic differences in feedback noise were observed for the two laser types : For type I, feedback noise (at R = 2.5%) exceeds the intrinsic noise level by 10 dB at $2 \cdot I_{th}$, whereas nearly intrinsic noise level is reached for type II (Fig.3). Thus, enhanced noise reduction with increased κL is clearly demonstrated.

Conclusions: Dry etched gratings with high κL reduce extrinsic noise influenced by back reflexion as well as intrinsic noise. Thus we have found a new tool to improve system performance of DFB-lasers by proper design of DFB-gratings.

88CH2609-8/88/0000/0138$1.00 1988IEEE

References:
/1/ F.Favre, IEEE J.Quantum Electron., QE-23, 81-88 (1987)
/2/ M.Schilling et al., Proc. 17th ESSDERC, Bologna 1987, p.799
/3/ K.Wünstel et al., Electron.Lett.22, 1144 (1986)

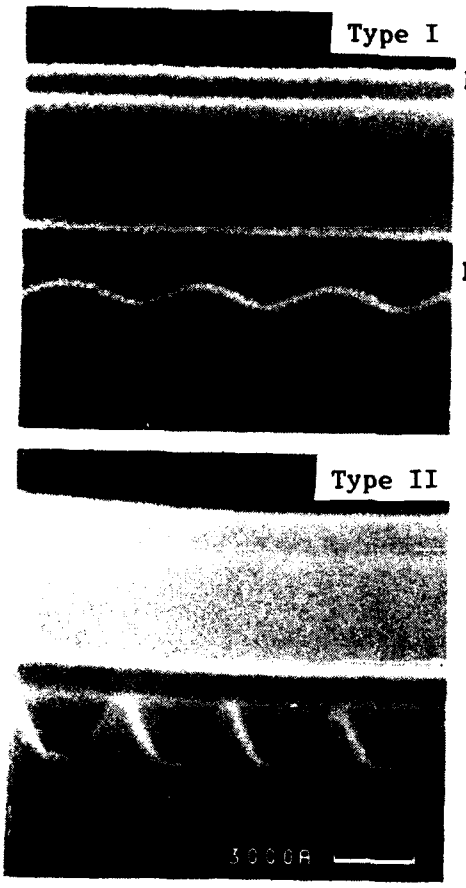

Fig.1: Cross sections of DFB-lasers with wet etched grating (type I) and dry etched grating (type II)

Fig.2: Emission spectra (cw) of laser with deep, dry etched grating

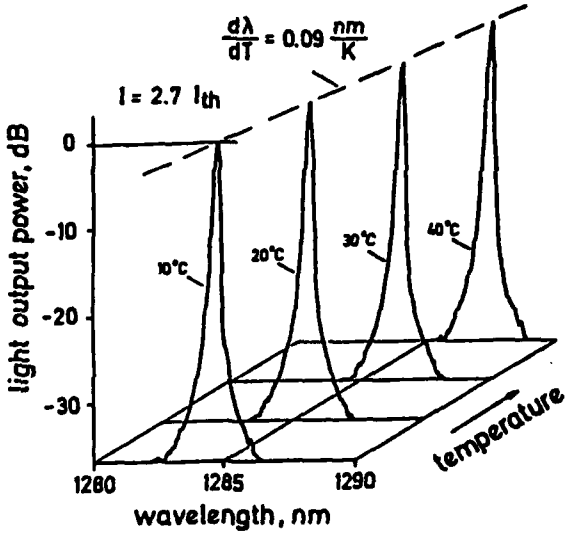

Fig.3: Intrinsic noise (dashed lines) and noise under optical feedback (solid lines) for lasers type I (κL = 1.5) and type II (κL = 4), as measured by TEN at 100 MHz

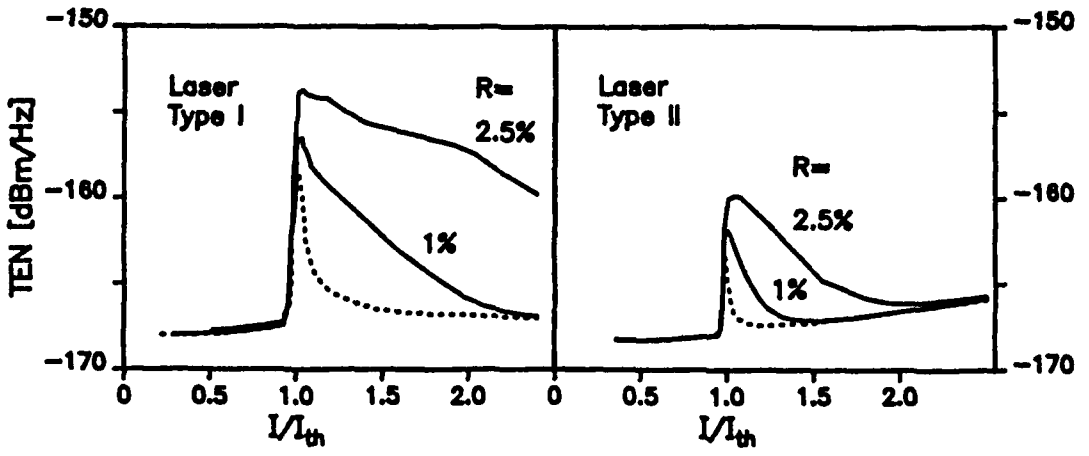

K—4

Feedback Induced Intensity Noise of InGaAsP-Semiconductor Lasers

Nikolaus Schunk and Klaus Petermann
Technische Universität Berlin
Institut für Hochfrequenztechnik
Einsteinufer 25, D-1000 Berlin 10, F.R.G.

It is well known that the linewidth of laser diodes is considerably broadened if the optical feedback for distant reflectors surpasses a certain critical level, corresponding to the "coherence-collapse" /1, 2/. In the "coherence-collapse"-regime also the relative intensity noise (RIN) drastically increases according to /3/. For stable laser operation it is thus desirable that the transition to the "coherence-collapse"-regime occurs at a feedback level as high as possible. From the numerical analysis in /3/ it has been concluded, that a low linewidth enhancement factor α (see Fig.1) and/or a large bias optical power are beneficial for shifting the "coherence-collapse" to larger optical feedback levels.

For verifying these results experimentally a fibre-optic set-up according to Fig.2 has been installed. The reflected power is measured via port ③ of the fibre-optic directional coupler. Using the variable attenuator feedback levels between 10^{-7} and $2 \cdot 10^{-2}$ may be reliably adjusted. In order to assure that the emitted and reflected light have the same polarization, linear polarization at the Al-mirror is adjusted using the polarization controller.

Figs.3a, 3b show the calculated and measured RIN relative to the RIN without feedback at 5 mW/facet. Theory and experiment are in good agreement yielding an increasing critical level of optical feedback for increasing light power.

This critical level shifts from $f_{ext} \approx 10^{-5}$ for P_1 = 1 mW to about $f_{ext} \approx 10^{-4}$ for P_1 = 5 mW.

In conclusion, the numerical model from /3/ has been verified experimentally yielding a decreasing feedback-induced intensity noise with increasing optical power.

References:

/1/ D.Lenstra, D.H.Verbeek and A.J. den Boef; IEEE J. Quant. Electron., QE-21, pp. 674-679, June 1985

/2/ R.W.Tkach and A.R.Chraplyvy; J. Lightwave Techn., LT-4, pp 1655-1661, Nov. 1986

/3/ N.Schunk and K.Petermann; IEEE J. Quant.Electron., QE-24, July 1988

88CH2609-8/88/0000/0140$1.00 1988IEEE

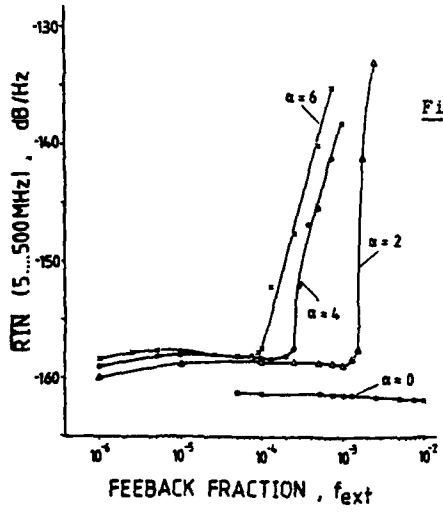

Fig.1: Calculated relative intensity noise RIN averaged over the frequency range 5...500 MHz for different linewidth enhancement parameters α at an output power P_1=5mW and an external cavity length L_{ext}=1m

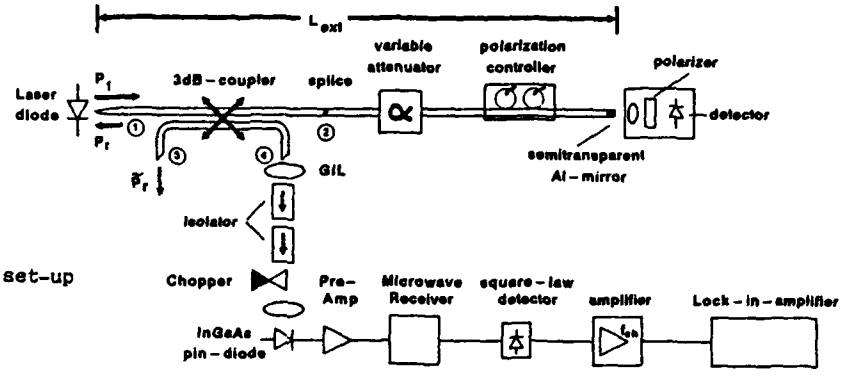

Fig.2: Experimental set-up

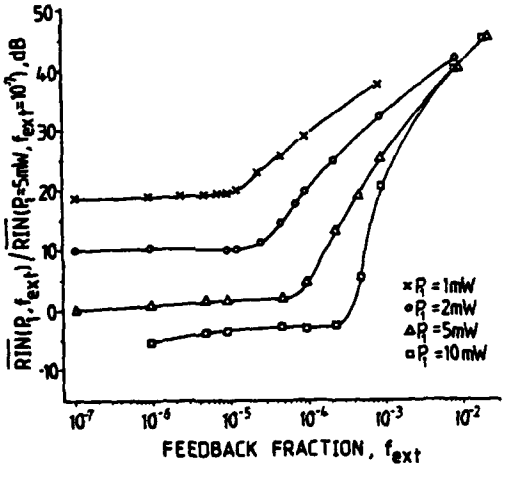

Fig.3a: Calculated relative intensity noise RIN averaged over the arbitrary chosen frequency range 5...500MHz and normalized to RIN (P_1=5mW, f_{ext}=10^{-7}) for different output powers P_1 at an external cavity length L_{ext}=1m and a linewidth enhancement factor α=6

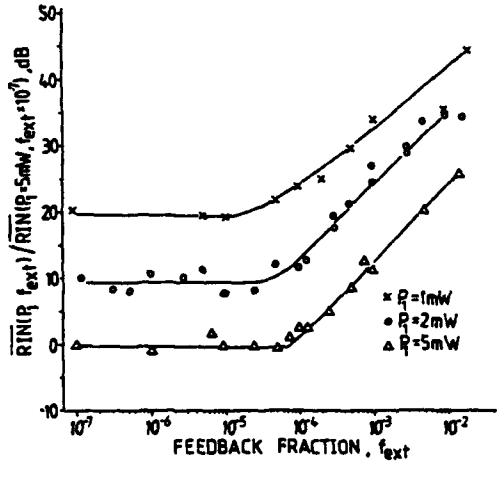

Fig.3b: Measured relative intensity noise RIN averaged over the frequency range 1755...2255MHz and normalized to RIN (P_1=5mW, f_{ext}=10^{-7}) for different output powers P_1 at an external cavity length L_{ext}=2m. A multimode BH-laserdiode Hitachi HLP5400 is used.

K—5

Improved Rate Equations for External Cavity Semiconductor Lasers

Hui Rongqing & Tao Shangping
(Beijing Inst. of Posts & Telecom. P.R.China)

Abstract: Improved rate equations for external cavity semiconductor laser (E.C.S.L.) is derived analytically.

The theory of E.C.S.L. is developing. Recently, R.F.Kazarinov and C.H.Henry[1] has made noticeable progress, they showed that chirp reduction and line narrowing ratio are simplely related, and have got improved rate equations of E.C.S.L. for strong feedback. They derived these mainly from physical properties of the slope of constant phase curve and loss curve of E.C.S.L.. On this research , we have also obtained similar form of improved rate equations as theirs before it published. Our derivation is based on the calculation of effective reflection coefficient r_e of a equivalent single cavity laser by the three mirror theory.
Considering the multiple reflections in the external cavity, then $r_e=r_2 f$, f is a complex feedback parameter and

$$\gamma_e=\gamma_2+R_3(1-\gamma_2^2)\sum_{p=1}^{\infty}\sqrt{\frac{I(t-\tau)}{I(t)}}(-\gamma_2 R_3)^{p-1}e^{i[p\omega\tau+\phi_n(t-p\tau)]} \qquad (1)$$

where r_1 and r_2 are the diode facet amplitude reflectivity, R_3 is the reflectivity of external cavity including coupling and scattering losses, I(t) is light intensity, $\phi_n(t)$ is phase deviation,τ is round trip time in the external cavity, ω is angular frequency, and $\beta(t)=\sqrt{I(t)}\exp[-i(\omega t+\phi_n(t))]$. As I(t) and $\phi_n(t)$ are random variables in stationary stochastic processes, satisfying

$$X[t-(n+1)\tau]-X(t-n\tau)=X(t-\tau)-X(t) \qquad (2)$$

With linear approximations, f can be simplified as follows

$$\lg(f)=(H_1+iP_1)+\tau(H_2+iP_2)[\dot{I}(t)/2I(t)-i\dot{\phi}_n(t)] \qquad (3)$$

where

$$H_1=0.5\ln\left[\frac{1+2(R_3/\gamma_2)\cos\varphi_0+(R_3/\gamma_2)^2}{1+2\gamma_2 R_3\cos\varphi_0+(\gamma_2 R_3)^2}\right] \qquad (4a)$$

$$P_1=\tan^{-1}\left[\frac{R_3(1-\gamma_2^2)\sin\varphi_0}{\gamma_2(1+R_3^2)+R_3(1+\gamma_2^2)\cos\varphi_0}\right] \quad ; \quad \varphi_0=\omega\tau \qquad (4b)$$

$$H_2=-\frac{1}{\tau}(dP_1/d\omega) \qquad (4c) \quad ; \quad P_2=-\frac{1}{\tau}(dH_1/d\omega) \qquad (4d)$$

As the term $k\beta(t-\tau)$ in [2] may be replaced by an added loss term lg(f) which represents the effect of external cavity, then Eq.(40) of [2] becomes

$$\dot{\beta}(t)=\left[-i\Omega+\frac{1}{2}\Delta G(1-i\alpha)+\frac{1}{\tau_i}\ln f\right]\beta(t)+F_\beta(t) \qquad (5)$$

88CH2609-8/88/0000/0142$1.00 1988IEEE

where τ_i is round-trip time of light in the laser diode cavity. Dividing the above equation into two coupled real variable differential equations of I(t) and $\phi_n(t)$ as follows

$$[1+(\tau/\tau_i)H_2]\dot{I}(t)=I(t)[\Delta G+\frac{2}{\tau_i}H_1-\frac{2\tau}{\tau_i}P_2\dot{\phi}_n(t)]+F_I(t) \qquad (6a)$$

$$[1+(\tau/\tau_i)H_2]\dot{\phi}_n(t)=(\Omega-\omega)+\frac{\alpha}{2}\Delta G-\frac{1}{\tau_i}P_1+\frac{\tau}{2\tau_i}\frac{\dot{I}(t)}{I(t)}P_2+F_\phi(t) \qquad (6b)$$

these are the derived improved Langevin rate equations of E.C.S.L

$$\Delta G=-\frac{2}{\tau_i}H_1 \qquad \text{(steady state gain condition)} \qquad (7a)$$

$$\omega=\Omega+\frac{1}{\tau_i}(\alpha H_1-P_1) \qquad \text{(steady state phase condition)} \qquad (7b)$$

here with α being taken into account its accuracy is better than the previous papers [3] in which α was ignored.
From Eq.(7b), the chirp reduction ratio can be calculated in small signal condition as follows

$$F = d\Omega/d\omega =[1+\frac{\tau}{\tau_i}(H_2-\alpha P_2)] \qquad (8)$$

where $d\Omega$ and $d\omega$ are small deviations of central frequency in the solitary laser diode and E.C.S.L. respectively.
From our improved rate equation (6) the line width narrowing ratio can be easily derived as F^2 . We have also shown that the dynamic stable condition of E.C.S.L. is $F>0$. Obviously, the stable region is on the upward side of the phase curve of Eq.(7b) , this fact has been pointed out [4] in weak feedback, here it is extended to arbitrary amount of feedback.
In short, our derived improved rate equations (6) and (7) are more general and complate then others.
It is noticeable that in very strong feedback,the laser will operate stably, not sensitive to the phase of feedback,and immune to external perturbations. It has been verified in our experiment on a semiconductor laser with strong optical feedback,no mode jumping was observed in more than 12 hours.

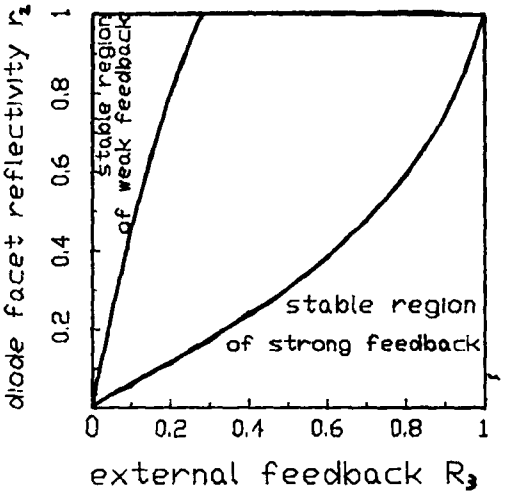

Fig.(3) stable regions of operation in any feedback phase

REFERENCE
[1] R.F.Kazarinov,et.al. J.QE-23, p1401, 1987
[2] C.H.Henry, J.QE-22 p298, 1986
[3] J.H.Osmundsen, et.al. J.QE-19, p465, 1983
[4] H.Olesen, et.al. J.QE-22, p760, 1986

K—6

Low Noise AlGaAs Lasers Grown by OMVPE

S.Yamashita, A.Ohishi, T.Kajimura, *M.Inoue, and *Y.Fukui
Central Research Laboratory, Hitachi, Ltd.
Kokubunji, Tokyo 185, Japan
*Consumer Products Research Center, Hitachi Ltd.
Totsuka, Yokohama 244, Japan

One of the most serious problems in using semiconductor lasers for practical systems such as optical disk systems is excess noise in the light output power. Video disk players in paticular require a high signal to noise ratio because they process analog signals. Light output power noise caused by optical feedback or longitudinal mode hopping is effectively suppressed by utilizing a self-pulsation phenomenon in the semiconductor laser.[1),2)] However, it was found that even in the self-pulsation lasers, pulsation frequency must be controlled to achieve low noise characteristics.

This paper reports the behavior of excess noise in self-pulsation lasers and demonstrates reproducible low noise AlGaAs lasers grown by organo-metallic vapor phase epitaxy (OMVPE). Fig.1 shows relative intensity noise (RIN) in a conventional self-pulsation laser fabricated by liquid phase epitaxy (LPE). Optical length from the laser to an optical disk is 60mm. Laser noise without optical feedback is less than $1\times10^{-13}Hz^{-1}$ over 3mW. However, under 3.2% optical feedback, excess noise is very large from 2mW to 6mW output power, and it decreases at around 7mW output power. Such behaviour was found to be due to the dependence of excess noise on self-pulsation frequency of the laser. Experimental results on the pulsation frequency (f_p) dependence of excess noise are shown in Fig.2. Optical feedback is 3-4% and output power is 3-7mW. As shown in Fig.2, excess noise is small when f_p is around 3GHz and lower than 1.2GHz. This means that the timing of feedback light affects RIN level in the self-pulsation lasers, as in the case of noise suppression by high frequency superposition.[3),4)] Pulsation frequency depends on light output power ($f_p \propto \sqrt{P_o}$). Therefore, it is difficult to control f_p at around 3GHz at the expected output power. It is more practical to control the pulsation frequency below 1.2GHz. It is confirmed experimentaly that the pulsation frequency can be controlled by changing the cavity length, impurity doping in the active layer, and reflectivity of the facet.

To realize reproducible low noise lasers, we devised a ridge waveguide self-aligned structure (RWSAS) laser grown by three step OMVPE as shown in Fig.3. The ridge waveguide structure was formed by chemically etching the p-AlGaAs cladding layer, and n-GaAs carrier blocking layers were selectively grown using a SiO_2 mask. Fig.4 shows the characteristics of pulsation frequency versus light output. By the introduction of undoped active layer and 300μm long cavity, pulsation frequency of the laser can be reduced to $\leq$1/2 compared with the conventional 250μm long laser with a Mg-doped active layer ($p\sim2\times10^{18}cm^{-3}$). The lasing spectra are presented in Fig.5. They show multi-longitudinal mode oscillation with wide line widths due to self-pulsation. The self-pulsation continued in the wide light output power range, 2-7mW. The experimental results of noise

88CH2609-8/88/0000/0144$1.00 1988IEEE

characteristics are shown in Fig.6. A RIN level below $10^{-13}Hz^{-1}$ was obtained at a light output power of 3-5mW with optical feedback of 3%. The increase in RIN level at light output powers over 5mW was caused by an increase in pulsation frequency, as stated above.

In conclusion, it was found that control of pulsation frequency is an important factor in reducting excess noise. Reproducible low noise AlGaAs lasers were realized by 3-step OMVPE. By controlling the pulsation frequency, a RIN level below $10^{-13}Hz^{-1}$ was obtained under optical feedback of 3%.

1) S.Matsui, et al., Appl. Phys. Lett. 43, 219 (1983).
2) T.Kawano, et al., 10th IEEE International Semiconductor Laser Conference, Technical Digest, 195, (1986).
3) A.Arimoto, et al., Applied Optics, 25, 1319 (1986).
4) M.Ojima, et al., Applied Optics, 25, 1404 (1986).

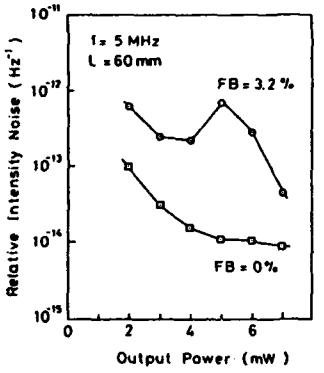

FIG.1.
Dependence of RIN on the light output power.

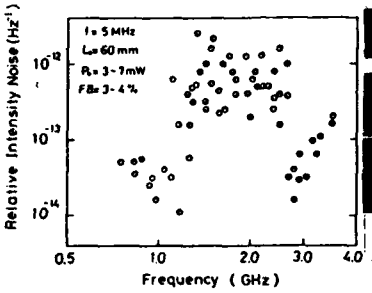

FIG.2.
Dependence of RIN on self-pulsation frequency.

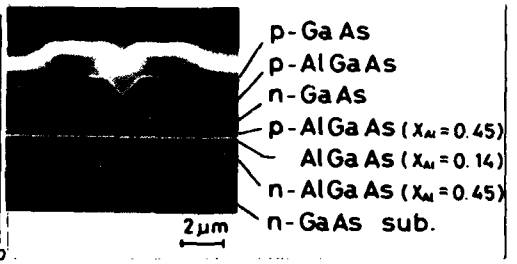

FIG.3.
Cross sectional structure of the low noise laser grown by OMVPE.

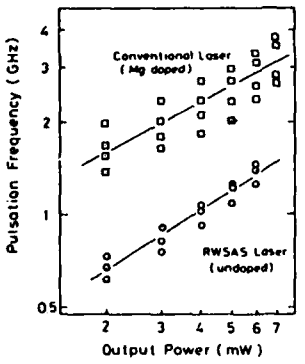

FIG.4.
Self-pulsation frequency vs. light output power characteristics.

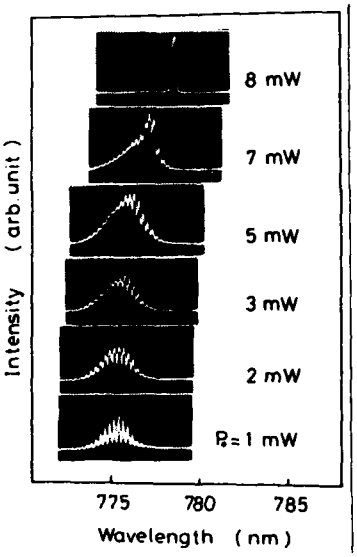

FIG.5.
Lasing spectra of the laser grown by OMVPE.

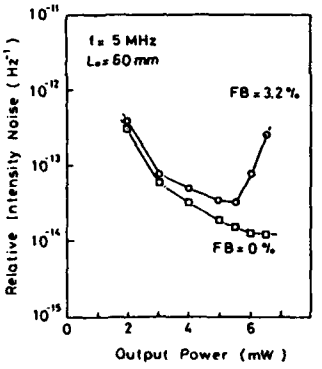

FIG.6.
RIN vs. light output power of the low noise laser grown by OMVPE.

Session L: High Power Fabry-Perot Lasers

L—1

50mW Stable Single Longitudinal Mode Operation of 780nm GaAlAs DFB Laser

S.Takigawa,T.Uno,M.Kume,K.Hamada,N.Yoshikawa,H.Shimizu and G.Kano
Electronics Research Lab. Matsushita Electronics Corp.
Takatsuki Osaka Japan

Stable single longitudinal mode (SLM) operation over 50mW of 780nm GaAlAs DFB lasers is described for the first time.

The following basic concepts, which allow the high power SLM operation, are applied to the present DFB laser.

(1) For the high quantum efficiency, the buried twin-ridge substrate (BTRS) structure [1] is used because of its high current confinement efficiency more than 90%.

(2) To obtain SLM operation under high output-power level, the coupling strength is designed to be as small as 0.5 so that the spacial hole burning along the laser axis can be avoided [2].

The schematic diagram of the GaAlAs DFB-BTRS laser is shown in figure 1. The diodes were successfully fabricated by means of the hybrid growth technique which consists of LPE method to grow flat epitaxial layers over two ridges in BTRS structure and MOCVD method to bury the corrugated GaAlAs guiding layer with high AlAs composition ratio. The corrugation period and height are 2310Å (2nd order grating) and 500Å, respectively. After the metallization and the cleavage, the front facet is coated with Al_2O_3 film and the rear facet is coated with Al_2O_3/Si/Al_2O_3/Si films. It is noticed that the coatings are designed to be power reflectivities of 10% and 94% (AR/HR-coating) on the front and rear facets, respectively.

Figure 2 shows the typical cw light-current characteristics of the AR/HR-coated DFB-BTRS laser at 22°C. The laser exhibits the threshold current of 94mA. The external differential quantum efficiency from the front facet is as high as 75% and the maximum output power is 62mW. The cw lasing spectra at the different power levels are shown in figure 3. The lasing wavelength is about 786nm. The SLM operation is maintained in the power range from 2mW to 50mW. In figure 4 cw lasing wavelength as a function of the heat sink temperature is shown. The SLM operations at 2mW, 20mW, and 50mW are maintained in the temperature ranges of -3°C to 60°C, -9°C to 52°C, and -17°C to 37°C, respectively. The temperature dependence of the lasing wavelength is 0.65Å/deg under SLM operation. Figure 5 shows the longitudinal mode spectrum under the pulsed operation at the frequency 250MHz, the duty cycle 50%, and the pulse height 50mW, which is superposed on the dc operation of 5mW. The SLM operation is maintained under this modulation and the suppresion ratio of the side mode is more than 30dB.

We have first reported the GaAlAs DFB-BTRS lasers which exhibit stable single longitudinal mode operation over 50mW in the wavelength of 780nm. This laser is hopefully expected to be applied to optical information processing systems, optical measurements and integrated optical circuits.

[1] K. Hamada et al., IEEE J. Quantum Electron., QE-21,623(1985)
[2] H. Soda et al., Electron.Lett.,22,1047(1986)

88CH2609-8/88/0000/0148$1.00 1988IEEE

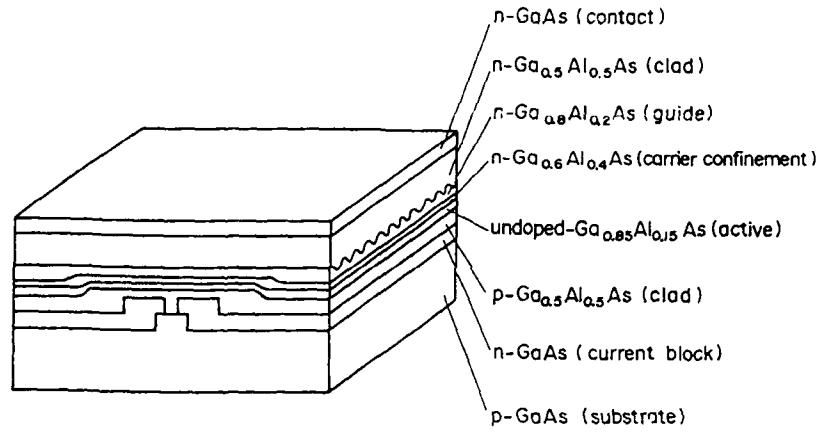

Fig.1 Schematic diagram of the GaAlAs DFB-BTRS laser.

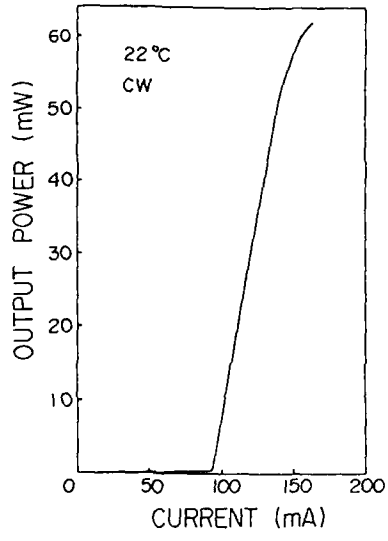

Fig.2
Light-current characteristics of the AR/HR-coated DFB-BTRS laser.

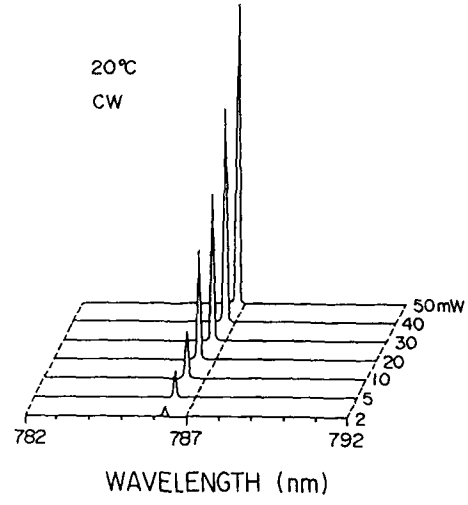

Fig.3 Lasing spectra at the different power levels.

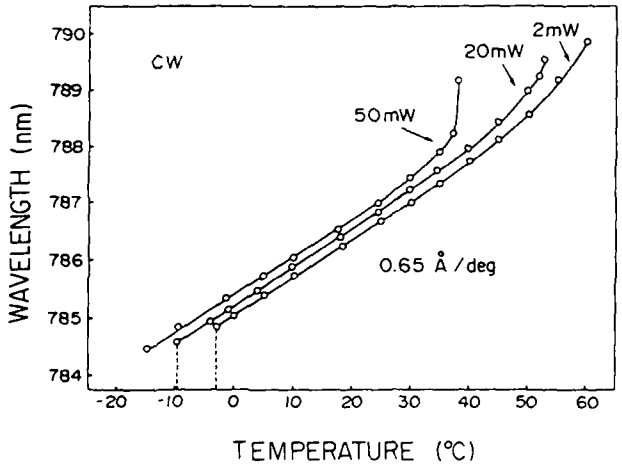

Fig.4 Lasing wavelength as a function of the heat sink temperature.

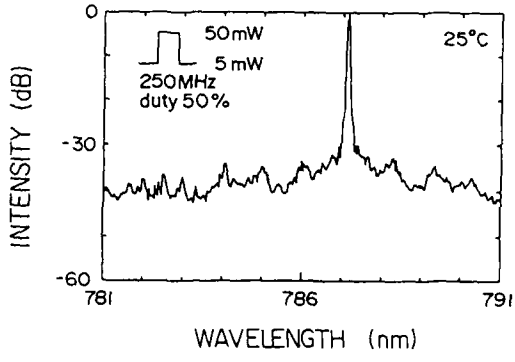

Fig.5
Longitudinal mode spectrum under pulsed operation.

L—2

Highly Reliable CW Operation of 100mW GaAlAs Buried Twin Ridge Substrate Lasers with Nonabsorbing-Mirrors

H.Naito,M.Kume,K.HAMADA,H.Shimizu and G.Kano
Electronics Research Laboratory Matsushita Electronics Corp.
Takatsuki Osaka Japan

In this paper, we demonstrate a high power GaAlAs laser with nonabsorbing-mirrors (NAM)[1)2)], in which highly stable operation over 3000 hours was achieved under 100mW cw output power at 50°C.

Much attention has recently been paid to the development of high power lasers which provide not only stable fundamental-transeverse-mode operation but also high reliability enough to meet requirements for optical systems.

The laser has been developed on the base of following two basic concepts.

(1) Formation of the NAM together with the current-blocked region[1)2)] is the most effective approach which leads to the dramatic suppression of mirror degradation due to the local heating at facets.

(2) The buried twin ridge substrate (BTRS)[3)] structure which allows the formation of the excellently uniform active layer is particularly suited for stabilizing the fundamental-transverse-mode in a high power operation.

These concepts were successfully applied to implementing the laser which is designated as the NAM-BTRS laser.

Figure 1 shows a schematic drawing of the NAM-BTRS laser. The large optical cavity BTRS structure with the current-blocked region[4)] is formed by the LPE growth. The epitaxial layers are etched down to the optical guide layer, followed by the growth of a cladding layer and a contact layer by MOCVD. It is noted that this fabrication process is suited for forming the NAM together with the current-blocking layer in the facet region. The guide layer permits suppression of the coupling loss between the active layer and the NAM region. The transverse mode is confined in the channel between two ridges.

Maximum output powers of 300mW and 1.2W were obtained under cw and 100ns pulsed operations, respectively as shown in Fig.2. Figure 3 indicates the fundamental-transverse-mode operation which is stably maintained up to 120mW. Figure 4 shows aging test results of the NAM-BTRS lasers under 100mW cw operation at 50°C. No increase of the operation currents was observed even after 3000 hours.

In conclusion, we have demonstrated the high power laser which posseses the stable transverse mode up to 120mW and the extremely high reliability operation over 3000 hours by applying NAM approach to the BTRS structure.

References

1)D.Botez et al.,9th IEEE Int.Semiconductor Laser Conf.,36(1984).
2)J.Ungar et al.,Electron.Lett.22,279(1986).
3)K.Hamada et al.,IEEE J.Quantum Electron.QE-21,623(1985).
4)T.Shibutani et al.,IEEE J.Quantum Electron.QE-23,760(1987).

88CH2609-8/88/0000/0150$1.00 1988IEEE

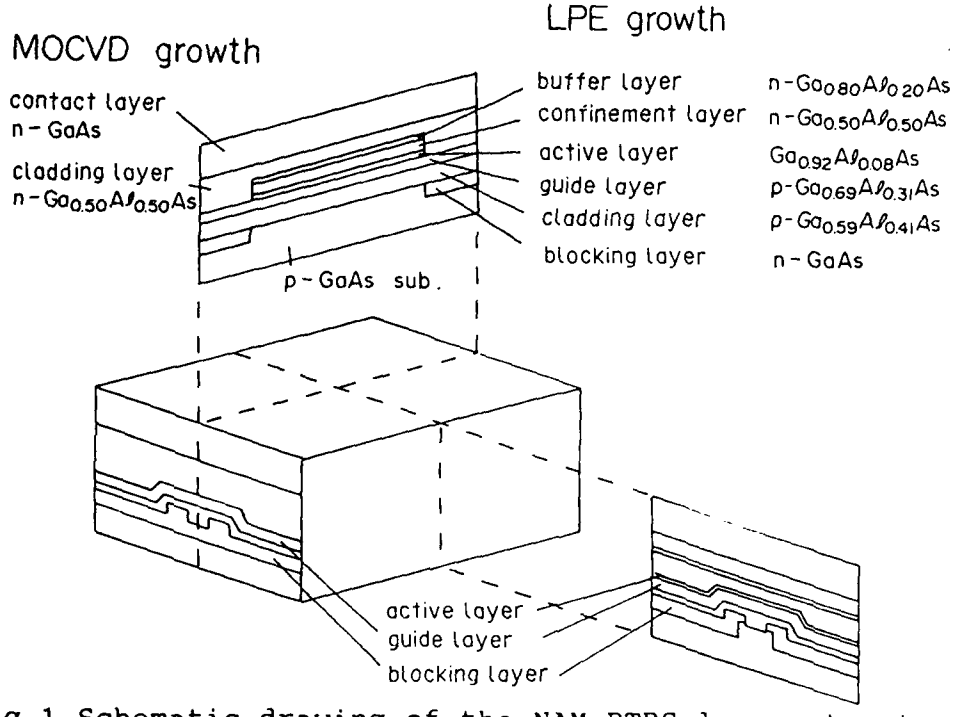

Fig.1 Schematic drawing of the NAM-BTRS laser structure.

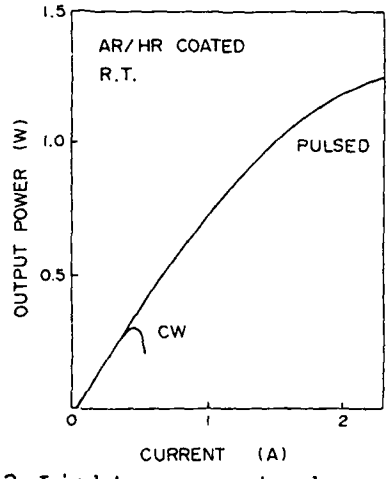

Fig.2 Light-current characteristics.

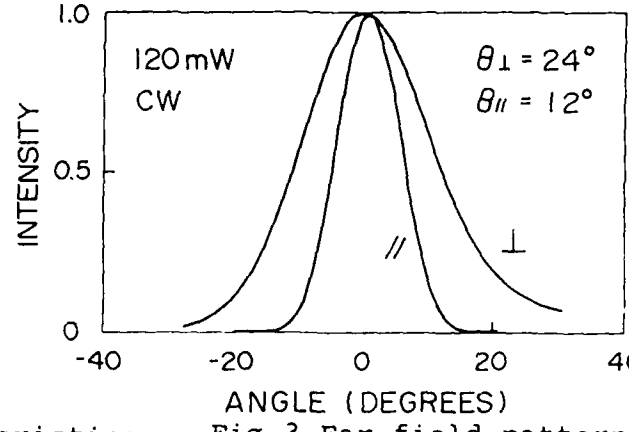

Fig.3 Far-field patterns.

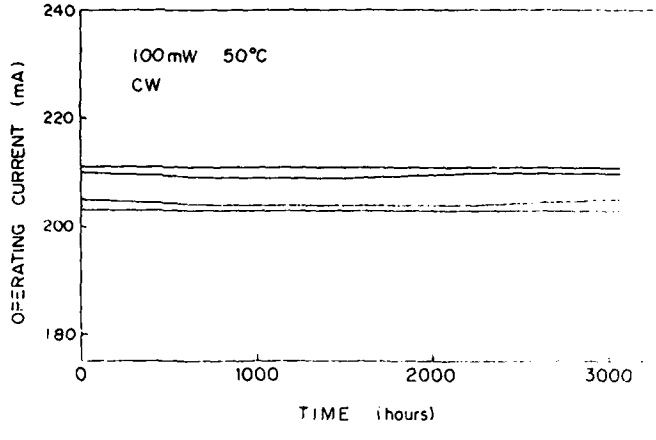

Fig.4 Aging test results.

L—3

This paper has been withdrawn

This paper has been withdrawn

L—4

High Peak Power AlGaAs/GaAs Stripe Laser Diodes on GaAs-on-Si Substrates Grown by Migration-Enhanced Molecular Beam Epitaxy

J.H. Kim, A. Nouhi, G. Radhakrishnan, R.J. Lang, and J. Katz
Jet Propulsion Laboratory, California Institute of Technology
Pasadena, California 91109, USA.

The main attraction of GaAs-on-Si technology is the possibility of monolithic integration (e.g., for optical interconnections) combining optical and electrical properties of III-V compound semiconductors with silicon VLSI technology and its mechanical and thermal properties. Recently, significant progress has been made in the heteroepitaxial growth of GaAs on Si substrates by MBE or MOCVD resulting in greatly reduced threshold currents in double heterostructure or quantum well lasers [1-4]. We report a high peak power low threshold AlGaAs/GaAs stripe laser on GaAs-on-Si substrates grown for the first time by a combination of migration enhanced molecular beam epitaxy (MEMBE) and metalorganic chemical vapor deposition. We also demonstrate low temperature migration-enhanced molecular beam epitaxy to grow the initial GaAs layer directly on Si substrates (i.e., without superlattice buffer layers), which is based on migration-enhanced epitaxy on GaAs proposed by Horikoshi et al. [5].

The growth procedures of our first technique start with the initial growth of 150 GaAs monolayers while supplying As with Ga and Si alternately by opening and closing the shutters. Following deposition of 150 monolayers of GaAs, this growth of GaAs layers continued up to a thickness of 2 μm at the rate of 1 monolayer/sec with all three sources open. A constant temperature (400 °C) was maintained during the entire procedures. A second growth technique was initiated by exposing a Si wafer to As for 4 sec at a substrate temperature of 300 °C. With the surface primed by As, the Ga source was opened and the GaAs was nucleated at the rate of 0.1 monolayer/sec. During deposition of 60 monolayers of GaAs the substrate temperature was gradually ramped up to 500 °C and the Ga and As fluxes were increased to the final growth values of 4×10^{-7} and 2×10^{-6} Torr, respectively. At this step faster growth was commenced at the rate of 1 monolayer/sec. Subsequently laser structures were grown on the GaAs-on-Si substrates by a conventional MOCVD technique. More recently, we try to combine several methods to reduce dislocation densities, which will be discussed at the conference in details.

As preliminary results we demonstrate a high peak power low threshold stripe laser diodes grown on Si substrates by hybrid MEMBE/MOCVD. The lasers were tested unmounted under pulsed conditions (i.e., 50 ns pulse width and 10 KHz repetition rate) at room temperature. These stripe lasers operated kink-free up to 185 mW per facet with a differential quantum efficiency of up to 30 % without mirror facet coating. (The maximum output power for pulsed operation is limited by catastrophic degradation of the mirror facets). A threshold current as low as 150 mA at room temperature for a cavity length of 350 μm has been measured, as shown in Fig.1. A pulsed intrinsic threshold current density has been estimated to be about 2 kA/cm^2 when taking current spreading and lateral diffusion effects into account. This can be further reduced for lasers with a quantum well (e.g., GRIN-SCH SQW) active region and advanced stripe (e.g., mesa or BH) lasers. This work on advanced stripe GRIN-SCH SQW lasers on Si substrates is in progress and further results will be reported at the conference. For comparison, the pulsed threshold current density of the broad area double heterostructure lasers on GaAs substrates was

88CH2609-8/88/0000/0154$1.00 1988IEEE

1.1 kA/cm^2 at room temperature. These results show the highest output peak power reported so far for conventional DH stripe laser diodes grown on Si substrates. Figures 2 and 3 show, respectively, the near and far-field patterns of AlGaAs/GaAs stripe lasers on Si parallel to the junction. These show stable operation of the lasers at currents above threshold. The near-field pattern with the full width at the half maximum (FWHM) of 6.5 μm shows single filament lasing and good current guiding in the lateral direction. A single-lobed far-field pattern with the FWHM of 10 was obtained. It should be noted that these parameters are comparable to those of the AlGaAs/GaAs lasers.

1. J. van der Ziel, R. Dupuis, R. Logan, R. Mikulyak, C. Pinzone, and A. Savage, Appl. Phys. Lett., 50(8), 454, 1987.
2. D. Deppe, N. Holonyak, D. Nam, K. Hsieh, G. Jackson, R. Matyi, H. Shichijo, J. Epler, and H. Chung, Appl. Phys. Lett., 51(9), 637, 1987.
3. H. Chen, A. Ghaffari, H. Wang, H. Morkoc, and A. Yariv, Appl. Phys. Lett., 51(17), 1320, 1987.
4. S. Sakai, H. Shiraishi, and M. Umeno, IEEE J. Quan. Elec., 23(6), 1080, 1987.
5. Y. Horikoshi, M. Kawashima, and H. Yamaguchi, Japan J. Appl. Phys., 25(10), 1986.

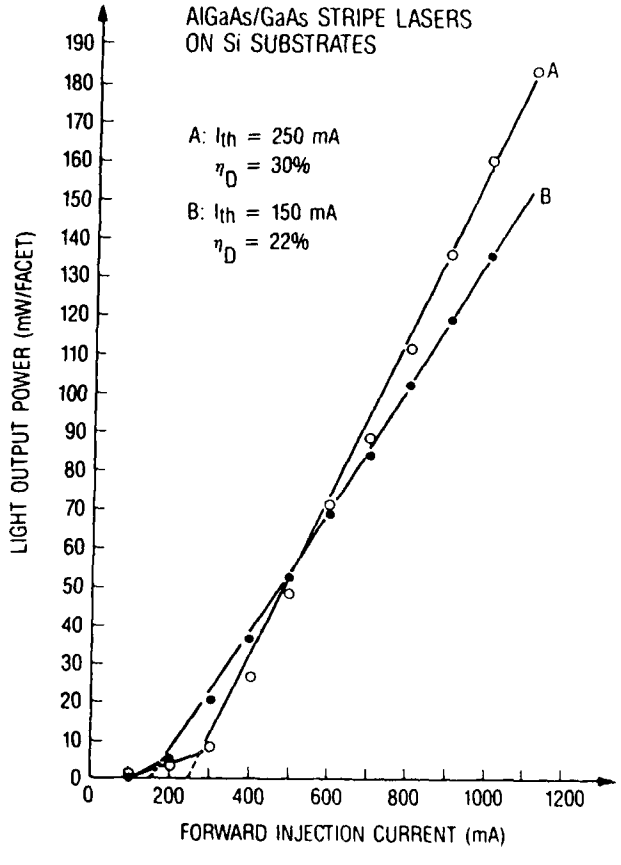

Fig.1. Light output power versus forward injection current characteristics.

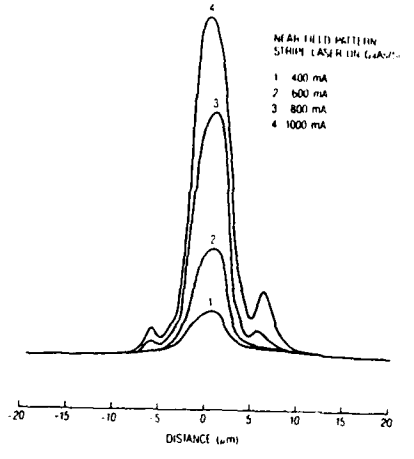

Fig.2. Near-field patterns of lasers.

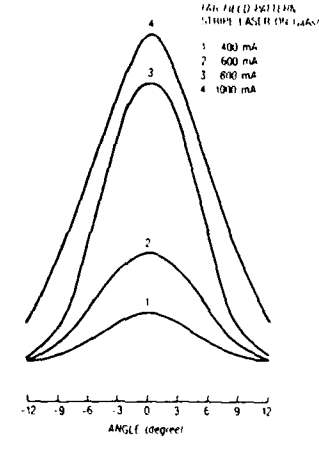

Fig.3. Far-field patterns of lasers.

L—5

Continuous Operation of High Power (200mW) Strained-Layer $In_xGa_{1-x}As$-GaAs Quantum Well Lasers with Emission Wavelengths $0.86 \leq \lambda \leq 1$ μm

P. Gavrilovic, K. Meehan, W. Stutius, J.E. Williams, and J.H. Zarrabi
Microelectronics Laboratory, Polaroid Corporation, Cambridge, MA 02139

High power GaAs/GaAlAs diode lasers are finding an increasing number of applications for optical pumping of solid-state lasers, such as Nd:YAG and Nd:glass. The pump wavelength here is typically around 0.805 μm. For optical pumping of rare earth glass lasers other than Nd:glass, e.g. Yb-sensitized Er:glass lasers with an emission wavelength of 1.54 μm, semiconductor lasers with emission wavelengths up to 1 μm are required. The longest wavelength attainable from GaAs quantum well lasers with an undoped GaAs quantum well is $\approx$ 0.87 μm .

Early attempts to shift the lasing emission to longer wavelengths relied on heavy p-type doping of the active region using Si, Ge, and Zn.[1] This approach, however, leads to an increase of the lasing threshold current density and poses reliability problems for the device. More recently, however, several reports of InGaAs/GaAs strained-layer quantum well lasers emitting near 1 μm, with threshold current densities as low as 152 A/cm^2 have been published.[2-4]

This paper describes the fabrication of separate-confinement double-heterostructure (SCDH) lasers with an $In_xGa_{1-x}As$-GaAs quantum well, grown by low pressure metalorganic chemical vapor deposition (MOCVD). These lasers are capable of high-power CW operation at emission wavelengths between 0.87 μm and 1 μm.

The laser structure was grown in a vertical cold-wall reactor at a pressure of 100 Torr and consists of the n-type (100) GaAs substrate, a 0.25 μm n-GaAs buffer layer, a 1.2 μm n-$Al_{0.8}Ga_{0.2}As$ cladding layer, an undoped 0.16 μm $Al_{0.25}Ga_{0.75}As$ / 150 ÅGaAs / 110 Å$In_xGa_{1-x}As$ / 150 ÅGaAs / 0.16 μm $Al_{0.25}Ga_{0.75}As$ waveguide region, followed by a 1.2 μm p-$Al_{0.8}Ga_{0.2}As$ cladding layer and a p^+-GaAs cap. The n-layers were Se doped, the p-cladding layer was doped with Mg, and the cap was doped with Zn. The growth temperature was 800 °C, except for the InGaAs quantum well, which was grown at 650 °C.

Both broad area devices and proton-isolated 10-stripe lasers were fabricated from the same wafer. The lowest measured threshold current density was 152 A/cm^2 for a 750 x 250 μm broad area device. The threshold current for a 250 μm long 10-stripe laser with a 100 μm aperture was 155 mA after facet coating, with a 35 % reflectivity for the front facet and 85 % reflectivity for the back facet. A typical plot of the CW output power versus current is shown in Fig.1. Accelerating aging of a device bonded p-side up for 150 hours at a heat sink temperature of 50 °C (corresponding to a junction temperature of 90 °C) and a CW power level of 100 mW indicated an increase of 0.1 mA/hour in operating current. This corresponds to a mean-time-to-failure of more than 20,000 hours at room temperature. No change in the near-field or far-field pattern was observed after aging.

These results suggest that lasers employing strained-layer quantum wells can operate as efficiently and reliably at high output power levels as lasers with unstrained quantum wells, thus enabling direct optical pumping of a diverse family of rare-earth glass and fiber lasers.

88CH2609-8/83/0000/0156$1.00 1988IEEE

References

[1] P.D. Dapkus N. Holonyak, Jr., J.A. Rossi, F.V. Williams, and D.A. High, J. Appl. Phys. **40**, 3300 (1969)

[2] W.D. Laidig, Y.F. Lin, and P.J. Caldwell, J. Appl. Phys. **57**, 33 (1985)

[3] D. Fekete, K.T. Chan, J.M. Ballantyne, and L.F. Eastman, Appl. Phys. Lett. **49**, 1659 (1986)

[4] S.E. Fischer, D. Fekete, G.B. Feak, and J.M. Ballantyne, Appl. Phys. Lett. **50**, 714 (1987)

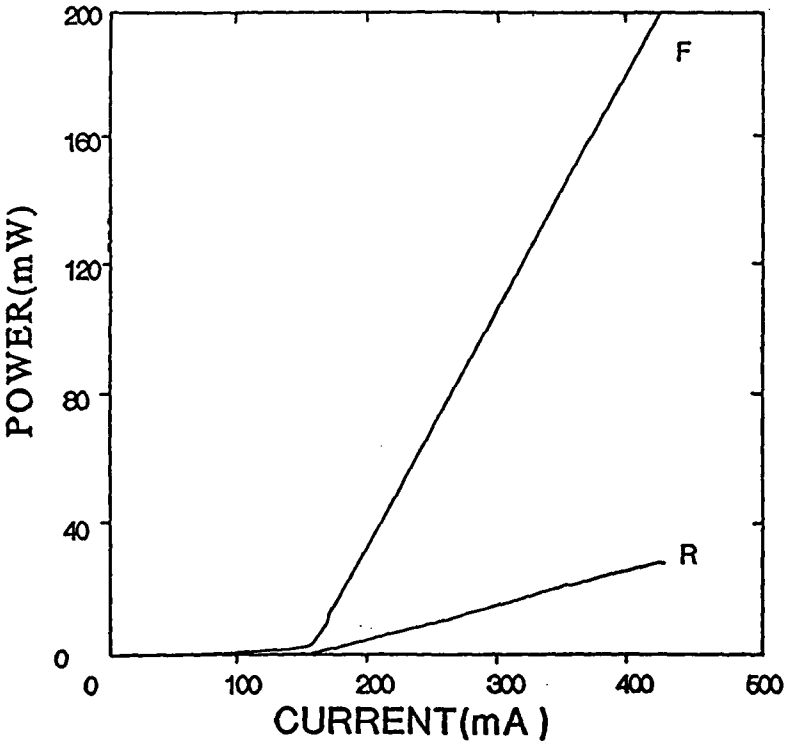

Figure 1. CW output power of front (F) and rear (R) facet of a 10-stripe $In_xGa_{1-x}As$-GaAs laser with 100 μm aperture and 250 μ cavity length.

L—6

High-Power Non-Planar Quantum Well Heterostructure Periodic Laser Arrays

C. A. Zmudzinski, M. E. Givens, R. P. Bryan and J. J. Coleman

Department of Electrical and Computer Engineering and
NSF Engineering Research Center for Compound Semiconductor Microelectronics
University of Illinois at Urbana-Champaign
1406 West Green Street
Urbana, Illinois 61801

ABSTRACT

Multiple stripe semiconductor laser arrays are a very promising source of high-power emission suitable for such applications as pumping solid state Nd:YAG lasers. The maximum output power before catastrophic optical damage occurs is determined primarily by the effective aperture width which is normally limited to a value less than the cavity length, unless lateral lasing and amplified spontaneous emission processes are suppressed. In order to fabricate diodes with a width greater than the laser cavity length, thereby allowing higher total output powers to be obtained, it is necessary to provide some structural change to inhibit lateral lasing. Previously reported methods of inhibiting lateral lasing and amplified spontaneous emission require extra processing steps in addition to the processing required to form the actual array elements, and also result in a portion of the array width which does not contribute to the laser output.

In this work, we report high-power operation of a simple non-planar index-guided graded barrier quantum well heterostructure (GBQWH) periodic laser array structure in which lateral lasing is prevented in a manner that still allows for uniform and continuous front facet light emission. Growth by metalorganic chemical vapor deposition (MOCVD) over a corrugated substrate is utilized for index-guiding and definition of the individual elements, and the resulting non-planar active region structure effectively suppresses lateral lasing and amplified spontaneous emission for the entire array. The structure is illustrated in Fig. 1 which shows a schematic cross section and a scanning electron micrograph of a portion of the laser array. No additional processing steps after growth, such as proton bombardment, chemical etching, diffusion, epitaxial regrowth, or insulator deposition, which may result in accelerated degradation due to the introduction of material defects, are required.

Fig. 2 shows the near field optical intensity pattern from two adjacent elements of a high power GBQWH periodic laser array at twice threshold. Two lasing spots, spaced by 1.5 μm, are located in the mesa near each edge. The observed near field pattern is stable over a wide range of drive currents, retaining its shape from threshold to at least 16 times threshold. The corresponding far field pattern in the plane of the junction is single lobed, with a relatively wide full width half maximum angle of 18°, indicating that, while it is possible that the individual emitter pairs are phase locked with each other, adjacent pairs spaced by 8 μm are not phase locked.

The L-I curve of Figure 3 shows the output from both an uncoated facet and a sawn edge of a typical laser array with a cavity length of 508 μm and a width of 700 μm. We observed no decrease in efficiency or increase in threshold current density as the width was varied from 0.5xl to 6.4xl, where l is the cavity length. Discrimination against lateral lasing is provided solely by the non-planar structure of the active region which is realized by epitaxial growth on a selectively etched substrate patterned with a periodic array of mesa stripes. The measured light intensity from the cleaved front facets at 2.0 A was typically more than 15 times the intensity of light from the sawn edges which is mainly scattered front facet emission. Data are presented in Fig. 4 on the high power light-current characteristics and optical near field measurements for uncoated laser bars with an aperture width of up to 3.1 mm (cavity length = 483 μm), showing output powers in excess of 8 W per uncoated facet for periodic laser arrays with threshold current densities of 120-220 A/cm^2.

88CH2609-8/88/0000/0158$1.00 1988IEEE

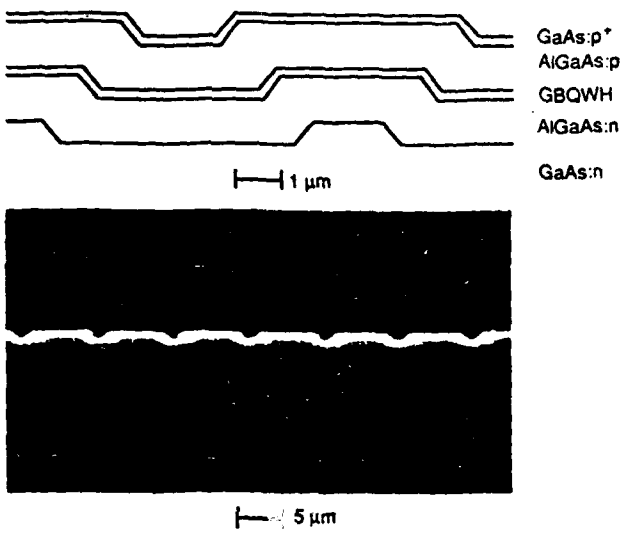

Figure 1

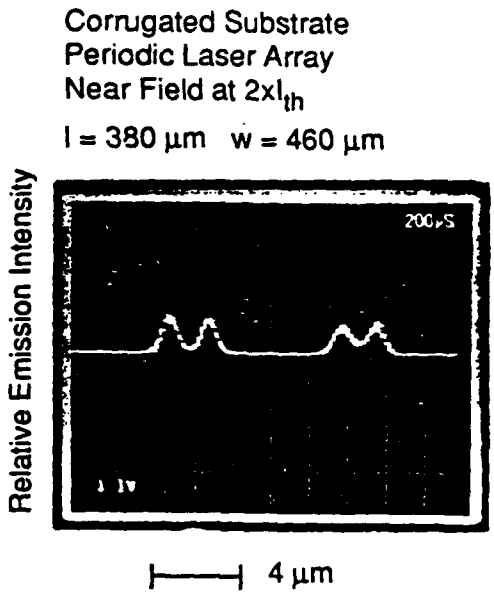

Figure 2

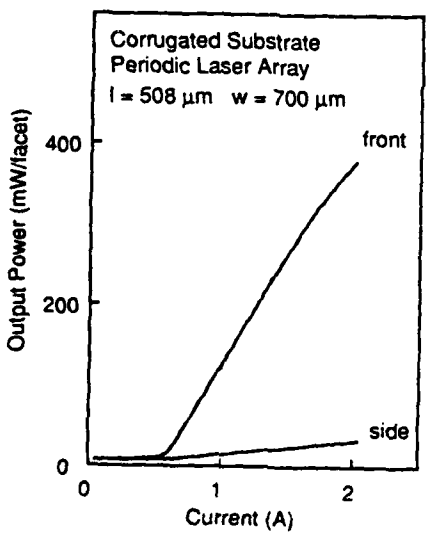

Figure 3

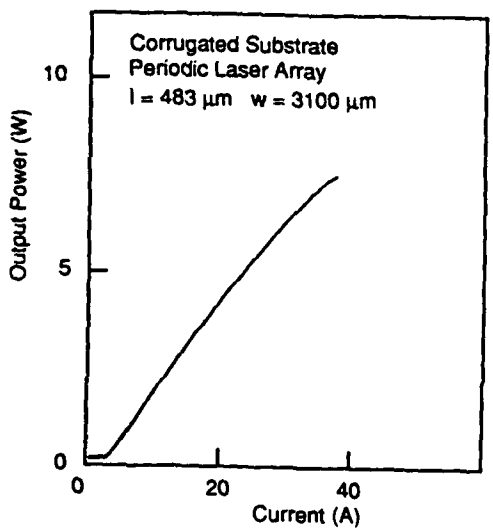

Figure 4

C. A. Zmudzinski, M. E. Givens, R. P. Bryan and J. J. Coleman

THURSDAY, September 1, 1988

Session N: Surface Emitters and Integration

N—1

A Vertical Cavity GaAlAs/AlAs DBR Surface Emitting Laser and Its Lasing Characteristics

T. Sakaguchi, F. Koyama and K. Iga
Tokyo Institute of Technology
4259 Nagatsuta, Midoriku, Yokohama 227, Japan, Fax 81-45-921-0898

This paper presents the first room temperature pulsed operation of a vertical cavity surface emitting (SE) laser with an electrically conductive GaAlAs/AlAs DBR. A necessary criterion for lasing operation of SE lasers [1] is discussed by using the result obtained.

A schematic structure of a GaAlAs/AlAs DBR surface emitting laser is shown in Fig. 1. A DH wafer with 20 pairs of $Ga_{0.9}Al_{0.1}As$/AlAs multilayers was grown by atmospheric pressure MOCVD. The multilayer was used for a light emitting side reflector, which is intentionally doped for current injection [2]. The maximum reflectivity of a grown DBR was 96% at 0.88μm of wavelength. A mesa cap structure [3] with an active layer thickness of 3μm and a diameter of 30μm was fabricated.

Figure 2 shows a light output/current characteristic and a typical lasing spectrum of a fabricated DBR surface emitting laser device. Room temperature pulsed operation has been achieved with a threshold I_{th}=200 mA, which is the lowest value for such a broad area structure. The threshold could be reduced to several miliamperes by introducing a circular buried heterostructure [4]. The maximum output power from fabricated DBR laser devices was 12 mW. These results indicate that the doped multilayer reflector works as a highly reflective mirror with low absorption loss.

Wide spectral widths (>10Å) are sometimes observed from surface emitting devices. From our lasers with a short cavity (L<10μm), on the other hand, a relatively narrow spectral width has always been observed even below the threshold. For the purpose of obtaining more exact criterion for oscillation of SE lasers, we paid attention to spectra below and above the threshold, which are shown in Fig. 3. Even below the threshold, the spectral width was less than 1Å which is limited by the resolution of

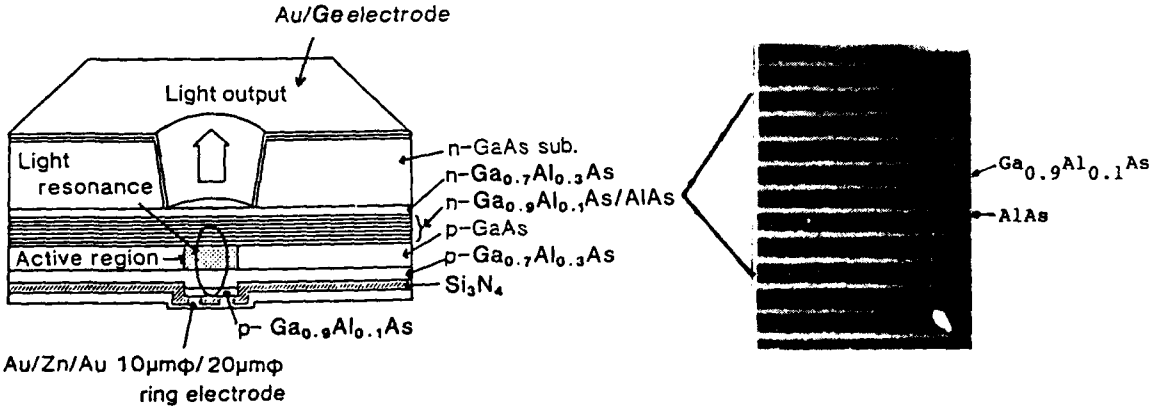

Fig. 1 A vertical cavity GaAlAs/AlAs DBR surface emitting laser.

88CH2609-8/88/0000/0162$1.00 1988IEEE

spectrometer used. The spectral width $\delta\lambda$ expected from the theory using the present laser parameters is plotted in Fig. 4. It is noted that $\delta\lambda$ was less than 2Å even below the threshold ($I>0.8\times I_{th}$). Spectral width of >10Å may indicate that the device is operating far below the threshold.

Next, we observed the center wavelength shifted below the threshold as plotted in Fig. 4 by the open circles. It was fixed above the current level I_{th} determined by the L-I break in Fig. 2. This is understood by the theory considering the increase and cramp of carriers. The spectral shift and cramp should be a better criterion of laser threshold.

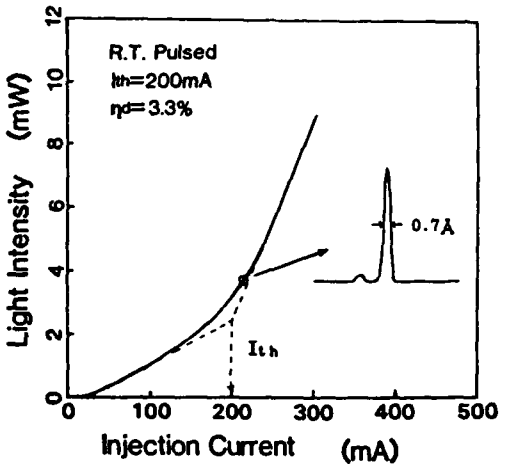

Fig. 2 Light output/current characteristic of a DBR surface emitting laser.

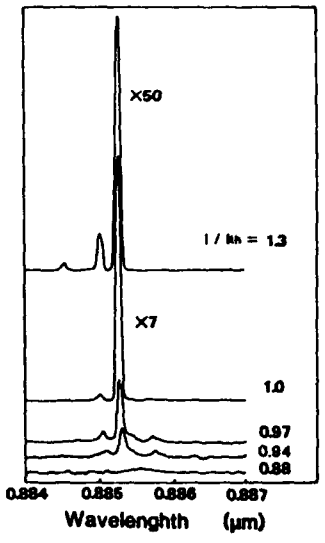

Fig. 3 Lasing spectra of DBR surface emitting laser with various injection levels. Spectral resolution is 0.5Å. Spectral width is less than 1Å even below the threshold.

We believe that a semiconductor multilayer DBR is effective for reducing the threshold and stacking other optical functional devices on the surface emitting laser.

The authors wish to thank Prof. Y. Suematsu of Tokyo Institute of Technology for encouragement. This work was supported by the Scientific Research Grant in Aid #61065002 from the Ministry of Education, Science and Culture.

References [1] H. Soda, K. Iga, C. Kitahara: Jpn. J. Appl. Phys., 18, p.2329-2330, 1979. [2] A. Chailertvanitkul, K. Iga and K. Moriki, Electron. Lett., 21, pp.303-304, 1985. [3] K. Iga, S. Ishikawa, S. Ohkouchi and T. Nishimura, IEEE J. Quantum Electron. QE-21, pp.663-668, 1985. [4] K. Iga, S. Kinoshita and F. Koyama, Electron. Lett., 23, pp.134-136, 1987.

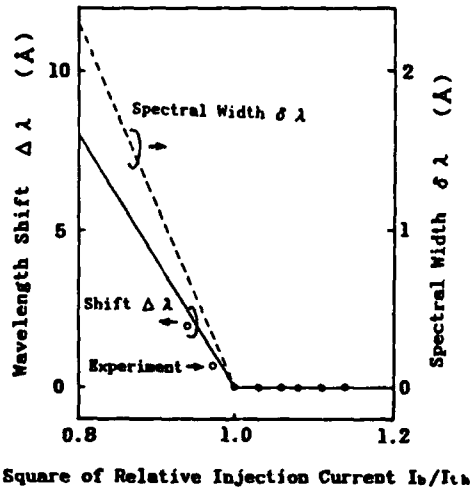

Fig. 4 Wavelength shift and spectral width of a resonant mode. (solid and dashed lines: theory, open circles: experiment)

N—2

GaAs/GaAlAs DBR Surface Emitting Laser With GaAlAs/AlAs and $Si0_2/Ti0_2$ Reflectors

A. Ibaraki, K. Kawashima, K. Furusawa, K. Ishikawa,
T. Yamaguchi and T. Niina

Semiconductor Research Center, SANYO Electric Co., Ltd.
1-18-13 Hashiridani, Hirakata, Osaka 573, Japan

Surface emitting (SE) lasers with a semiconductor multilayer Bragg reflector have two main merits: they can be formed in the same process as the growth of the DH layers, and the carriers can be injected through the reflector (1),(2). They are very attractive for two-dimensional laser arrays and OEICs.

This report concerns the performance of a SE laser with a $Ga_{0.9}Al_{0.1}As$/AlAs multilayer Bragg reflector grown by OMVPE and a SiO_2/TiO_2 dielectric multilayer reflector. A significantly high slope efficiency was achieved, which is much higher than the value previously obtained in SE lasers.

The structure of the DBR SE laser is shown in Fig. 1, where the $Ga_{0.9}Al_{0.1}As$/AlAs multilayer Bragg reflector is used for the rear mirror with high reflectivity, and light output is obtained through the front mirror with the high reflectivity and low loss of the SiO_2/TiO_2 (4 pairs) dielectric multilayer reflector.

The eptaxial layers, n-GaAs buffer layer (Se-doped, 0.5 μm), n-Ga . $Al_{0.1}As$/AlAs multilayers (Se-doped, 30 pairs), n-Ga . $Al_{0.35}As$ cladding layer (Se-doped, 1.0 μm), p-GaAs active layer (Zn-doped, 1.8 μm), p-$Ga_{0.65}Al_{0.35}As$ cladding layer (Zn-doped, 1.7 μm) and p-$Ga_{0.94}Al_{0.06}As$ cap layer (Zn-doped, 1.2 μm), were successively grown on Si-doped GaAs substrates under atmospheric pressure (Fig. 2).

The reflectivity of the 30-pair n-$Ga_{0.9}Al_{0.1}As$/AlAs multilayer Bragg reflector was 96% at a wavelength of 0.875 μm, which corresponds to the lasing wavelength of the GaAs/GaAlAs SE laser. The reflectivity and transparency of the 4-pair SiO_2/TiO_2 dielectric multilayer reflector were about 97% and 3%, respectively. As a result of this multilayer Bragg reflector, no sophisticated etching process for the GaAs substrate is necessary for an n-side mirror formation.

A mesa structure with a 20-μmϕ/10-μmϕ ring electrode is formed on the p-side surface.

Fabricated DBR SE layers have operated under a room-temperature pulsed condition. The light-output/current characteristic is shown in Fig. 3, and the threshold current is 107 mA. The slope efficiency (s_d) of this sample is 0.14 mW/mA, which is about four times higher than the s_d of a sample with an Au/SiO semi-transparent reflector (loss ~3%) instead of the SiO_2/TiO_2 dielectric multilayer reflector. The current dependence of the spectrum is shown in Fig. 4. The spectrum at I/Ith = 0.95 has three peaks. The one at 875 nm is a lasing longitudinal mode, and the others are

88CH2609-8/88/0000/0164$1.00 1988IEEE

small peaks, which are nonlasing neighboring longitudinal modes. The longitudinal mode spacing is about 13 nm. A single mode operation up to 1.8 times the threshold value was obtained.

Acknowledgements

The authors wish to thank Prof. K. Iga of Tokyo Institute of Technology for his helpful discussions.

Reference

(1) A. Ibaraki et. al.: to be published in J. Crystal Growth.
(2) A. Chailertvanitkul, K. Iga and K. Moriki: Electron. Lett. 21, 303 (1985)

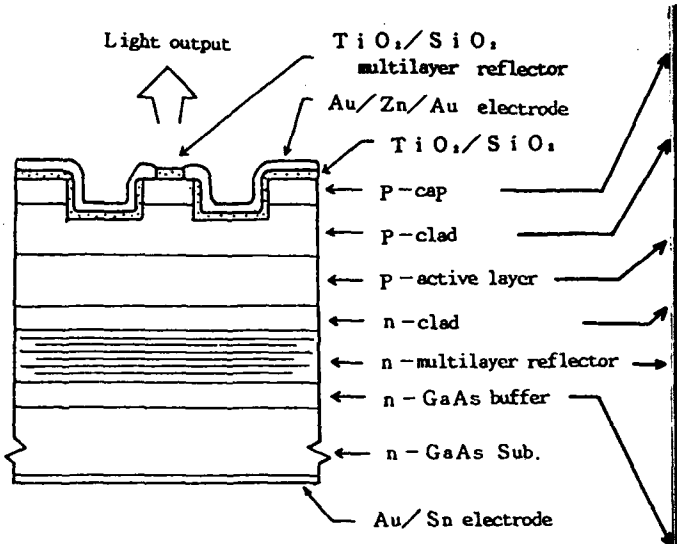

Fig. 1 Structure of a GaAs/GaAlAs DBR SE Laser with semiconductor mulitilayer and dielectric multilayer reflectors.

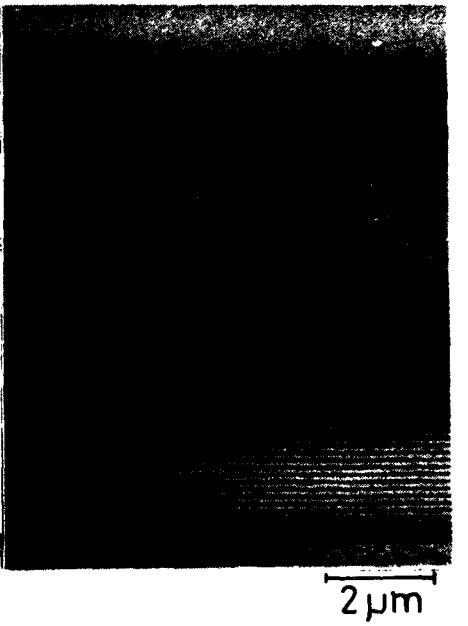

Fig. 2 Cross sectional SEM photograph of the DBR SE Laser.

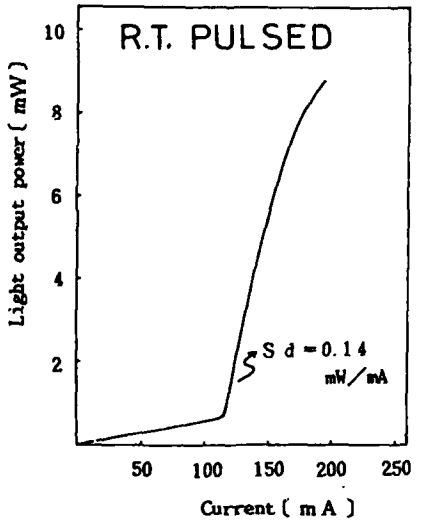

Fig. 3 Light output power vs current characteristic under a room-temperature pulsed condition.

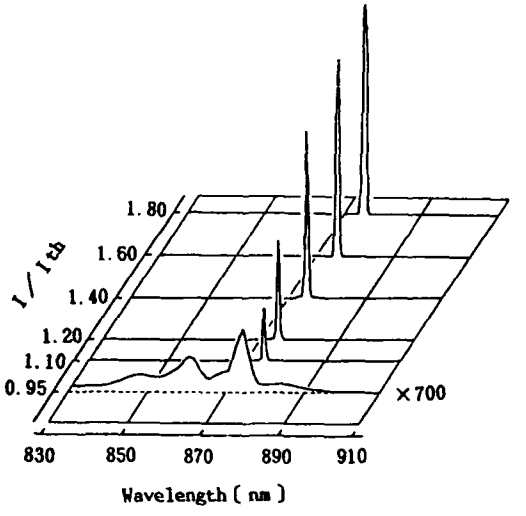

Fig. 4 Current dependence of the spectrum characteristics.

N—3

Two Dimensional, Coherent Grating Surface Emitting Laser Arrays

G. A. Evans[a], N. W. Carlson[a], J. M. Hammer[a], M. Lurie[a], J. K. Butler[a], M. Ettenberg[a], J. Connolly[a], L. A. Carr[a], F. Z. Hawrylo[a], E. A. James[a],C. J. Kaiser[a], J. B. Kirk[a], W. F. Reichert[a], S. R. Chinn[b], J. R. Shealy[b], and P. S. Zory[b]

[a]David Sarnoff Research Center, CN 5300, Princeton, NJ 08543-5300
[b]General Electric Electronics Laboratory, Syracuse, NY 13221

Objective: The objectives of this work were to fabricate and characterize monolithic, coherent two dimensional 10 X 10 arrays of grating surface emitting (GSE) semiconductor lasers.

Background: Grating surface emission from distributed feedback (DFB) and distributed Bragg reflector (DBR) lasers were reported in the mid-1970's by several research groups [1]. The use of quantum well AlGaAs lasers has resulted in large increases in the power and efficiency of individual [1,2] and one-dimensional coherent arrays [3] of GSE lasers.

Technique: Two dimensional arrays of grating surface emitting DBR lasers were fabricated using 1) graded index separate confinement heterostructure (GRINSCH) single quantum well (SQW) wafers with superlattice cladding and graded regions; 2) conventional GRINSCH-SQW wafers (no superlattices); and 3) multiple quantum well (MQW) wafers. The approximate thicknesses and compositions of the GRINSCH SQW wafers were 0.2 μm thick linearly graded regions (graded from about 80% AlAs to 40% AlAs) with 80 to 150 Å GaAs quantum wells. The cladding regions of the GRINSCH SQW structure contained 80% AlAs. The MQW wafers consisted of six 80 Å GaAs wells separated by five 60 Å barriers containing 30% AlAs. The cladding regions of the MQW structure contained 40% AlAs. These two dimensional laser arrays use either Y-guides or evanescent coupling in the lateral direction to maintain coherence; in all cases, the arrays were ten elements wide. Illustrations of four sections of a) a two dimensional Y-guide array and b) a two dimensional evanescently-coupled array are shown in Figure 1. For both types, the length of the gain sections are 150 μm while that of the passive grating emitting regions are 300 μm. A lateral index step of approximately 8×10^{-3} in the gain region was achieved by removing the p-clad material outside the ridges to within about 500 - 1000 Å of the graded region. We fabricated and operated Y-guide and evanescently-coupled arrays both with and without ridge guides in the passive grating sections. The ridge guides in the passive grating emitting region had a lateral index step of approximately 3×10^{-3} which resulted from a 200 - 500 Å ridge height in the passive grating regions.

The SEM micrograph in Fig. 2 shows the Y-guide gain section pattern (defined by ion-beam etching) before the submicron grating is fabricated.

Results: The emitting apertures of these 10 x 10 arrays were about 0.05 mm (Y coupled) or 0.06 mm (evanescently coupled) x 5.0 mm. A 10 X 10 evanescently-coupled array far-field, shown in Fig. 3, is single-lobed and measures about $1^{o} \times 0.01^{o}$--which is within 30% of the diffraction-limited beam divergence from a uniformly illuminated 60 μm x 5000 μm aperture. The inset in the power-current curve (Fig. 4) shows that the mode spectra is contained in a 3 Å interval at 1.13 W.

Impact: This is the first demonstration of a new class of high-power, coherent semiconductor lasers which have beam divergences of ~ 1/1000 of conventional devices and a narrow spectrum. Because of their high brightness, these sources are expected to find numerous applications such as satellite communications, optical recording, laser printing, and laser radar.

References: 1). G. A. Evans, N. W. Carlson, J. M. Hammer, M. Lurie, J. K. Butler, S. L. Palfrey, L. A. Carr, F. Z. Hawrylo, E. A. James, C. J. Kaiser, J. B. Kirk, W. F. Reichert, Appl. Phys. Lett., 52, 1988, and references therein. 2). K. Kojima, S. Noda, K. Mitsunaga, K. Kyuma, and K. Hamanaka, Appl. Phys. Lett., 50, 1705, 1987. 3). N. W. Carlson, G. A. Evans, J. M. Hammer, M. Lurie, L. A. Carr, F. Z. Hawrylo, E. A. James, C. J. Kaiser, J. B. Kirk, W. F. Reichert, and D. A. Truxal, Appl. Phys. Lett., 52, 1988.

88CH2609-8/88/0000/0166$1.00 1988IEEE

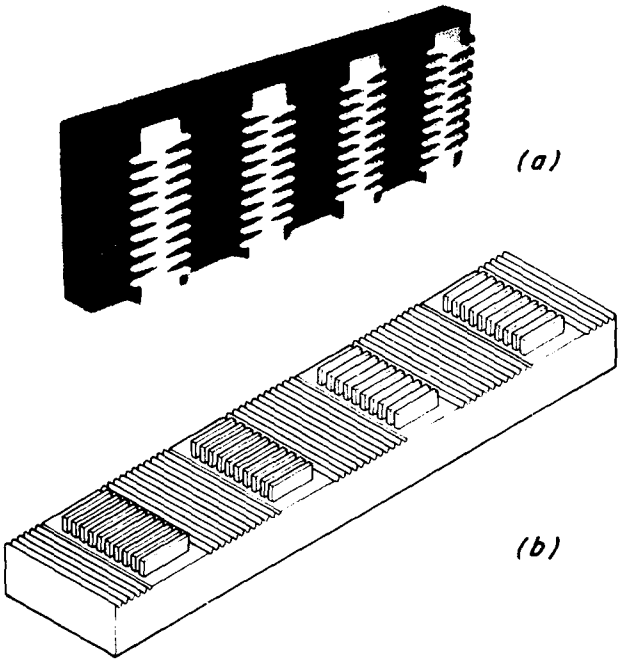

Figure 1. a) model of four sections of a two dimensional Y-guide array; b) sketch of four sections of a two dimensional evanescently coupled array.

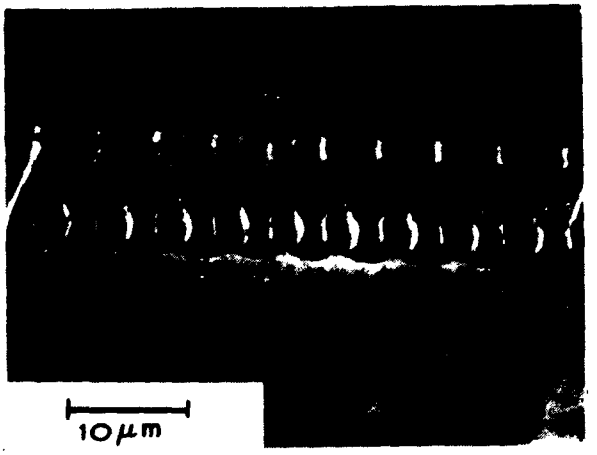

Figure 2. Scanning electron micrograph of the Y-guide gain region before the grating fabrication step.

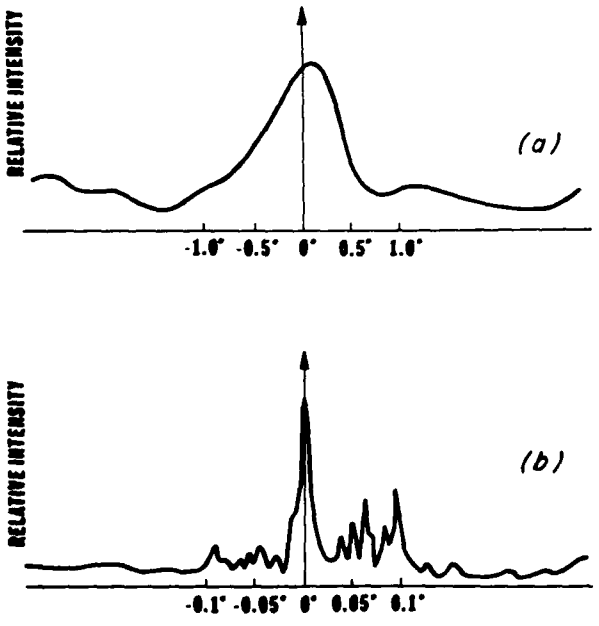

Figure 3. Far-field intensity patterns of a 10 X 10 evanescently coupled GSE array a) parallel to the grating lines (60 μm aperture) and b) perpendicular to the grating lines (5 mm aperture).

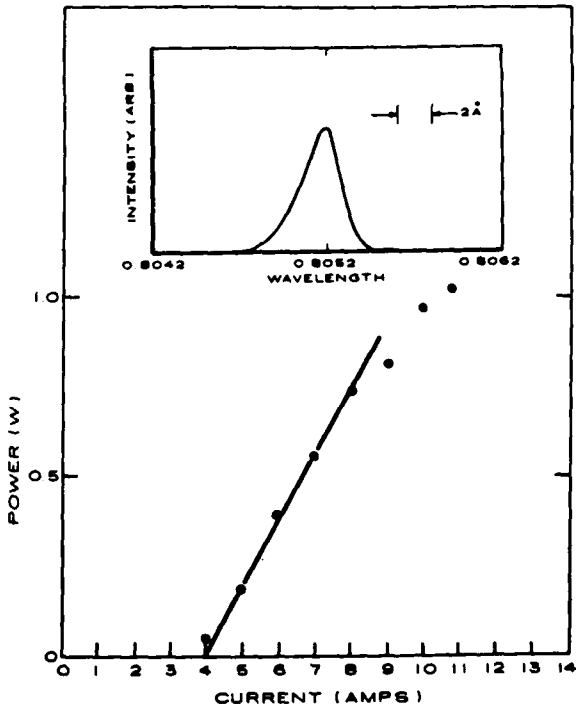

Figure 4. Peak power versus current curve and mode spectrum (at 1.13 W) for a 10 X 10 evanescently coupled array.

N—4

New Developments in Monolithic Two-Dimensional GaInAsP/InP Laser Arrays*

Z. L. Liau, J. N. Walpole and V. Diadiuk
Lincoln Laboratory, Massachusetts Institute of Technology
Lexington, Massachusetts 02173-0073

Monolithic two-dimensional arrays of GaInAsP/InP surface-emitting lasers have been further developed for low threshold (6 mA per array element), high output power (1.3 W) and better uniformity. To collimate the array output and to greatly increase the array fill factor, a new technique has been developed to fabricate high-quality f/1 lenslets in InP by mass transport.

The laser arrays consist of buried-heterostructure lasers with integrated 45° mirrors, as described previously.[1,2] Techniques have been developed for better fabrication control and better array uniformity. Figure 1 shows the threshold currents of all 16 lasers in a 4×4 array with an overall size of 1 × 1 mm. Note that the array has fairly good uniformity and the room-temperature cw threshold current of 6 mA is the lowest to date. To further improve the array uniformity, liquid-phase epitaxial growth of the starting wafers has been optimized. InP layers approximately 3 μm thick have been grown with a thickness variation of only 3% across the 1-cm wafer dimension. Improved GaInAsP active layer uniformity has also been observed by optimizing the growth morphology.

To achieve high output power from large arrays, a microchannel heatsink has been developed and is capable of dissipating up to 500 W cm^{-2} with a temperature rise of only 0.05°C W^{-1} cm^2.[3]. Figure 2 shows a total output of 1.3 W achieved by using a 1 × 4 mm array which contains 164 lasers. It should be noted, however, that this particular array has a relatively high threshold and low efficiency. With better arrays as previously reported (approximately half the threshold and twice the efficiency), considerably higher output powers can be achieved by using the microchannel heatsink.

To greatly reduce the beam divergence and increase the array fill factor, high quality f/1 lenslets with diameters up to 130 μm have been fabricated in InP by using mass transport to smooth out etched cylindrical multilevel mesa structures.[4] Very smooth lens surface and accurately controlled lens profiles have been obtained. Figure 3 shows a two-dimensional array of the mass-transported lenslets and the array of images it formed. Figure 4 shows a nearly diffraction-limited beam divergence obtained for a lenslet of 67-μm diameter. Work is underway to combine the present laser and lenslet arrays in an external cavity for coherent phase locking. In addition, the mass-transport phenomenon has recently been observed on GaP, strongly indicating that similar lenslets can be fabricated in this material and will be useful for shorter wavelength lasers.

1. J. N. Walpole and Z. L. Liau, Appl. Phys. Lett. 48, 1636 (1986).

2. Z. L. Liau and J. N. Walpole, Appl. Phys. Lett. 50, 528 (1987).

3. L. J. Missaggia, J. N. Walpole and Z. L. Liau, unpublished.

4. Z. L. Liau, V. Diadiuk, J. N. Walpole and D. E. Mull, unpublished.

*This work was sponsored by the Department of the Navy for SDIO and by the Department of the Air Force.

88CH2609-8/88/0000/0168$1.00 1988IEEE

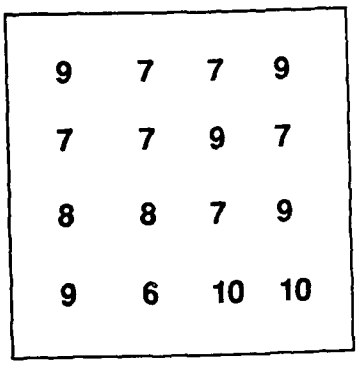

Fig. 1 Map of room-temperature cw threshold currents (in mA) in a monolithic two-dimensional laser array.

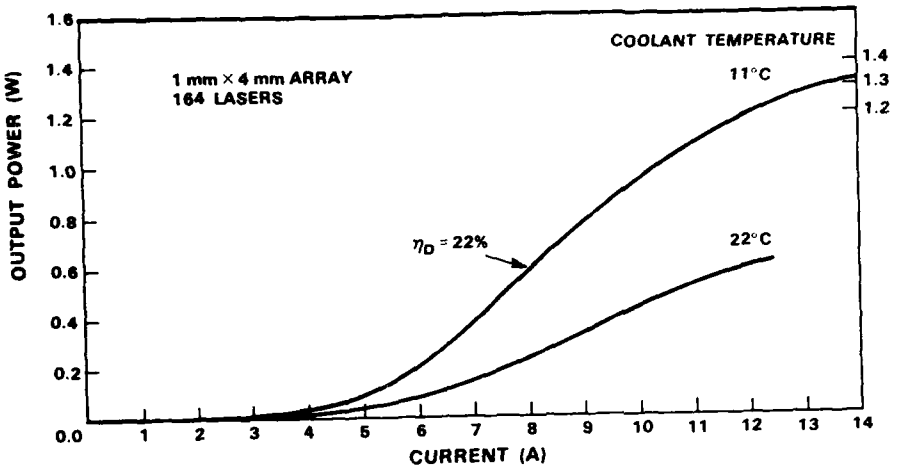

Fig. 2 Output power of a 2D laser array mounted on a microchannel heatsink.

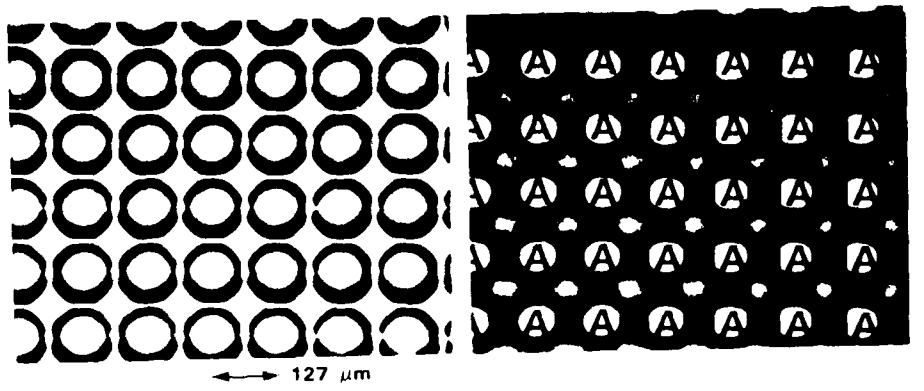

Fig. 3 An array of mass-transported f/1 lenslets and the array of images it formed.

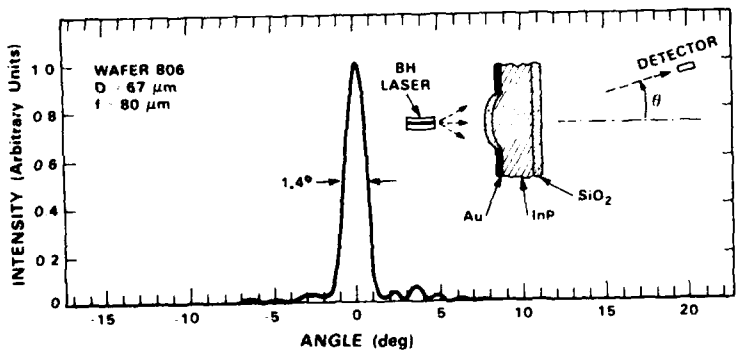

Fig. 4 A nearly diffraction-limited far-field pattern obtained by using a mass-transported lenslet to collimate a buried-heterostructure laser output.

N—5

A Hybrid Approach to Two-Dimensional Surface-Emitting Diode Laser Arrays*

J.P. Donnelly, R.J. Bailey, C.A. Wang, G.A.Simpson and K. Rauschenbach
Lincoln Laboratory, Massachusetts Institute of Technology
Lexington, Massachusetts 02173-0073

In this paper, we report a hybrid approach for fabricating two-dimensional surface-emitting diode laser arrays that takes advantage of both the advanced state of development of linear laser arrays with conventional cleaved end facets[1] and the rapid development of Si heat-sink technology.[2,3] A complete hybrid two-dimensional diode laser array is illustrated schematically in Fig. 1. For this initial demonstration of the hybrid approach, arrays were fabricated without the cooling fluid microchannels in the bottom of the Si substrate and the Cu conductors on top of each linear array. We have demonstrated these omitted features separately, however, and it appears that their inclusion in future arrays should be straightforward.

The flat-bottom grooves with 45° sidewalls are etched in (100) Si using conventional photolithography and an orientation-selective etch. A sawed cross section of an etched groove is shown in Fig. 2. For the hybrid arrays presented here, the grooves are 210 μm deep with 400-μm-long flat bottoms. After etching, the surface of the Si wafer is metallized with Cr/Au. Reflections of the cleaved end facets of GaAs/AlGaAs linear bar arrays mounted in these grooves are clearly visible in the 45° deflecting mirrors.

The linear bar arrays were fabricated from an OMVPE-grown GaAs/AlGaAs separate-confinement heterostructure wafer containing a 20-nm GaAs quantum well symmetrically positioned in a 660-nm large optical cavity. Stripe lasers 40 μm wide on 250-μm centers were defined by a proton bombardment that penetrated to a depth approximately 0.2 μm above the top of the large optical cavity. An additional proton bombardment at higher energies was performed to introduce sufficient optical loss in 10-μm-wide stripes midway between the lasers to suppress lasing in the transverse direction. After the wafer was thinned to 75 μm and an ohmic contact made to the n^+-GaAs substrate, linear bar arrays with 400-μm-long laser cavities were cleaved from the wafer.

Three linear bar arrays approximately 4 mm wide, each containing 15 or 16 lasers, were mounted in three adjacent metallized grooves etched in a Si substrate. The hybrid array was then mounted on a header and wires bonded to the top of each bar array from both ends. The near-field pattern of the laser emission from this array is shown in Fig. 3. There is some nonuniformity due to series resistance along the top of each bar. Otherwise, the pattern appears to be a composite of the patterns obtained directly from the cleaved end facets of the individual bars before mounting.

The pulsed power out of the hybrid array was measured with all three linear bar arrays driven in parallel and with each of them driven separately. Because of limitations in current available from the pulser, higher currents per laser could be obtained by driving the linear bar arrays one at a time. The output power vs pulsed current obtained from each of the bars driven separately is shown in Fig. 4. Approximately 10W of peak power perpendicular to the array surface was obtained from each bar with currents in the 11- to 12-A range. The differential quantum efficiencies are high, 65 to 70%, indicating that the 45° metallized Si mirrors are deflecting essentially all of the light emitted from the laser facets.

This hybrid approach can be used with other semiconductor lasers besides the GaAs/AlGaAs lasers illustrated here. High-power CW operation of large arrays should be possible by incorporating an integral microchannel heat sink in the bottom of the Si substrate (see Fig. 1).

1. D.F. Welch, W. Streifer, R.L. Thornton, and T.L. Paoli, Electron. Lett. 23, 525 (1987).
2. D.B. Tuckerman and R.F.W. Pease, IEEE Electron Device Lett. EDL-2, 126 (1981).
3. L.A. Missaggia, J.N. Walpole and Z.L. Liau, to be published

*This work was sponsored by The Department of the Navy for SDIO and by the Department of the Air Force.

88CH2609-8/88/0000/0170$1.00 1988IEEE

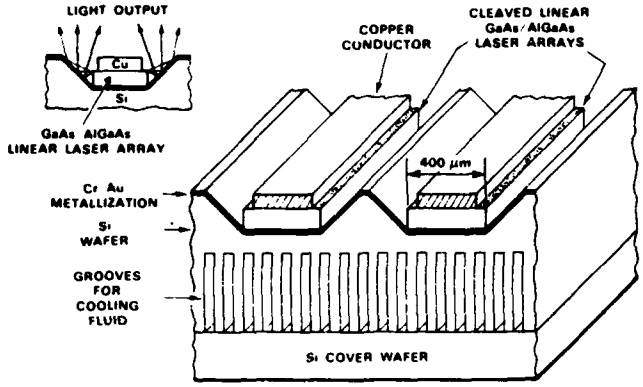

Fig. 1 Schematic illustration of hybrid two-dimensional surface-emitting diode laser array.

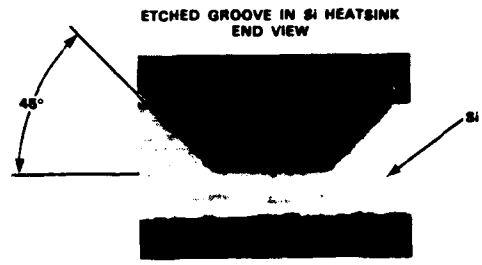

Fig. 2. Sawed cross section of groove etched in Si with flat bottom and 45° sidewalls.

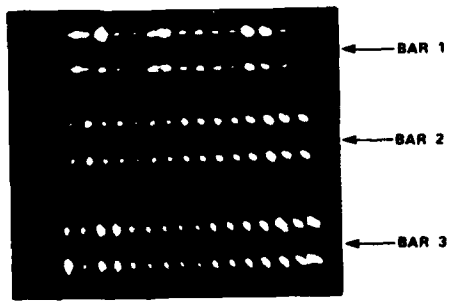

Fig. 3. Near-field pattern of a hybrid two-dimensional surface-emitting laser array consisting of three 4-mm-wide GaAs/AlGaAs linear bar arrays mounted in three separate grooves on the same Si substrate.

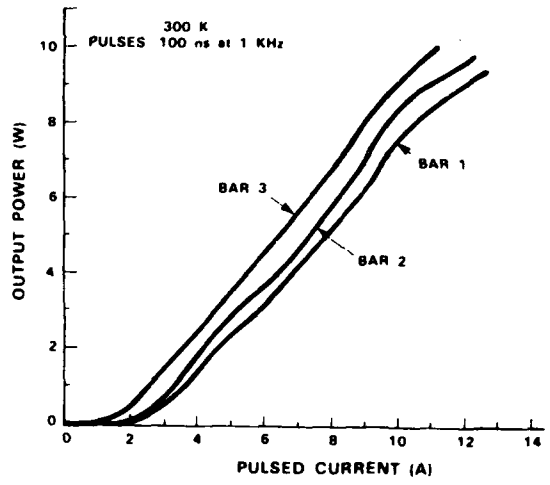

Fig. 4. Power output vs pulsed current of the hybrid array whose near-field pattern is shown in Fig. 3 with the linear bar arrays driven one at a time.

The views expressed are those of the author and do not reflect the official policy or position of the U.S. Government.

N—6

A New Monolithic Laser Waveguide Butt-Coupling Scheme Based on a Single-Step MOVPE

L. MENIGAUX, D. REMIENS, L. DUGRAND, P. SANSONETTI*, A. CARENCO
Centre National d'Etudes des Telecommunications
Laboratoire de Bagneux
196 avenue Henri Ravera - 92220 BAGNEUX _ FRANCE
* BERTIN S.A. - BP 22 - LES MILLES - FRANCE

An important issue in the realization of monolithic optical circuits is the coupling of laser to optical waveguide. Over the past few years, several attempts have been successfully reported, mainly based on butt-coupling technique using several-step epitaxy or coupled-cavity technique requiring a precise control of the epitaxy. Here, we propose a simple new means of butt-coupling between Optical Waveguides using a single-step epitaxy (1). We demonstrate the concept in the GaAs system by realizing a laser constituted of an active region and two passive guides.

The structure is illustrated in fig. 1. The alignment between the active and passive cavity levels results from the trench in the substrate realized before the epitaxy. The step height and the layers thicknesses are designed in such a way that the active layer and the transparent optical waveguides are directly butt-jointed. The thickness of the confining layer sandwiched between the active and the guiding layer is large enough to avoid any directional coupling between them. The preliminary operation in the device fabrication is the realization of a 300μm wide, 1.6μm deep trenches in a (100)n^+ substrate. Then, the layers are grown by atmospheric pressure MOVPE. At the difference of LPE, no levelling is induced by the vapor phase technique and the step profile is maintained during the growth. As indicated in fig.1 by the dashed line, the structure is made planar by chemical etching. 5μm wide ridges are patterned for light confinement. Ohmics contacts are then deposited in order to form a 300μm long active area (in the trench region). Finally, the wafers are cleaved in such a way that each device contains an active part and either one or two butt-coupled optical waveguides.

Laser operation has been obtained from the various devices. A typical characteristics of the optical power as a function of the pulsed current injected in the 300μm active region is given in fig. 2 for a 1020μm long device, constituted by two transparent optical waveguides, respectively 490μm and 230μm long. The emission is very similar for both facets (threshold 82mA), in spite of the dissymmetry of the output waveguide lengths. The same figure shows the laser performance of a single active cavity of 240μm length, cleaved in the trench region of the same wafer (threshold 52mA). Wavelength spectrum measurement reveals that the laser is influenced by internal reflections between the active and passive regions, in spite of a theoretical low internal reflection value. Some strong frequency selectivity resulting from the coupled cavity effects has been observed.

In conclusion, a new technique has been reported involving a single MOVPE for direct butt-coupling of optical waveguides. A 1 mm long laser constituted of an active guide butt-jointed to two transparent waveguides has been succesfully demonstrated in the GaAs system. Performance could be furhter improved by a better control of the process (trench quality, crystal orientation,...) and some optimization of the optical structure. This growth principle could simplify the implementation of opto-electronics functions, like wavelength stabilization or linewidth reduction of emitters ; since the planar component presented here is particularly well suited for DBR fabrication.

(1) L. MENIGAUX et al., French Patent n° 8405053, 1984.

88CH2609-8/88/0000/0172$1.00 1988IEEE

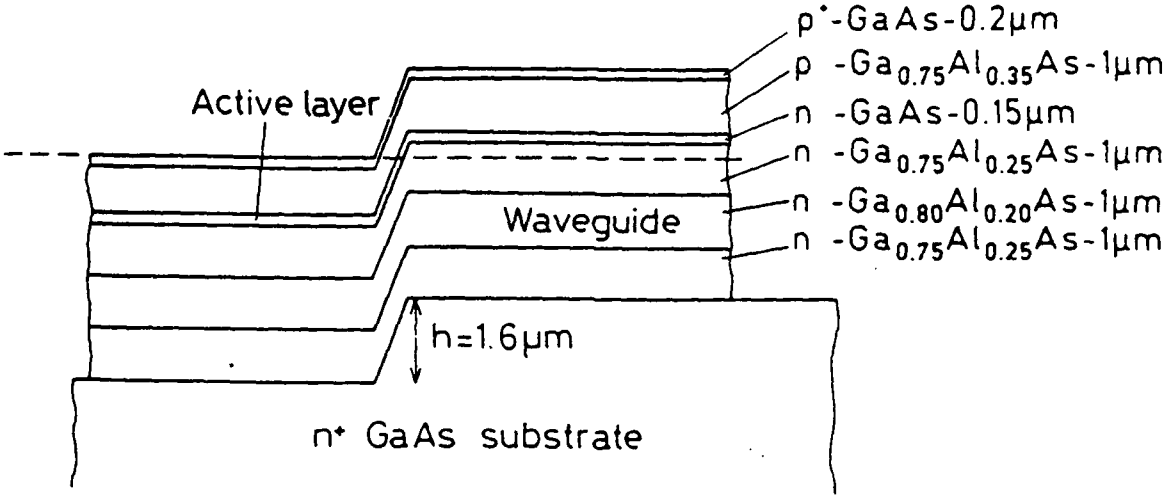

Fig. 1 : Scheme of the device with the active layer butt-jointed to the optical waveguide at both trench ends. The dashedline indicates the final level of the structure.

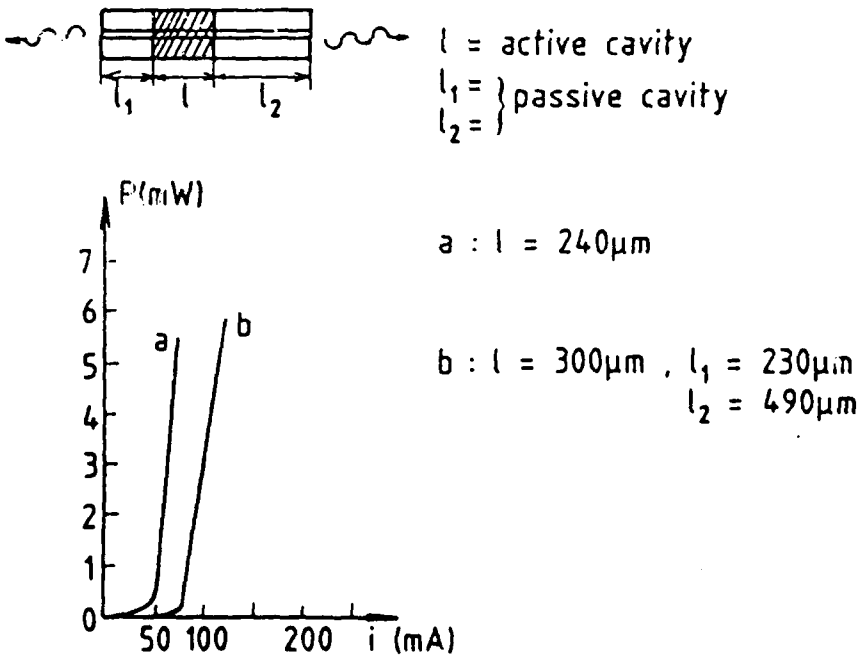

Fig. 2 : Light output versus current.

Session O: Four-Wave Mixing and Nonlinear Gain

O—1

Four-Wave Mixing in Semiconductor Lasers due to Beat Frequency Inversion Modulation

W. Elsässer, R. Nietzke, P. Panknin, and E.O. Göbel
Philipps–Universität, Fachbereich Physik, Renthof 5
D–3550 Marburg, FRG

Direct experimental evidence for beat frequency inversion modulation as the microscopic origin of Four–Wave Mixing signals in semiconductor lasers is presented.

The nonlinear optical properties of semiconductor lasers have gained increasing interest, recently. Intracavity Four–Wave Mixing (FWM) has been employed as a direct access to the nonlinear optical constants. The generation of high efficient cascade FWM signals in an electrically pumped semiconductor laser by external light injection from a dye laser has been reported /1,2/ and these signals have been described on the base of a third order susceptibility /2/. The microscopic origin of the FWM has been attributed to a modulation of the carrier system where either the concentration or the intraband population is modulated with the beat frequency of the two fundamental frequencies (population pulsation PP) /3/.

In the present paper, we provide the first direct experimental evidence that both, reflection induced relaxation oscillations (RO) as well as FWM signals are caused by an inversion modulation of the carrier system. The frequency of these PP is given by the relaxation frequency ω_{RO} in the case of reflection induced RO. Instead, in the case of FWM the frequency corresponds to the beat frequency $\Delta\omega = \omega_2 - \omega_1$. The modulation of the carrier system with the respective frequencies is directly demonstrated by analyzing the HF noise spectrum of the driving DC current.

All experiments have been performed in a GaAs/(GaAl)As CSP laser at a wavelength of 830 nm. Fig. 1 depicts the experimental set–up for the simultaneous determination of the optical spectra of the generated light signals and of the power spectrum of the injection current. SL 1 denotes the laser in which the mixing process takes place.

The experimental results for RO induced optical sidebands generated by external reflection are shown in Fig. 2 (upper part). FWM signals as generated by external light injection from a second semiconductor laser (SL 2) into the active volume of laser 1 are depicted in Fig. 3 (upper part). In both cases the HF noise spectrum of the injection current (Fig. 2 and 3 lower part) shows a pronounced signal at the corresponding modulation frequency, i.e. the eigenfrequency ω_{RO} of the electron photon system for the induced RO and the beat frequency $\Delta\omega$ for FWM. This provides direct evidence for the transformation of the optical beat frequency into a modulation of the carrier density with this characteristic beat frequency.

FWM signals have been observed up to a frequency spacing of 21 GHz, which is appreciably higher than the RO frequency. This experimental result indicates that for beat frequencies much larger than the RO frequency a new microscopic process on a much faster time scale, as, e.g. intraband processes has to be considered.

88CH2609-8/88/0000/0176$1.00 1988IEEE

References

/1/ H. Nakajima, R. Frey, IEEE J. Quant. Electron. QE–22, 1349 (1986)

/2/ R. Nietzke, P. Fenz, W. Elsässer, E.O. Göbel, Appl. Phys. Lett. 51, 1298 (1987)

/3/ G.P. Agrawal, J. Opt. Soc. Am. B5, 147 (1988)

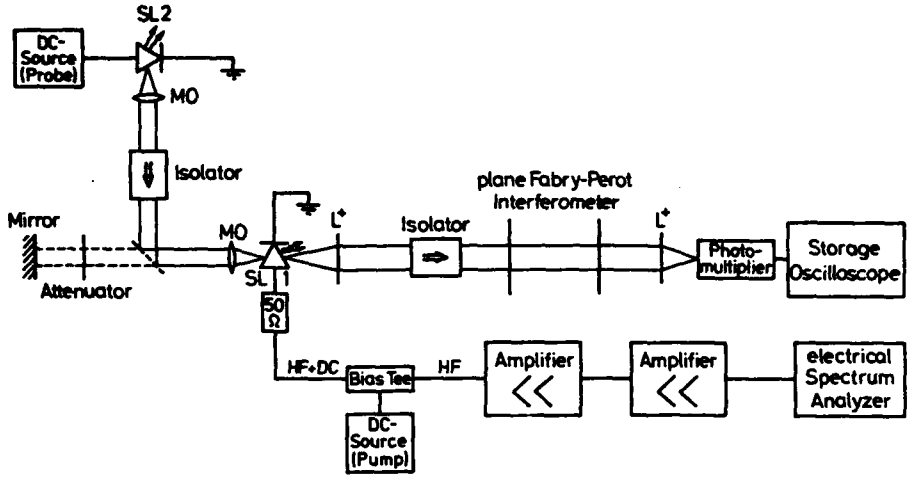

Fig. 1 Experimental set–up

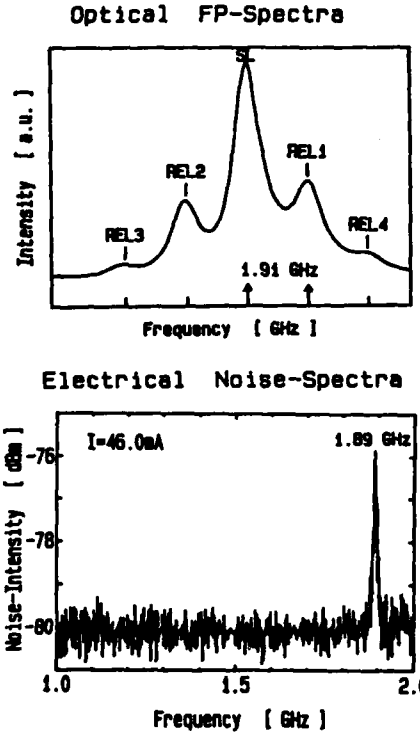

Fig.2 Optical Fabry–Perot spectra of the light emitted from semiconductor laser 1 with feeedback induced relaxation oscillations (upper part) and HF noise spectrum of the injection current (lower part).

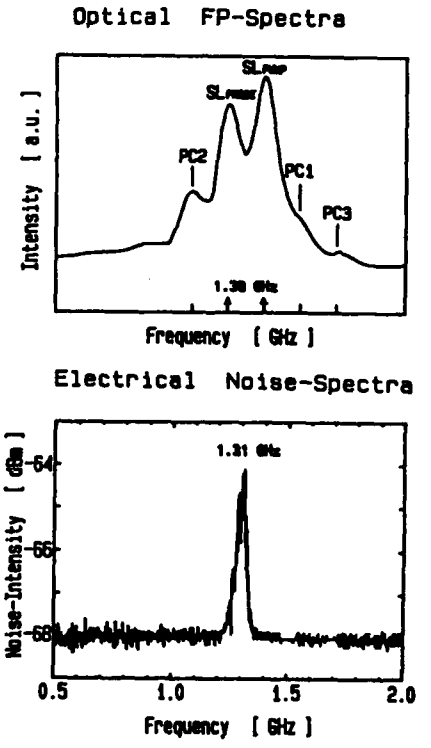

Fig.3 Optical Fabry–Perot spectra of the light emitted from semiconductor laser 1 with FWM signals generated by external light injection from semiconductor laser 2 (upper part) and HF noise spectrum of the injection current (lower part)

O—2

An Improved Density-Matrix Analysis of Nonlinear Optical Phenomena in Semiconductor Injection Lasers

Nagaatsu Ogasawara and Ryoichi Ito
Department of Applied Physics, University of Tokyo
7-3-1 Hongo, Bunkyo-ku, Tokyo 113, Japan

A density matrix formalism is presented whereby an improved description of nonlinear optical phenomena in laser diodes (LD's) can be achieved.

In such nonlinear optical phenomena in LD's as longitudinal mode coupling and 4-wave mixing, two dynamic effects of optical intensity beat at inter-mode frequency on carrier population are known to play important roles; they are (1) pulsation of carrier population in the levels directly involved in the laser transition (population pulsation) and (2) pulsation of whole carrier density in a band (carrier-density pulsation). Until now, however, no formulation that describes both pulsations in a closed form has been presented; contributions of these pulsations to the third order nonlinear susceptibility have been evaluated separately using different formalisms: (1) the density matrix equation[1,2] and (2) the rate equation for carrier density.[3]

For this reason, we have reexamined the third order nonlinear susceptibility in LD's on the basis of density matrix formalism.

The reexamination has revealed that, in order to properly describe intraband carrier relaxation, a refinement should be introduced in treating density matrix formalism. By virtue of the new treatment, the beat-induced pulsation of carriers is shown to be indeed expressed as a sum of a population pulsation term and a carrier-density pulsation term. In Fig. 1, the broken line depicts a saturated gain spectrum calculated taking account of these pulsations. The saturated gain is asymmetric with respect to the lasing frequency ($\delta\lambda = 0$) owing to the asymmetric nonlinear gain arising from carrier-density pulsation (the dash-dotted line). Population pulsation, on the other hand, causes symmetric gain suppression (the solid line). The difference in the dispersion of these nonlinear gains is interpreted as originating from the difference in the spectral distributions of carrier population involved in these pulsations. Laser power is analyzed to decrease upon mode jumping toward longer wavelengths and increase upon mode jumping toward shorter wavelengths as shown in Fig. 2. These results agree with the mode competition behavior experimentally observed in AlGaAs lasers.[4]

In the previous density matrix analyses,[1,2] carrier density pulsation has not been taken into account and, therefore, asymmetry in gain saturation could not be accounted for. In the rate equation analysis,[3] symmetric gain suppression arising from the population pulsation has not been included. In contrast, both the symmetric and asymmetric contributions have been derived in a closed form in the present analysis. It should be emphasized that the present closed-form formulation can be applied to the analysis of 4-wave mixing and high-speed direct modulation as well.

1) M. Yamada and Y. Suematsu: J. Appl. Phys. 52 (1981) 2653.
2) R. F. Kazarinov et al.: J. Appl. Phys. 53 (1982) 4631.
3) A. P. Bogatov et al.: IEEE J. Quantum Electron. QE-11 (1975) 510.
4) N. Ogasawara and R. Ito: Jpn. J. Appl. Phys. 25 (1986) L617.

88CH2609-8/88/0000/0178$1.00 1988IEEE

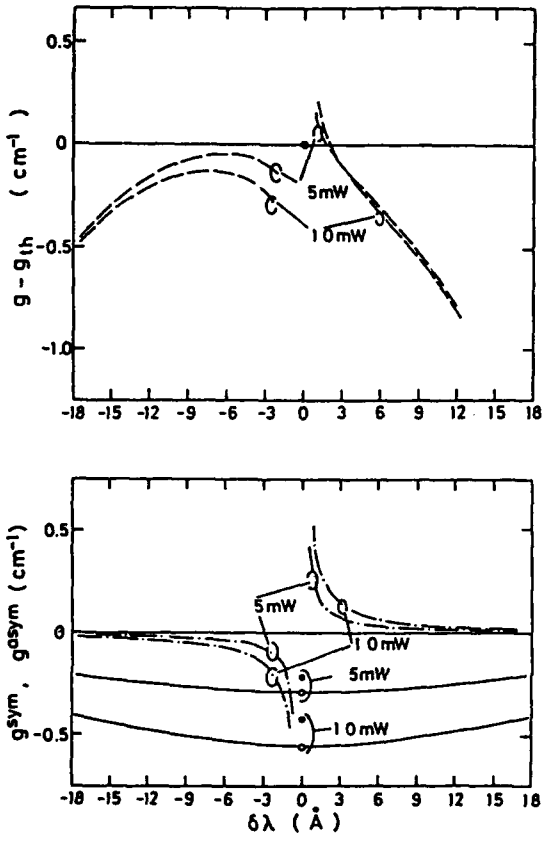

Fig. 1 Calculated gain spectra.
Broken line: saturated gain that includes both symmetric and asymmetric nonlinear contributions.
Dash-dotted line: asymmetric nonlinear contribution.
Solid line: symmetric nonlinear contribution.
Output power = 5, 10 mW. The linewidth enhancement factor $\alpha = 3$. The intra-band relaxation time $T_2 = 0.12$ ps.

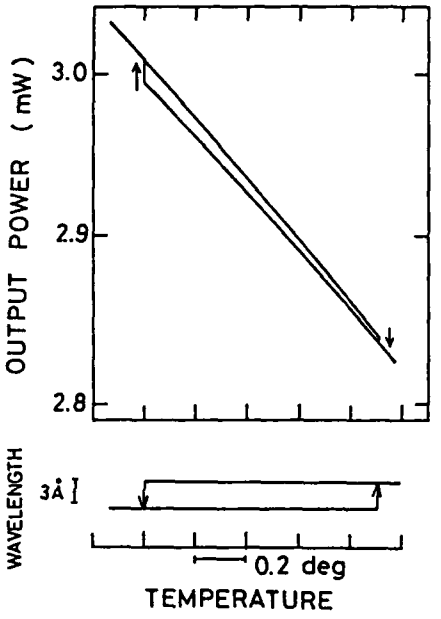

Fig. 2 Output power versus temperature (upper) and lasing mode versus temperature (lower) characteristics. $\alpha = 3$. $T_2 = 0.12$ ps.

O—3

Measurement of Nonlinear Gain Coefficient in 1.3 μm InGaAsP DFB Lasers

H.Schweizer, R.J.Lang*, A.Mozer, H.P.Mayer, F.Schuler, W.Idler, M.Schilling and K.Wünstel
Standard Elektrik Lorenz AG, Research Centre Stuttgart, FRG
*Micorelectronic Devices Laboratory, JET Propulsion Laboratory, Pasadena, USA

Introduction : Nonlinear optical gain plays an important role in semiconductor lasers with strong impact on wavelength chirp and maximum attainable modulation speed. In recent publications values for the nonlinear gain coefficient ε have been reported varying from $4\text{-}8*10^{-17}$ cm^3 for undoped structures. The methods employed until now are mainly based on small signal frequency response measurements from where ε is estimated by a curve fitting procedure. We measured the fine structure in the field spectrum of DFB-single mode lasers with optical and terminal electrical noise (TEN) methods which allow a direct determination of ε without the unavoidable effects of the RL and RC influence affecting electrical small signal measurements. From the relation between damping and current the coefficient ε is determined. We compare the results obtained by the new measuring techniques to the results obtained with conventional small signal response measurements and find typically smaller values for ε.

Experimental: The optical field spectrum of a 1.3 μm InGaAsP/InP DFB laser /1/ has been recorded over the current range of 1.1-2.0 I_{th} with a planar Fabry Perot interferometer. Fig.1 shows an example of these measurements at I/I_{th} =1.34. Around the main mode (p=0) well resolved side modes up to the third order ($p=\pm1,\pm2,\pm3$) are visible being the result of an amplitude and phase coupling in the active laser cavity. They are located symmetrically around the main mode and separated by multiples of the internal resonance frequency ν_r. From the intensity ratio between main peak and side modes, the intrinsic damping rate γ can be determined (fig.2). An estimate of the nonlinear gain coefficient ε from these plots reveals a value of $2.7*10^{-17}$ cm^3. Due to the equivalence of optical noise and TEN we can also determine the damping rate γ from the electrical noise spectra. We measured TEN spectra of the same lasers and observed side modes up to the third order near threshold. The evaluation of the TEN spectra yields similar results as optical measurements.
In addition to the optical and electrical noise measurements we also performed small signal frequency response measurements (fig.3). The dots represent the frequency response of the laser versus the modulation frequency. The full line is the best fit to the measured response including the parasitic RL and RC influence and the intrinsic relaxation behaviour. From the fitting procedure a nonlinear gain coefficient ε of $1.3*10^{-17}$ cm^3 is obtained. Compared with the other methods the nonlinear gain coefficient found with electrical frequency response measurements is about 50% smaller over the entire current range.

Conclusion: The nonlinear gain coefficient ε has been measured with three independent methods. For the first time, ε was determined from optical field spectra and electrical noise measurements. As a main advantage of these methods the result is not influenced by the external laser parasitics. Compared to the other methods the values of ε obtained by small signal frequency response measurements are about 50% smaller which we ascribe to laser parasitics.

/1/ K.Wünstel et al, Electron. Lett. 22, 1144 (1986)

88CH2609-8/88/0000/0180$1.00 1988IEEE

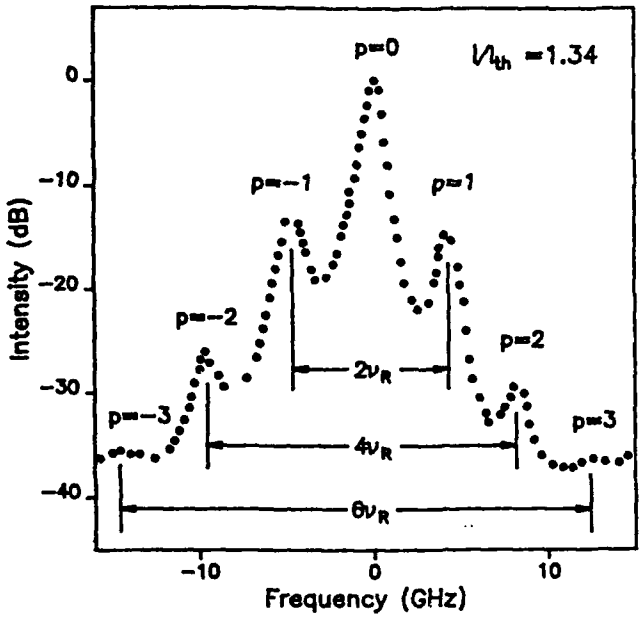

Fig.1: Field spectrum of an InGaAsP DFB laser. Laser threshold is 13 mA instrumental bandwidth : 2 GHz

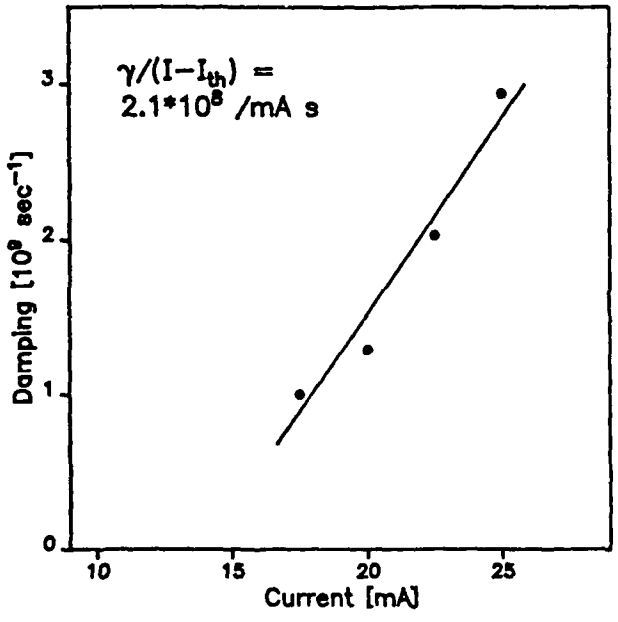

Fig.2: Damping constant vs. current from field spectra (dots) and least-square fit (solid line)

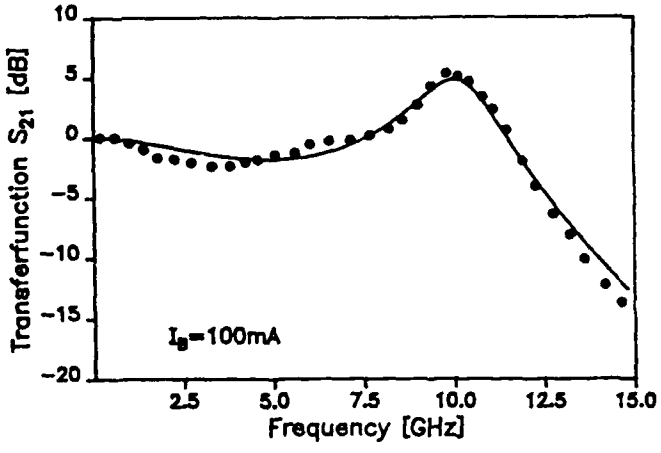

Fig.3: Small signal frequency response (dots) with fitted curve (solid line). The 3dB corner frequency is 12 GHz.

Session P: Quantum Wells III

P—1

Measurements of Linewidth Enhancement, Gain and Spontaneous Emission in InGaAs Quantum Well Lasers with InGaAsP Barriers

L.D. Westbrook, D.M. Cooper, P.C. Spurdens
British Telecom Research Laboratories
Martlesham Heath
Ipswich, UK.

Quantum well lasers are potentially superior to double heterostructure (bulk) lasers with sub-milliampere lasing thresholds having already been reported for GaAs/GaAlAs quantum wells [ref. 1]. In addition to lower threshold currents, it is predicted [ref.2] that quantum well lasers should have narrower linewidths and wider modulation bandwidths compared with the bulk, as a result of the smaller linewidth enhancement factor (α) and larger gain constant ($\partial g/\partial N$) in these devices. Quantum well lasers in the InGaAs/InP system are of especial interest because of their potential use in high capacity optical fibre systems operating in the 1.3-1.6μm fibre window. We report here the first measurements of the linewidth enhancement, gain and spontaneous emission in InGaAs multi-quantum well lasers with InGaAsP barrier layers designed to improve carrier confinement.

Figure 1 shows the spontaneous emission spectra recorded for a single quantum well InGaAs/InGaAsP broad area laser having a well width of 100Å and 0.95eV barrier/confinement layers. In order to minimise self-absorption and re-emission of the light, spontaneous emission was observed through the device substrate. The emission peaks at 0.8eV and 0.87eV are attributed to the n=1 and n=2 electron to heavy-hole transitions, respectively. A third peak at 0.95eV is the result of emission from the barrier/cladding layers. For comparison, in figure 2 we show a theoretical spontaneous emission spectrum for this quantum well structure assuming both unbroadened (broken curve) and broadened transitions (solid curve).

In figure 3 we show measured gain spectra (obtained from the Fabry-Perot resonances in the sub-threshold emission) for a ridge-waveguide InGaAs/InGaAsP multi-quantum well laser at various injection levels. As with reported measurements on quantum well lasers in other material systems, neither the gain nor spontaneous spectra exhibit sharp peaks at the sub-band edges indicating strong broadening of the transitions. From the measured gain spectra, together with measurements of the differential quantum efficiency as a function of device length, we estimate the gain constant $\partial g/\partial N$ to be of the order of 1×10^{-15} cm^2, compared with 2.5×10^{-16}cm^2 in bulk 1.5μm InGaAsP/InP lasers.

In figure 4 we show the dispersion of the linewidth enhancement factor α, also derived from the sub-threshold emission spectra, for the multi quantum well laser used in figure 3. Also shown in this figure is the analytic theoretical expression for α of reference 3 (broken curve). The value of $|\alpha|$ at the lasing energy was approximately 2-3, compared with 5-6 in bulk InGaAsP.

These preliminary measurements suggest therefore that InGaAs/InGaAsP multi-quantum well lasers are likely to offer improved characteristics over bulk devices for long wavelength fibre applications.

References:
1) K.Y. Lau, P.L.Derry & A.Yariv, Appl. Phys. Lett., 1988, 52, pp88-90

88CH2609-8/38/0000/0184$1.00 1988IEEE

2) Y.Arakawa & A.Yariv,IEEE J. Quantum Electron.,1986,QE-22,pp1887-1899
3) L.D. Westbrook & M.J. Adams Electron. Lett., 1987, 23, pp1223-1225

Fig. 1
Spontaneous emission spectrum from an InGaAs/InGaAsP single quantum well laser.

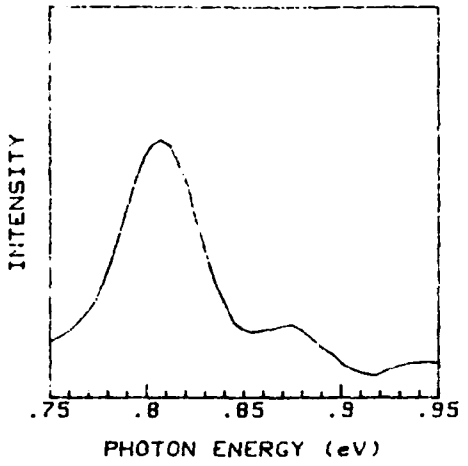

Fig. 3
Gain spectra at various injection levels for an InGaAs/InGaAsP MQW laser.

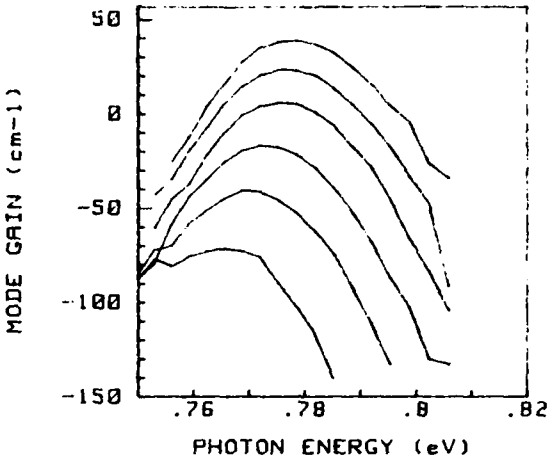

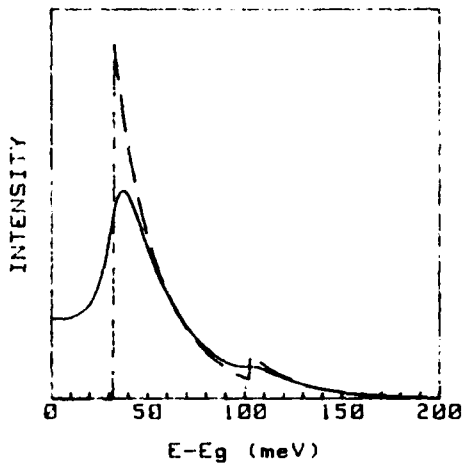

Fig. 2
Theoretical spontaneous emission spectrum.

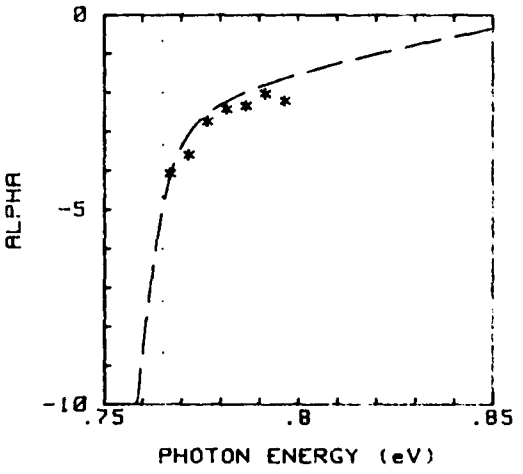

Fig. 4
Linewidth enhancement factor for an InGaAs/InGaAsP MQW laser.

P—2

The Effect of Doping on the Optical Gain and the Spontaneous Emission Factor in Quantum Well Amplifiers and Lasers Studied by Simple Analytical Expressions

C. E. Zah, NVC3X361, Bell Communications Research, Red Bank, NJ 07701, USA
Kerry J. Vahala, 128-95 California Institute of Technology, Pasadena, CA 91125, USA

Introduction: To optimize a quantum well active layer for improved device performance it is desirable to have simple expressions for optical gain and related quantities as a function of excitation, doping, well width, temperature, etc. Semiconductor Lasers employing the appropriately designed single or multiple quantum well active layers exhibit lower threshold current densities, reduced phase noise, and improved dynamic response as compared to their conventional counterparts.[1,2,3,4] Optical amplifiers employing quantum well active layers should also exhibit improved performance. In this paper we will show that very simple approximate expressions for optical gain, spontaneous emission, and the spontaneous emission factor can be derived for quantum well structures.

Theory: We assume throughout this analysis that all subbands are parabolic and optical transitions obey rigorous k-selection rules. Transition broadening is neglected. We focus on gain resulting from the lowest energy subband in the conduction and valence bands. The point of maximum gain in this case always occurs for the band edge transitions. Under these assumptions the maximum optical gain G_{max}, the spontaneous noise S ,and the spontaneous emission factor n_{sp} at the gain peak are given by the following expressions,

$$G_{max} = G_o(f_c(n) - f_v(n)) \tag{1}$$

$$S = G_o f_c(n)(1 - f_v(n)) \tag{2}$$

$$n_{sp} = \frac{S}{G_{max}} \tag{3}$$

G_o is a constant. The quantities $f_c(n)$ and $f_v(n)$ are Fermi electronic occupancies for states *at the lowest energy* conduction and valence subband edges, respectively. We assume quasi neutrality so that each occupancy is determined by knowledge of the electron density. For quantum wells we have found the following very simple approximate formulas,

$$f_c(n) = 1 - e^{-\frac{n}{N}} \quad \text{and} \quad f_v(n) = e^{-\frac{n}{P}} \tag{4}$$

where, for example,

$$N = \sum_{l=0} n_l e^{-\epsilon_{cl}} \quad \text{and} \quad n_l = \frac{\kappa_B T m_{cl}}{\pi \hbar^2 L_z} \tag{5}$$

and where L_z is the well width and m_{cl} is the effective mass of the l^{th} conduction subband whose band edge located ϵ_{cl} (in units of $\kappa_B T$) higher in energy than the lowest energy subband edge (i.e., ϵ_{c0}=0). Equations similar to (5) hold for the valence bands with N, ϵ_{cl}, n_l, and m_{cl} replaced by P, ϵ_{vl}, p_l, and m_{vl}, respectively.

Application: As an application of these expressions we use them to investigate the effect of p- and n-type doping on the gain and the spontaneous emission factor in a 100Å InGaAs/InP quantum well structure. To test the approximation we have plotted f_c and f_v versus carrier density at several donor (figure 1) and acceptor (figure 2) concentration levels using eqns. (4) and (5) and the exact form for comparison. At room temperature, the approximation is actually valid over an extremely wide range of carrier densities ($n << 4.7 \times 10^{19} cm^{-3}$). Notice that the inclusion of donors or acceptors merely shifts the appropriate curve along the horizontal axis by the amount of doping level. By simple graphical means, one can estimate the transparency shifts under various conditions from the intersection of the exponential functions f_c and f_v. G_{max} per quantum well for TE modes and n_{sp} are plotted versus carrier density in figures 3 and 4 at various donor and acceptor concentration levels. N-type doping is most effective in reducing the transparency level and the spontaneous emission factor

88CH2609-8/88/0000/0186$1.00 1988IEEE

whereas p-type doping enables increased gain at a given excitation level. One can also study the differential gain by differentiating the G_{max} w.r.t. carrier density. The differential gain of the quantum well is, in fact, reduced by doping at a given injection level. P-type doping causes a minor reduction and n-type doping causes a large reduction. The slight p-type induced reduction can be offset, however, by the ability to operate at a lower carrier density since transparency is also reduced. This idea has been demonstrated experimentally in the multiple quantum well laser with p-type modulation doping which leads to high differential gain and modulation speed.[4] These same conclusions apply in other material systems having a strong conduction band/valence band effective mass asymmetry such as the GaAs(AlGaAs) system.

Conclusion: we propose that n-type modulation doping of quantum well active layers may have certain benefits to lasers and amplifiers. First, the ability to reduce the transparency excitation level when combined with a reduction in the overall laser cavity losses could reduce lasers thresholds beyond the already impressive limits that have been set in quantum well lasers.[3] Second, n-type modulation doping in a quantum well amplifier could significantly improve the noise figures of these devices (Note: $NF \approx 2n_{sp}$). For the same reason laser intensity noise and phase noise will also be reduced.

The authors are grateful for several stimulating discussions with T. P. Lee of Bellcore.

[1] Y. Arakawa, K. Vahala, and A. Yariv, *Appl. Phys. Lett.*, **45**, p. 950 (1984).
[2] S. Noda *el al.*, *Appl. Phys. Lett.*, **50**, p. 863 (1987).
[3] P. L. Derry, *el al.*, *Appl. Phys. Lett.*, **50**, p. 1773 (1987).
[4] K. Uomi, T. Mishima, and N. Chinone, *Appl. Phys. Lett.*, **51**, p. 78 (1987).

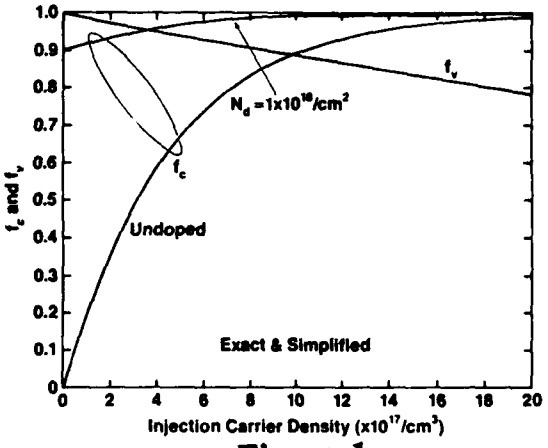

Figure 1

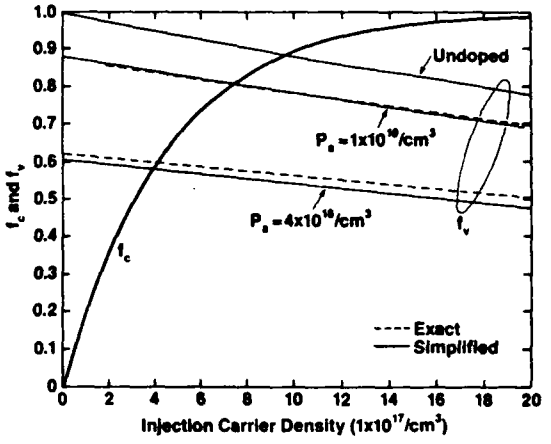

Figure 2

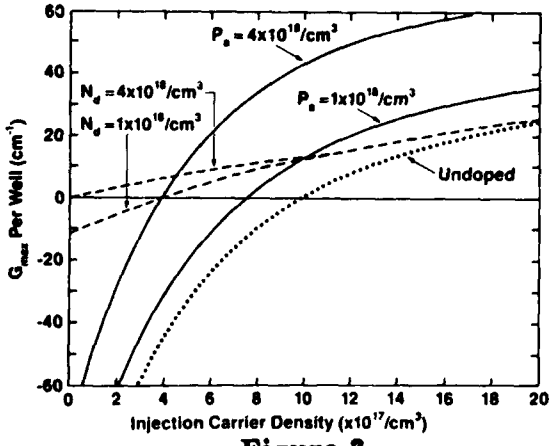

Figure 3

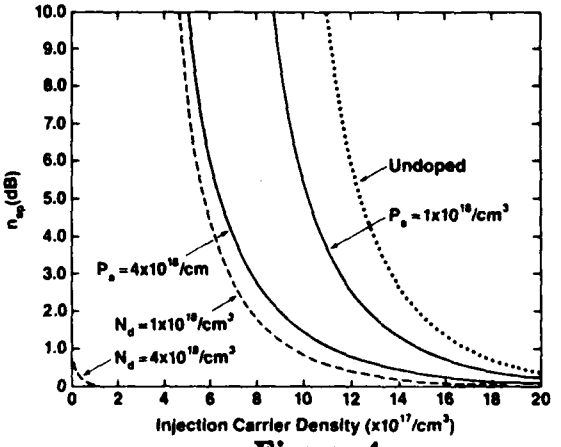

Figure 4

P—3

Optical Gain and Loss Processes in GaInAs/InP MQW Laser Structures

E. Zielinski, F. Keppler , M.H. Pilkuhn,
4. Physikalisches Institut, Universität Stuttgart, Pfaffenwaldring 57, D-7000 Stuttgart 80, FRG,
R. Sauer, and W.T. Tsang
AT&T Bell Laboratories, Holmdel, USA

Recently, a significant improvement of important laser parameters (such as enhanced T_0 values of 80K and reduced threshold current densities of 1.5kAcm^{-2}) have been demonstrated for GaInAs/InP multiple Quantum-Well laser structures /1/. In spite of this progress, threshold data indicate that strong loss processes, due to inter valence band absorption (IVBA) and Auger recombination (AR) are still present in two dimensional (2D) GaInAs lasers and differ insignificantly from 3D laser structures. We present a detailed analysis of the optical gain, absorption losses and recombination processes in GaInAs/InP MQWH structures, leading to a quantitative comparison between 2D and 3D lasers.

We have measured unsaturated optical gain spectra of CBE-grown GaInAs/InP MQW structures using the stripe variation technique. MQWs with $L_z \geq 150$Å exhibit a pronounced step-like line shape of the optical gain spectra, directly reflecting the two dimensional nature of the carrier system. As shown in fig. 1, the peak gain switches from low energy n=1 subband transitions to higher energy n=2 subband transitions with increasing carrier density. At low temperatures net gain values resulting from n=1 and n=2 subband transitions agree well with the two dimensional density of states. However, at room temperature the net gain is considerably lowered by optical absorption, leaving the difference between n=1 and n=2 contributions basically unchanged. Applying a detailed line shape analysis, absorption coefficients up to 400cm^{-1} at carrier densities of $n^{2D}=6\cdot10^{12}$cm^{-2} and an intra band relaxation time of 50fs were derived. The absorption originates from IVBA processes, which are expected to be stronger in 2D than in 3D lasers /2/.

Our temperature dependent data of the differential quantum efficiency in MQW lasers show a breakpoint behavior similar to that in 3D lasers: below 200K, η_d is nearly constant, whereas at higher temperatures, a steep decrease is observed. This is explained by a temperature and density dependent absorption process.

We have quantitatively investigated CHSH AR in 2D lasers. CHSH processes, where a recombining electron-hole pair transfers energy and momentum to a heavy hole which is excited into the split-off band, give rise to a weak emission (1 photon/sec.) at the energy of $E_g+\Delta_0$. This $E_g+\Delta_0$ luminescence is used to investigate the population of the split-off band via CHSH processes. We have investigated the E_g and the $E_g+\Delta_0$ emission under comparable experimental conditions. The temperature and excitation power dependence of both emissions was analyzed applying coupled carrier rate equations for the conduction and the valence subbands including the split-off band. An example is shown in fig.

88CH2609-8/88/0000/0188$1.00 1988IEEE

2 for a well width of 70Å at room temperature. Information on the actual carrier density is obtained by line shape analyses of the E_g emission using the same model as for the optical gain. Density values up to $4.5 \cdot 10^{12} cm^{-2}$ were determined. The most important results are: i) the dominant population process of the split-off band is the CHSH Auger process, and ii) AR coefficients of $C = 1 \cdot 10^{-28} s^{-1} cm^6$ at room temperature have been derived. Our results are in agreement with lifetime measurements /3/ and confirm calculations which predict similar AR rates in QW and bulk GaInAs /4/.

In summary, no significant reduction of the band-structure inherent loss mechanisms is observed in QW lasers. The improved laser parameters (T_0, j_{th}) are explained by the decreased temperature sensitivity of the inversion density n_i and the higher differential gain $\partial g / \partial n$ in QW structures, resulting from the modified density of states.

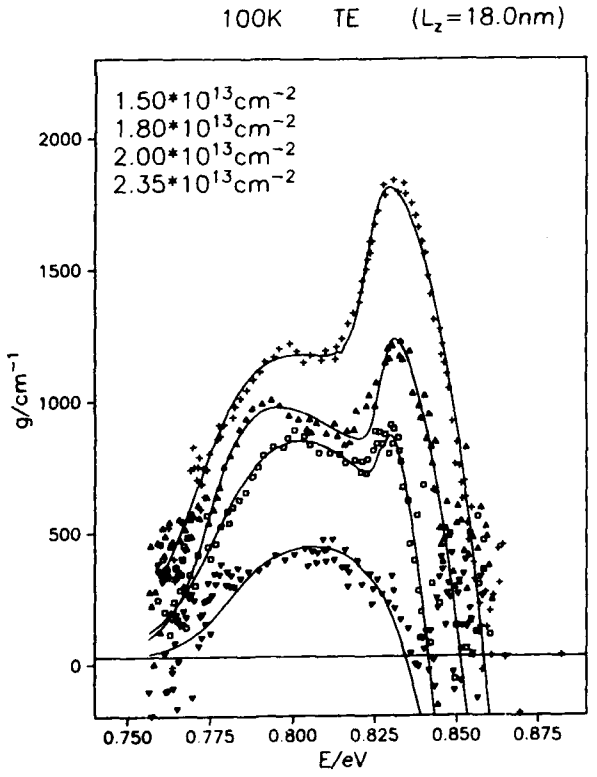

fig. 1: Optical gain spectra exhibit band filling effects with increasing excitation level. Actual carrier densities were obtained by line-shape fits (solid lines).

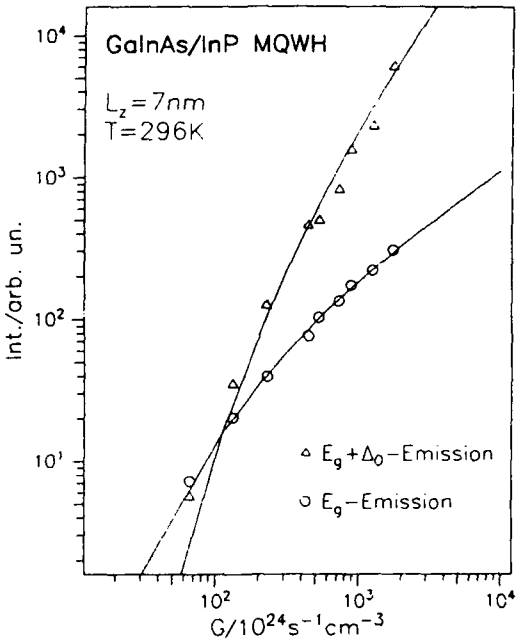

fig. 2: The luminescence intensity at the energy E_g and $E_g+\Delta_0$ (open symbols) are analysed using coupled carrier rate equations (solid lines). From these steady-state experiments, recombination coefficients are derived.

References:

/1/ W.T.Tsang, IEEE J. Quant. Electron. **QE-23**, 936 (1987)

/2/ M.Asada, A.Kameyama, Y.Suematsu, IEEE J. Quant. Electron. **QE-20**, 745 (1984)

/3/ B.Sermage, D.S.Chemla, D.Sivco, A.Y.Cho, Physica **134B**, 417 (1985)

/4/ M.G.Burt, R.I.Taylor, Electron. Lett. **21**, 733 (1985)

Session Q: Linewidth and Chirp Reduction

Q—1

Spectral Linewidth Reduction by MOVPE Grown 1.5 μm SCH Quantum Well DFB LDs

S.Takano, T.Sasaki, H.Yamada, M.Kitamura and I.Mito
Opto-Electronics Research Laboratories., NEC Corporation
4-1-1 Miyazaki, Miyamae-ku, Kawasaki, 213 JAPAN

Narrow linewidth single frequency laser diodes (LDs) are extremely important for coherent optical communication systems. A distributed feedback laser diode (DFB LD) with quantum well (QW) active layer is the most promising candidate [1], though attempts to achieve it have not been successful [2]. This paper reports, for the first time, a marked spectral linewidth reduction by 1.5μm QW-DFB LDs.

The InGaAs/InGaAsP QW heterostructure was fabricated on (001)InP substrates with 2400Å period grating by low pressure (76Torr) MOVPE technique. MOVPE was carried out in a horizontal reactor at 625°C. Figure 1 is an SEM photograph. High QW-DFB wafer qualities were evidenced by photoluminescence (PL) measurement. The intensity and FWHM for the PL spectra were comparable to those for QW wafers grown on flat InP substrates.

The active region, whose energy band diagram is depicted in Fig.2, was constituted as the separate confinement hetero-structure (SCH). Three 60Å thick InGaAs wells were separated by 200Å thick InGaAsP (λ_g=1.3μm) barriers. 1000Å thick InGaAsP (λ_g=1.15μm) optical confinement layer was employed. QW-DFB wafers were buried into DC-PBH by LPE technique and were processed into 300-400μm long cavity chips.

Threshold currents were 15-20mA. Stable single frequency cw operations were maintained at more than 20mW light output power level. Spectral linewidths were measured by the delayed self-homodyne method. Figure 3 shows a beat spectrum for the minimum linewidth. 2.0MHz was achieved at 6mw output, which is the smallest value among 1.5μm DFB LDs with conventional 300-400μm long cavity.

Spectral linewidths were plotted as a function of inverse power in Fig.4, with the linewidths for a MQW-DFB-DC-PBH LD (ten 75Å InGaAs wells separated by 120Å thick InGaAsP barriers) and for a λ/4 shifted DFB-DC-PBH LD with a bulk active layer as references. The minimum linewidth power product values were also plotted as a function of the cavity length in Fig.5, together with some reported values [3,4]. The linewidths for MQW-DFB-DC-PBH LD and SCH-QW-DFB-DC-PBH LD were much smaller than that for a λ/4 shifted DFB-DC-PBH LD with a bulk active layer. This is due to the reduced linewidth enhancement factor in QW LDs with stepped density of states. Even smaller linewidth in SCH-QW-DFB-DC-PBH LD, compared to MQW-DFB-DC-PBH LD, can be interpreted as reduced number of spontaneous emission events coupled to the lasing mode for QW-DFB LD with smaller total well volume [1]. The linewidth power products for SCH-QW-DFB-DC-PBH-LDs were much smaller than that for the very long cavity (1.2mm) DFB-LDs [3].

In summary, the spectral linewidth reduction by quantum effect was realized for the first time experimentally. The 2.0MHz minimum linewidth and the 5 MHz*mW minimum linewidth power product were obtained in 1.5μm SCH-QW-DFB LDs.

88CH2609-8/88/0000/0192$1.00 1988IEEE

REFERENCES
[1] Y.Arakawa et al.,IEEE J.Quantum Electron.QE-21,pp.1666(1985).
[2] N.Dutta, et.al.,Appl.Phys.Lett.,48,pp.1419(1986).
[3] S.Ogita, et.al.,Trans.IECE of Japan, No.263,Oct.(1987).
[4] K.Chinen, et.al.,Appl.Phys.Lett.,51,pp.273(1987).

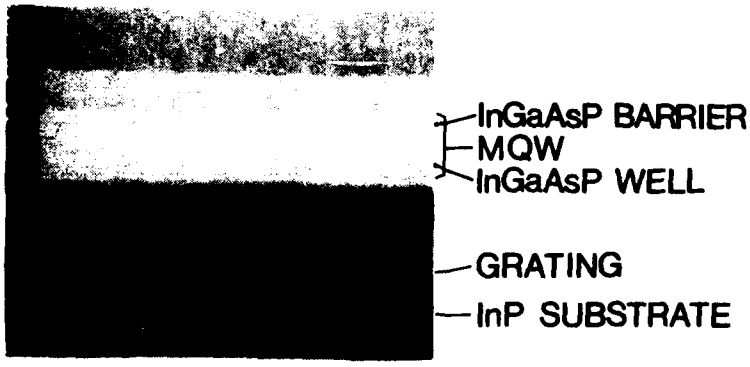

Fig.1 SEM cross section of QW structure grown on InP grating.

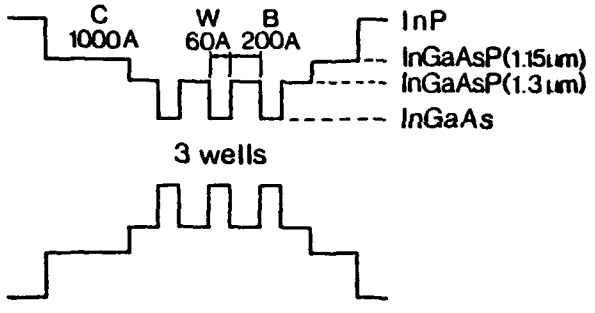

Fig.2 Band diagram of SCH-QW-DFB LD active region.

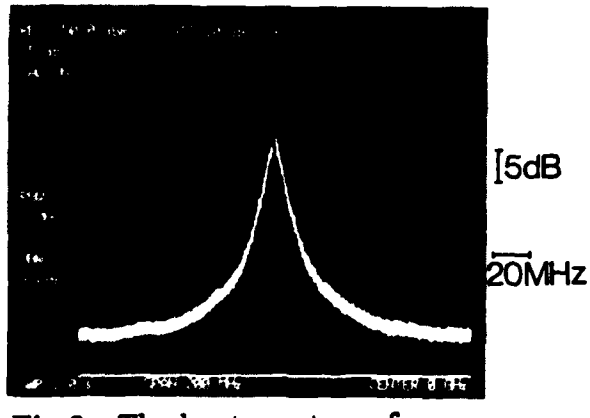

Fig.3 The beat spectrum for the minimum linewidth LD.

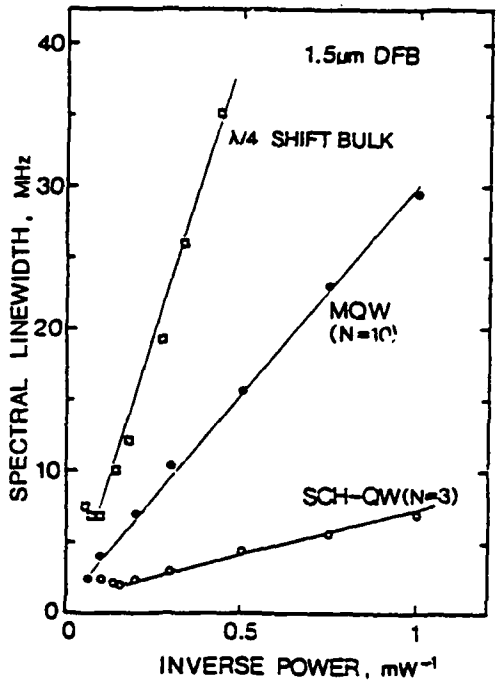

Fig.4 Spectral linewidth vs. inverse power.

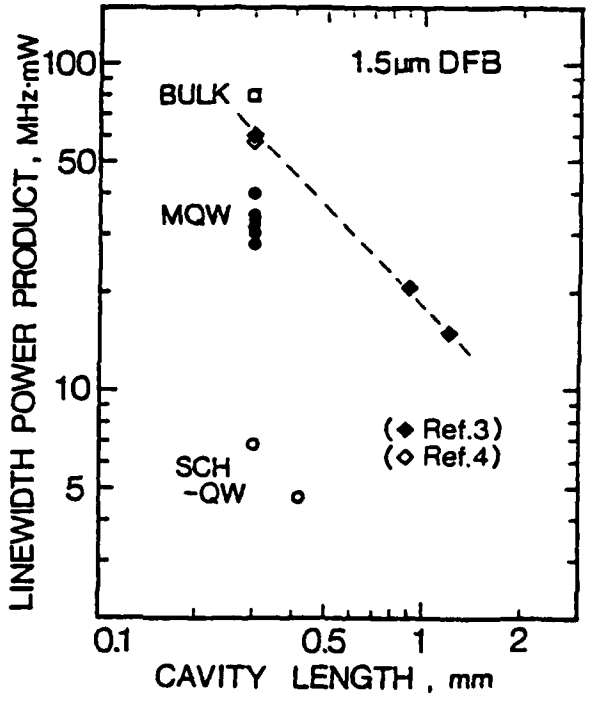

Fig.5 Linewidth power product vs. cavity length.

Q—2

Narrow Spectral Linewidth of MBE-Grown GaInAs/AlInAs MQW Lasers in 1.55 μm Range

Yuichi MATSUSHIMA, Katsuyuki UTAKA and Kazuo SAKAI

KDD Meguro R&D Laboratories
2-1-23 Nakameguro, Meguro-ku, Tokyo 153 Japan

GaInAs/AlInAs multiquantum-well (MQW) lasers made by molecular beam epitaxy (MBE) are promising candidates as a light source in 1.55μm wavelength range. We have recently reported the first successful room-temperature CW operation of the GaInAs/AlInAs MQW lasers [1]. This paper describes the spectral behaviors of these MQW lasers.

A schematic structure of a ridge-type GaInAs/AlInAs MQW laser is illustrated in Fig.1. The wafers were grown by conventional metal-source MBE on Sn-doped (100) InP substrates. The n-type MQW active layer was composed of 10 GaInAs wells (L_Z=80Å) and 9 AlInAs barriers (L_B=20Å). The laser diodes were mounted in p-side-up configuration on a diamond heat sink using Sn solder.

The lasers were continuously operated up to the heat-sink temperature of 35 °C, and the lasing wavelength was around 1.57μm as shown in Fig.2. The rather single-longitudinal-mode dominated spectrum appears to indicate a narrower gain spectrum of the MQW laser compared with a conventional DH-laser. The threshold current densities were typically 2-4kA/cm^2 for the diodes with 300-600μm cavity length.

The spectral linewidth of MQW lasers was evaluated by a delayed self-homodyne scheme with 3km optical fiber. The measurements were carried out at 5°C stabilized within ± 0.01°C. Fig.3 shows the measured spectral linewidth as a function of inverse output power for the diode of 570μm cavity length. The minimum linewidth of 3.6MHz was achieved at the output power of 7mW. The effect of cavity length on the linewidth was also confirmed. At the output power of 5mW, the linewidth of about 3MHz was obtained for a diode with 750μm cavity length. These facts indicate the good uniformity of the MBE-grown wafers. These measured linewidths are less than half values of the InGaAsP DH-DFB lasers [2].

The dynamic spectral linewidth (called chirping) is an important parameter in terms of actual optical transmission systems. Fig.4 shows the chirping characteristics of the main longitudinal mode. The threshold current and the bias current in this case were 120mA and 135mA, respectively, and the modulation current was a parameter. The linewidth was defined as the full width at 1/10 maximum. Decreases of linewidth over 2GHz may be due to the frequency response limited by RC time constant of the diode. At 1GHz the chirping was as small as 1.5Å, which was about half of that of the conventional DH-DFB laser [3].

In conclusion, we demonstrated the narrow spectral linewidth and small chirping characteristics of MBE-grown GaInAs/AlInAs MQW lasers for the first time. These lasers are considered to have high potential as a light source of coherent and IM-DD transmission systems.

The authors wish to thank Drs.T.Muratani, T.Yamamoto and Y.Kushiro for discussion and encouragement, and Mr.O.Takeuchi for assistance.

References

1) Y.Matsushima et al., Electron. Lett., 24, 1271 (1987)
2) T.P.Lee, IOOC-ECOC '85, Venezia, Tech.Digest II-189, (1985)
3) S.Yamamoto et al., IEEE J.Lightwave Technol., LT-5, 1518 (1987)

88CH2609-8/88/0000/0194$1.00 1988IEEE

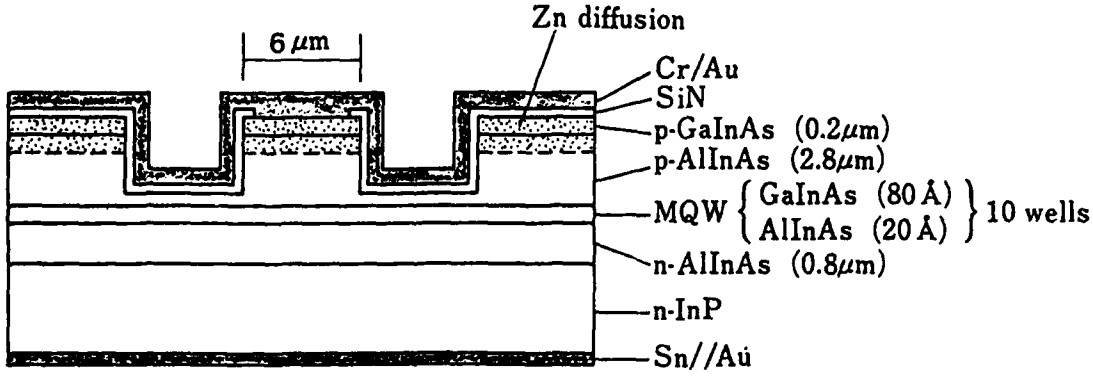

Fig.1 Schematic structure of ridge-type MBE-grown GaInAs/AlInAs MQW laser.

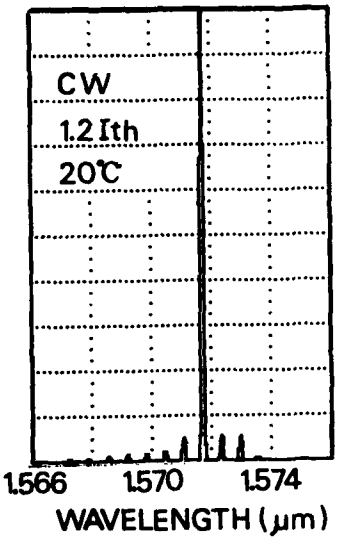

Fig.2 Typical spectrum of MQW laser under CW condition at room temperature.

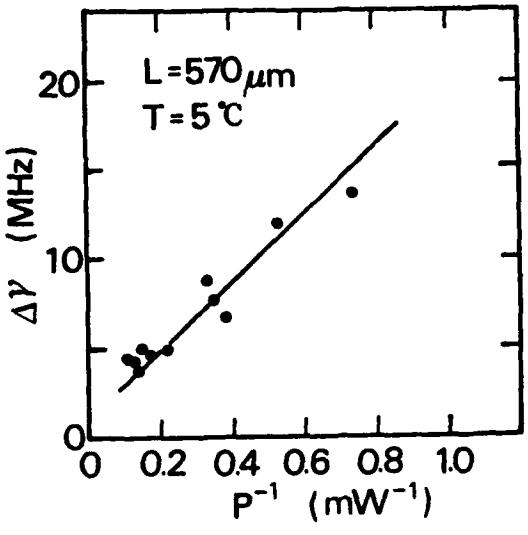

Fig.3 Spectral linewidth as a function of inverse output power.

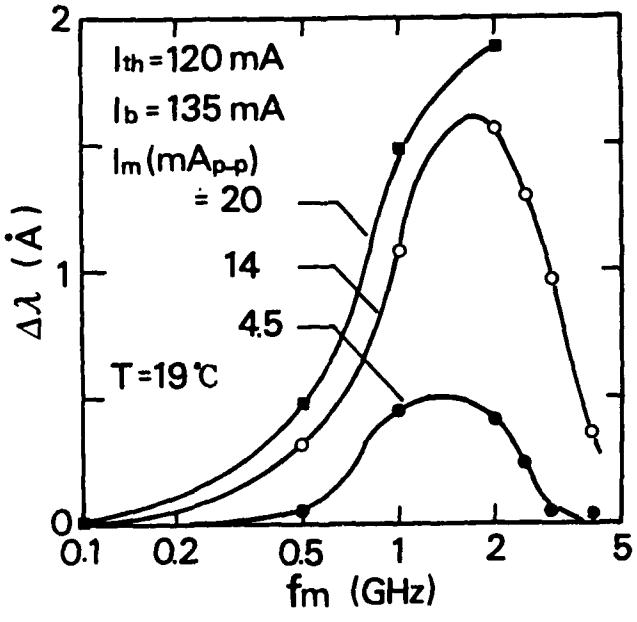

Fig.4 Chirping characteristics against modulation frequency with parameter of modulation current.

Q—3

Reduction of Spectral Chirping in Modulation Doped Multiquantum Well (MD-MQW) Lasers

K.Uomi, N.Chinone, and T.Mishima

Central Research Laboratory, HITACHI, Ltd., Kokubunji, Tokyo, 185

To realize semiconductor lasers for multi-gigabit long-span optical communications, key factors are as follows; 1) increase of the relaxation oscillation frequency, f_r ($f_r \propto (dg/dn)^{1/2}$, g: optical gain coefficient, n: carrier concentration) and 2) decrease of spectral chirping width, $\Delta\nu$ ($\Delta\nu = 2\ln 2/(\pi \Delta t)(1+\alpha^2)^{1/2}$, α: linewidth enhancement factor$\propto (dg/dn)^{-1}$, Δt:optical pulse width). These parameters can be improved by enhancing differential gain, dg/dn. Recently, we proposed a modulation-doped multi-quantum well (MD-MQW) laser [1] for the increase of dg/dn, and experimentally demonstrated f_r was enhanced 5 times (up to 30GHz) compared with DH lasers [2]. In this letter, we report theoretical and experimental results of the spectral chirping in p-type MD-MQW lasers.

Figure 1 shows the band diagram of the MD-MQW structure in which carriers from impurity atoms in barrier layers are relaxed and localized in well layers. Figure 2 shows the gain coefficient versus injected electron density at various acceptor concentrations. The dg/dn increases as the increase of acceptor concentration, which is due to the fact that laser oscillation takes place at very low injected electron density. The calculated α factor of MD-MQW lasers normalized by that of undoped MQW lasers for various acceptor concentrations is shown in Fig.3. It is seen that the α factor of the MD-MQW lasers is 1/4 times smaller than that of MQW lasers. Therefore, we can expect the chirping width is decreased by utilizing MD-MQW structure.

We investigated the frequency chirping width $\Delta\nu$ of MD-MQW lasers[2] grown by our home-made MBE system [3]. $\Delta\nu$ was measured using the CHP method [4]. The MD-MQW structure is composed of four undoped GaAs wells (105Å) separated by five Be doped GaAlAs barriers (117Å). Be was selectively doped in the center region of the barrier layers ($Be=2\times10^{19}cm^{-3}$). The threshold current was about 50mA. In Fig.4, the measured $\Delta\nu$ of both MD-MQW lasers and undoped MQW lasers is shown as a function of FWHM, Δt, of the optical pulse.

88CH2609-8/88/0000/0196$1.00 1988IEEE

The chirping width of both lasers increases inversely proportional to Δt. As can be seen in Fig.4 , the chirping width of MD-MQW lasers was about 1/5 times of that of MQW lasers. This suppression factor (1/5 times) roughly coinsides with the theoretical analysis.

In conclusion, we have demonstrated that the spectral chirping width was drastically reduced utilizing the MD-MQW structure, and that MD-MQW lasers have superior properties for high bit rate optical communications such as low spectral chirping and high f_r.

References

1) K. Uomi et al., 10th IEEE Semicond. Laser conf., M-6, 1986
2) K. Uomi et al., 13th ECOC'87 Techn. Digest vol.I, p.29 1987
3) T. Mishima et al., Inst. Phys. Conf. Ser., No.79, p.445, 1985
4) M. Osinski et al., IEEE QE-23, p.9, 1987

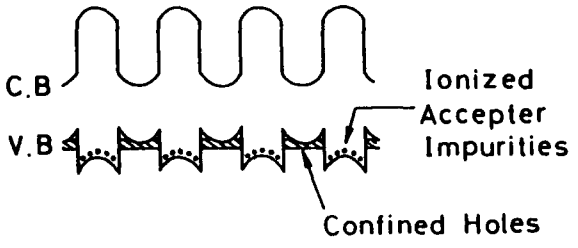

Fig. 1 Band diagram of MD-MQW structure.

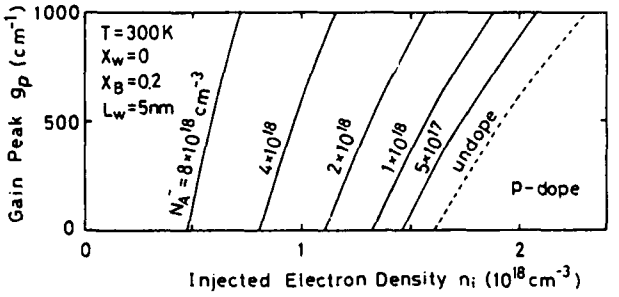

Fig. 2 Calculated gain versus injected electron density at various accceptor concentrations in p-type MD-MQW lasers.

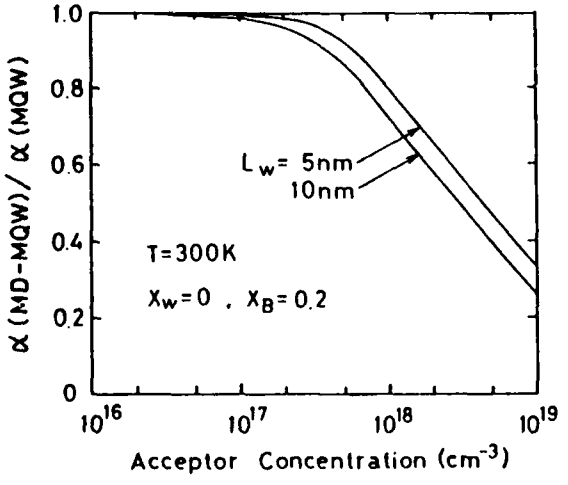

Fig. 3 Calculated α factor of MD-MQW lasers.

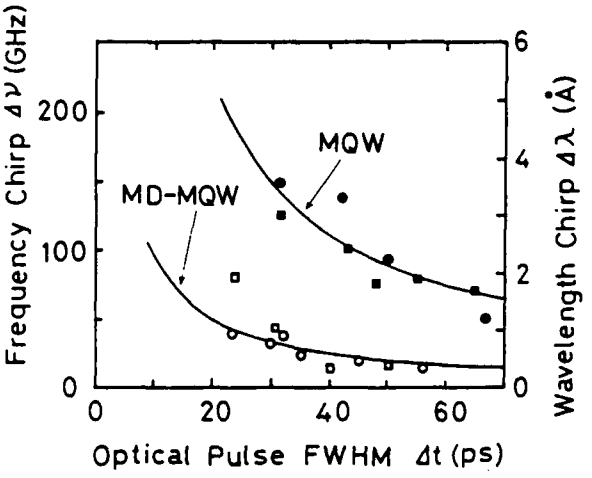

Fig. 4 Measured spectral chirping of p-type MD-MQW lasers(o□) and undoped MQW lasers(●■).

Q—4

Spectral Linewidth of DBR Single-Mode Lasers

M. Takahashi, Y. Michitsuji, M. Yoshimura
Y. Yamazoe, H. Nishizawa, T. Sugimoto

Application Specific Devices R&D Department
SUMITOMO ELECTRIC INDUSTRIES LTD.
1-1-3 Shimaya Konohana OSAKA 554, JAPAN

In recent years, reduction of the spectral linewidth of laser diodes has been required for the application of coherent optical communication system and measurement systems. In this report, we have measured the spectral linewidth of DBR (Distributed Bragg Reflector) lasers and have verified that the DBR lasers with long DBR region show a very narrow linewidth. The lowest linewidth we have achieved is 3.2 MHz at P=1.5 mW.

The DBR lasers used in these experiments are fabricated by using the liquid phase epitaxy and holographic exposure method. The structure of DBR laser is shown in Fig. 1(1). The coupling coefficient κ was estimated to be 40 cm^{-1} from the mode spacing of the lasing spectra. The length of the active region, La, and that of the rear DBR region, Lg2, were fixed to 300μm and 400μm, respectively. On the other hand, the length of the front DBR region varied from 0 to about 300μm.

Typical opto-electronic properties of DBR lasers are shown in Fig.2 and Fig.3. As shown in Fig.2, the threshold current is 30 mA at 30°C, and this laser can be operated up to the power of 7mW without mode jump. The lasing spectra is shown in Fig.3. The side mode suppression ratio (SMSR) is 35.2 dB, and SMSR values of other lasers used in our experiments were better than 32 dB.

Fig.4 shows the dependences of the spectral linewidth on the inverse power for three different lasers. The linear relation between the spectral linewidth and the inverse power can be explained by the theory proposed by Schawlow and Townes(2). However, the residual linewidth was observed in some lasers when the power was extrapolated to infinity. It is reported that the residual linewidth is due to the 1/f-noise(3).

The relation between the normalized linewidth $\Delta\nu \cdot P$ and the length of the front DBR region is shown in Fig.5. The shaded area in Fig.5 is due to the effect of the randomness of the phase angle of the grating at the front facet. The experimental results well agree to the theoretical curve(4). These results suggest that the long DBR region is effective for reducing the linewidth.

The maximum power of the DBR laser was about 7 mW, but it was improved to a value larger than 10 mW by using the anti-reflection coating on the front facet. In addition, the excess broadening of the linewidth was not observed in all coated lasers.

The authors would like to thank Prof. Y. Suematsu and Dr. S. Arai of Tokyo Institute of Technology for their helpful discussion.

88CH2609-8/88/0000/0198$1.00 1988IEEE

REFERENCES
(1) Y. Tohmori, et al.: Jpn. J. Appl. Phys., 24, (1982), 399
(2) D. Welford, et al.: Appl. Phys. Lett., 40, (1982), 865
(3) K. Kikuchi, et al.: Electron. Lett. 21, (1985), 1011
(4) H. Tsubokawa, et al.: National Conference Record Part 2, November 1987, Kumamoto, IEICE of JAPAN, p.54

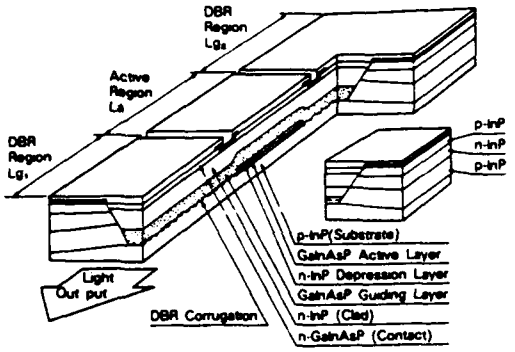

Fig.1 Structure of the fabricated DBR-laser

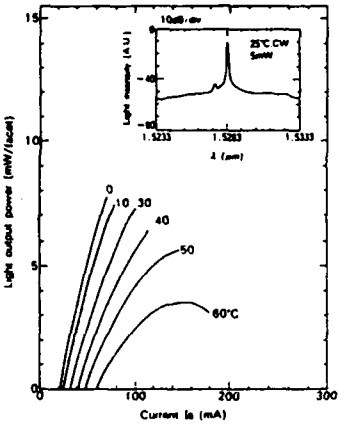

Fig.2 Output power of the DBR-laser

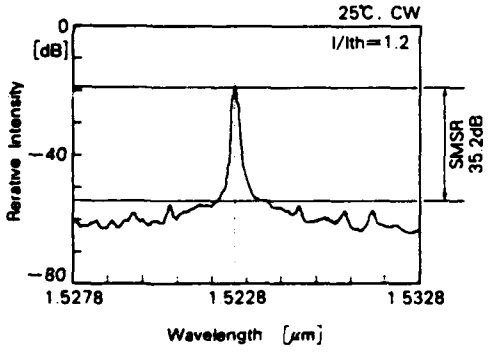

Fig.3 Lasing spectra of the DBR-laser

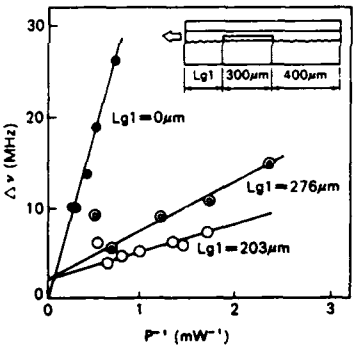

Fig.4 Dependence of spectral linewidth on the inverse power

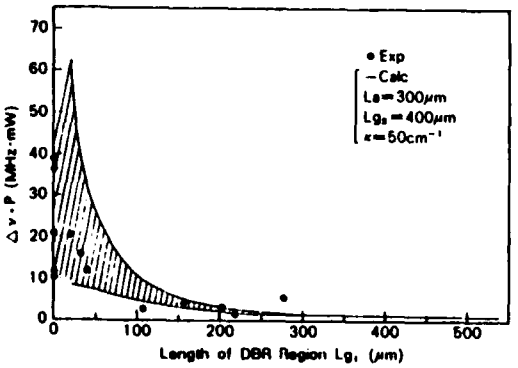

Fig.5 Dependence of the normalized linewidth on the length of DBR region

Q—5

Compact Silicon-Chip Bragg Reflector Hybrid Laser with 110kHz Linewidth

D. A. Ackerman, C. Y. Kuo[*], *V. L. Silva, E. J. Wagner*[*]

AT&T Bell Laboratories
Murray Hill, New Jersey 07974
*Allentown, PA 18103

A single frequency hybrid laser consisting of a conventional semiconductor laser coupled to a glass-on-silicon distributed Bragg reflector is observed to produce a very narrow minimum linewidth of 110kHz.

External cavity semiconductor lasers have been previously reported to produce linewidths of <1MHz through use of distant reflectors or monolithically integrated distributed Bragg reflectors.[1] These devices suffer from severe mechanical instability and low yield, respectively. The silicon-chip Bragg reflector (SCBR) laser has been reported to produce single longitudinal mode operation with linewidths ~1MHz as well as significantly reduced chirp.[2]

We report a hybrid device incorporating an SCBR in an optimized configuration yielding a compact, robust, very narrow linewidth semiconductor laser. The SCBR (Figure 1) consists of a SiO_2 clad Si_3N_4 core, ridge waveguide of length ~3mm with a first order diffraction grating imposed on the top-most cladding layer surface.[2] The laser and reflector are attached to submounts which permit very high accuracy butt-coupling alignment of the laser cavity and SCBR waveguide with a typical misalignment of ±0.15μm. Nearly matched laser and reflector mode sizes resulted in <5dB overall round-trip coupling loss of power reinjected into the <1% anti-reflection coated laser facet. The resulting side-mode suppression ratio was observed to be ≤–40dB.

Linewidth measurements of the optimized hybrid device (Figure 2) reveal a temperature range of ≥10°C for which Δν<0.2MHz with a minimum of 110kHz. As predicted in ref. 2, the linewidth minima occur at temperatures just below mode transitions. Mode transition spacing of ~17°C results from differential thermo-optical properties of the dielectric reflector and semiconductor laser. Variations of threshold current and wavelength of the hybrid laser as a function of temperature are illustrated in Figure 2. Highest threshold and longest wavelength which occur coincidently with narrowest linewidth are consistent with the predictions of ref. 2 and the measured 6Å wide reflection band of the Bragg reflector. FM modulation of the narrow line hybrid laser is plotted in Figure 3 and is observed to decrease (for a given modulation current and frequency of 40MHz) with decreasing linewidth as $dF/dI \propto (\Delta\nu)^{1/2}$. Thus the resultant chirp reduction is simply the square root of the linewidth reduction due to the feedback from the Bragg reflector.

The compact design of the hybrid SCBR laser and the narrow linewidth of the single mode output make this device ideal for application within a coherent optical communications system. Stringent requirements on device-to-device wavelength variations are met by highly controlled processing of the SCBR's. Devices of this nature have been tested for 10 kh under accelerated aging conditions and indicate the potential for stable, reliable use.

References

1. See for example, R. Wyatt and W. J. Devlin, "10kHz linewidth 1.5μm InGaAsP external cavity laser with 55 nm tuning range," Electron. Lett. *19*, 110 (1983).

2. R. F. Kazarinov and C. H. Henry, "The relation of line narrowing and chirp reduction resulting from the coupling of a semiconductor laser to a passive resonator," J. Quantum. Electron. *QE-23*, 1401 (1987) and references cited within.

88CH2609-8/88/0000/0200$1.00 1988IEEE

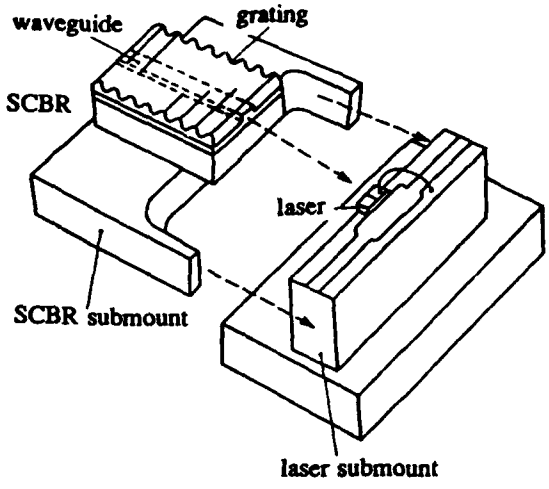

Figure 1

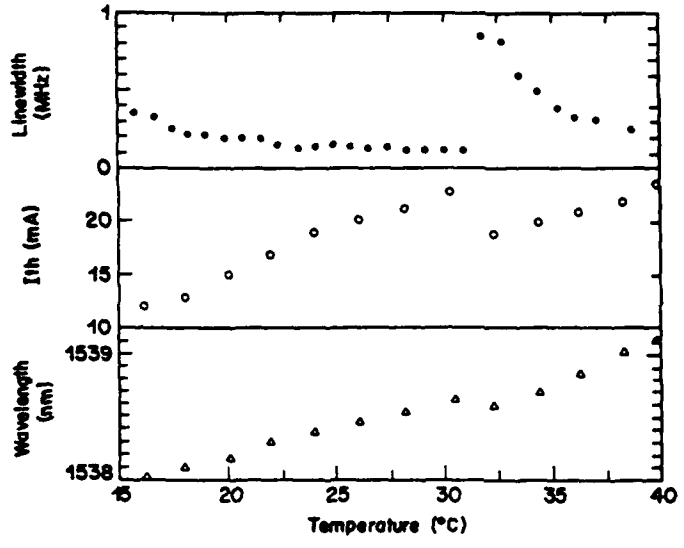

Figure 2

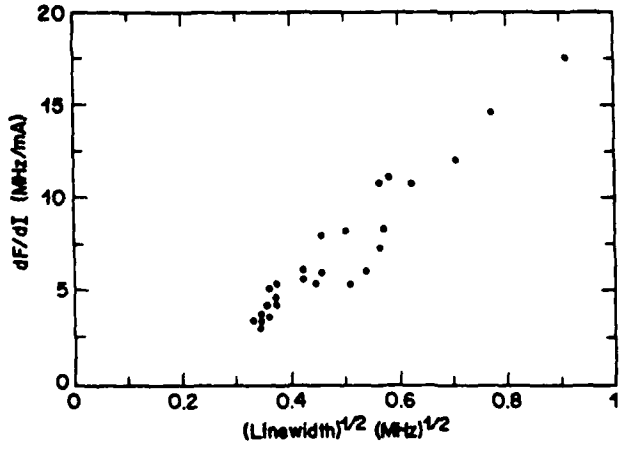

Figure 3

Q—6

Theory of the Single-Mode Emission Spectrum of Semiconductor Laser

A.P.Bogatov, P.G.Eliseev
P.N.Lebedev Physical Institute, Acad. of Sci. of the USSR,
Leninsky prospect 53, Moscow 117924, USSR

A b s t r a c t

The problem of the bandwidth and spectral shape of the emission line of the semiconductor laser, especially in a single-mode case of operation, is of serious scientific and practical interest. It is well known that in lasers there are significant deviations from Shawlow-Townes formula for the linewidth /1,2/.

In the single-frequency case one can observe a broadened line on the superluminescent background of emission. The spectral shape is formed which is affected by the intensity fluctuations as well as the fluctuations of the refractive index and the gain. In contrast to the plurality of previous treatments of the problem, the analysis of the spectra of the frequency and intensity fluctuations of laser emission has been made with taking into account not only the spontaneous noise, but also the thermodynamic fluctuations of temperature and density of the semiconductor medium. The calculation of the spectral shape of the laser line and superluminescent pedestal has been made for the first time. The optical nonlinearity of the medium provides the disturbance of the superluminescence distribution in the vicinity of a strong laser line. As a result, the symmetrically detuned field oscillations, in respect to the laser line, appear to be coupled. The splitting occurs of the longitudinal resonances corresponding to the neighbour modes. Magnitudes and spectral positions of the resonances depend on the laser emission intensity /3/.

In a well developed oscillation regime the shape may be quite close to a Lorentzian, and the main contributions to the linewidth are from fluctuations of the spontaneous emission and from temperature fluctuations. The contribution $\Delta\omega_T$ from the latter is independent of the laser optical power and is expressed by:

$$\Delta\omega_T = (K/2)(c/n)^2(T\partial g/\partial T)^2(\alpha_T-\alpha_N)^2 R_T,$$

where c is the light velocity, n is the refractive index, T is absolute temperature, α_T and α_N are the partial coefficients of amplitude-phase coupling, namely, temperature coefficient $\alpha_T = (\partial \mathrm{Re}\beta/\partial T)/(\partial \mathrm{Im}\beta/\partial T)$ introduced in /4/ and concentra-

88CH2609-8/88/0000/0202$1.00 1988IEEE

tion one (α_N), respectively, β is the longitudinal propagation constant of the guided mode, K is the Boltzmann constant, R_T is the thermal resistance of the active medium. Estimation of $\Delta\omega_T$ for a laser with typical parameters leads to 10-20 kHz.

Thermodynamic fluctuations of carrier concentration and the medium density lead to the modification of the spectral contour, therefore, to deviation from the Lorentzian, especially, in the wings of the line. As to the concentration fluctuation, the conclusion has been made in /2/.

In summary, this work shows that the distribution of spectral density of the emission is affected by fluctuations of intensity, refractive index and gain, but for correct estimation it is necessary to take into account spontaneous noise and thermodynamic fluctuations. Analysis of the superluminescent spectrum at the frequency distances comparable with the intermode spacing allows one to explain and compute symmetry of the spectral peaks and other features of laser emission and noise spectra.

References

1. C.H.Henry. IEEE J.Quant.Electron., 1982, 18, 2, 259-263.
2. K.Vahala, A.Yariv. IEEE J.Quant.Electron., 1983, 19, 6, 1102-1110.
3. A.P.Bogatov, P.G.Eliseev, O.G.Okhotnikov, M.P.Rakhvalskii, K.A.Khairetdinov. Kvant.Elektronika, 1983, 10,9, 1851-1865 (in Russian).
4. R.Lang, K.J.Vahala, A.Yariv. IEEE J.Quant.Electron., 1985, 21, 5, 443-451.

Session R: Electrical Properties & Design

R—1

Observation of Strong Carrier Density Increase Above Threshold and Its Effect on P-I and I-V Characteristics of 1.3 μm InGaAsP Lasers

Joanne LaCourse and Robert Olshansky
GTE Laboratories, 40 Sylvan Road, Waltham, MA 02254; Telephone 617-466-2494

The low differential quantum efficiencies and sublinear power-current curves of InGaAsP lasers are widely observed and poorly understood. Proposed mechanisms such as heating and leakage currents are not sufficient to explain the observed behavior for all cases, such as for pulsed operation or for lasers with leakage currents eliminated by the lack of burying layers. In this paper, measurements of spontaneous emission provide direct evidence of an increase in injected carrier density above threshold (Fig. 1). Spectrally resolved data eliminates the possibility of contributions from scattered stimulated emission or 960 nm emission from homojunction leakage currents. The combination of the measured carrier density increase above threshold and a carrier-dependent internal loss provide a quantitative explanation of the reduced internal efficiency and the observed decrease in differential quantum efficiency with current (Fig. 2).

For the case of an internal loss which continues to increase above threshold, the expression for the differential quantum efficiency becomes:

$$\eta_d(I) = \eta_i \alpha_m/(\alpha_m+\alpha_{i_{th}}+\Delta\alpha_i(I)) \qquad (1)$$

where $\eta_i = 1-(d\alpha_i/dN)/(dg/dN)$ is the new expression for the internal efficiency, α_m is the mirror loss, $\alpha_{i_{th}}$ is the internal loss at I_{th}, $\Delta\alpha_i$ is the increase above the threshold value, N is the carrier density, and $g = \Gamma G - \alpha_i$ is the net gain measured from the emission spectrum below I_{th}.

- $dN/dI = 7\times10^{15}$ cm^{-3}/mA is found from the observed increase in spontaneous emission above threshold (through a window in the substrate metallization), as Fig. 1 shows. The dependence of the spontaneous power on N is found by fitting carrier lifetime and spontaneous emission data below threshold.[1] Since N increases linearly with I above threshold, Eq. 1 predicts a quantum efficiency which decreases approximately linearly with current, in agreement with observation.
- $\Delta\alpha_i$ is found from the decrease in η_d with I:

$$\Delta\alpha_i = (d\alpha_i/dN)(dN/dI)(I-I_{th}) = 0.12 \text{ cm}^{-1}/\text{mA } (I-I_{th})$$

where $d\alpha_i/dN = 1.8\times10^{-17}$ cm^2 in approximate agreement with previous determinations of intervalence band absorption.[2,3]

- $\eta_i = 0.8$, since measured $dg/dN = 1.1\times10^{-16}$ cm^2.

Figure 2 shows the predicted and observed P-I and η_d-I curves in pulsed operation with a 100 nsec pulse. The agreement is excellent except at very high currents (above 10 mW), where homojunction leakage currents become significant, as verified by observation of 960 nm emission from the homojunctions beside the active layer.

SUMMARY:

The observed strong increase in the carrier density above threshold quantitatively explains:

- the reported values of 0.8[5] for η_i, contrary to classical models in which $\eta_i = 1$; and
- the observed linear decrease of η_d with current even in pulsed operation.

88CH2609-8/88/0000/0206$1.00 1988IEEE

References

1) J. LaCourse and R. Olshansky, Appl. Phys. Lett. 49, 128 (1986).
2) A.P. Mozer et al., IEEE J. Quantum Electron. QE-21, 719 (1985).
3) C. Henry et al., IEEE J. Quantum Electron. QE-19, 947 (1983).
4) S. Kakimoto et al., IEEE J. Quantum Electron. QE-24, 29 (1988).

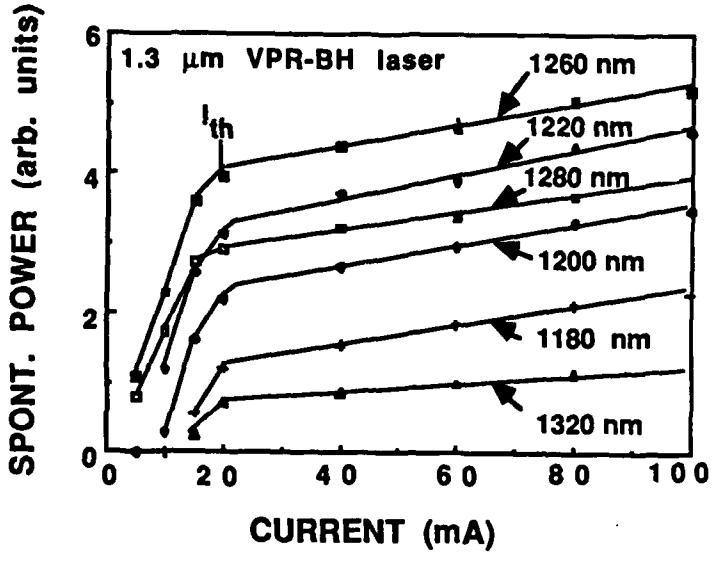

Fig 1:

Spontaneous power (measured through substrate) increases above threshold. From this, $dN/dI = 7 \times 10^{15} cm^{-3}/mA$

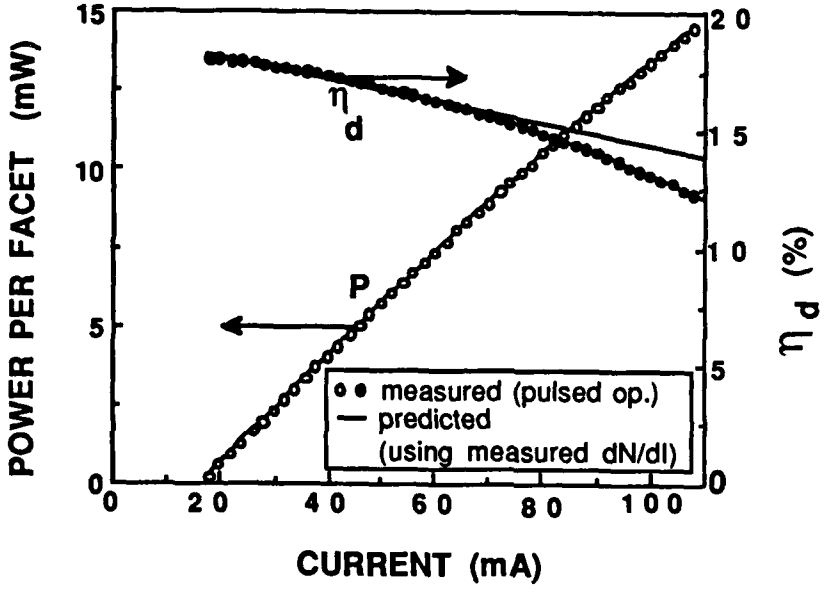

Fig. 2:

Observed facet power and η_d vs I agree with predicted (solid line) using measured dN/dI. Deviation at high I is attributed to homojunction leakage currents.

R—2

Carrier Capture and Tunnelling Effects in Long Wavelength InGaAs/InP Multiple Quantum Well Lasers

D. J. Robbins, P.J. Williams, R. Cush and A.C. Carter

PLESSEY RESEARCH CASWELL LIMITED
Allen Clark Research Centre
Caswell, Towcester, Northants, U.K.

The object of this work is to study carrier capture and transfer effects in the operation of InGaAs/InP Multiple Quantum Well (MQW) lasers.

Preferential capture of carriers into the first few wells of an MQW laser active region can lead to a variation in injection rates among the different wells, so degrading device performance. Largely as a result of the rapid development of single well GRIN-SCH and Modified QW lasers in the Ga As-based system, such effects have been unimportant and have received only limited attention (1). By contrast, in long wavelength InP-based materials, provision of an outer confinement region presents difficulties for materials growth, and to date most published results have been for InGaAs/InP MQW structures where the problem persists.

Our experimental investigations on 8-well InGaAs/InP MQW lasers are summarised in Table 1. These include optically and electrically pumped lasing characteristics and show that narrowing the barrier width contributes significantly towards achieving low threshold room temperature operation. To provide a theoretical framework to describe these lasing characteristics a rate equation model linked to a calculation of the spectral gain has been developed which describes an MQW system under different injection regimes. In addition to the usual loss mechanisms, terms describing the interwell tunnelling transfer of carriers are also included. The capture of the heavy holes determines the carrier distribution and is described by a mean capture length α_p^{-1} which characterises the exponential decay of the hole density into the MQW. As is shown in Figure 1, the predicted threshold current depends strongly on both the capture length and the tunnelling time, T^{-1} between the wells. α_p is estimated to be $\sim 2.5 \times 10^6 cm^{-1}$ for this system. To balance this assymmetry and promote strong carrier redistribution Figure 1 shows that T^{-1} must be less than 0.5 ns, i.e. barrier widths must be around 25-30A, in good agreement with the observed results.

The model presented here goes well beyond previous descriptions of carrier capture effects in MQW laser systems. It not only leads to a good understanding of the observed lasing characteristics, but will also lead to further optimisation of the device design.

(1) Kroemer H and Okamoto H. Jap J Appl Phys (1984) 23 970-974

Support by the Air Force Systems Command DoD under project number F19628-85-C-0172 is acknowledged.

88CH2609-8/88/0000/0208$1.00 1988IEEE

BARRIER THICKNESS (A)	OPTICAL PUMP INTENSITY ($kW.cm^{-2}$)	THRESHOLD CURRENT DENSITY ($A.cm^{-2}$)	
		INFERRED OPTICAL J_{th}(opt)at 20^0C	ELECTRICAL J_{th}(elec)
100	4	1100	3500 at -40^0C
55	3	820	8000 at -12^0C
25	3.3	700	3200 at 20^0C

TABLE I Threshold Current Densities under Optical and Electrical Injection

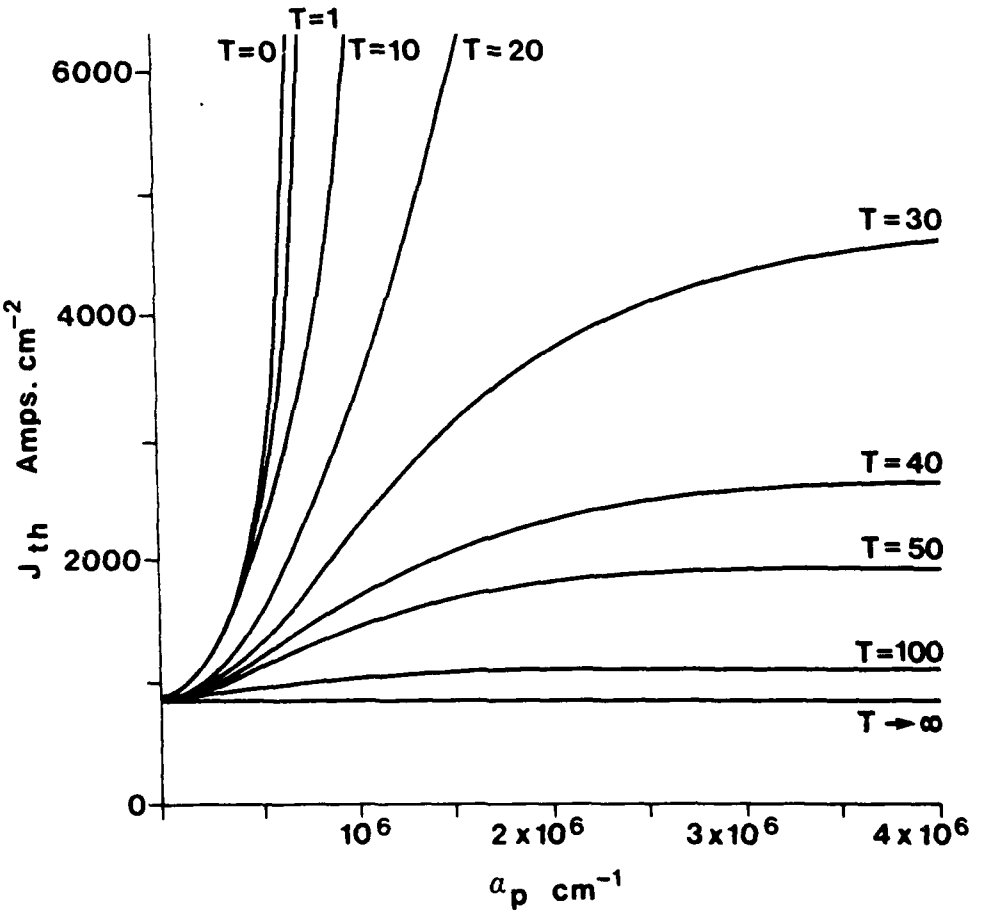

Figure 1: Predicted threshold current for an 8-well InGaAs/InP MQW laser as a function of the inverse hole capture length. $Tx10^8$ s^{-1} is the inverse tunnelling time between the wells.

R—3

Current Leakage Mechanism in InGaAsP/InP Buried-Heterostructure Lasers

T. Ohtoshi, K. Yamaguchi, and N. Chinone
Central Research Laboratory, Hitachi, Ltd.
Kokubunji, Tokyo 185, Japan

This paper reveals the mechanism of current leakage or spreading at high bias levels in InGaAsP/InP buried-heterostructure (BH) lasers. The purpose is to improve high-temperature operation of such lasers.

A full two-dimensional analysis of current distributions at various bias conditions is performed [1]. Figure 1 shows calculated current-flow distributions at around 3mW in 1.3-μm BH lasers with p-n-p-n current-blocking layers. At 85°C, considerable current leaks through the p-n-p-n layers. Diagrams of calculated energy bands in the interior of the device at 85°C are shown in Fig. 2. The relationships $\phi_n^A \approx \phi_n^C$ and $\phi_p^B \approx \phi_p^D$ are satisfied (see Figs. 2(a),(c)). This is because quasi-Fermi potentials ϕ_n and ϕ_p for majority carriers should be nearly flat in a structure whose n-substrate is common and whose p-cladding layer and p-burying layer are connected between the central p-n diode and the p-n-p-n layers. Therefore, each junction in the p-n-p-n layers is forward-biased. That is, no reverse junction exists, unlike in ordinary thyristors. Even at room temperature, no junction is reverse-biased.

Until now it has been widely accepted that it is the reverse junction formed in p-n-p-n layers which confines current. Here it is found that current confinement is due to the electrically floating region where carriers are not directly supplied from electrodes. This region corresponds to the n-burying layer in Fig. 1. This is a key point for understanding the mechanism of current leakage or spreading at high bias levels and for designing current-confinement structures. It is clarified for the first time that the confinement mechanism differs from that in conventional thyristor models.

It is also found that a p-substrate improves

88CH2609-8/88/0000/0210$1.00 1988IEEE

high-temperature performance. This is because the resulting structure's n-mesa has low resistivity which reduces the applied voltage at the junctions of p-n-p-n layers. Moreover, mass-transported BH lasers which do not have the above-mentioned floating region show considerable current leakage in high-temperature operation.

References

[1] T. Ohtoshi, K. Yamaguchi, C. Nagaoka, T. Uda, Y. Murayama, and N. Chinone, Solid-State Electron. 30, 627 (1987).

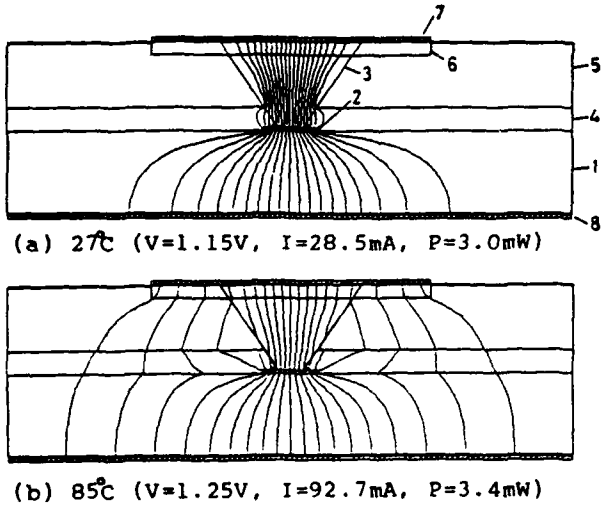

Fig. 1 Current-flow distributions in 1.3-μm BH lasers at (a) 27°C, (b) 85°C.
1: substrate (n-InP)
2: active layer (p-InGaAsP)
3: cladding layer (p-InP)
4: burying layer (p-InP)
5: burying layer (n-InP)
6: Zn-diffused region
7: p-type electrode
8: n-type electrode

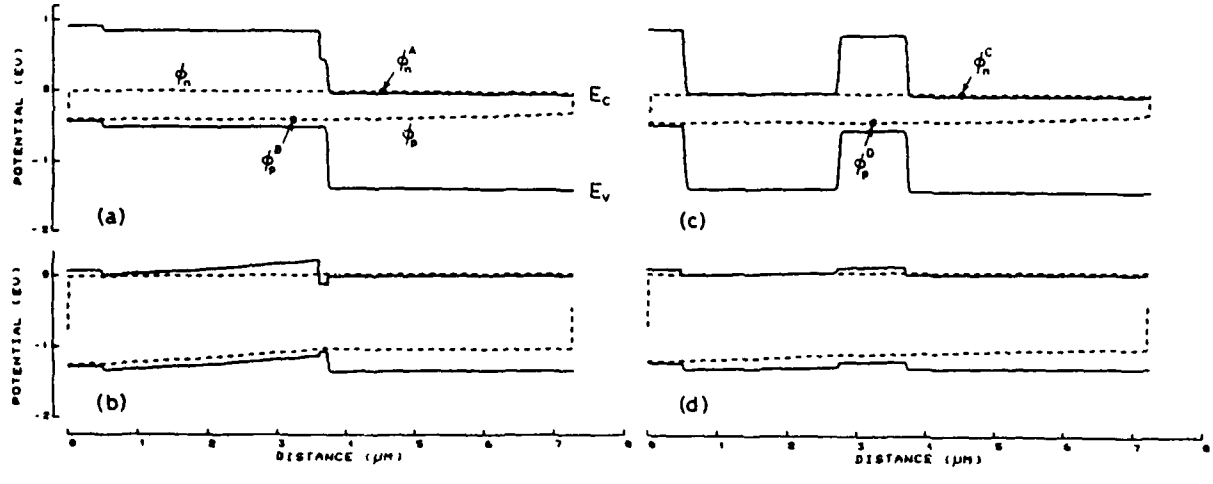

Fig. 2 Diagrams of energy bands in BH laser at 85°C.
(a),(b) cross-section of central p-n junction
(c),(d) cross-section of p-n-p-n blocking layers
(a),(c) 0.40V, (b),(d) 1.25V

R—4

Leakage Current Analysis of Buried Heterostructure Lasers with Semi-Insulating Blocking Layers

S. Asada, S.Sugou, K. Kasahara and K. Kumashiro*

Opto-Electronics Research Laboratories, NEC Corporation,
Kawasaki 213, Japan

*VLSI CAD Engineering Division, NEC Corporation,
Kawasaki 211, Japan

A reduction method for leakage current in buried heterostructure (BH) lasers with semi-insulating InP blocking layers has been obtained from the current analysis using a newly developed compound semiconductor device simulator, in which deep levels are taken into account.

Semi-insulating current blocking layers are important for both current-isolation and current-confinement in high-speed electrical and optical devices.[1] As a useful tool for analyzing these devices, a versatile two-dimensional device simulator BIUNAP-C (BIpolar and UNipolar device Analysis Program for Compound semiconductor devices)[2] has been developed. A standard model for semi-insulating InP layers was used. This model's high resistivity arises from the compensation for shallow background levels by deep levels (electron trap levels). Calculated current-voltage relations were checked and found to agree with measured values in planar configurations, which consist of a semi-insulating InP layer on n-InP or p-InP layers.

Figure 1 shows calculated current distributions for a semi-insulating InP blocked BH laser. Figure 1 shows the existence of the leakage current passing through the semi-insulating layers near the p-InP mesa. The leakage current to total current ratio was about 10 %, but was not sufficiently small, as shown in Fig.2 (Curve a). This leakage current arises from hole diffusion from the p-InP mesa. This residual leakage current can be reduced by adding a thin wide-band-

88CH2609-8/88/0000/0212$1.00 1988IEEE

gap semiconductor layer in the semi-insulating regions at the mesa boundaries. For example, assuming that the valence band gap barrier from InP mesa region is 0.15 eV (60 % of the ΔE_g), a 100-200 Å $Ga_{0.3}In_{0.7}P$ layer, whose thickness is less than the estimated critical thickness[3] without misfit dislocation, will be effective in reducing the leakage current, as shown by curve b in Fig.2.

1. C.E.Zah et al., Electron. Lett. 23,52(1987).
2. S.Asada et al., Appl. Phys. Lett. 52,703(1988).
3. J.W.Matthews and A.E.Blakeslee, J.Crystal Growth 27,118(1974).

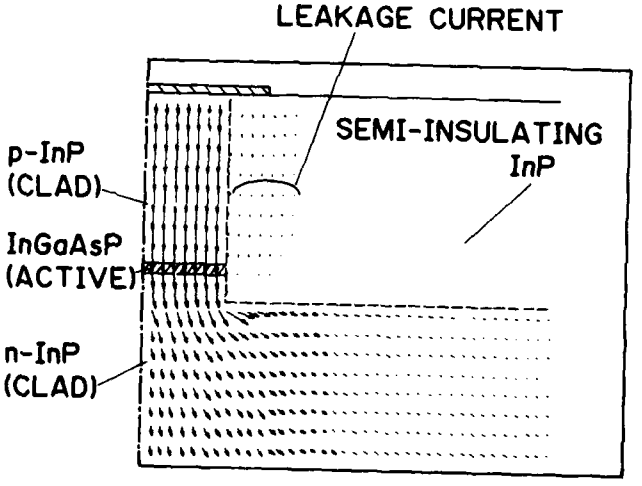

Fig. 1. Current vector distributions in BH InGaAsP/InP laser cross section.

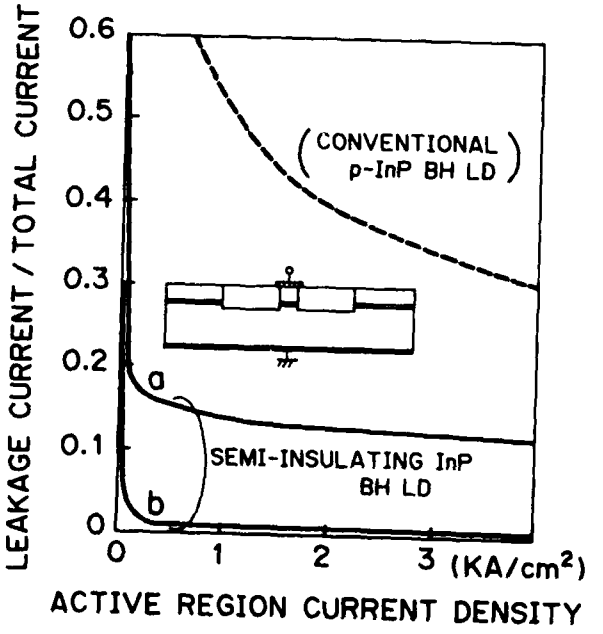

Fig. 2. Leakage current ratio vs active-region current density for semi-insulating InP BH lasers. Without and with a thin GaInP layer in the semi-insulating InP regions at the mesa boundaries (Curves a and b). The broken line shows calculated results for a 5×10^{17} cm^{-3} p-InP BH laser.

R—5

Design and Performance of InGaAsP-InP Planar Buried-Ridge-Structure Lasers

W. Thulke, A. Zach, B. Borchert, and M.-C. Amann
Siemens AG Research Laboratories
Otto-Hahn-Ring 6, D-8000 München 83, Fed. Rep. of Germany

It is demonstrated by the calculation of leakage current densities and by the fabrication of PBRS lasers (1) (fig.1) emitting at 1.3 μm and 1.55 μm that neither reverse-biased junctions nor high-resistivity blocking layers are needed in the shunt-current path of InGaAsP-InP BH lasers to obtain low threshold current, high-temperature cw operation, and high reliability, if the lasers are appropriately designed.

The omission of blocking layers is desirable, especially with regard to monolithic integration, because they are difficult to fabricate by large-scale production techniques such as MOVPE and because their capacitances are detrimental to the modulation performance of the device.

With PBRS lasers, current confinement to the active region is exclusively achieved by the different turn-on voltages of the p-n heterojunction and the adjacent p-n homojunctions. In order to get an estimate of the leakage current across the p-n homojunctions, the forward bias voltage U_H across these junctions normalized by the overall forward bias voltage U and the heterojunction voltage U_Q is calculated by conformal mapping (fig. 2). The calculation of the leakage current I_H (fig. 3) shows that the device performance mainly depends on the series resistance and the p-side contact stripe width. With resistances below 3 Ω and contact stripe widths around 4 μm, leakage currents are negligible up to diode currents of 40 mA.

PBRS lasers are fabricated by liquid-phase epitaxy. The fabrication process - growth of a double heterostructure, dry etching, overgrowth and formation of the contact stripe - is highly reproducible. Neither facet coating nor proton-bombardment (2) of the homojunctions are applied. Nevertheless, threshold currents as low as 6.4 mA and a light output of more than 10 mW even at elevated operation temperature are obtained. Cw operation above 110 °C (λ = 1.3 μm) and 100 °C (λ = 1.55 μm) is achieved (fig.4). Due to low parasitic capacitances, the 3 dB small-signal-modulation bandwidth exceeds 9 GHz at 80 mA diode current (fig.5). Reliability tests are being performed at 60 °C and 50 mA. Threshold-degradation rates are as low as 1.5 mA/kh within the first 2000 h. This corresponds to a lifetime of more than 10^5h at 25 °C, if an activation energy of 0.4 eV is assumed and a threshold current of 50 mA is defined as failure criterion.

(1) W. Thulke et al., Siemens Forsch.-u.Entw.-Ber. 17 (1988), 1-5
(2) M. Krakowski et al., IEEE J. LT 4 (1986), 1470-1474

88CH2609-8/88/0000/0214$1.00 1988IEEE

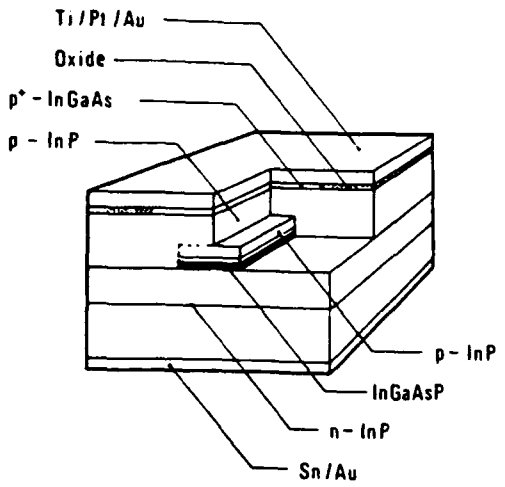

Fig.1: Schematic representation of the PBRS laser

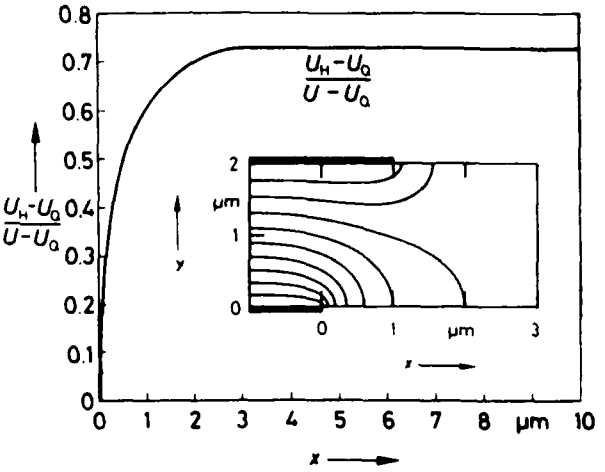

Fig.2: Normalized forward bias voltage $(U_H-U_Q)/(U-U_Q)$ across lateral InP p-n junction as a function of the lateral distance x from the active stripe (inset: geometry and equipotential lines)

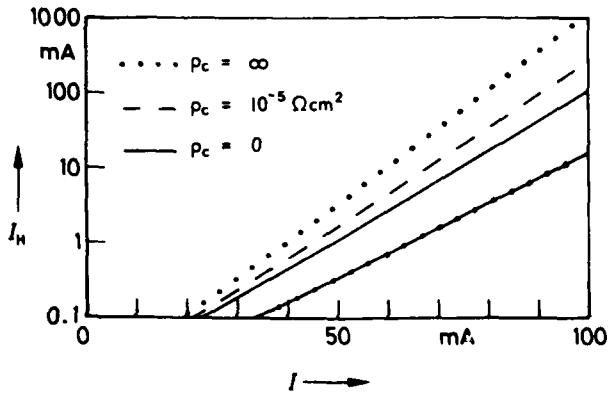

Fig.3: Leakage current I_H as a function of the diode current I for contact stripe widths of 4 μm (lower solid line) and 8 μm (upper lines) and different contact resistances.

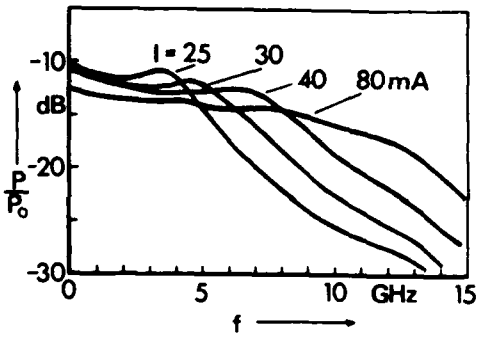

Fig.5: Small-signal frequency response P/P_o of a 1.55 μm PBRS laser

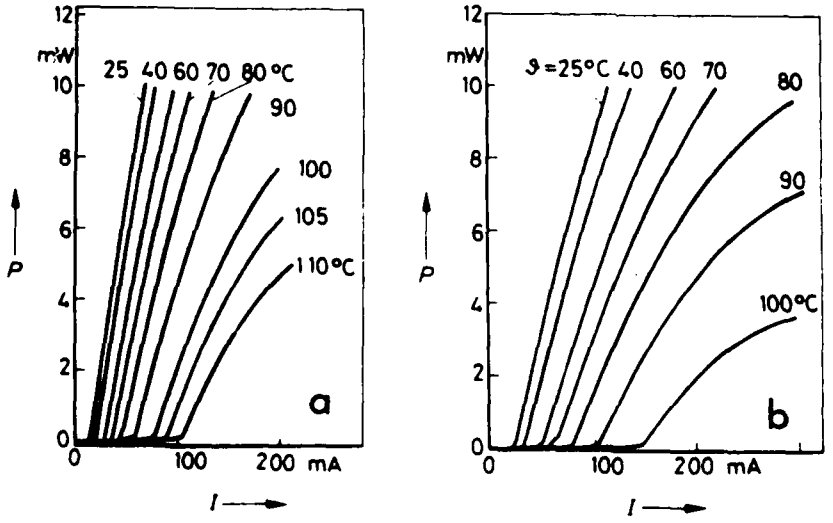

Fig.4: Cw light output power per facet P versus diode current I of upside-down mounted PBRS lasers emitting at 1.3 μm (a) and 1.55 μm (b) at various heatsink temperatures

R—6

Double Injection Leakage Currents in Channel Substrate Buried Heterostructure Lasers with Semi-Insulating InP: Fe Current Blocking Layers

E. J. Flynn, L. J. P. Ketelsen, J. L. Zilko, D. T. C. Huo and L. A. Koszi

AT&T Bell Laboratories
Murray Hill, N. J. 07974

In this paper we show that channel-substrate buried heterostructure (CSBH) lasers with InGaAsP active layers grown by liquid phase epitaxy (LPE) and semi-insulating InP:Fe current blocking layers grown by metallo-organic chemical vapor deposition (MOCVD) exhibit current leakage through the blocking layers via the mechanism of double-injection. Semi-insulating (si) layers are widely used for current confinement in BH lasers, but the importance of the double-injection problem has not been clearly recognized. Leakage currents, which partially shunt the active layer and degrade device performance, flow through si material despite the high (single-carrier) resistivity of InP:Fe layers. The existence of p-si-n leakage currents is demonstrated by analysis of light- and voltage- versus current (LIV) data, and by means of scanning electron microscope (SEM), electron beam induced current (EBIC) and electroluminescence (EL) imaging of laser facets. The observation of homojunction EL distributed spatially along si-p interfaces in both n-substrate and p-substrate devices, as shown in Figure 1, is compelling evidence of double-injection carrier transport across the semi-insulating layers. These data are consistent with the n-type behavior of si material under double-injection conditions. Numerical estimates using existing theory show that double-injection currents will flow through InP:Fe layers of thickness ~1μm at voltages well below levels relevant to laser operation. Moreover, double-injection behavior in specially fabricated p-si-n chips has been demonstrated explicitly. Elimination of double-injection currents will require proper design of structures that incorporate InP:Fe layers.

88CH2609-8/88/0000/0216$1.00 1988IEEE

CSBH/MOCVD LASERS
-HOMOJUNCTION EMISSION-

EL IMAGES
($\lambda < 0.98\mu m$)

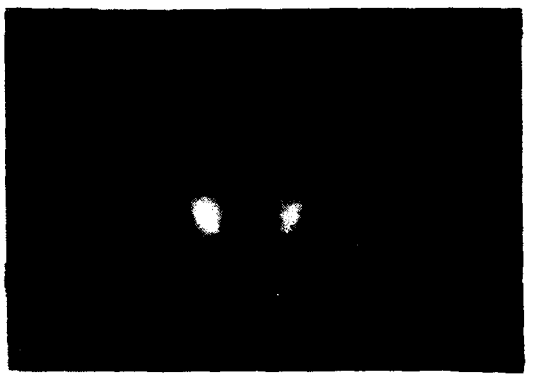

LUMINESCENCE MAP

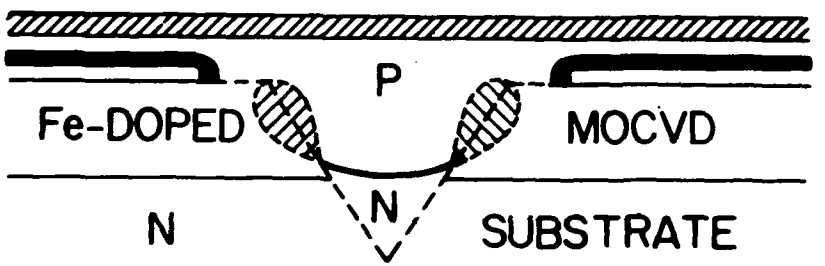

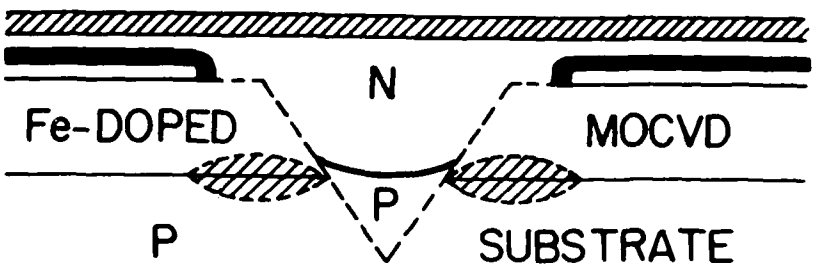

AUTHOR INDEX